This document was prepared for the ETI by third parties under contract to the ETI. The ETI is making these documents and data available to the public to inform the debate on low carbon energy innovation and deployment.

Programme Area: Marine

Project: PerAWAT

Title: Tidal Basin Modelling: the Alderney Race, the Pentland Firth and the Paimpol-Bréhat Sites Modelled in Telemac Software

Abstract:

This document describes four different numerical models of sites. The sites are Paimpol-Brehat, the Alderney Race, and the Pentland Firth. The Paimpol-Brehat site has been modeled in 2D and in 3D. The site selection was made with the PerAWaT consortium at the beginning of the PerAWaT project. This work layed the foundations for the basin scale modeling, as it enabled the study of the influence of the presence of tidal farms.

Context:

The Performance Assessment of Wave and Tidal Array Systems (PerAWaT) project, launched in October 2009 with £8m of ETI investment. The project delivered validated, commercial software tools capable of significantly reducing the levels of uncertainty associated with predicting the energy yield of major wave and tidal stream energy arrays. It also produced information that will help reduce commercial risk of future large scale wave and tidal array developments.

PerAWAT WG3 WP3 D1

Tidal basin modelling: The Alderney Race, the Pentland Firth and the Paimpol-Bréhat sites modelled in Telemac software

Project	PerAWAT
Work package	WG3
Deliverable	WG3 WP3 D1 Candidate sites without farm
Responsible author	Vanessa Martin, Chi-Tuân Pham, Sylvain Saviot (EDF)
Second reading	Jean-François Dhédin, Clarisse Fil (EDF)
Circulation	Among all authors and readers
To be approved by	Robert Rawlinson-Smith (GH)
Date	10/12/2012
Issue	V2.0

Document revision history

Issue	Date	Summary
V1.0	21/06/2012	Document sent to GH.
V1.1	05/10/2012	Document sent to GH with EDF response to ETI comments
V2.0	10/12/2012	Document sent to GH without track changes after ETI approval

Table of content

1 INTRODUCTION

1.1 Scope of this document

This document describes four different numerical models of sites. The sites are Paimpol-Brehat, the Alderney Race, and the Pentland Firth. The Paimpol-Brehat site has been modeled in 2D and in 3D. The site selection was made with the PerAWaT consortium at the beginning of the PerAWaT project.

This work lays the foundations for the basin scale modeling, as it will enable the study of the influence of the presence of tidal farms.

1.2 Purpose of the basin scale modelling

The purpose of the coastal basin modelling is to:

- Develop a numerical model for modelling of tidal farms performance and wake at large scale,
- Assess the large scale effects of tidal energy extraction from UK sites,
- Provide results for cross-comparison with another model (WG3 WP6 UoO),
- Provide input data (boundary conditions) to array scale models (WG3 WP2 UoE),
- Provide results for validation of the engineering tool (WG3 WP4).

1.3 Specific tasks associated with WG3 WP3

- D1 – 2D shallow water equation model(s) of candidate site(s).
- D2 – Code development for 2D shallow water model in Telemac 2D of the Telemac software suite, in order to allow for the implementation of parametric characterization of arrays.
- D3 – Incorporation of the parametric characterization of an axial flow turbine array (obtained in WG3 WP2) into the 2D basin scale numerical models.
- D4 – Assessment of the effects of energy extraction at various UK sites using the 2D model: Macroscopic, but still reliable, study of the large-scale impact of a tidal farm on the hydrodynamics of the area, and accurate assessment of the site tidal resource.
- D5 – Cross-comparison in terms of energy extraction of 2D and 3D results for the selected site.

D1 Content

- 2D shallow water equation models of candidate sites + 3D modelling of one site.
- Construction of numerical models for the candidate sites. This will require accurate digitized bathymetry and tidal characteristics data for the boundary conditions. Calibration of the models will be performed with various data, such as real basin scale data where this is available (ie ReDAPT for the EMEC site), and charts otherwise.

D1 Deliverables

a) Input files for candidate sites
b) Report: model methodology, performance and validation (for 2D and 3D: 2D for each of the different sites and 3D for one site)

1.4 WG3 WP3 D1 Acceptance criteria

c) Module software code provided in Telemac software – 2D and 3D versions – for sites as specified in WG0 D2.
d) Report contains the following:
   - Description of model methodology, assumptions and algorithms
   - Assessment of model performance and Calibration/validation against measurements from WG4 WP4 and chart data for the selected sites.

- Provision of boundary conditions for the array scale models (WG3 WP2 UoE).

2 MODELLING SOFTWARE: TELEMAC-2D AND TELEMAC-3D

The TELEMAC-2D and TELEMAC-3D softwares have been developed by the LNHE department (National Hydraulics and Environment Laboratory) of EDF R&D. They allow the modelling and simulation of free surface flows and are based on finite element methods. TELEMAC-2D solves the Saint-Venant equations (or shallow water equations) in a two-dimensional (plane) computational domain. Its principle variables are the water depth and the vertically averaged velocity components, at every point within the domain. The underlying assumptions to the use of TELEMAC-2D are: hydrostatic pressure (the vertical acceleration caused by the pressure balances gravity), negligible vertical velocities (this is linked to the hypothesis of hydrostaticity that requires vertical acceleration to be insignificant) and impermeability of the surface and of the bottom (no transfer of water either through the bottom or from the surface, a particle of water located on one of these two interfaces will remain there). TELEMAC-3D software solves the Navier-Stokes equations for free surface flows in three dimensions. It can solve the Navier-Stokes equations with or without the hydrostatic assumption. TELEMAC-2D and TELEMAC-3D can take into account the following phenomena:

- bed friction,
- impact of the Coriolis effect,
- effects of meteorological phenomena: atmospheric pressure and wind,
- turbulence,
- subcritical and supercritical flows,
- tidal flats (sections of the shore exposed during ebb tide that are treated as dry areas in the computational field), an option that has been utilised in this study.

These programmes have complete user documentation [G1]-[G5]. TELEMAC-2D has been available in Open Source since 2010 (from version 6.0) whereas TELEMAC-3D became available in Open Source in 2011 (from version 6.1).

The TELEMAC-2D software uses a number of input and output files, some of which are optional. The input files are the following:

- The geometry file (obligatory). This is a binary file in Selafin format, and can thus be read by FUDAA-PREPRO software and created either directly by MATISSE, JANET or BLUEKENUE or else by the STBTEL module from the file(s) produced by the mesh generator. The structure of the Selafin format is described in [G3],
- The steering file (obligatory). This is a text file created by a text editor or by the FUDAA-PREPRO software. In a way, it represents the control panel of the computation. It contains a number of keywords to which values are assigned,
- The boundary conditions file (obligatory). This is a formatted file generated automatically by MATISSE, JANET, BLUEKENUE or STBTEL. It can be modified with a standard text editor. It describes the contour of the domain trigonometrically, starting from the bottom left-hand corner (X + Y minimum) and then the islands in a clockwise direction,
- The bottom topography file (optional),
- The FORTRAN file (optional, but very often used),
- The open boundary file (optional),
- The previous computation file (optional),
- The binary data file (optional, but sometimes used here),
- The formatted data file (optional, but used here),
- The reference file (optional).

The output files are the results file, the listing printout, the formatted data file (optional) and the binary data file (optional).

3 THE ALDERNEY RACE

3.1 Introduction

The aim of this study is to provide a precise characterisation of the tidal conditions, *i.e.* the sea levels and tidal currents, in the vicinity of Alderney where strong tidal currents are experienced. The TELEMAC-2D software is used to build the free surface flow numerical model covering the study area (see Figure A1).

The model is calibrated against ADCP current speed measurements and validated against Vessel Mounted ADCP (VMADCP) current speed measurement and predicted tidal heights for the harbours of Braye (Alderney) and Goury (France). In addition to bathymetric data provided by oceanographic services, refined bathymetry data (from multi-beam survey) is locally integrated into the numerical model.

3.2 Geographic location of the site

The Alderney Race (also known as “Raz Blanchard” in French) is located off the western tip of the Cotentin peninsula in Normandy, France. Figure A1 shows that the bathymetric morphology is complex, with trenches, banks and irregular isobaths. The major ports in the study area are Braye on the island of Alderney and Goury on the French coast.

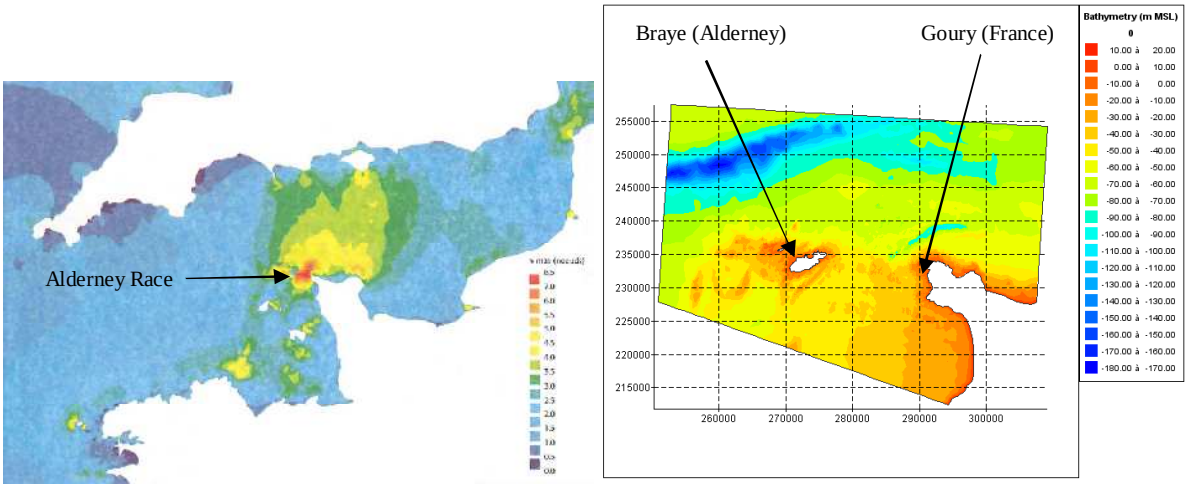

Figure A1: Left panel: Maximal tidal velocities over the English Channel during a mean spring tide (in knots), source [A1]. Right panel: Alderney Race study area, bathymetry (m MSL) and extent of the TELEMAC-2D local model, Lambert 1 North coordinate system (m)

3.3 Tidal sea levels

The sea level data, which are characteristic of astronomical tides, are provided by the French Marine Hydrographic and Oceanographic Service (SHOM) and referenced with respect to Chart Datum for the two ports: Goury, the major port on the French coast in the study area, and Braye on the island of Alderney (©SHOM-2011).

Table A1 gives sea level data for the following tides:

- Highest Astronomical Tide (HAT),
- Mean High Water Springs (MHWS),

- Mean High Water Neaps (MHWN),
- Mean Sea Level (MSL),
- Mean Low Water Neaps (MLWN),
- Mean Low Water Springs (MLWS),
- Lowest Astronomical Tide (LAT).

Port	Source	HAT	MHWS	MHWN	MSL	MLWN	MLWS	LAT
Goury	[A2]	8.98 m CD	8.15 m CD	6.60 m CD	5.06 m CD	3.50 m CD	1.40 m CD	0.29 m CD
Braye	[A3]	x	6.2 m CD	4.7 m CD	x	2.5 m CD	0.9 m CD	x

Table A1 : Sea levels characteristic of astronomical tides at Goury (French coast) and Braye (Alderney), (source [A2]-[A3], ©SHOM-2011)

The following tidal ranges are thus obtained:

Port	Source	Mean spring tide - tidal range	Mean neap tide - tidal range
Goury	[A2]	6.75 m	3.10 m
Braye	[A3]	5.3 m	2.2 m

Table A2: Tidal ranges at Goury (French coast) and Braye (Alderney)

Certain meteorological conditions can lead to differences between the predicted tide and the actual tide, in particular a combination of a HAT and a surge (extreme high water level), or conversely, a conjunction of a LAT and a receding surge (extreme low water level).

3.4 Measurement campaign

Multi-beam bathymetry data were provided to EDF by ACRE. They were collected using a GeoAcoustic GeoSwath Plus system. The processed sounding spacing of the survey is of 5 m. This allows a good representation of the local features of the sea bed morphology, enhancing the quality of the numerical modelling along the South South-East side of Alderney, over the Alderney South Banks. The ACRE survey area is shown in Figure A4. Figure A2 shows the seabed morphology over this area with sandbank ripples that are likely to change in size and shape with time depending on the long term pattern of sediment transport.

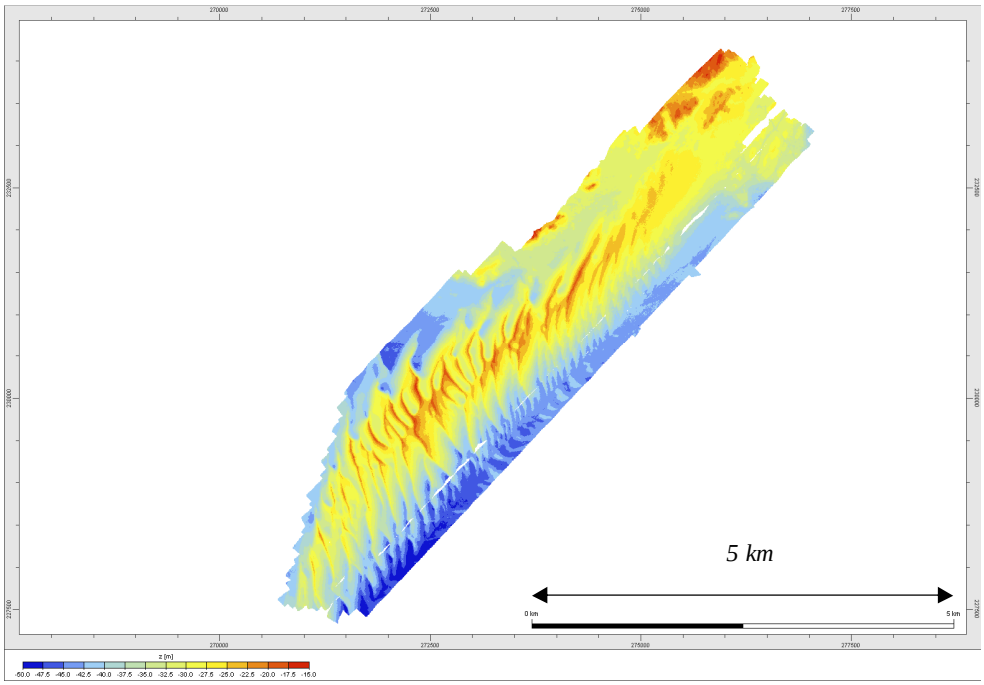

Figure A2: ACRE multi-beam bathymetry data

ACRE also provided EDF with VMADCP continuous records over 40 to 50 minute transects [A5]. Each transect consists of five lines that cross the South Banks survey area for a total distance of approximately 6.5 km (cf. Figure A3 and Table A3). Seven transects had been completed on the 17th August 2011.

The instrument used was a 600 kHz Teledyne RDI Workhorse Sentinel vessel-mounted ADCP. The instrument used single-ping ensembles, and was set to 1 second interval between ensembles. Fifty bins with a 1 m depth cell size were used as the basis for data collection.

Unfortunately, the vessel coordinates of transects number 5 and 7 were not available and thus these transects were not analysed. Besides, the average speed of vessel was about 2.5 m/s, which is superior to the recorded water flow velocities. Due to the turbulent nature of the marine flow, current speed measurements are usually based on average speeds over a period of at least 1 minute. At a vessel speed of 2.5 m/s, a distance of 150 m is covered in 1 minute. Flow fluctuations thus vary significantly, because of intrinsic flow turbulence and the spatial variability of the marine flow.

VMADCP data are therefore not considered as fully reliable for validation purposes and will only be regarded as an indication of the order of magnitude of the flow. To this end, data is averaged over the water column and compared to the TELEMAC-2D results.

	Start of line		End of line	
Line	Latitude	Longitude	Latitude	Longitude
1	49°40.898526’	2°10.825458’	49°42.041065’	2°10.765214’
2	49°42.041065’	2°10.765214’	49°42.194765’	2°11.478455’
3	49°42.194765’	2°11.478455’	49°41.724829’	2°10.972991’
4	49°41.724829’	2°10.972991’	49°41.278457’	2°10.139377’
5	49°41.278457’	2°10.139377’	49°41.583643’	2°9.815782’

Table A3: Transect lines

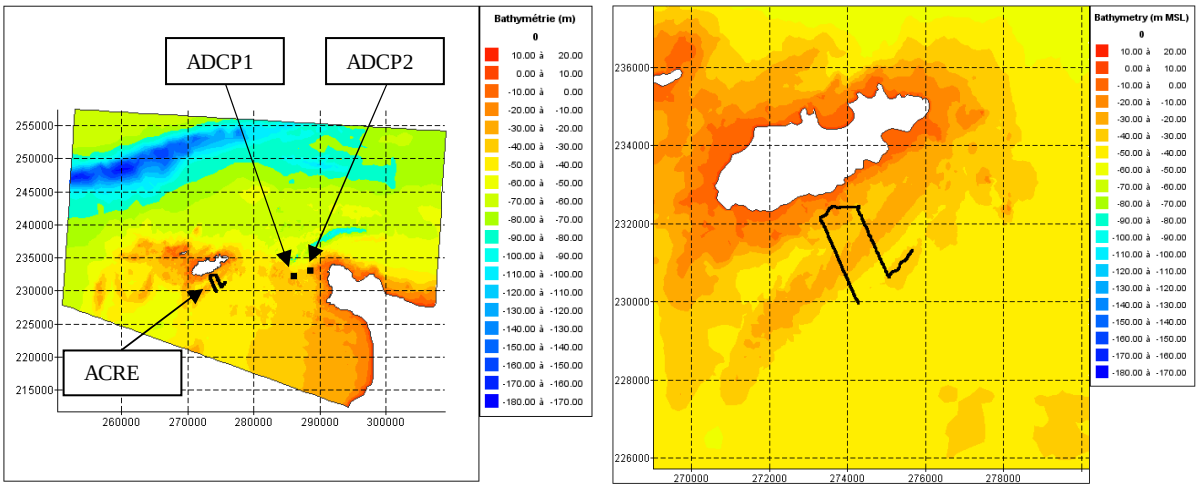

Figure A3: ACRE VMADCP transect measurements and EDF DPIH ADCP1 and ADCP2 locations (left panel) – Focus on ACRE VMADCP transect measurements over the Alderney South Banks (right panel)

Complementary to ACRE data, two ADCPs were deployed off the French coast on the 31st July 2009 for around 6.5 months by EDF DPIH (see Table A4). Three tidal cycles were made available in order to provide calibration data. They correspond to a mean neap tide (13/10/2009 – tidal coefficient: 45), a mean spring tide (17/10/2009 – tidal coefficient: 95) and a stronger spring tide (01/02/2010 – tidal coefficient: 112).

Data collection was performed continuously for ADCP1 during the entire period. However, ADCP2 did not record any data during 15 days at the end of August 2009. It has been assumed that the device moved and flipped upside down.

Note: The tidal coefficient ('coefficient de marée' in French) corresponds to the ratio between the semi-diurnal tidal range in Brest and the mean tidal range of equinox spring tides, set at 6.1 m in Brest. The tidal coefficient is a dimensionless number that is usually expressed by multiplying its value by 100, so that it varies between 20 and 120.

The current velocities were averaged over the vertical in order to fit the TELEMAC-2D model outputs.

	ADCP 1	ADCP 2
Latitude (WGS84)	49°42.508' N	49°43.041' N
Longitude (WGS84)	2°01.163' W	1°59.115' W
Approx. depth (m CD)	-34.3	-29.4
Instruments	AWAC 600 kHz WPR1287	AWAC 600 kHz WPR 1290
Cell size	1 m	1 m
Number of layers	50	50
Measurement interval	10 or 20 min	10 min
Averaging interval (sample duration)	60 s	60 s

Table A4: Characteristics of the EDF DPIH measurement campaign

3.5 Numerical model construction

All modelled flow velocities shown hereafter only take into account the astronomic tide. In particular, no meteorological effects (atmospheric pressure, wind, surge/wane) or wave effects have been considered in the numerical model.

Moreover, in this section, any reference made to the current velocity resulting from the TELEMAC-2D numerical model or measurement data refers to the vertically averaged velocity. The results given from TELEMAC-2D are averages in the Reynolds sense, *i.e.* after smoothing out of the turbulence effects.

The sea levels are referenced with respect to MSL.

3.5.1 Code version

The TELEMAC-2D software used in this study is version 6.0.

3.5.2 Definition of the domain area

The domain covers an area extending approximately 40 km from North to South and 50 km from West to East. Its extent can be seen in Figure A1. The domain extent of the numerical study is, in the WGS84 coordinate system, contained between longitudes 1° 43' and 2° 30' W. The southern boundary of the domain (segment [E4, E5]) is oblique, so that the tidal current flows perpendicularly to this segment. The boundary coordinates of the domain covered by the study are given in Table A5 and are illustrated in Figure A5.

The domain extent encloses the areas where tidal flows are expected to be the strongest and thus where tidal turbines would be profitable. The model boundaries are also defined so that the domain size maintains computation time of simulations to reasonable values (cf. § 3.7). It is acknowledged that the integration of an industrial tidal farm within the model will disturb the flow and thus will question the domain extent. The fluid – structure interactions due to tidal turbines will be examined in detail in on-coming studies (*e.g.* WG3 WP3 D03). Then, boundaries could be adjusted to allow an accurate assessment of the impacts of the turbines on the hydrodynamics conditions depending on fluid – structure interaction conditions.

Boundary extents	WGS84		Lambert 1 North	
	Longitude	Latitude	E (m)	N (m)
E1	1°43' W	49°40' N	307575	226413
E2	1°43' W	49°55' N	309070	254176
E3	2°30' W	49°55' N	252915	257493
E4	2°30' W	49°39' N	251012	227897
E5	1°50.5' W	49°31.5' N	297693	211175

Table A5: Boundary coordinates of the numerical domain extent (Figure A5).

The hydrodynamic numerical model was built with its horizontal geographic coordinates expressed in the Lambert 1 North projection coordinate system (in metres, with the point of origin at the Lambert 1 North projection origin).

3.5.3 Bathymetry

In addition to the ACRE multi-beam survey, bathymetric data has been purchased from the "Service Hydrographique et Océanographique de la Marine" (SHOM – French Navy Hydrographic and Oceanographic Service) and Seazone. It includes:

- 100 km x 100 km SHOM bathymetric tile "FRA-03-69-2009", covering an area within 300,000 to 400,000 m E and 6,900,000 to 7,000,000 m N (RGF93 – Lambert 93)
- digitalised depth and shoreline data from nautical chart number $6{,}966_L$
- 2° x 2° Seazone tile "NW24800040", covering an area within 4° to 2° W and 48° to 50° N

Figure A4 shows the extent of each data source over the study area.

All bathymetric data were reduced to MSL and all numerical results are therefore referenced with respect to MSL. Bathymetric data (SHOM and Seazone) were provided in the form of ASCII files. They required very little conditioning to be converted into "xyz ASCII file" directly readable by the mesh generator (Janet v2.7.8) that manages large input files (over millions of data points).

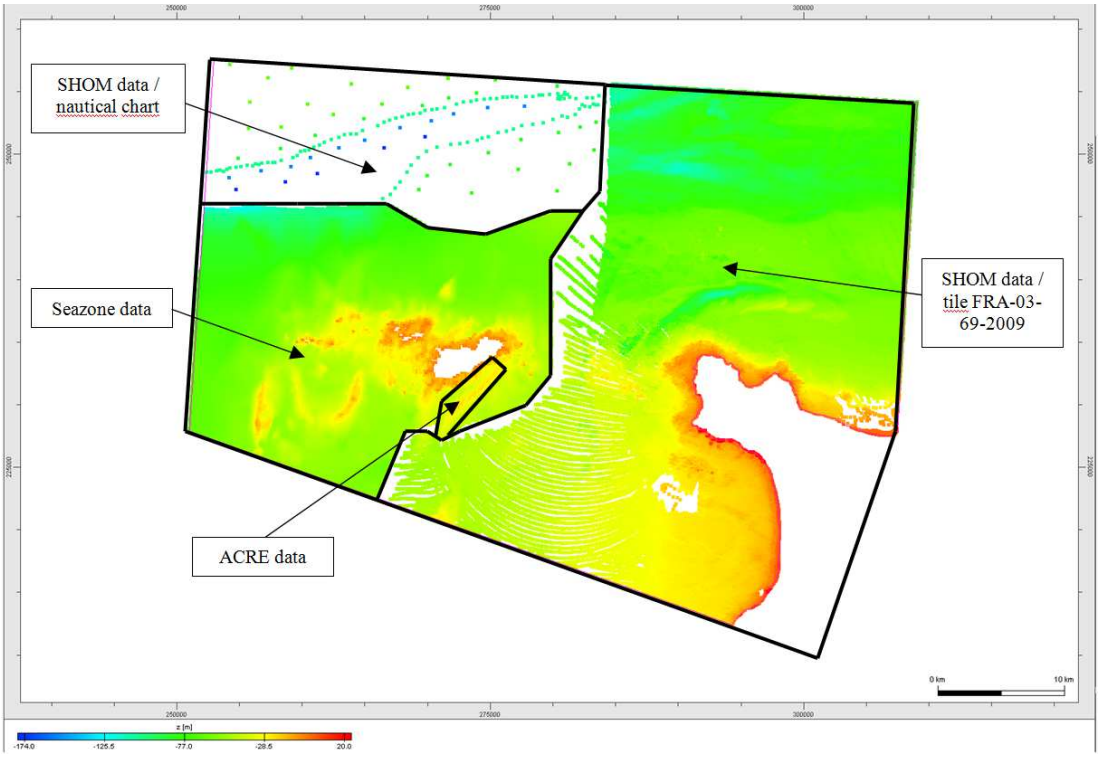

Figure A4: Alderney Race study area, bathymetry data (m MSL)

3.5.4 Mesh

The finite element mesh, built with Janet v2.7.8, is composed of 29,304 nodes and 58,074 triangular elements. The mesh size varies progressively from 60 m, at the shoreline and within the areas of interest, to 2 km offshore (western and eastern sectors of the model) (see figure below).

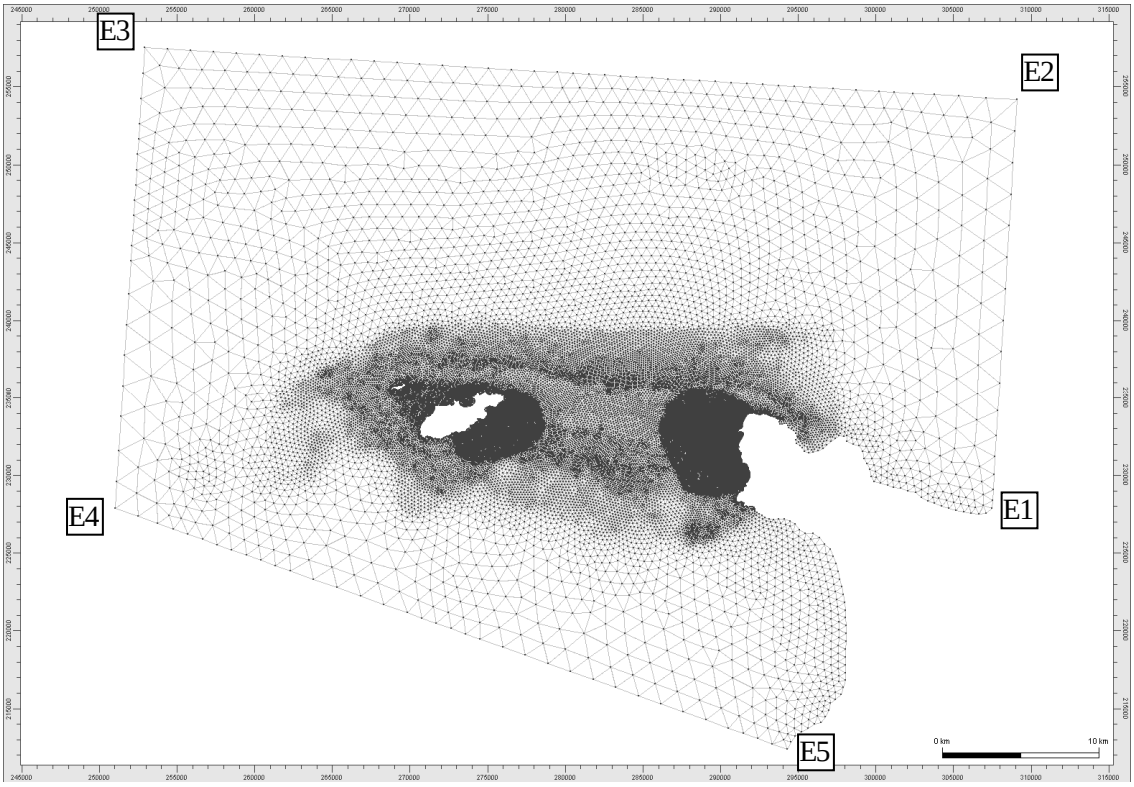

Figure A5: Model mesh (Lambert 1 North coordinate system)

3.5.5 Boundary conditions

The boundary conditions are derived from the NEA (North East Atlantic) model processed by NOVELTIS/LEGOS in the frame of the COMAPI project, funded by CNES [A6]-[A7]. The atlas covers the North East part of the Atlantic, from Mauritania to the South of Norway (see Figure A6). The model gives amplitudes and phases for the tidal elevation and for the two horizontal components of the current. The latest version (Spring 2010) has 47 harmonic constituents. The resolution is roughly 20-25 km in the ocean and 4 km closer to the shore.

In this study, real tide cases were recomposed from the NEA forcing.

Water depths or velocities on the boundary are imposed using Thompson-type boundary conditions [G7].

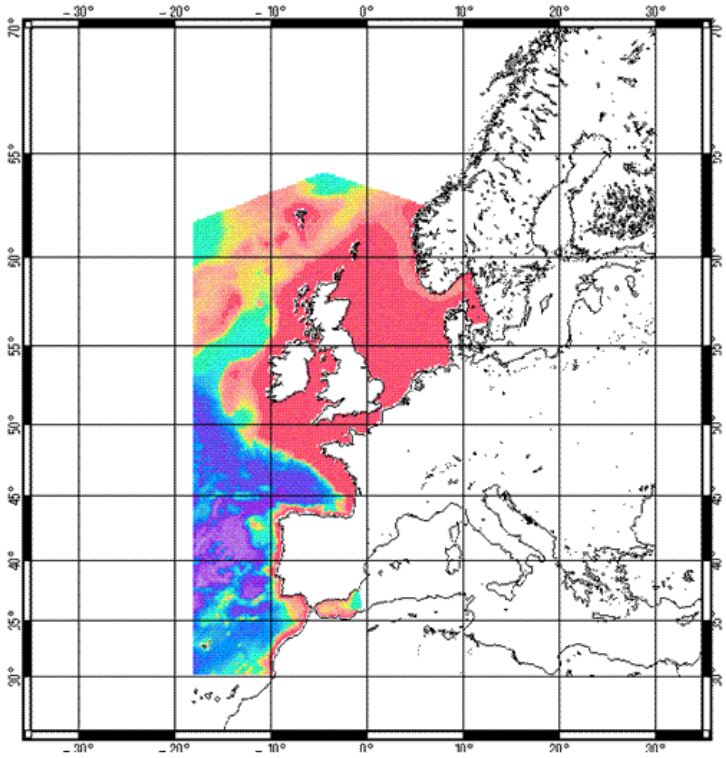

Figure A6: Extent of the NEA model, processed by NOVELTIS/LEGOS in the frame of the COMAPI project, funded by CNES

3.5.6 Modification of standard sources

In order to take into account the modification of some of the subroutine arguments, the TELEMAC--2D routine was amended accordingly.

As discussed previously, tidal signals for the boundary conditions at the liquid border are reconstituted from the NEA model [A6]-[A7] comprising 47 harmonic constituents (including Z0). A velocity ramp (*i.e.* a linear increase of the velocity intensity) is imposed at the beginning of each simulation, during the first half hour of physical simulation, so that the simulation does not freeze or crash during this period. These modifications are found in the subroutines TIDAL_MODEL_T2D, BORD, BORD_TIDE_LEGOS, NODALF_SCHUREMAN, and NODALUPV_SCHUREMAN which isolate the treatment of the tide on the liquid boundaries and will be integrated into version 6.2 of the TELEMAC-2D software.

A calibration parameter was used to correctly reproduce the tidal current speeds. This parameter is called CTIDEV. It is a multiplier coefficient which acts on the amplitude of the tidal signal (sum of sinusoids of the harmonic constituents for the two horizontal velocity components). It is set at CTIDEV = 0.8 to keep results consistent when using the LNHE 4-harmonic constituents numerical model forcing with the same bottom friction characterisation. This parameter modulates the tidal current imposed at the boundary condition of the model. It is a correction parameter of the tidal current intensity provided by the NEA model.

The subroutine STRCHE was edited in order to impose a spatially varying bed friction coefficient over the study domain (cf. § 3.5.9).

3.5.7 Parameters

An example of the parameter files (taken from July 2010 tide cycles) is reproduced in Appendix A1.

Real tide cycles are modelled, with a varying duration for the physical computation (keyword NUMBER OF TIME STEPS associated with the keyword TIME STEP).

The initial condition chosen is a free-surface elevation that is constant over the entire domain extent (keyword INITIAL CONDITIONS assigned to the value 'CONSTANT ELEVATION'), taken as equal to the water level (in MSL) at the port of Goury (value of the keyword 'INITIAL ELEVATION').

The graphic outputs (variables and variable names in the parameter file), routinely viewed for this type of hydrodynamic study, are: the horizontal velocity components U and V (averaged over the vertical) and the free-surface elevation S.

For this numerical model and for every real tide cycle, the chosen time step (keyword TIME STEP) was 5 s.

In order to capture the tidal wave characteristics and to optimise the output file size, the computational results are written to the output file every 10 or 5 minutes (real time) = 120 × 5 s or 60 × 5 s (keyword GRAPHIC PRINTOUT PERIOD = 120 or 60 according to the chosen time step).

3.5.7.1 Physical parameters

Dissipation through bed friction was modelled using a Strickler coefficient Ks, spatially varying over the study domain split into two parts (LAW OF BOTTOM FRICTION = 3, default value – see map § 3.5.9).

The Coriolis force was taken into account (keyword CORIOLIS = YES) with the value of the Coriolis coefficient equal to 1.11×10^{-4}. (= $2\omega\sin(l)$ value obtained for a latitude l equal to 49.75°N, with $\omega = 2\pi/T$, T = 86,164 s, duration of a sidereal day. This value is thus assigned to the keyword CORIOLIS COEFFICIENT).

Meteorological effects (wind and atmospheric pressure) were not taken into account in the numerical simulations (keywords WIND and AIR PRESSURE = NO, default values).

No specific turbulence model was employed (value left at 1 by default for keyword TURBULENCE MODEL). Therefore, a constant coefficient of viscosity equal to the default value of 10^{-4} is applied over the whole domain (keyword VELOCITY DIFFUSIVITY) to model the Reynolds stress terms by using the gradient diffusion hypothesis.

3.5.7.2 Numerical parameters

The boundary conditions for the open liquid boundaries at which the tidal conditions (depth and/or velocity) were imposed, were treated using the Thompson method [G7] with calculation of characteristics (keyword OPTION FOR LIQUID BOUNDARIES = 2).

The discretisation uses linear triangular elements (DISCRETIZATION IN SPACE = 11; 11 default values) with matrix storage by segments to optimise calculation times (keyword MATRIX STORAGE = 3, default value). For the suppression of free-surface parasite oscillations, the keyword FREE SURFACE GRADIENT COMPATIBILITY was taken equal to 0.9 (recommended value).

Equations were solved in the wave equation form (keyword TREATMENT OF THE LINEAR SYSTEM = 2).

The numerical schemes used were: the method of characteristics for the advection of velocities and, for the water depth, a conservative scheme (keyword TYPE OF ADVECTION = 1; 5 default values).

For solving the propagation step, the conjugate gradient method was the chosen solver (keyword SOLVER = 1), with an accuracy of 10^{-4} which is the default value (keyword SOLVER ACCURACY), a maximum number of 500 iterations (keyword MAXIMUM NUMBER OF ITERATIONS FOR SOLVER) and a diagonal preconditioning (keyword PRECONDITIONING = 2, default value).

3.5.8 Treatment of tidal flats

The tidal flats (keyword TIDAL FLATS = YES, default value) were treated using the first treatment option, which consists of the correction of the free surface computations by elements, to take account of the tidal flats (keyword OPTION FOR THE TREATMENT OF TIDAL FLATS = 1, default value). More information can be found in [G2] p. 41.

In order to ensure that water depths remain positive over the entire study domain (particularly given the presence of tidal flats), an innovation, introduced from TELEMAC version 6.0 and above, was used. This consists of taking the combination of the following four keywords: no upwind for SUPG (SUPG OPTION = 0; 0), total mass-lumping for depth (keyword MASS-LUMPING ON H = 1.), correction of velocities at the points with imposed depth where the continuity equation has not been solved (keyword CONTINUITY CORRECTION = YES) and a treatment to suppress negative depths by a limitation of fluxes (keyword TREATMENT OF NEGATIVE DEPTHS = 2).

3.5.9 Calibration / Validation

The calibration parameter is the Strickler coefficient Ks ($m^{1/3}/s$), representing the energy dissipation by bottom friction. The best fit is obtained for Ks_{West} = 35 $m^{1/3}/s$ over the western part of the domain area and Ks_{East} = 30 $m^{1/3}/s$ over the eastern part. Comparisons of tidal range and tidal current are presented below.

The domain separation for bottom friction is based on past experience of comparison between model simulation and measurements available in the English waters. Unfortunately, measurements are not available for the present study but the proposed domain separation for bottom friction is thought as the best option.

Given the complex feature of the bathymetry and the geology with strong and irregular spatial variations over the whole domain, the variation of the bottom friction is not based on seabed properties. That is why the eastern / western separation is rather schematic without accounting for seabed characteristics. It is acknowledged that it could be further refined with complementary measurement data over various locations.

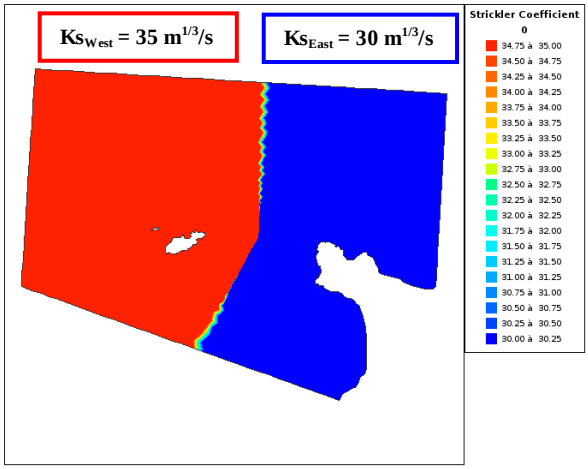

Figure A7: Spatial variation of the Strickler coefficient over the study area

3.5.9.1 Model calibration - Tidal current

First, model results are compared to EDF DPIH ADCP measurements to set the most appropriate Strickler coefficient Ks to represent bed frictions over the eastern part of the domain area. Both tidal flow intensity and direction are examined. The best fit is obtained for Ks_{East} = 30 $m^{1/3}/s$ over the eastern part of the domain area.

As stated in § 3.4, two ADCPs were deployed off the French coast on the 31st July 2009 for around 6.5 months by EDF DPIH (see Table A4). Three tidal cycles were made available in order to provide calibration data for the purpose of the present study. They correspond to a mean neap tide (13/10/2009 – tidal coefficient: 45), a mean spring tide (17/10/2009 – tidal coefficient: 95) and a stronger spring tide (01/02/2010 – tidal coefficient: 112). The numerical model simulated these three periods starting with an initial 2-day spin-up period to set up the model.

At ADCP1 location, the combination of Ks_{West} = 35 $m^{1/3}/s$ and Ks_{East} = 30 $m^{1/3}/s$ leads to excellent agreement between simulation and measurements for tidal speed intensities and directions. At ADCP 2 location, we can observe a slight overestimation in the numerical model, especially during ebb tide. Indeed, the ebb / flood dissymmetry is clearly observable from ADCP2 measurement with a peak current speed reduction of roughly 25% from flood to ebb tide. At both ADCP locations, there is good agreement concerning the direction. Flood and ebb tidal directions are diametrically opposed along the North - South axis. During slack tide, measured current directions are changing very quickly and rather chaotically (high variations of current directions over the water column). Due to the quality of the bathymetric data (lead sounding-weight measurements realised in 1922) and the more complex features of the sea bed in the ADCP2 zone, it is preferable that model calibration be based on ADCP1. Consequently, only comparisons to ADCP1 measurements will be quantified and ADCP2 measurement will be analysed qualitatively.

The ADCP measurements and modelled current speeds are 30 min out of phase at both locations. This phase shift has not been observed for tidal surface elevation. An error in the time reference for ADCP measurements or a phase shift in the tidal current forcing may lead to such differences.

Apart from the phase shift, quality indices (therefore calculated from synchronized time-series: the modelled velocity time-series were shifted so that they are in phase with the measurements to allow an appropriate quantification of error estimates) show very good agreement between model outputs and measurements with a mean error below 5% (see Appendix G1 for more information about calculated quality indices).

The non dimensional bias of current speeds varies from -0.03 to 0.00 for the three study tide cycles when the modelled bed friction is set to Ks_{East} = 30 $m^{1/3}/s$, *i. e.* over the eastern part of the domain area. The RMS error of current speeds remains relatively high (up to 0.31 m/s for Ks_{East} = 30 $m^{1/3}/s$), but this can be explained by the nature of the measured tidal speeds. The signal is rather noisy due to the turbulent nature of the flow. Besides, the model only accounts for the tidal forcing, whereas on-site measurements capture wind, wave and atmospheric pressure effects on currents.

For Ks_{East} = 30 $m^{1/3}/s$ at ADCP1 location, the non dimensional bias of tidal directions varies from -0.03 to 0.01 (*i.e.* below 5%) for the three study tide cycles. The corresponding non dimensional RMS error of tidal directions appears to be high with values ranging from 0.10 to 0.26. However eliminating the turn of the tide periods (when measured current directions are changing very quickly and rather chaotically) from the analysis reduces the non dimensional RMS error to values ranging from 0.04 to 0.06 for the three study tide cycles. The non dimensional bias then equals -0.01 for the three tide cycles.

For Ks_{East} = 25 $m^{1/3}/s$, velocities are constantly underestimated compared to ADCP1 measurements with a negative bias of approximately 10%. At ADCP2 locations, peak velocities during the flood are still underestimated but there is a good agreement with measurements during the ebb tide.

For Ks_{East} = 35 $m^{1/3}/s$, velocities are constantly overestimated. At ADCP1 location, the bias is always positive and at ADCP2 location, peak velocities exceed the measurements by, at least, 0.5 m/s during spring tides (see Figure A12 and Figure A13).

Quality indice	Ks_{East} = 25 $m^{1/3}/s$ Ks_{West} = 35 $m^{1/3}/s$	Ks_{East} = 30 $m^{1/3}/s$ Ks_{West} = 35 $m^{1/3}/s$	Ks_{East} = 35 $m^{1/3}/s$ Ks_{West} = 35 $m^{1/3}/s$
Bias or mean error	-0.12	-0.02	0.06
Non dimensional bias	-0.09	-0.01	0.04
RMS error	0.26	0.16	0.15
Non dimensional RMS error	0.19	0.11	0.11
Pearson correlation coefficient	0.95	0.98	0.99

Table A6: Quality indices of computed tidal velocity intensities compared to ADCP1 raw measurements during a mean neap tide (13/10/2009) for Ks_{East} = 25, 30 and 35 $m^{1/3}/s$ and Ks_{West} = 35 $m^{1/3}/s$

Quality indice	Ks_{East} = 25 $m^{1/3}/s$ Ks_{West} = 35 $m^{1/3}/s$	Ks_{East} = 30 $m^{1/3}/s$ Ks_{West} = 35 $m^{1/3}/s$	Ks_{East} = 35 $m^{1/3}/s$ Ks_{West} = 35 $m^{1/3}/s$
Bias or mean error	-0.22	0.00	0.18
Non dimensional bias	-0.10	0.00	0.08
RMS error	0.35	0.19	0.29
Non dimensional RMS error	0.15	0.08	0.12
Pearson correlation coefficient	0.98	0.98	0.98

Table A7: Quality indices of computed tidal velocity intensities compared to ADCP1 raw measurements during a mean spring tide (17/10/2009) for Ks_{East} = 25, 30 and 35 $m^{1/3}/s$ and Ks_{West} = 35 $m^{1/3}/s$

Quality indice	Ks_{East} = 25 $m^{1/3}/s$ Ks_{West} = 35 $m^{1/3}/s$	Ks_{East} = 30 $m^{1/3}/s$ Ks_{West} = 35 $m^{1/3}/s$	Ks_{East} = 35 $m^{1/3}/s$ Ks_{West} = 35 $m^{1/3}/s$
Bias or mean error	-0.32	-0.08	0.10
Non dimensional bias	-0.13	-0.03	0.04
RMS error	0.50	0.31	0.31
Non dimensional RMS error	0.20	0.12	0.12
Pearson correlation coefficient	0.95	0.97	0.97

Table A8: Quality indices of computed tidal velocity intensities compared to ADCP1 raw measurements during a stronger spring tide (01/02/2009) for Ks_{East} = 25, 30 and 35 $m^{1/3}/s$ and Ks_{West} = 35 $m^{1/3}/s$

From Figure A9 to Figure A13, model outputs for different values of Ks and ADCP measurements are compared during tides representative of a mean neap tide, a mean spring tide and a stronger mean spring tide (tidal coefficient of 112):

- in blue: ADCP measurements,
- in green: model outputs for Ks_{East} = 25 $m^{1/3}/s$ & Ks_{West} = 35 $m^{1/3}/s$,
- in red: model outputs for Ks_{East} = 30 $m^{1/3}/s$ & Ks_{West} = 35 $m^{1/3}/s$,
- in purple: model outputs for Ks_{East} = 35 $m^{1/3}/s$ & Ks_{West} = 35 $m^{1/3}/s$.

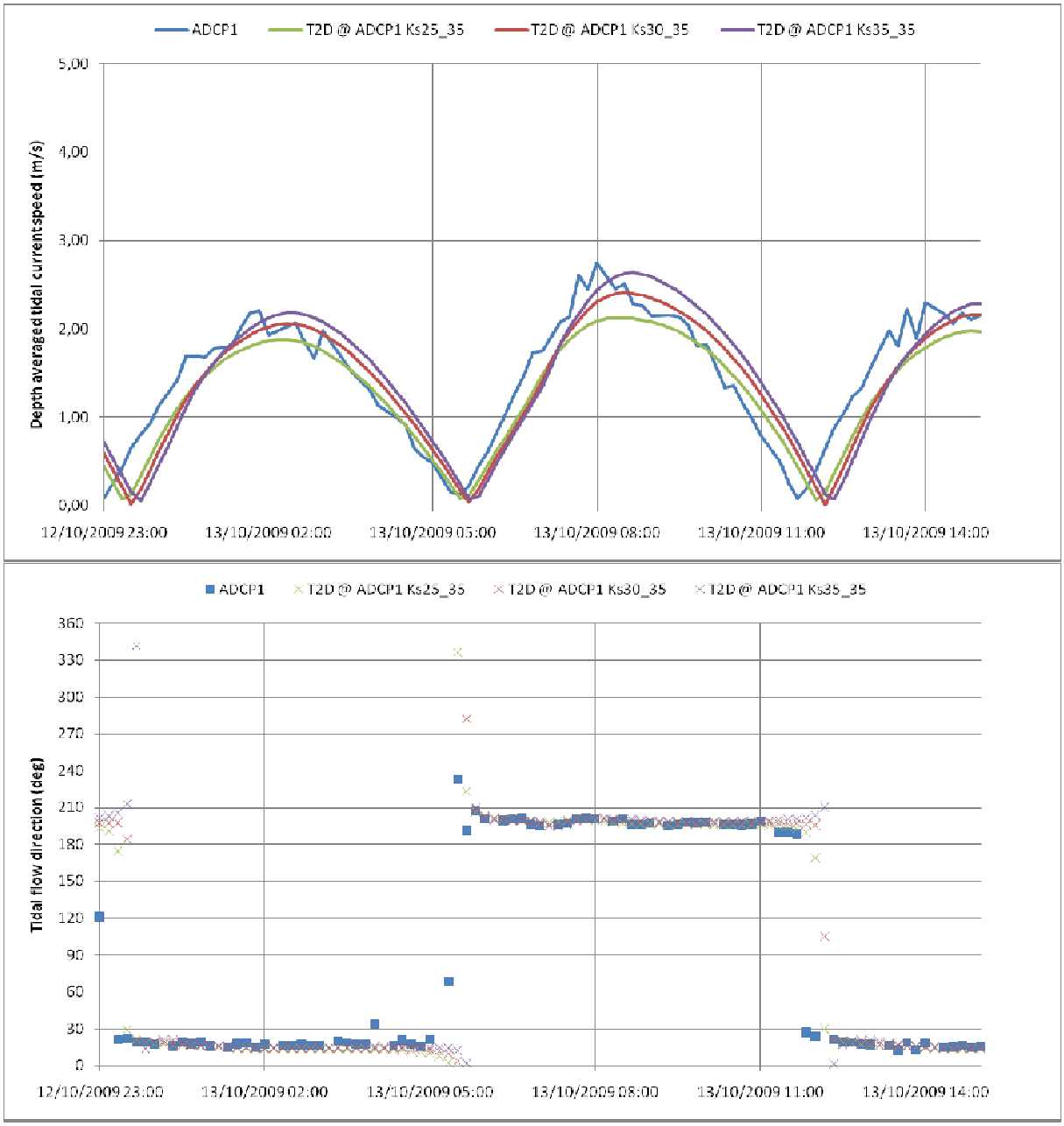

Figure A8: Upper panel: Depth averaged tidal current speed (m/s); Lower panel: Depth averaged tidal current direction (degrees, from North, clockwise). Tide representative of a mean neap tide at ADCP1 location.

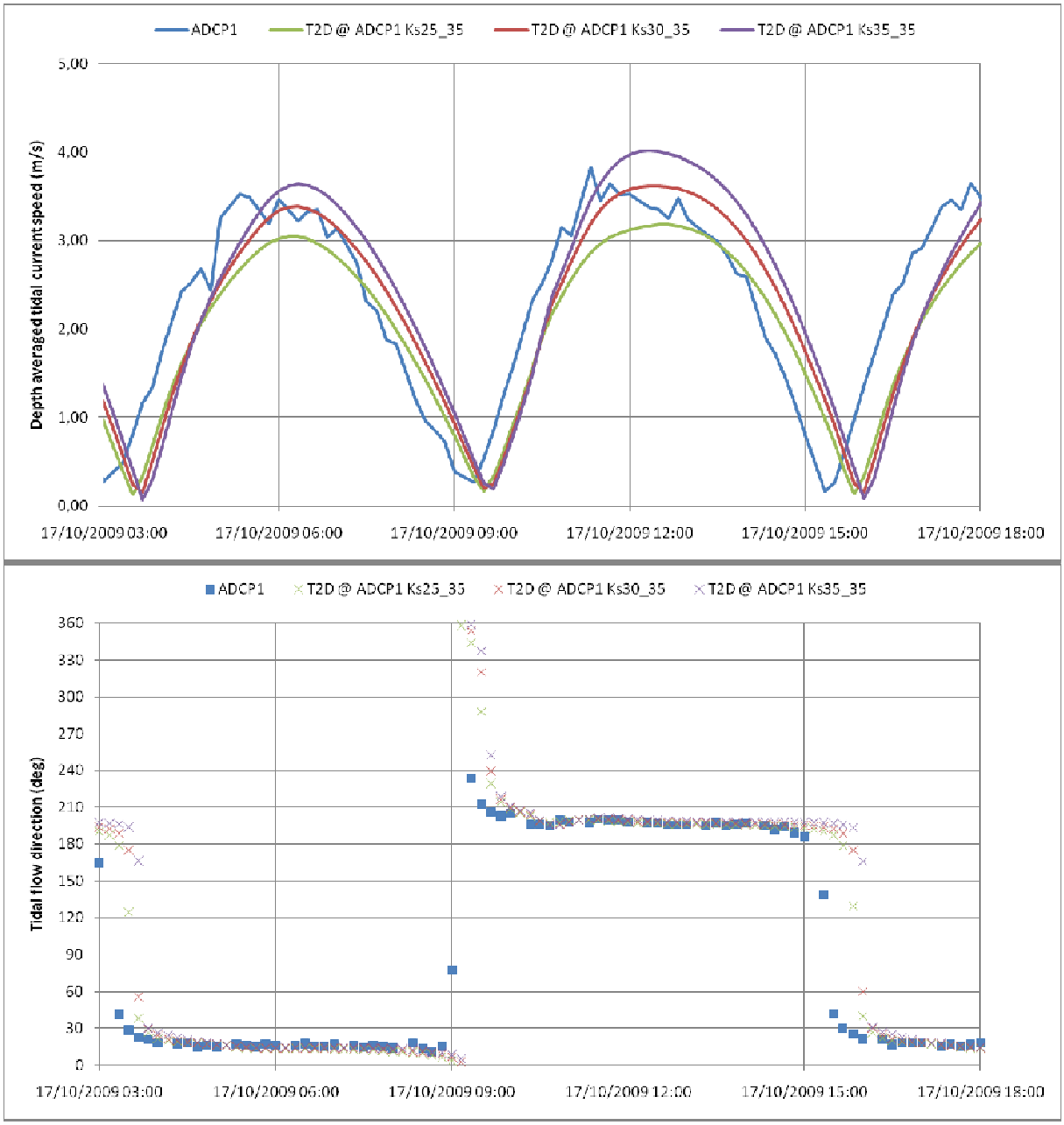

Figure A9: Upper panel: Depth averaged tidal current speed (m/s); Lower panel: Depth averaged tidal current direction (degrees, from North, clockwise). Tide representative of a mean spring tide at ADCP1 location.

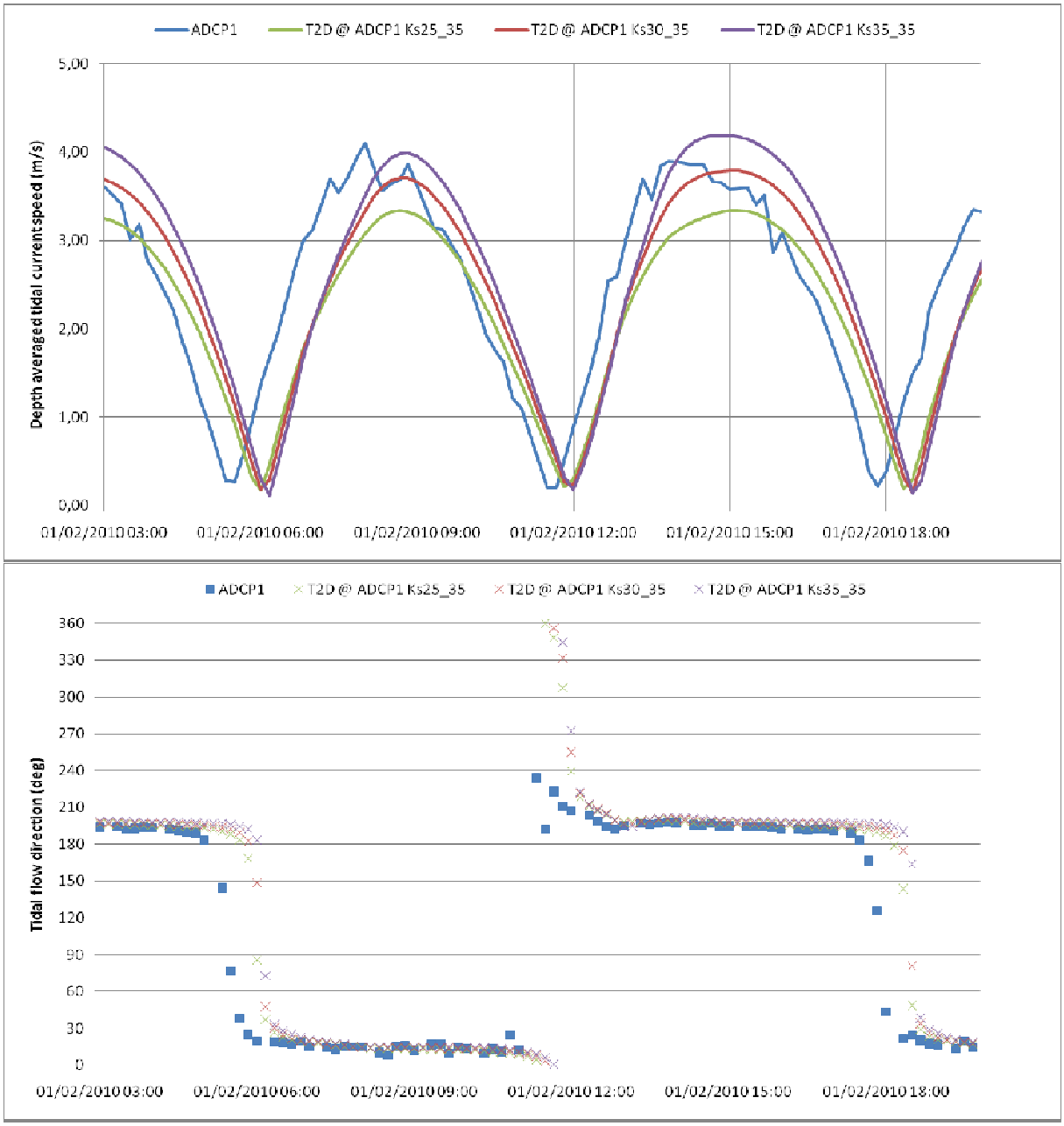

Figure A10: Upper panel: Depth averaged tidal current speed (m/s); Lower panel: Depth averaged tidal current direction (degrees, from North, clockwise). Tide representative of a spring tide (tidal coefficient of 112) at ADCP1 location.

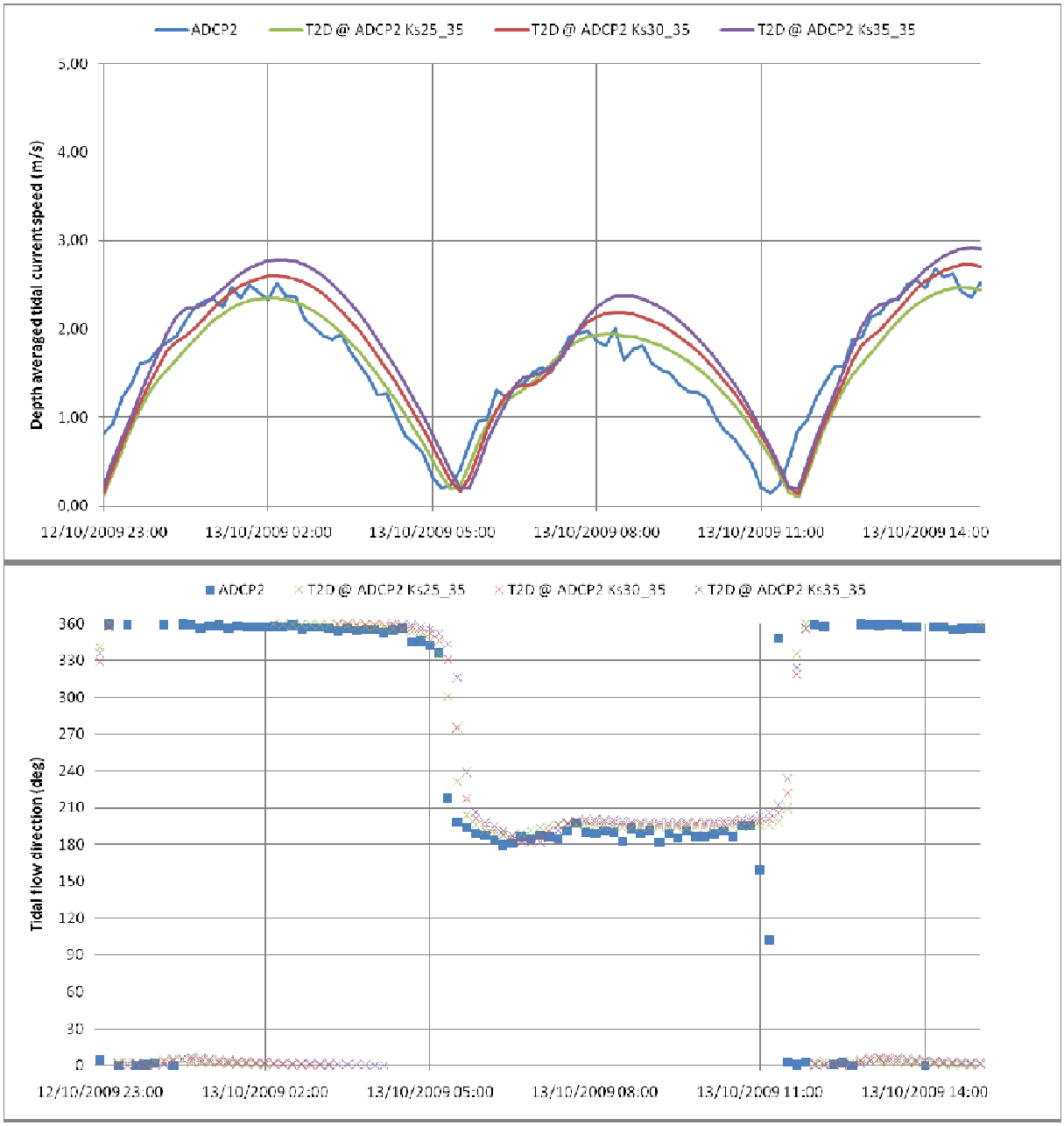

Figure A11: Upper panel: Depth averaged tidal current speed (m/s); Lower panel: Tidal current direction (degrees, from North, clockwise). Tide representative of a mean neap tide at ADCP2 location.

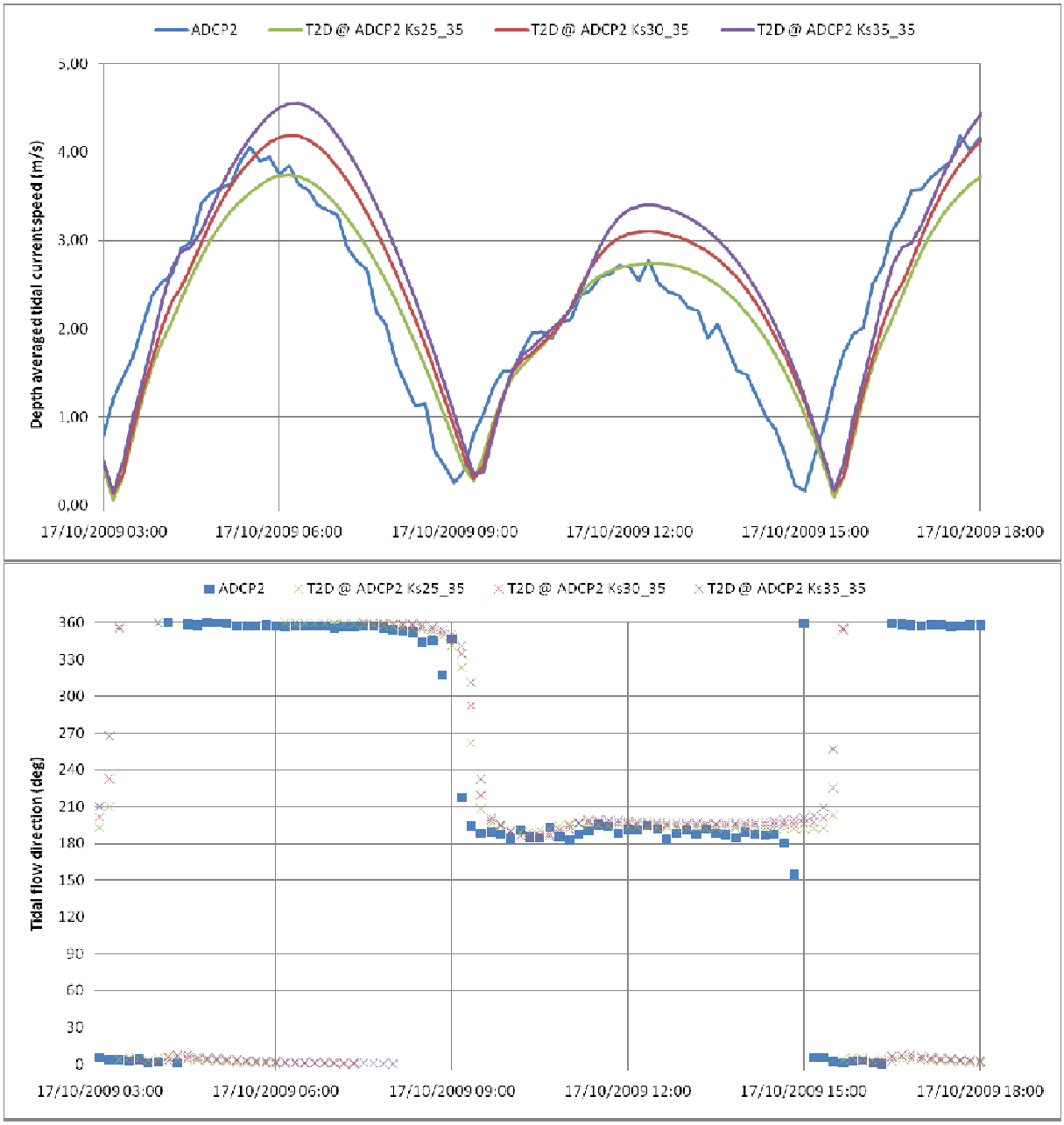

Figure A12: Upper panel: Depth averaged tidal current speed (m/s); Lower panel: Depth averaged tidal current direction (degrees, from North, clockwise). Tide representative of a mean spring tide at ADCP2 location.

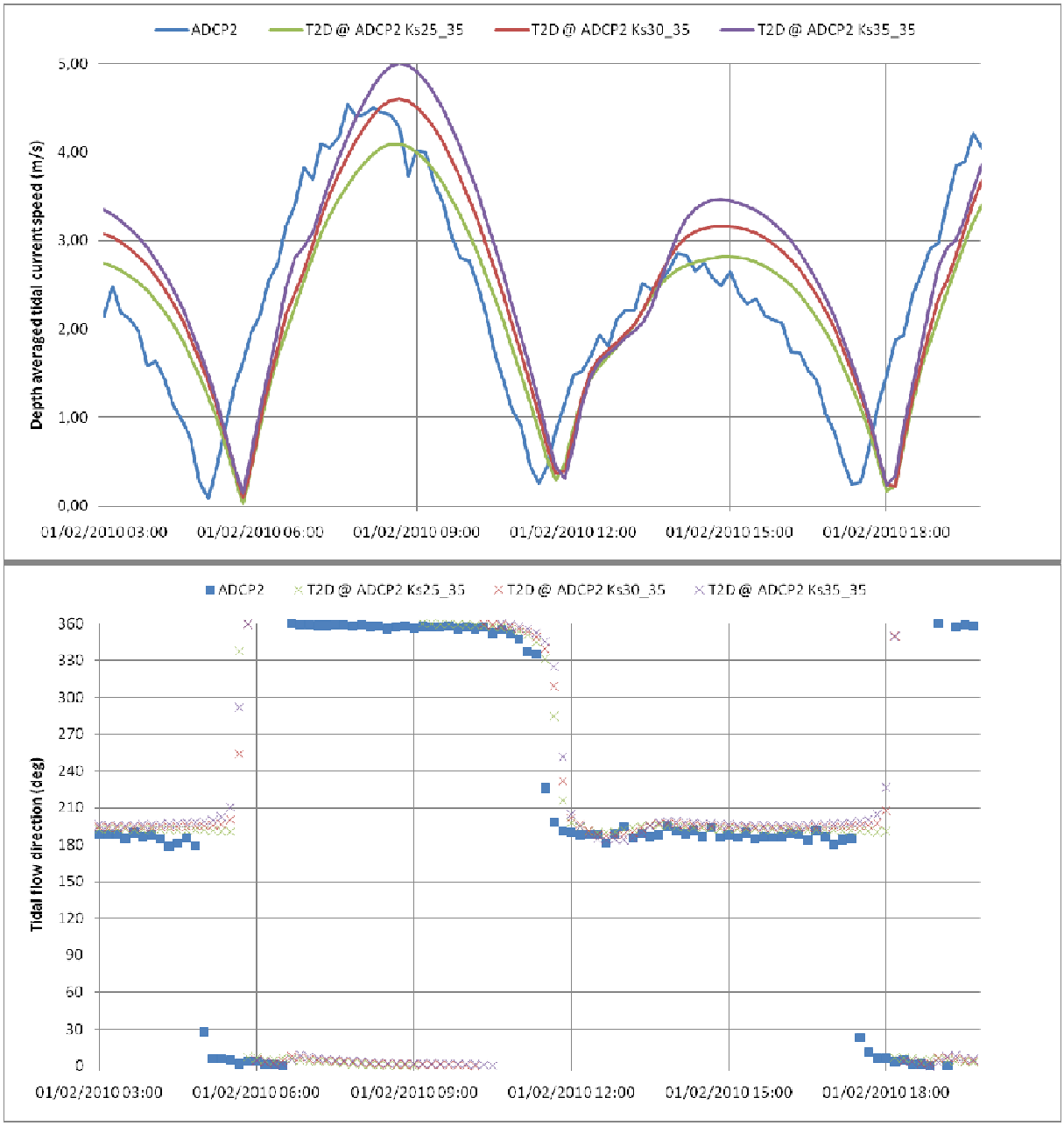

Figure A13: Upper panel: Depth averaged tidal current speed (m/s); Lower panel: Depth averaged tidal current direction (degrees, from North, clockwise). Tide representative of a spring tide (tidal coefficient of 112) at ADCP2 location.

3.5.9.2 Model validation - tidal range

The tidal range is simulated at the reference ports of Goury and Braye. The Telemac-2D results are compared to the SHOM data throughout the month of July 2010 (see Figure A14 to Figure A17). Model outputs are extracted every 10 min for Ks_{West} = 35 $m^{1/3}/s$ over the western part of the domain area and Ks_{East} = 30 $m^{1/3}/s$ over the eastern part. SHOM free surface elevation reference values are extracted from the SHOM website (www.shom.fr). They correspond to hourly predictions from harmonic analysis of tidal gauge measurements, so that they are not influenced by meteorological conditions.

The computed surface elevation compares well with SHOM tidal gauges in terms of tidal range. At Goury, the mean error (bias) is of 0.02 m, the RMS error equals to 0.18 m and the correlation coefficient is of 0.995. At Braye, quality indices get slightly better with a mean error equals to 0.00 m, a RMS error of 0.12 m and a correlation coefficient of 0.998.

The standard non dimensional bias and scatter index are not used as the average of measured values tends to 0. The non dimensionalisation of the bias and the RMS error are done by dividing their value by the tidal range during a mean spring tide at corresponding harbours (cf. Table A2). Resulting non dimensional indicators are as follows:

Quality indice	At Goury	At Braye
Non dimensional bias	0.00	0.00
Non dimensional RMS error	0.03	0.02

Table A9: Non dimensional bias and RMS error of the computed sea surface elevation compared to SHOM data

It should be noted that the numerical model leads to spatial variations of the MSL. Its major feature is an important decrease in the water level off Goury (several decimetres). Figure A18 shows the spatial variation of the computed MSL, calculated as the average of modelled free surface elevations over July 2010, from the initial bathymetry referenced to the MSL. At Braye the computed MSL is 1 cm below the initial MSL whereas at Goury the computed MSL decreases to 28 cm below the initial MSL.

In order to compare the tidal range, from Figure A14 to Figure A17 the free surface elevation is referenced to the computed MSL (*i.e.* the average of modelled free surface elevations over July 2010 at Goury and Braye harbours) for the numerical results and to the initial MSL for SHOM data.

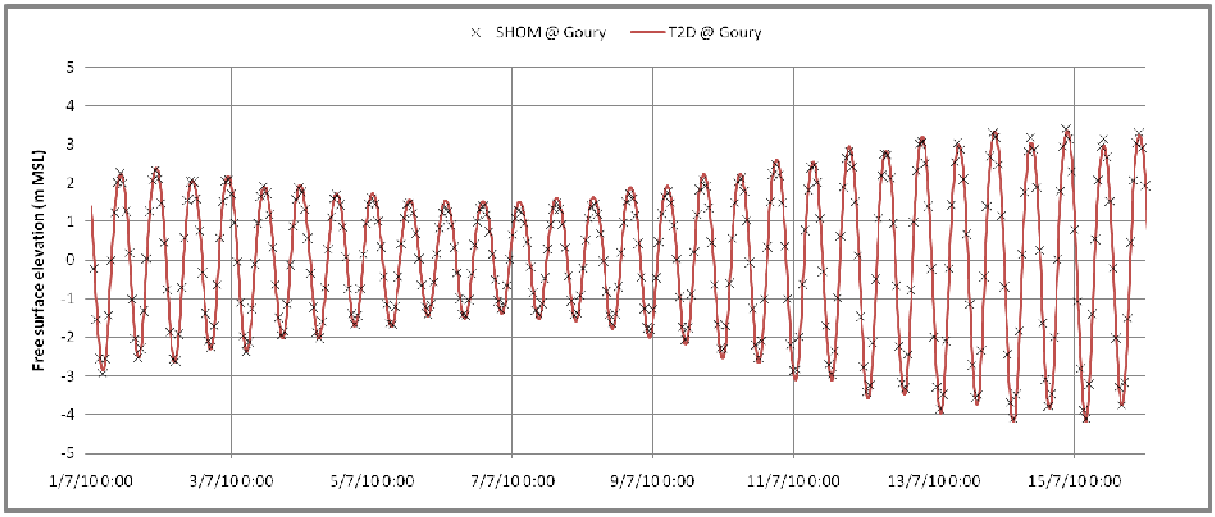

Figure A14: Free surface elevation (m MSL) at Goury (black crosses: SHOM predictions, red curve: numerical results)

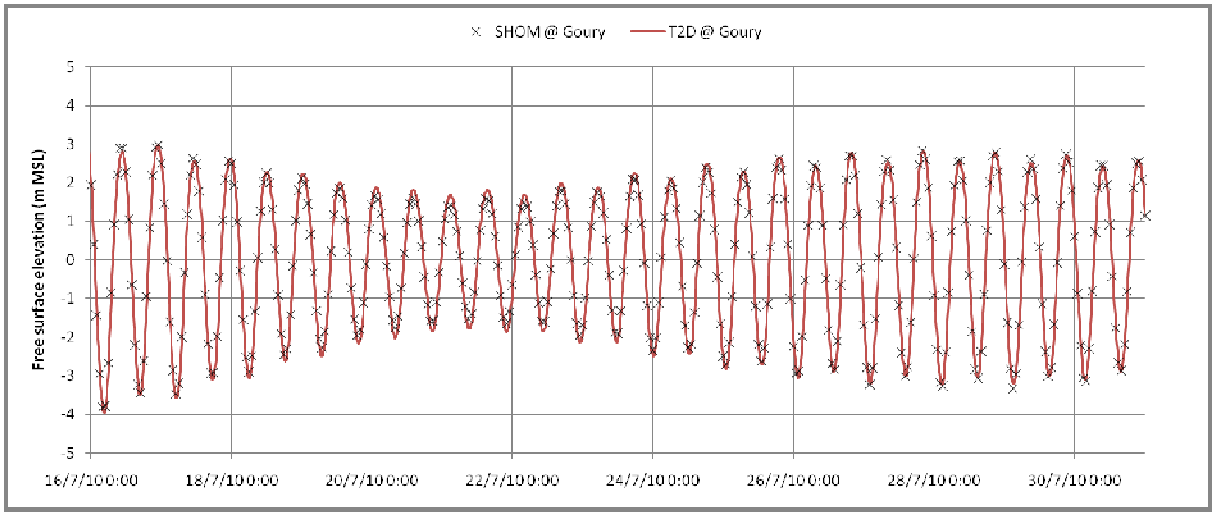

Figure A15: Free surface elevation (m MSL) at Goury (black crosses: SHOM predictions, red curve: numerical results)

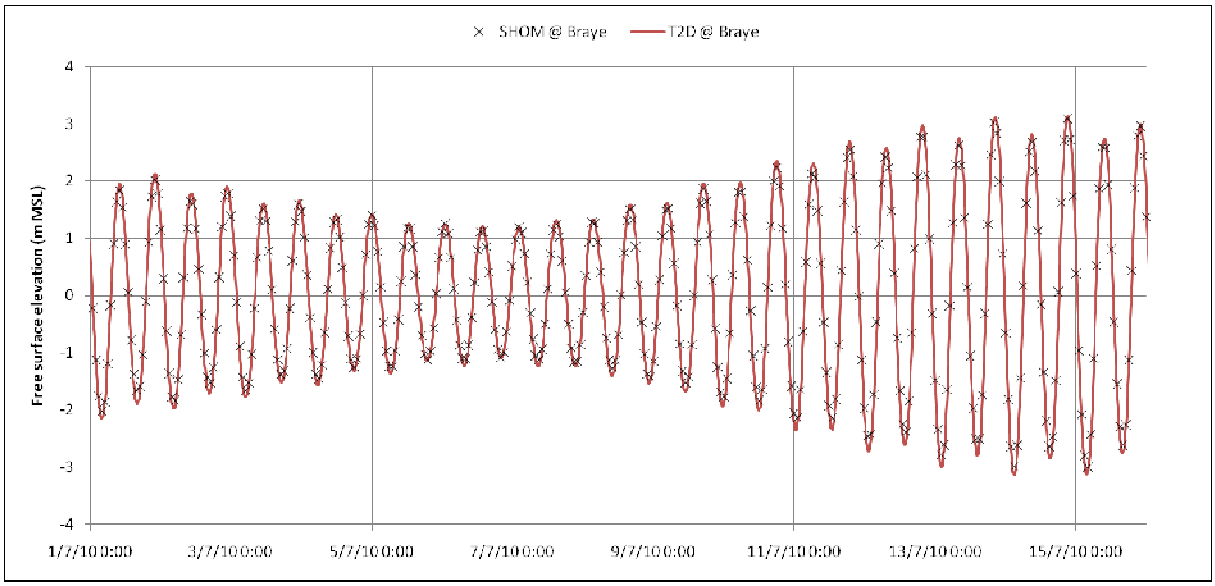

Figure A16: Free surface elevation (m MSL) at Braye (black crosses: SHOM predictions, red curve: numerical results)

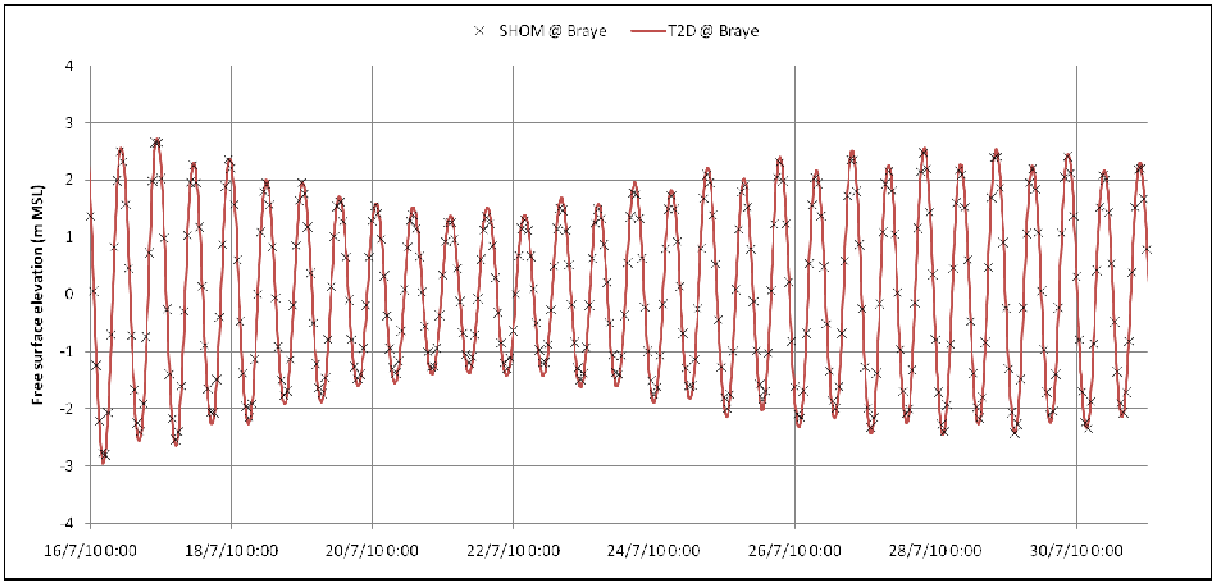

Figure A17: Free surface elevation (m MSL) at Braye (black crosses: SHOM predictions, red curve: numerical results)

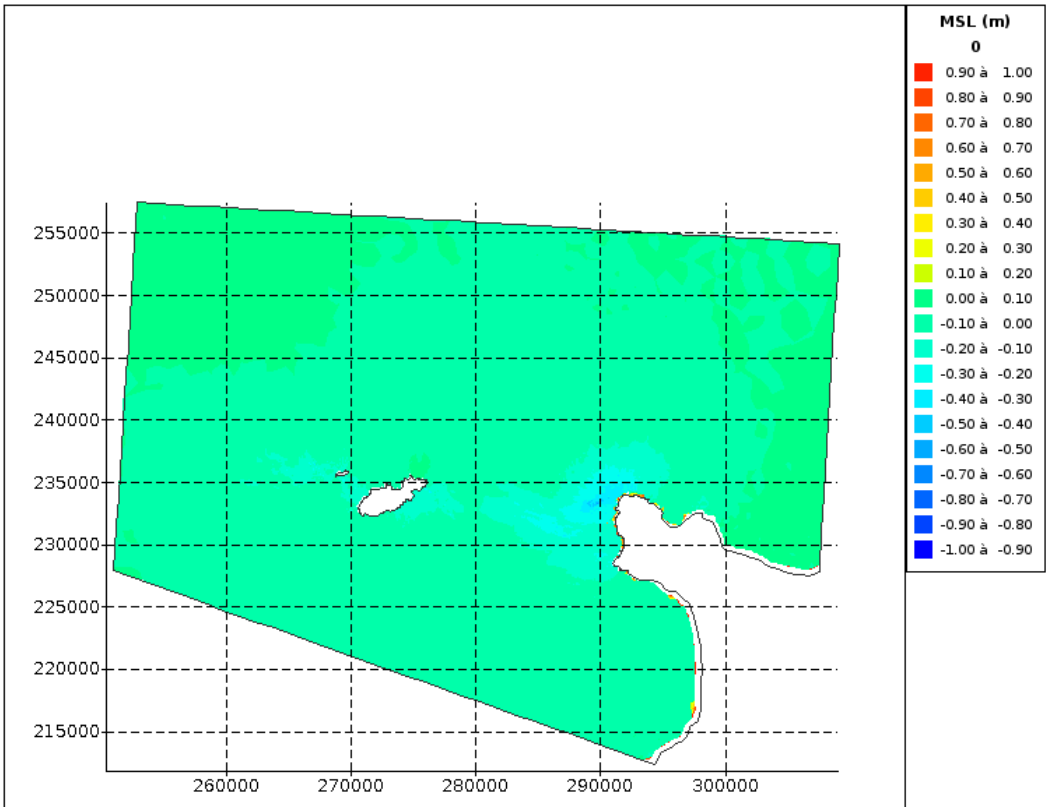

Figure A18: Variation of MSL (m) over the study domain

3.5.9.3 Model validation - ACRE VMADCP measurements

As discussed in § 3.4, VMADCP data are taken into account only to give an order of magnitude of the flow velocities (no quality indices are thus calculated). To this end, ACRE data are averaged over the water column and compared to the TELEMAC-2D results.

Graphical outputs of the model are recorded every 5 min in order to provide sufficient data for qualitative validation (see Figure A19 to Figure A23).

Overall, a good visual agreement is observed between model and measurements. Differences are specifically observed during the third and fourth transects. Slight errors in phase can lead in this case to significant discrepancies, in addition to the constraints of the measurement campaign (vessel speed higher than recorded current speeds, complex bathymetry, tidal flow highly variable in space).

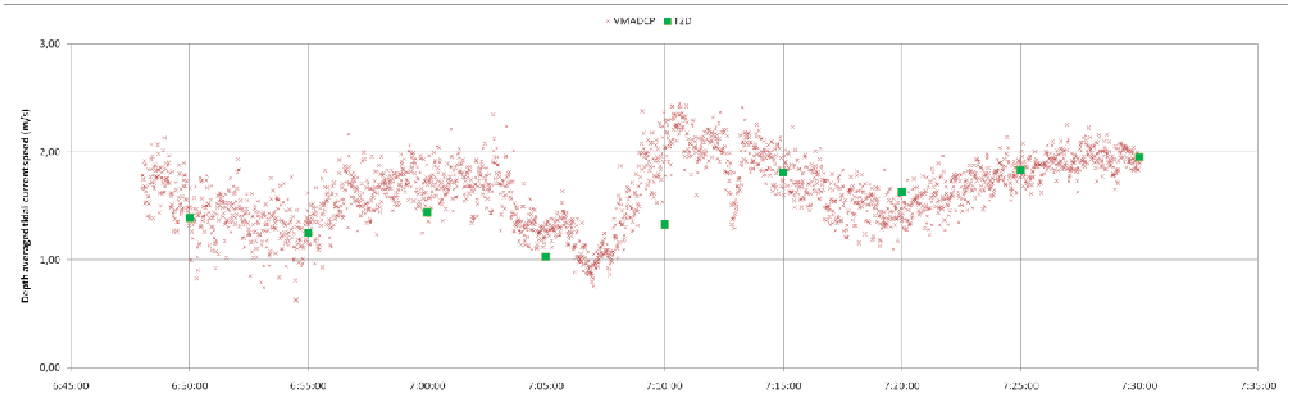

Figure A19: Depth averaged current speeds (m/s) from ACRE VMADCP measurements (red crosses) and model results (green squares) throughout the first ACRE transect.

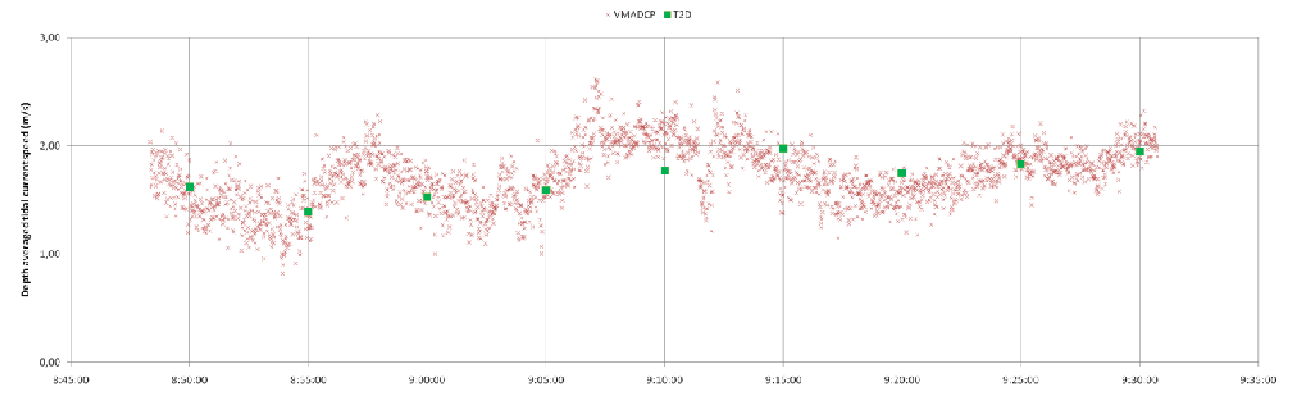

Figure A20: Depth averaged current speeds (m/s) from ACRE VMADCP measurements (red crosses) and model results (green squares) throughout the second ACRE transect.

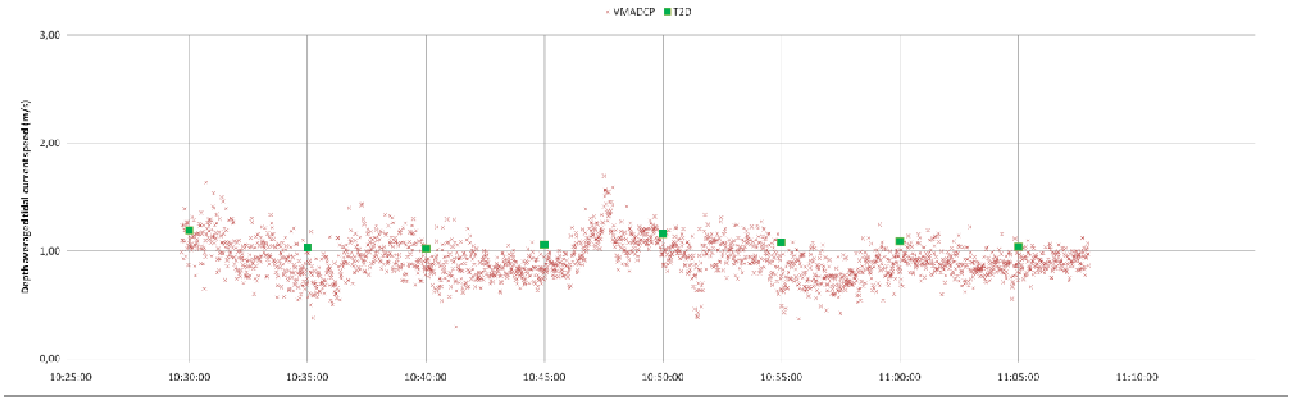

Figure A21: Depth averaged current speeds (m/s) from ACRE VMADCP measurements (red crosses) and model results (green squares) throughout the third ACRE transect.

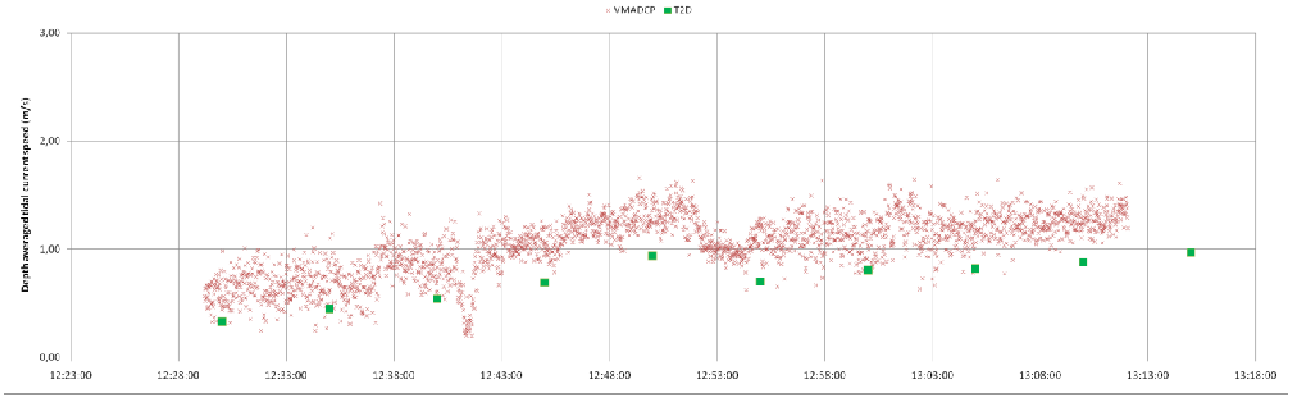

Figure A22: Depth averaged current speeds (m/s) from ACRE VMADCP measurements (red crosses) and model results (green squares) throughout the fourth ACRE transect.

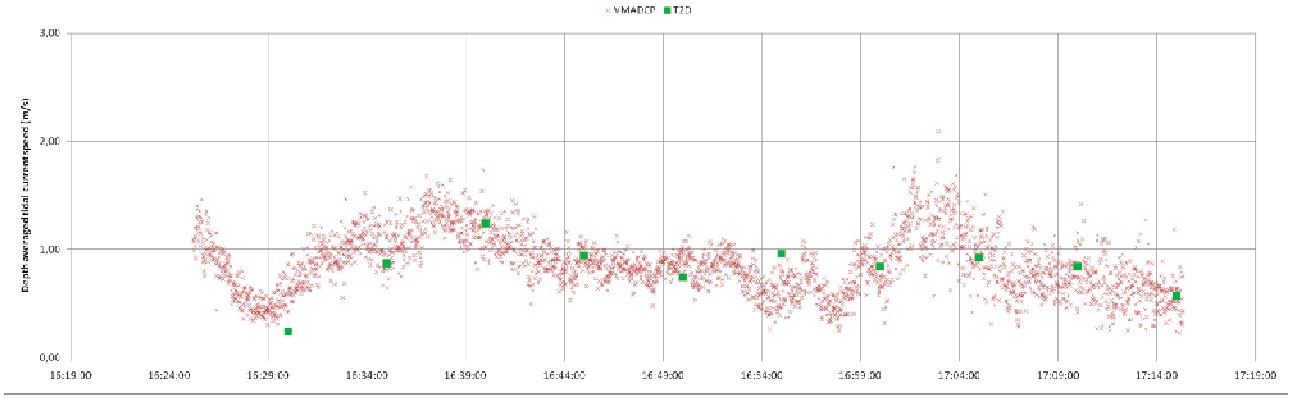

Figure A23: Depth averaged current speeds (m/s) from ACRE VMADCP measurements (red crosses) and model results (green squares) throughout the sixth ACRE transect.

3.5.10 Analysis

The tidal flow conditions are examined in detail during the mean spring tide of 17th July 2009. The figures below show hourly tidal flow patterns with tidal current speeds (m/s) and directions (black vectors on a regular grid) from low water (at 00:10 on 17/10/2009) to next low water (at 12:30 on 17/10/2009):

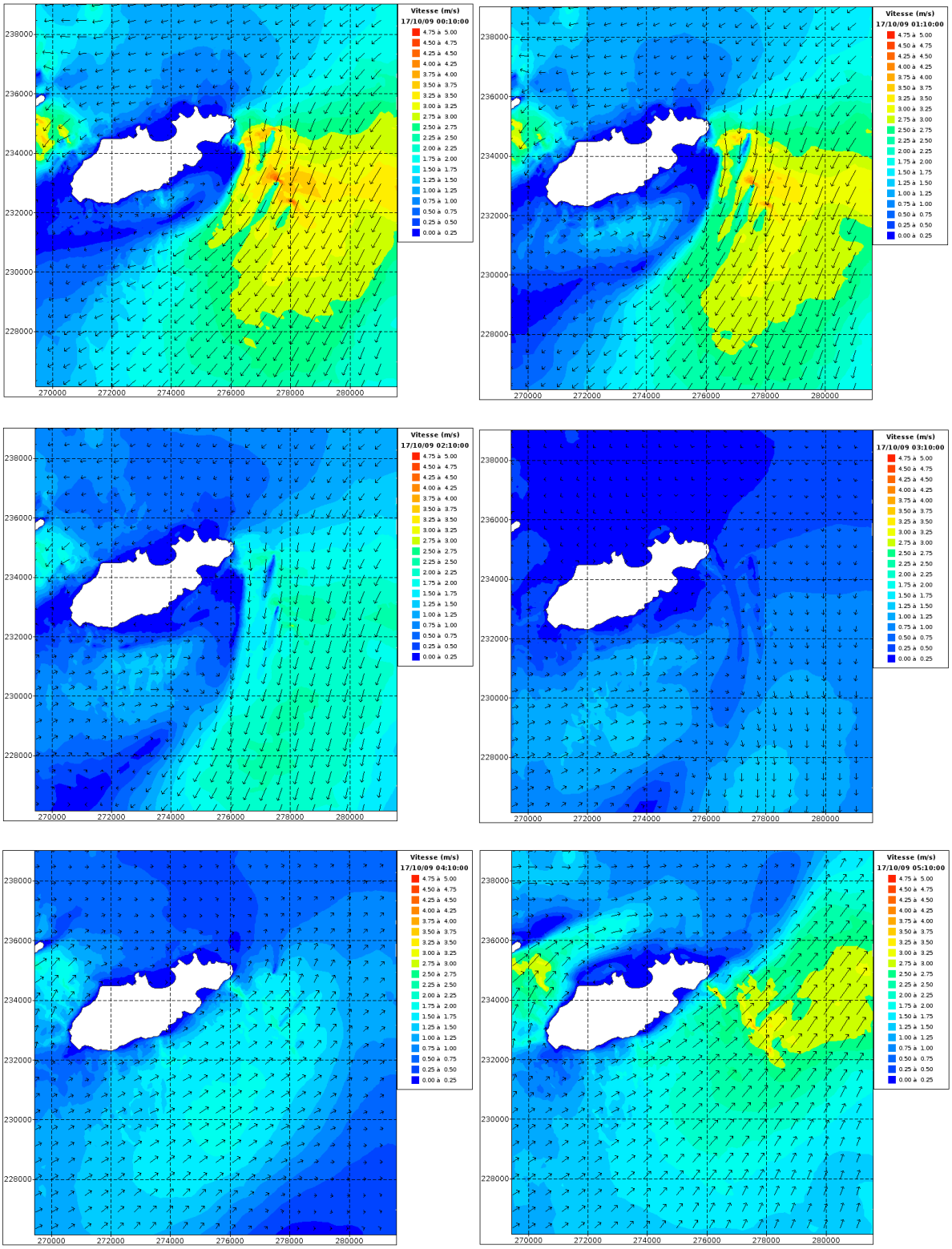

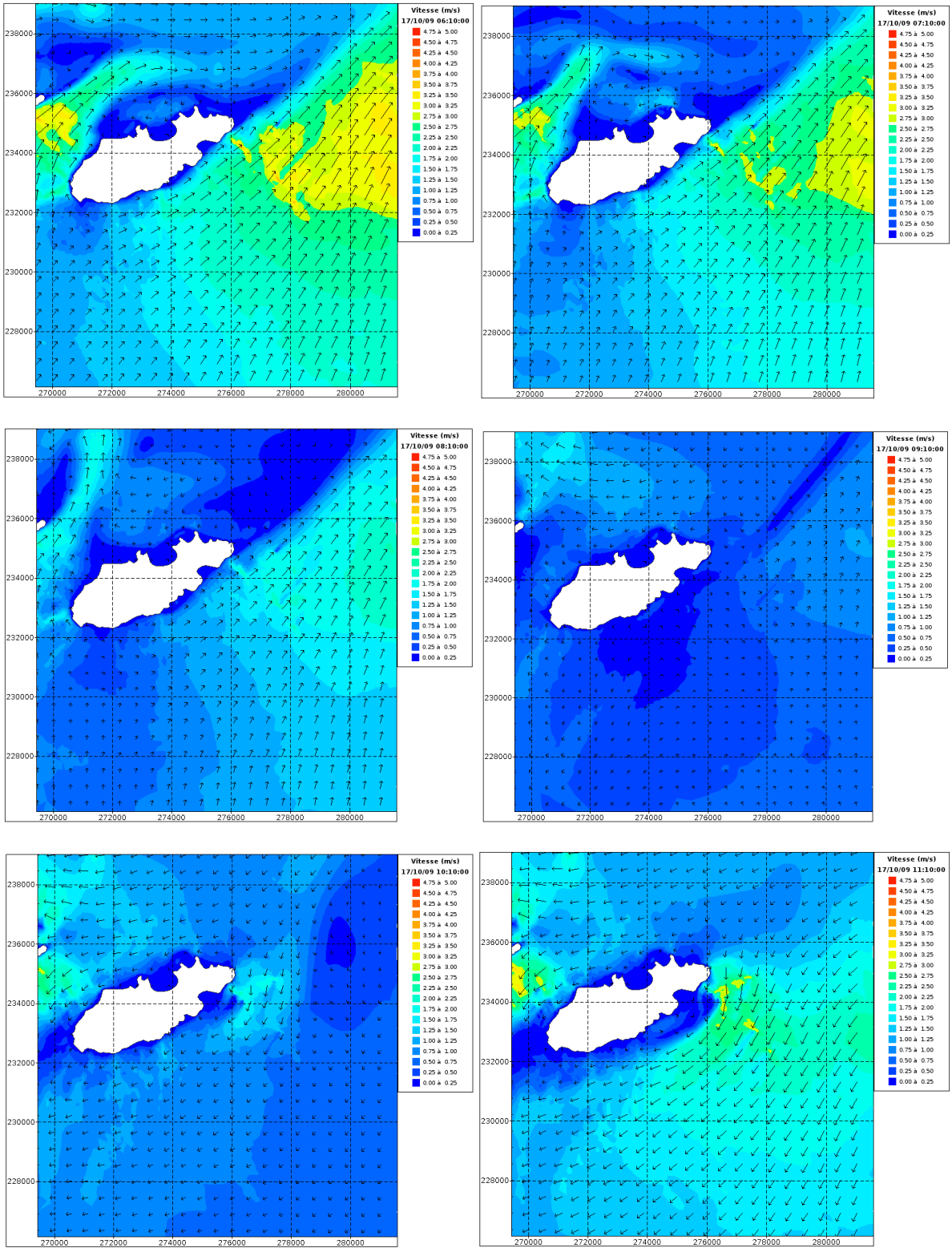
Vitesse (m/s)
17/10/09 06:10:00
17/10/09 07:10:00
17/10/09 08:10:00
17/10/09 09:10:00
17/10/09 10:10:00
17/10/09 11:10:00
4.75 à 5.00
4.50 à 4.75
4.25 à 4.50
4.00 à 4.25
3.75 à 4.00
3.50 à 3.75
3.25 à 3.50
3.00 à 3.25
2.75 à 3.00
2.50 à 2.75
2.25 à 2.50
2.00 à 2.25
1.75 à 2.00
1.50 à 1.75
1.25 à 1.50
1.00 à 1.25
0.75 à 1.00
0.50 à 0.75
0.25 à 0.50
0.00 à 0.25
238000
236000
234000
232000
230000
228000
270000
272000
274000
276000
278000
280000

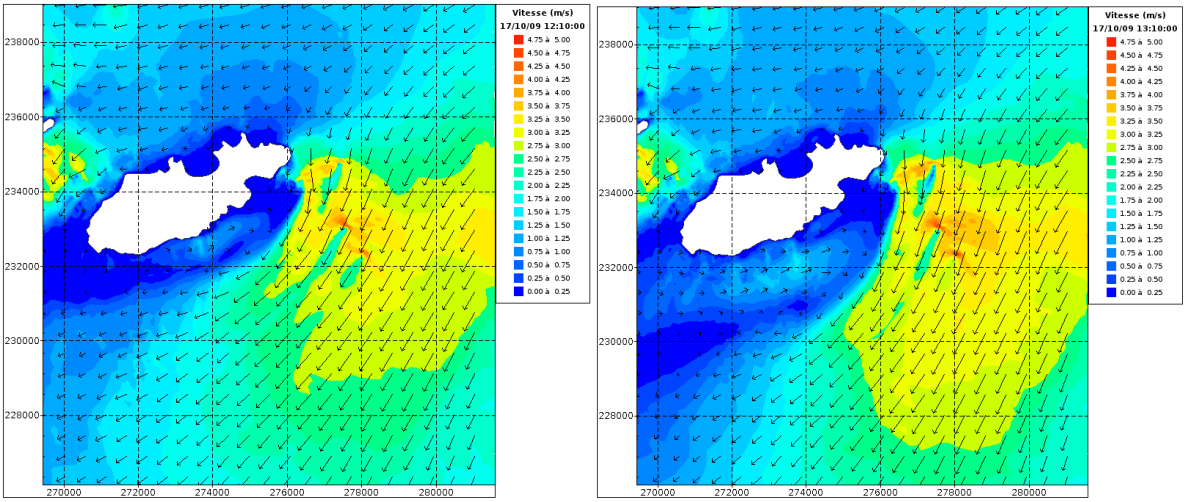

The speed peaks occur close to high waters and low waters, which is characteristic of the progressive tidal wave that occurs in the English Channel. Overall, the flood current flows towards North East and the ebb current flows towards the South West. The strongest tidal currents are observed on the east of Alderney during ebb tide, with tidal speeds reaching roughly 4.5 m/s. During flood tide, maximal speeds can locally exceed 3.5 m/s.

The tidal flow around Alderney is strongly variable in space with a complex flow pattern. The bathymetry in this area is indeed rather irregular, with rocky prominences, banks and fissures (see Figure A24). For example, sharp and high prominences create local obstacles to the flow (as it can be observed during ebb tide on the eastern side of Alderney) or the complex morphology of the bathymetry generates recirculation patterns around Alderney (as it is also mentioned in nautical charts: see Figure A25). Besides, the height of the prominences can be over-estimated because of the use of bathymetric data extracted from nautical charts that originally aim at providing information for navigational safety.

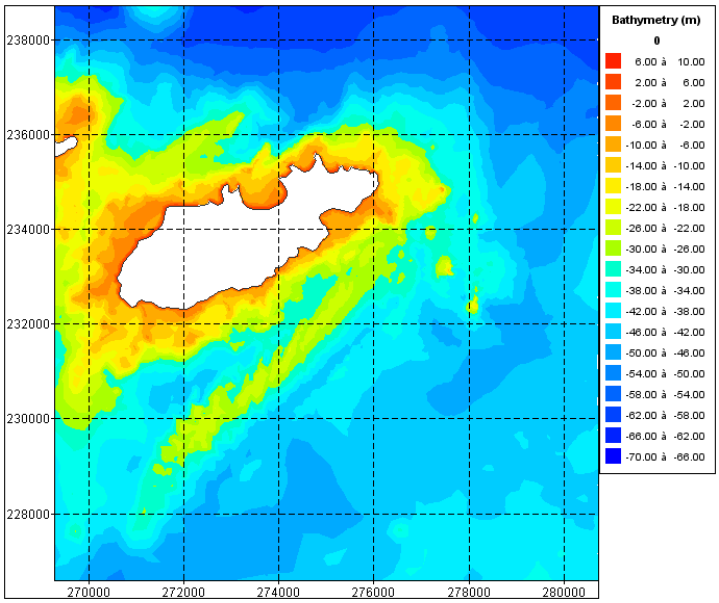

Figure A24: Local bathymetric features around Alderney

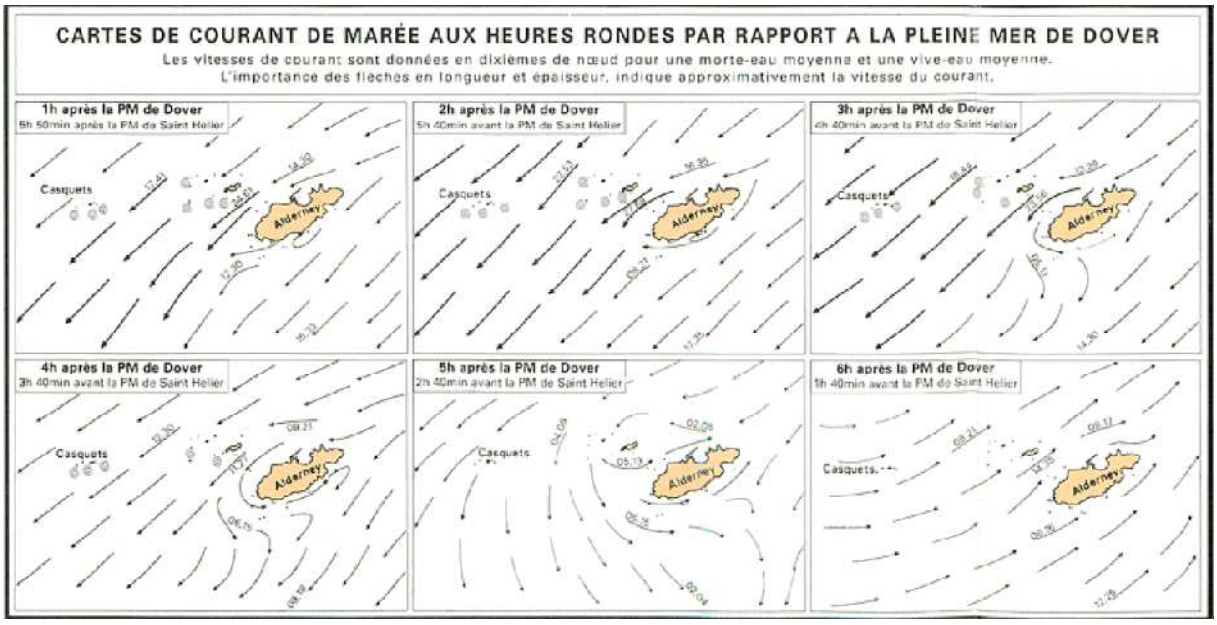

Figure A25: Tidal current fields during the ebb tide given at an hourly time step (time reference: high water at Dover), source: SHOM [A3]

3.6 Uncertainties

The main source of uncertainties regarding the presented results is due to the bathymetric data for the study zone. Apart from the ACRE multi-beam survey, they were obtained from commercially available SHOM or Seazone data (digital bathymetric grids, DTMs, charts). The sounding density of such data is in the order of 20 m to 200 m. SHOM and Seazone charts provide data mainly for navigational safety and can hence display conservative soundings (*i.e.* the sea bed can be over-estimated). Therefore, it does not accurately represent the local features of the sea bed morphology that strongly influence the tidal current patterns. Measurement campaigns for the SHOM digital bathymetric grids were undertaken from 1922 to 1999, with a wide range of devices (from lead sounding-weights to single-beam soundings or even sometimes "unknown").

The numerical errors which are propagated within the TELEMAC-2D model are not quantified at this stage. This extremely complex topic is currently under investigation outside of the PerAWaT project, and may not be available before the end of 2013.

In addition, this study used the TELEMAC-2D modelling software, which solves the Saint-Venant two-dimensional equations based on the shallow-water assumption (shallow waters being, in principle, satisfactory for tide representation).

3.7 Computation time

The TELEMAC-2D computations were carried out on a processor running at 2.33 GHz. The CPU time required for a simulation of 1 day is approximately 1 hour.

3.8 Conclusion

The present study enabled the characterisation of tidal flow conditions in the Alderney Race zone. It was based on numerical modelling at local scale. The numerical model was built with the TELEMAC-2D hydro-informatics software developed at EDF R&D.

Overall, good agreement is found between measurements and simulation results. Calibration was performed against ADCP measurements during three tidal cycles (real tide cycles, tides representative

of a mean neap tide, mean spring tide and a stronger spring tide of tide coefficient of 112). At ADP1 location, the best agreement between model outputs and measurements is found for Ks_{East} = 30 $m^{1/3}/s$ over the eastern part of the domain area. The mean error for tidal current speeds and directions remains below 5% (see § 3.5.9.1). The modelled tidal range was validated throughout the month of July 2010 (making a 31-day validation period) at Goury and Braye harbours. Model outputs match the SHOM predictions with a non dimensional bias equals to 0.00 and a non dimensional RMS error below 5% (see § 3.5.9.2). A qualitative validation of the tidal speeds was performed using ACRE data. A good visual agreement is observed between model and measurements (see § 3.5.9.3). Finally, the tidal flow conditions are examined in detail during the mean spring tide of 17th July 2009 off Alderney. Hourly tidal flow patterns with tidal current speeds and directions are provided (see § 3.5.10).

3.9 References

[A1] Simon B. (2007). La marée océanique côtière. Institut océanographique éditeur, p. 280.

[A2] SHOM (2011). Références altimétriques maritimes – Ports de France métropolitaine et d'outre-mer. Cotes du zéro hydrographique et niveaux caractéristiques de la marée. Edition 2011. Site Internet SHOM: www.shom.fr. [Marine altimetric references (Chart Datums) – SHOM 2011].

[A3] SHOM (2007). Alderney (Aurigny) et le Casquets. Nautical chart n°6934_L.

[A4] SHOM (2006). Des Héaux-de-Bréhat au Cap Lévi. Nautical chart n°6966_L.

[A5] Confidential information disclosure and limited use agreement between EDF and ACRE – May 2012.

[A6] Pairaud I.L., Lyard F., Auclair F., Letellier T., Marsaleix P. (2008). Dynamics of the semi-diurnal and quarter-diurnal internal tides in the Bay of Biscay. Part 1: Barotropic tides. Continental Shelf Research 28 (2008) 1294– 1315.

[A7] Pairaud I.L., Auclair F., Marsaleix P., Lyard F., Pichon A., (2010). Dynamics of the semi-diurnal and quarter-diurnal internal tides in the Bay of Biscay. Part 1: Baroclinic tides. Continental Shelf Research 30 (2010) 253– 269.

4 THE PENTLAND FIRTH

The aim of this study is to provide a precise characterisation of the tidal conditions, *i. e.* the sea levels and tidal currents, in the vicinity of the Pentland Firth where the strongest tidal currents in Europe are found. The TELEMAC-2D software is used to build the free surface flow numerical model covering the study area (see Figure B26 – Geographic location of the Pentland Firth).

The mesh comes from the Tidal Resource Modelling project, which is also commissioned and funded by the Energy Technologies Institute. The boundary conditions come from TPXO data. The bathymetric data come from Seazone and Gebco. The model is calibrated against tidal diamonds from gardline surveys at three different locations in the Pentland Firth.

4.1 Geographic location of the site

The Pentland Firth is located off the north coast of Scotland, in the United Kingdom. The site is well known for its high current velocities.

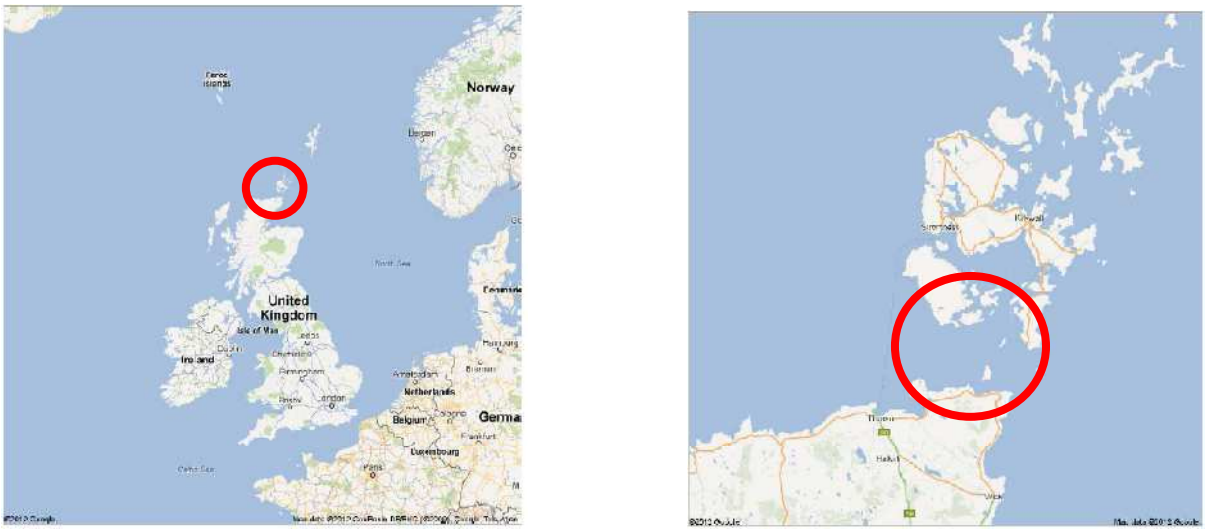

Figure B26 – Geographic location of the Pentland Firth (Google maps).

4.2 Numerical model construction

All modelled flow velocities shown hereafter only take into account the astronomic tide. In particular, no meteorological effects (atmospheric pressure, wind, surge/wane) or wave effects have been considered in the numerical model.

Moreover, in this section, any reference made to the current velocity resulting from the TELEMAC-2D numerical model or measurements data refers to the vertically averaged velocity. The TELEMAC-2D results given are averages in the Reynolds sense, *i. e.* after smoothing out of the turbulence effects.

The sea levels are referenced with respect to MSL (Mean Sea Level).

4.2.1 Code version

The TELEMAC-2D version used in this study is version 6.2, which will be available in open source in August 2012.

4.2.2 Definition of the domain area

The domain covers an area extending approximately 1000 km from North to South and 1000 km from West to East. Its extent can be seen below. More information can be found in [B1].

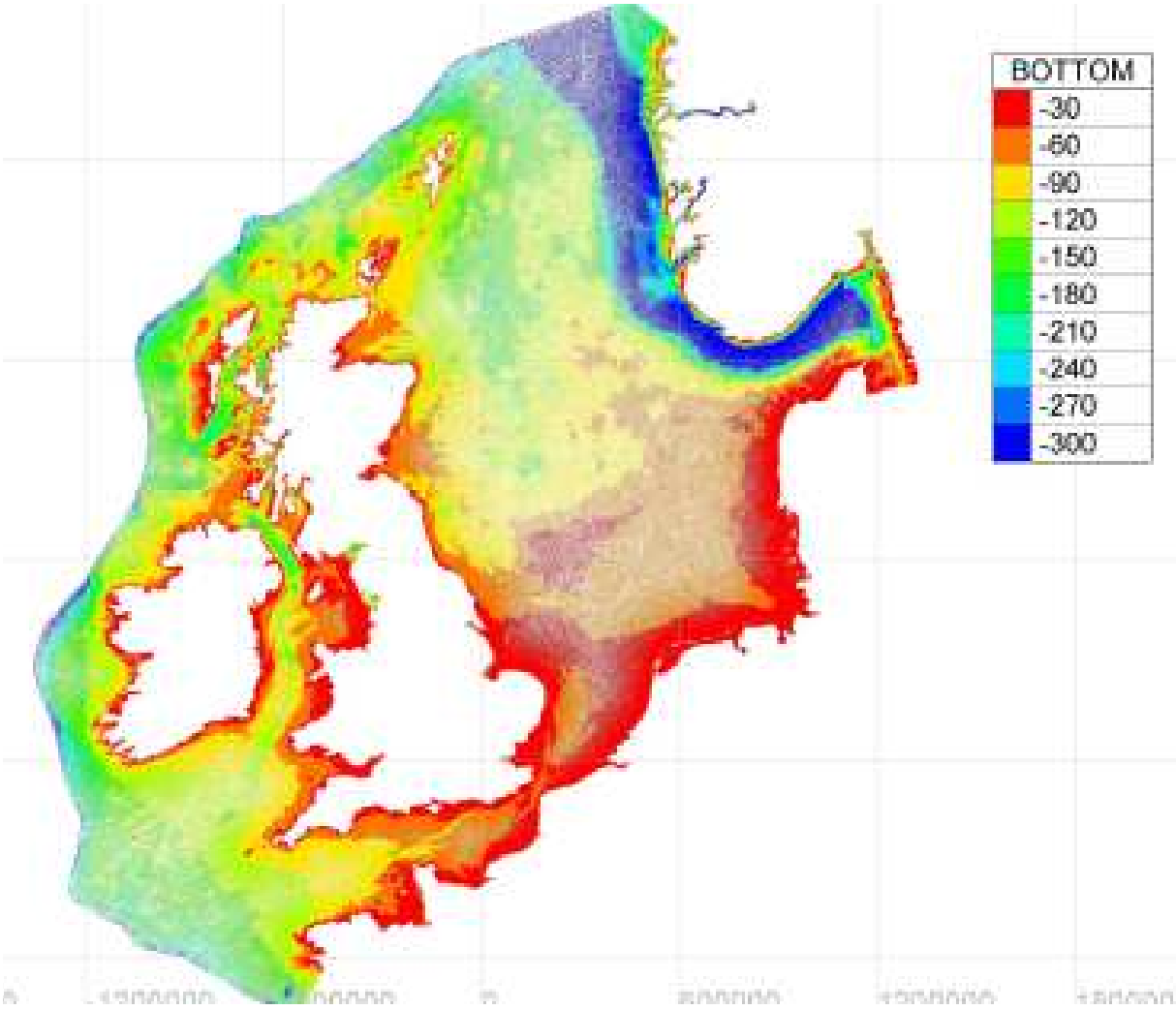

Figure B27 – Model coverage and bathymetric data (Mercator-Telemac projection, MSL).

The hydrodynamic numerical model was built with its horizontal geographic coordinates expressed in Telemac-Mercator projection coordinates.

4.2.3 Bathymetry

The GEBCO_08 Grid (General Bathymetric Chart of the Oceans) freely available data are used for most of the model. They are in MSL.

The GEBCO_08 Grid is a continuous terrain model for ocean and land with a spatial resolution of 30 arc-seconds. The bathymetric portion of the grid has largely been generated from a database of ship-track soundings with interpolation between soundings guided by satellite-derived gravity data. However, in areas where they improve on the existing GEBCO_08 grid, data sets generated by other methods have been included. [B2]

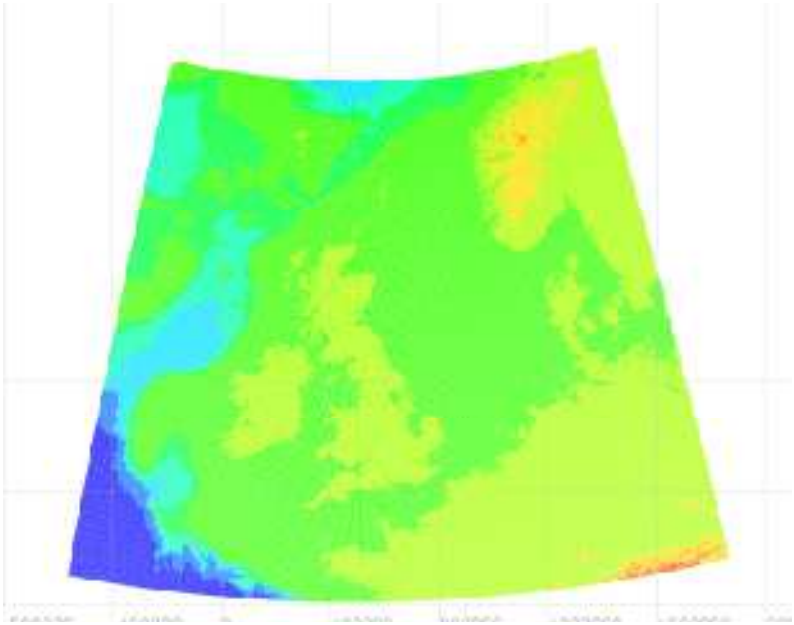

Figure B28 – GEBCO data coverage (Lat Long coordinates)

Locally, around the Pentland Firth, several Seazone data sets were used. These data are subject to a licence bought by the University of Oxford in the framework of the PerAWaT project for both the Oxford and the EDF use (www.seazone.com). These data sets were provided in the form of ASCII files. They were converted into xyz-ASCII files and the header characters were removed in order for the file to be readable by the mesh generator (Janet v2.6).

First, the Seazone charted grids [B3] help refine the bathymetry. These data are referenced to chart datum. However, the comparison of these refined data to the Gebco MSL data shows that there is no correction required to use the Seazone CD data.

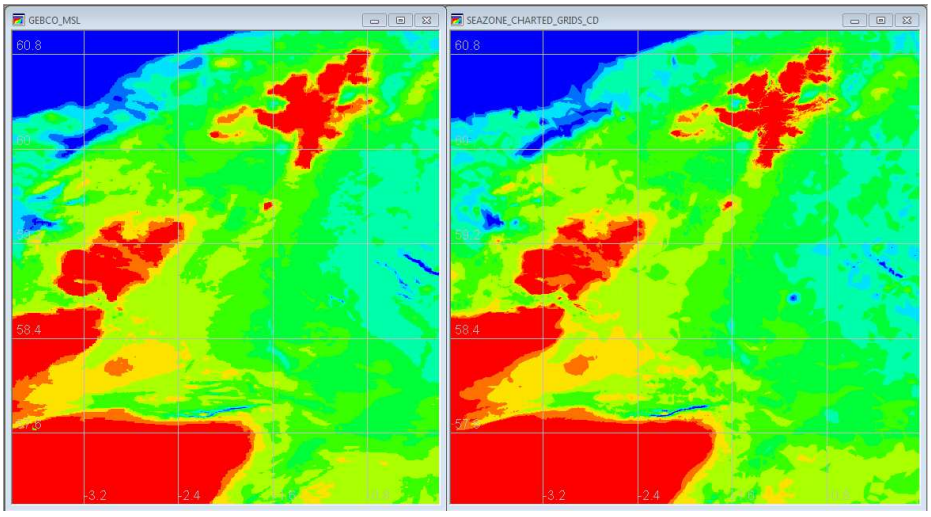

Figure B29 – Comparison between Gebco MSL data and Seazone charted grid CD data. – Mercator-Telemac coordinates.

Second, the higher-resolution Seazone survey grids [B3] allow an extremely detailed description of the bathymetry, as shown on the figure below.

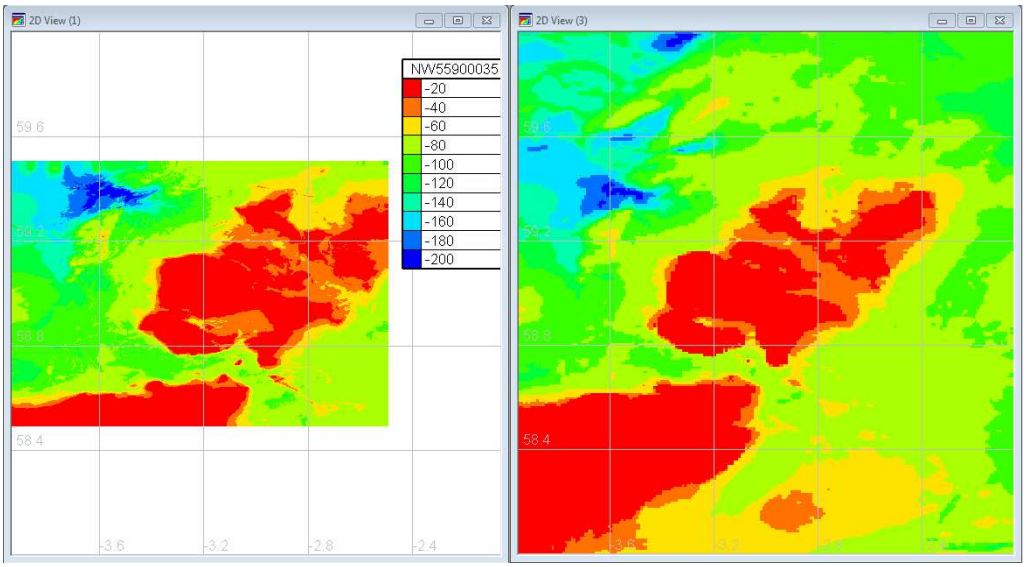

Figure B30 – Comparisons between Seazone survey MSL data and Gebco MSL data. Mercator-Telemac coordinates.

The final bathymetry for the model can be seen in Figure B27.

4.2.4 Mesh

The finite element mesh is derived from the Tidal Resource Modelling Coarse CSM model [B1]. It was refined in the area of interest, as shown below. The refinement was performed with Janet v2.7.8. The final model is made up of 457 771 nodes and 893 404 triangular elements. The mesh size varies progressively from 200 m to 20 km offshore (see figure hereafter).

The strong benefit from using the already existing coarse CSM model mesh was to use the TPXO boundary conditions. HR Wallingford developed and implemented a routine which enables the TPXO boundary conditions to be used for the model. This routine will be freely available in August 2012 in Telemac2D v6p2.

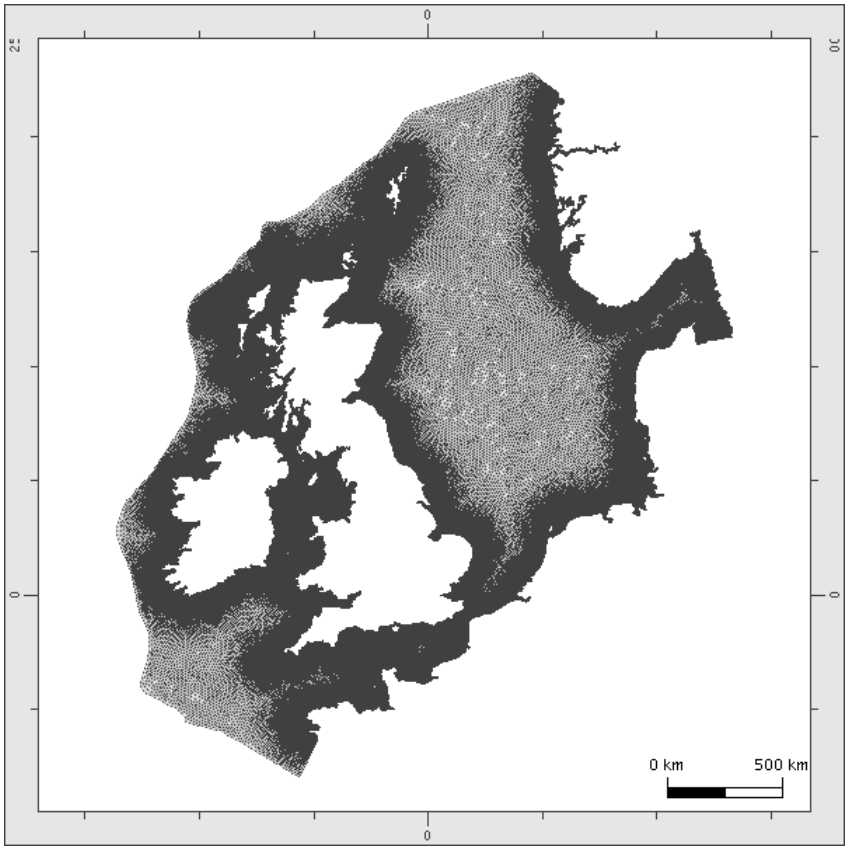

Figure B31 - Model mesh (Mercator projection)

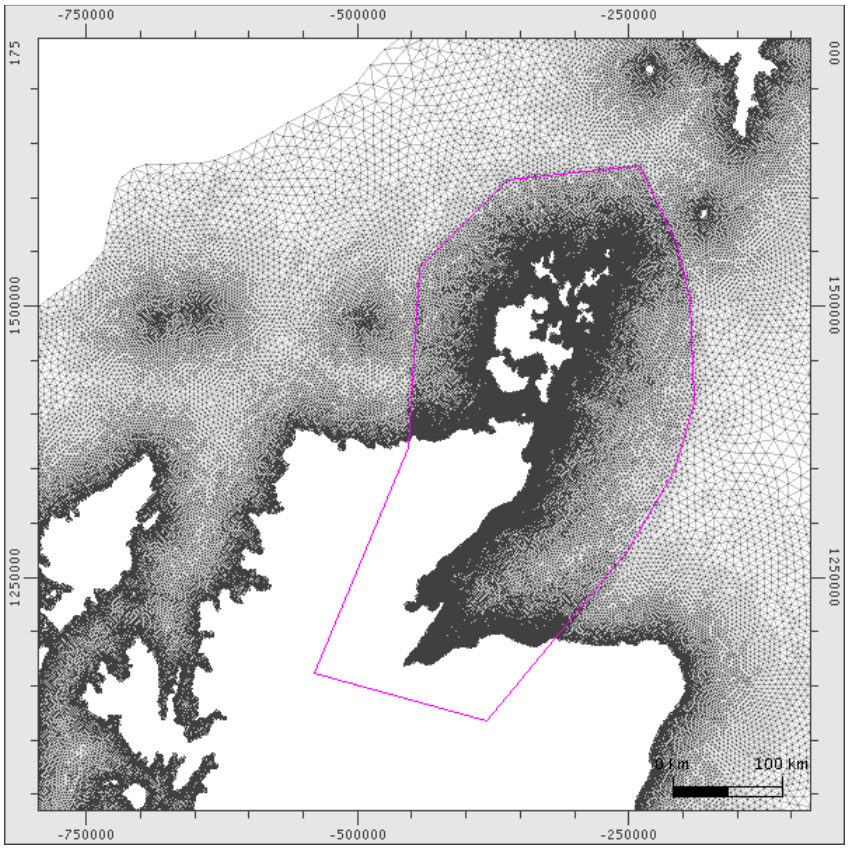

Figure B32 - Model mesh, refined down to 200 m inside the Pentland Firth area (Mercator projection)

4.2.5 Boundary conditions

As written in the previous paragraph, the boundary conditions come from the TPXO database.

TPXO is the current version of a global model of ocean tides, which best-fits, in a least-squares sense, the Laplace Tidal Equations and along track averaged data from TOPEX/Poseidon and Jason (on TOPEX/POSEIDON tracks since 2002). The methods used to compute the model are described in detail by Egbert, Bennett, and Foreman,1994 and further by Egbert and Erofeeva, 2002 [B4].

The tides are provided as complex amplitudes of earth-relative sea-surface elevation for eight primary (M2, S2, N2, K2, K1, O1, P1, Q1), two long period (Mf, Mm) and 3 non-linear (M4, MS4, MN4) harmonic constituents, on a 1440x721, 1/4 degree resolution grid (for versions 6.* and later). [B5]

4.2.6 Parameters

An example of the parameter files is reproduced in Appendix B1.

Real tide cycles are modelled, with a varying duration for the physical computation (keyword NUMBER OF TIME STEPS associated with the keyword TIME STEP). For this numerical model, the chosen time step was 60 s. In order to perform a 28-day simulation, 40320 time steps were required.

The chosen initial conditions are the TPXO satellite altimetry over the domain (keyword TPXO SATELLITE ALTIMETRY).

The graphic outputs routinely viewed for this type of hydrodynamic study are: the horizontal velocity components U and V (averaged over the vertical axis), the free-surface elevation, S, and the water height H.

In order to obtain the tidal wave characteristics and to optimise the output file size, the computational results are added to the output file every 15 min (real time) (keyword GRAPHIC PRINTOUT PERIOD = 15).

4.2.6.1 Physical parameters

Dissipation through bed-friction was modelled using a Chézy coefficient C.
The roughness appears in the Chézy coefficient calculation, via the Manning-Strickler formula:

$$C = K \times Rh^{1/6}$$

Where K is the Strickler coefficient, and Rh is the hydraulic radius. The value of the Chézy coefficient was set during the calibration of the model (please refer to § 4.2.7).

The Coriolis force was taken into account (keyword CORIOLIS = YES) with the value of the Coriolis coefficient equal to 1 10^{-6}. This value is thus assigned to the keyword CORIOLIS COEFFICIENT). It appears that this value is erroneous, as it corresponds to a Coriolis force which is lower than the existing one under these latitudes. This does not call the model into question, as it has been calibrated against measurements with that value, however it will have to be modified in the next deliverable (and the calibration will be modified accordingly, if necessary).

Meteorological effects (wind or atmospheric pressure) were not taken into account in the numerical simulations.

No specific turbulence model was used (value left by default at 1 for keyword TURBULENCE MODEL). A constant coefficient of viscosity equal to the value of 10^{-6} was applied over the whole domain (keyword VELOCITY DIFFUSIVITY).

4.2.6.2 Numerical parameters

For the suppression of free-surface parasite oscillations, the keyword FREE SURFACE GRADIENT COMPATIBILITY was taken equal to 0.9 (recommended value).

Equations were solved in the wave equation form (keyword TREATMENT OF THE LINEAR SYSTEM = 2).

The numerical schemes used were: the method of characteristics for the advection of velocities and, for the water depth, a conservative scheme (keyword TYPE OF ADVECTION = 1; 5 default values).

For solving the propagation step, the conjugate gradient method was the chosen solver (keyword SOLVER : 1) with an accuracy of 10^{-4}, which is the default value (keyword SOLVER ACCURACY) and a diagonal preconditioning (keyword PRECONDITIONING = 2, default value).

4.2.7 Calibration

The calibration parameter is the Chézy coefficient C ($m^{1/2}/s$), which is high when the roughness is low. Because the interest lies in the spatially restricted Pentland Firth region, one single roughness coefficient was chosen for the entire domain, which allows a good estimation of the tidal currents in the area of interest.

Identifying different roughness coefficients for different areas of the model would involve an extremely complex inverse problem, and is outside the scope of this study.

The best fit is obtained for C = 80 $m^{1/2}/s$ over the entire domain. In the literature, this value corresponds to a silt seabed. However, this parameter is used over such a large area that it does not reflect the state of the seabed itself but rather the equivalent friction force which is applied on the flow by the seabed, with all its unevenness.

Three moored ADCPs were deployed for a month, between 14th September 2001 and 15th October 2001 by the Oceanography Department of Gardline Surveys [B6]. The ADCPs were placed in the middle of the Pentland Firth. The exact locations C1, C2 and C3 are provided in the table below, and are shown on the following figure.

	Latitude	Longitude
C1	58.7180555555 58°43’34’’N	-3.2333333333 3°14’11’’W
C2	58.7166666666 58°43’01’’N	-3.0841666666 3°05’09’’W
C3	58.6522222222 58°40’13’’N	-2.9675000000 2°58’35’’W

Table B10 – ADCP Latitude / Longitude coordinates

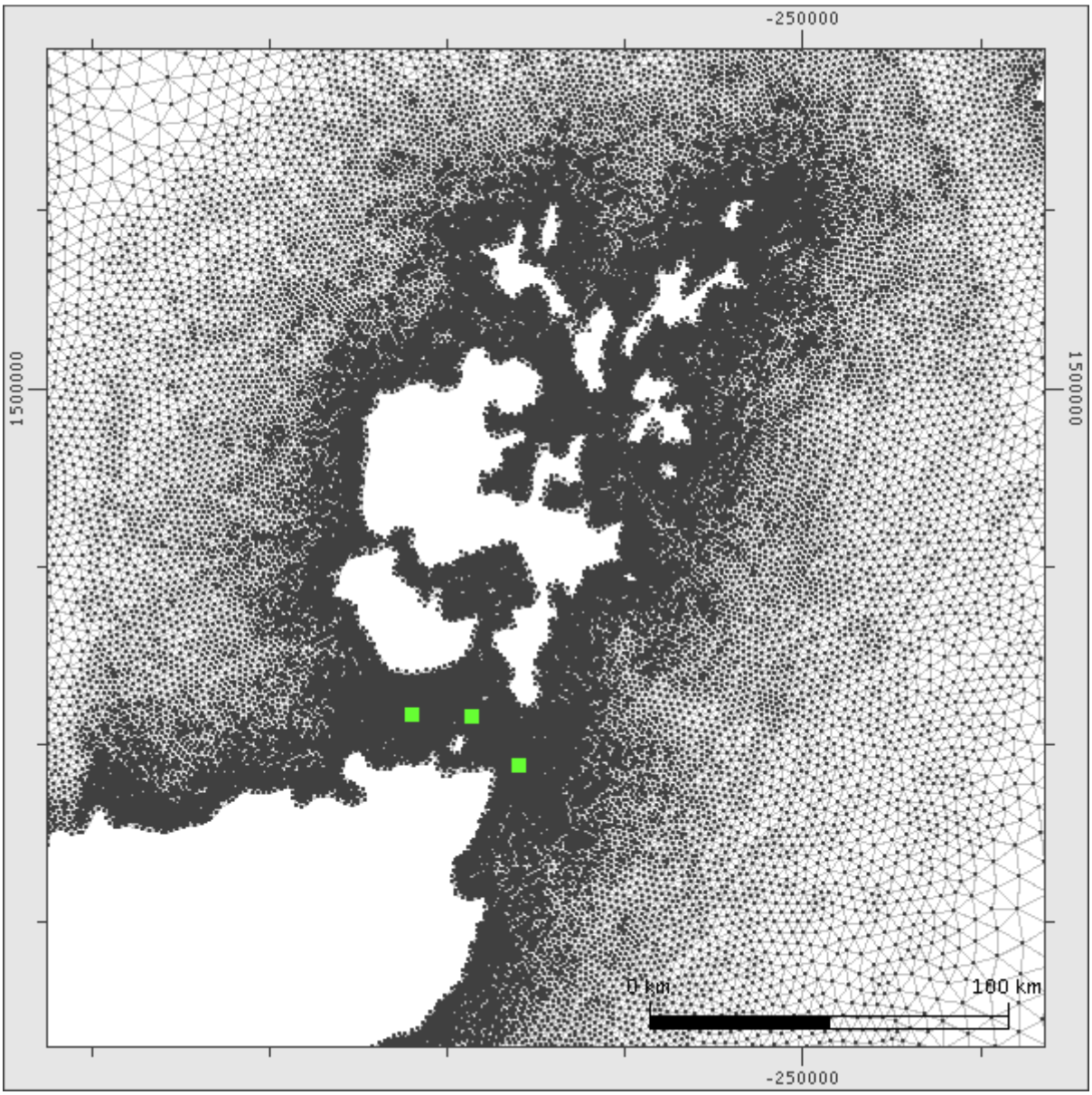

Figure B33 – ADCP locations.

The measurement campaign report provides the tidal diamonds for the mean spring tide and the mean neap tide, in hours, referenced to high water in Aberdeen. The Aberdeen tide tables were obtained for that period, and the interesting periods of time were identified.
The comparison between measurements and simulations are provided in the following figures. The calibration was performed on the 2nd ADCP (called C2) which is located in the middle of Pentland Firth. After that calibration, comparisons were performed for C1 and C3 which, although showing less good agreement than for C2, still give acceptable results.

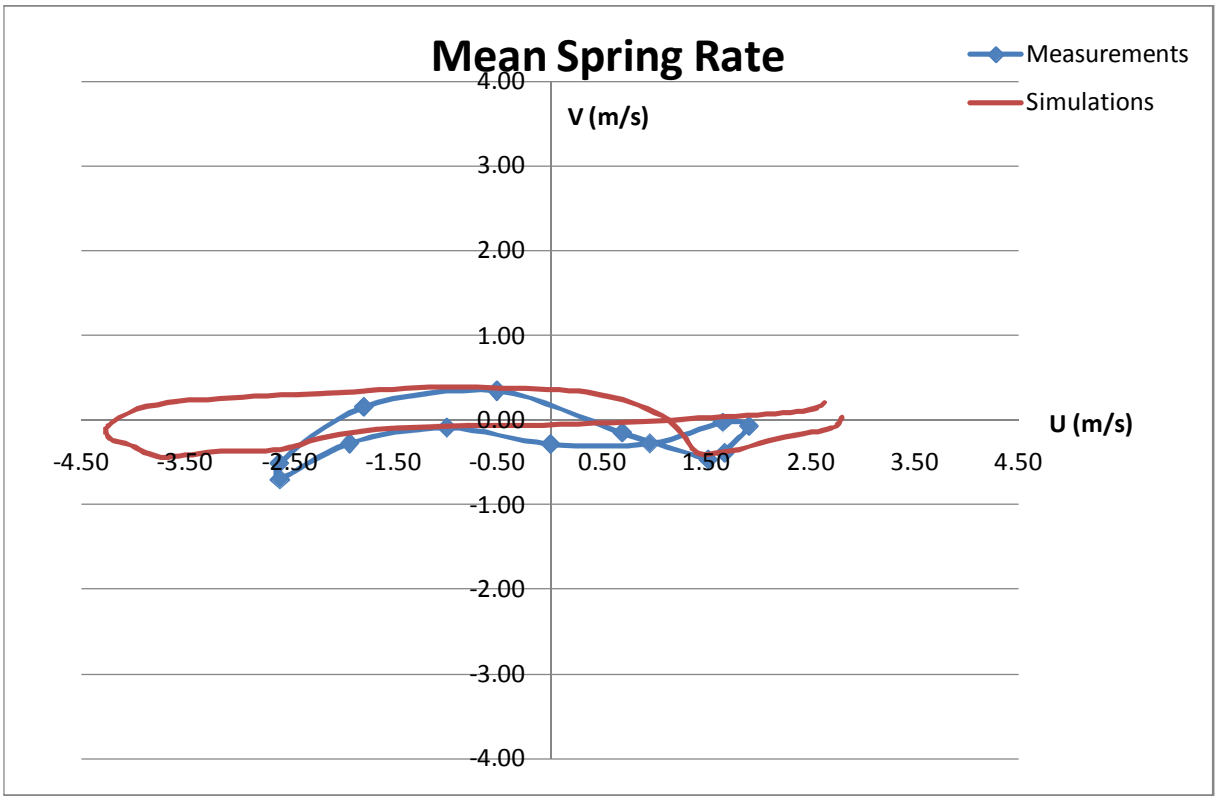

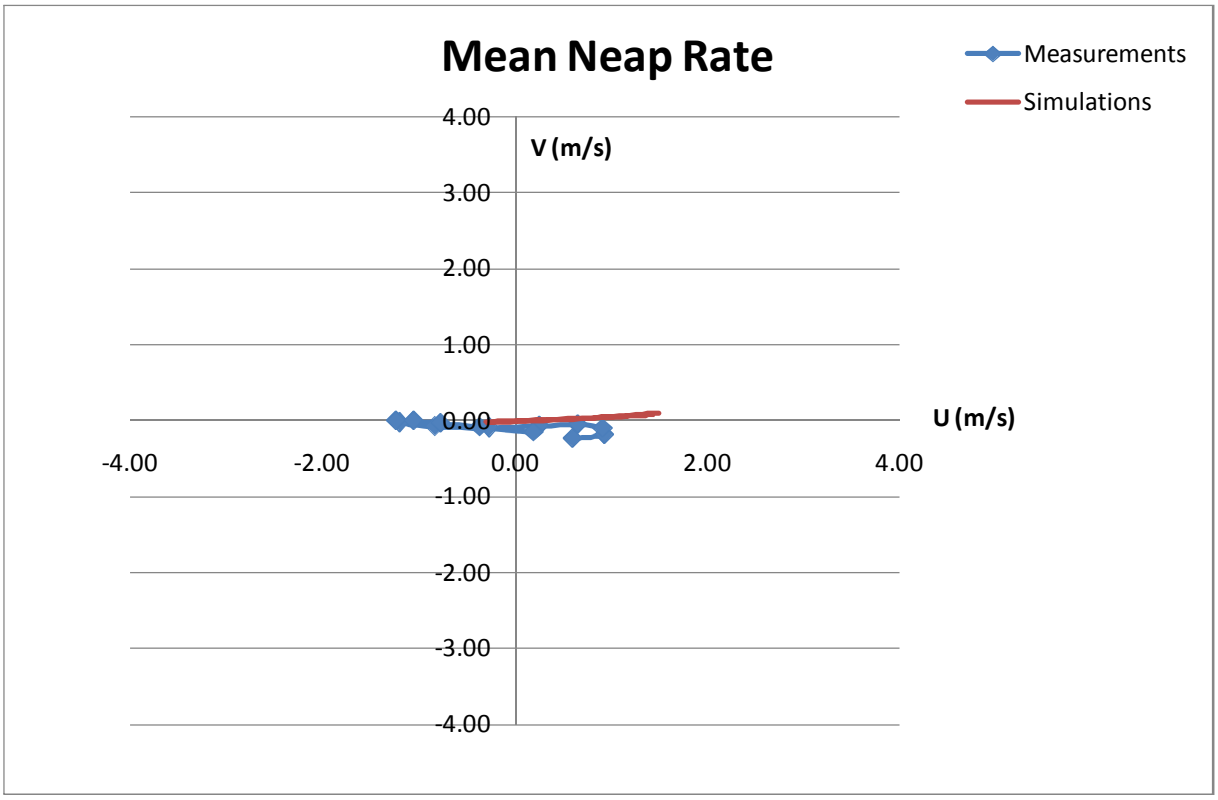

Figure B34 - Tidal diamonds for C1.

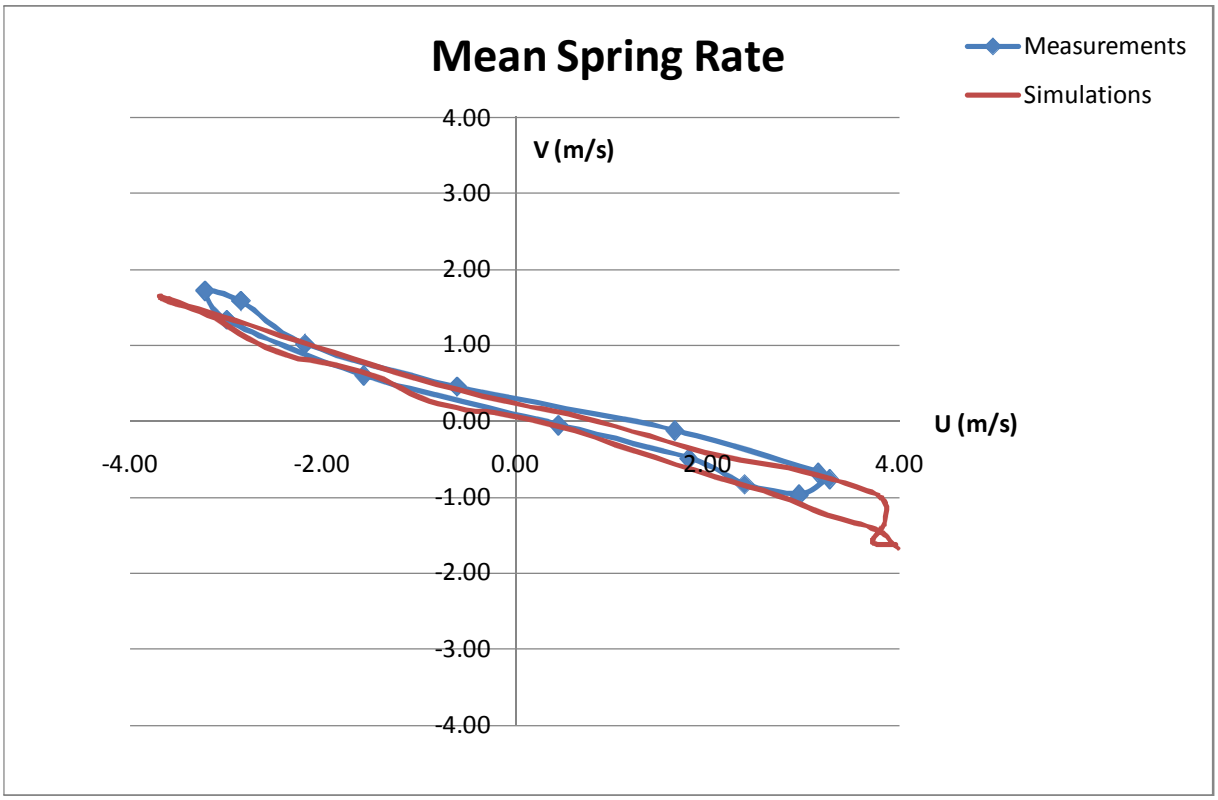

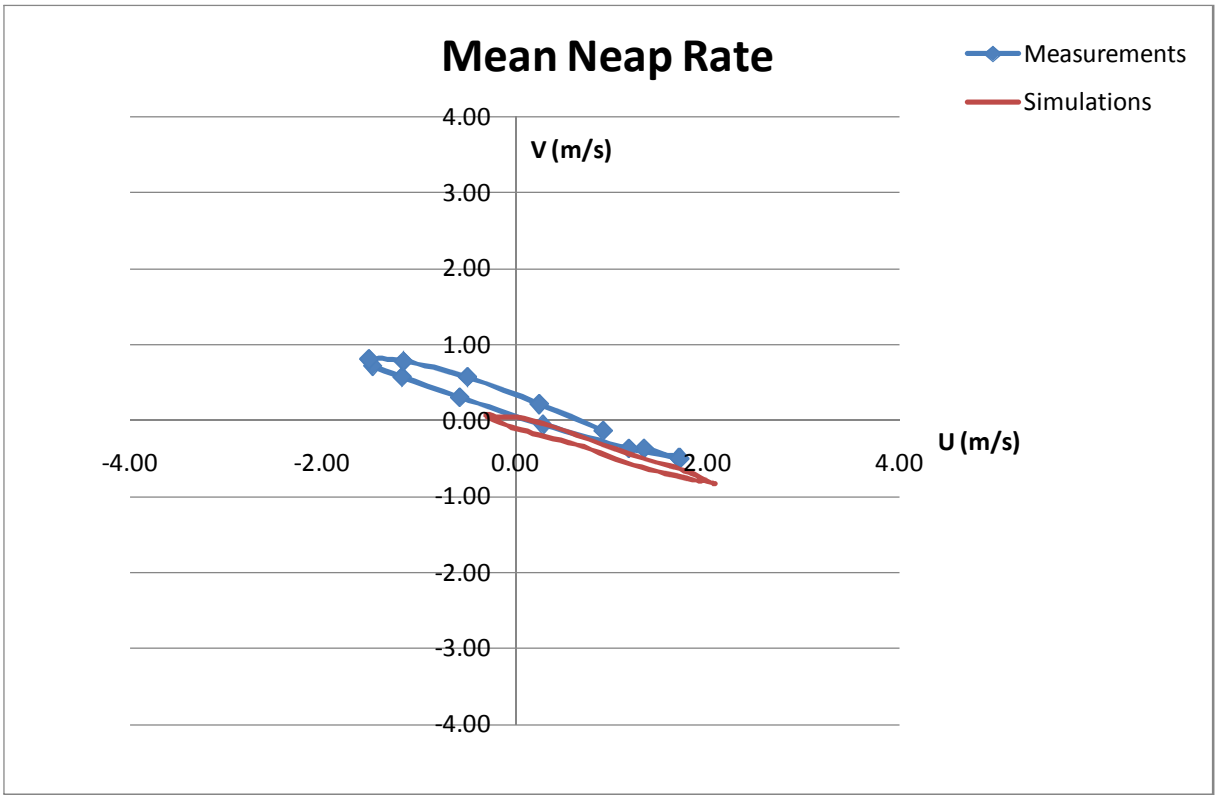

Figure B35 - Tidal diamonds for C2.

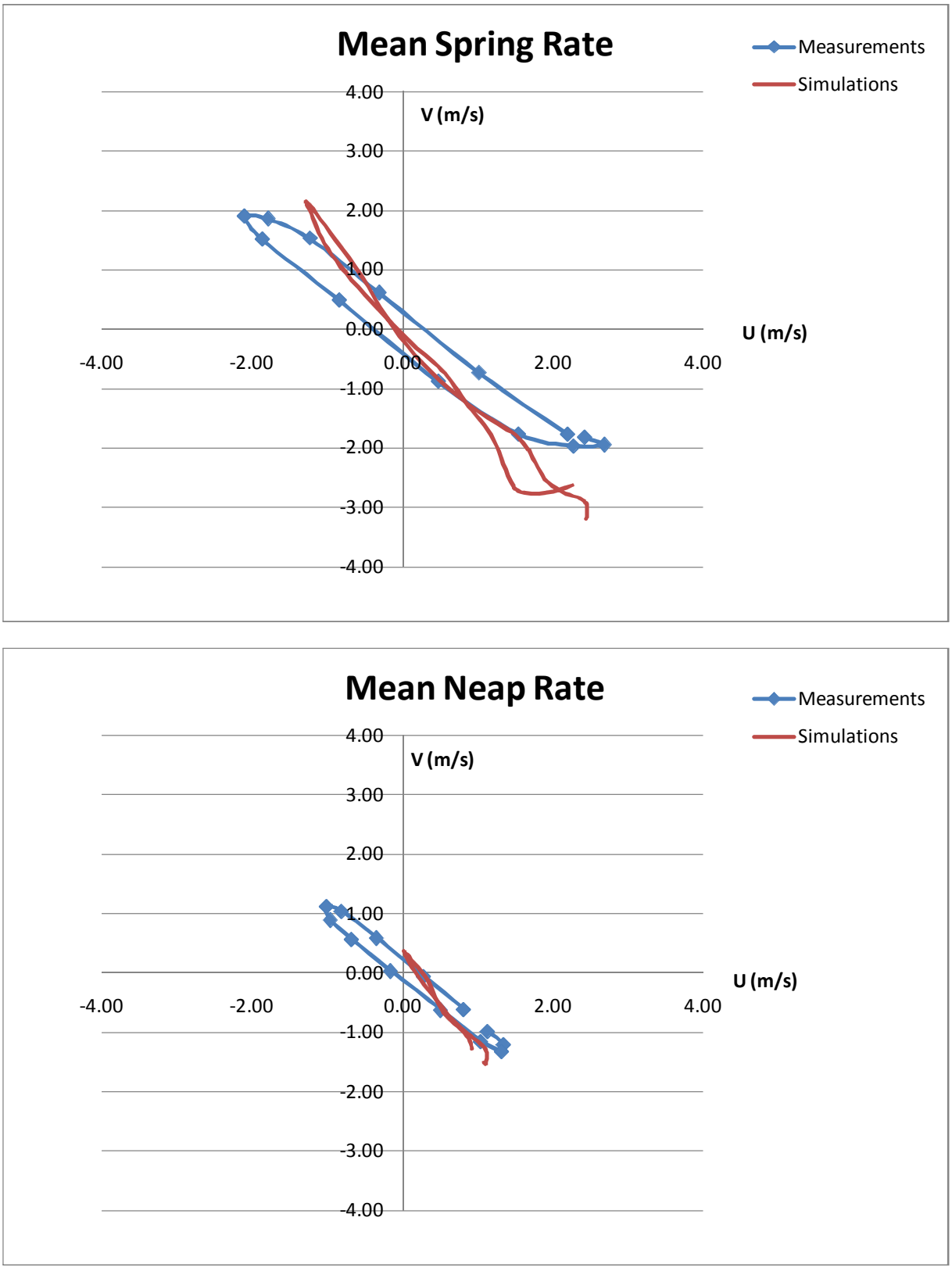

Figure B36 - Tidal diamonds for C3.

The measurements and the model show excellent agreement in terms of directions, for both the mean spring and mean neap tides, and at the three locations.

The current velocity amplitudes are more difficult to reproduce in the case of the mean neap tide than in the case of the mean spring tide, for all three locations, and this may be partially explained by the

fact that low velocities are reproduced with less accuracy than high velocities. The amplitude is underestimated for the mean neap tide, and overestimated for the mean spring tide in location C1.

The ability to say that there is or is not a good agreement between measured and simulated data is based on:

- The resolution of the numerical model, and its associated uncertainties
- The quality of the bathymetry data
- The quality of the boundary conditions
- The content of the measurement data (how much information?)
- The quality of the measurements and their associated uncertainties (acquisition frequency, average data, experimental uncertainties, etc...)
- The site hydrodynamic complexity
- The ability to reach better agreement when tuning various parameters

In the present case, at location C1, there are two aspects which could explain why the comparison between measured and simulated velocities is not as good as expected. These are the resolution of the model and the site hydrodynamic complexity.

- The bathymetry data around C1 come from Seazone Survey grids (25 m resolution), however since the model resolution at this location is 200m, it is impossible for the model to take into account the unevenness of the detailed bathymetry. Moreover, as seen on Figure B37 – Zoom on the C1 location (red cross) with bathymetry data in metres.Figure B37 and Figure B38, C1 is located in a region where the bathymetry gradients are more pronounced than in the C2 region, and therefore discrepancies between measurements and simulations at C1 may be greater than those at C2.
- The hydrodynamic complexity of the area around C1 is observed in § 4.2.8.

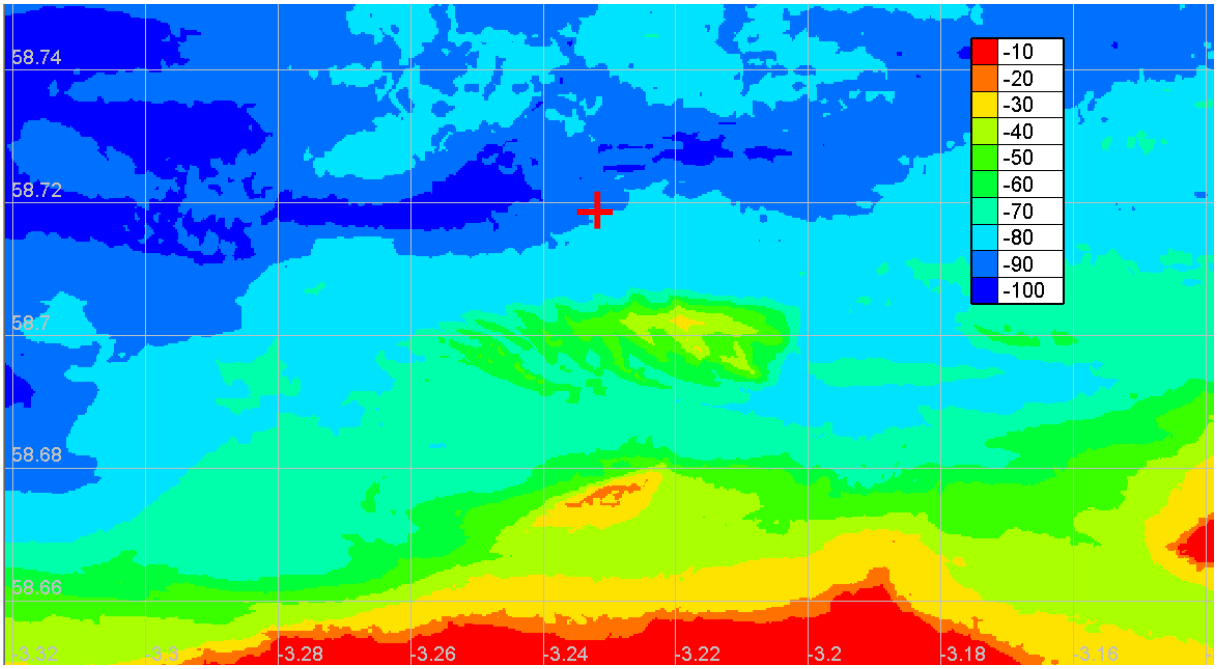

Figure B37 – Zoom on the C1 location (red cross) with bathymetry data in metres.

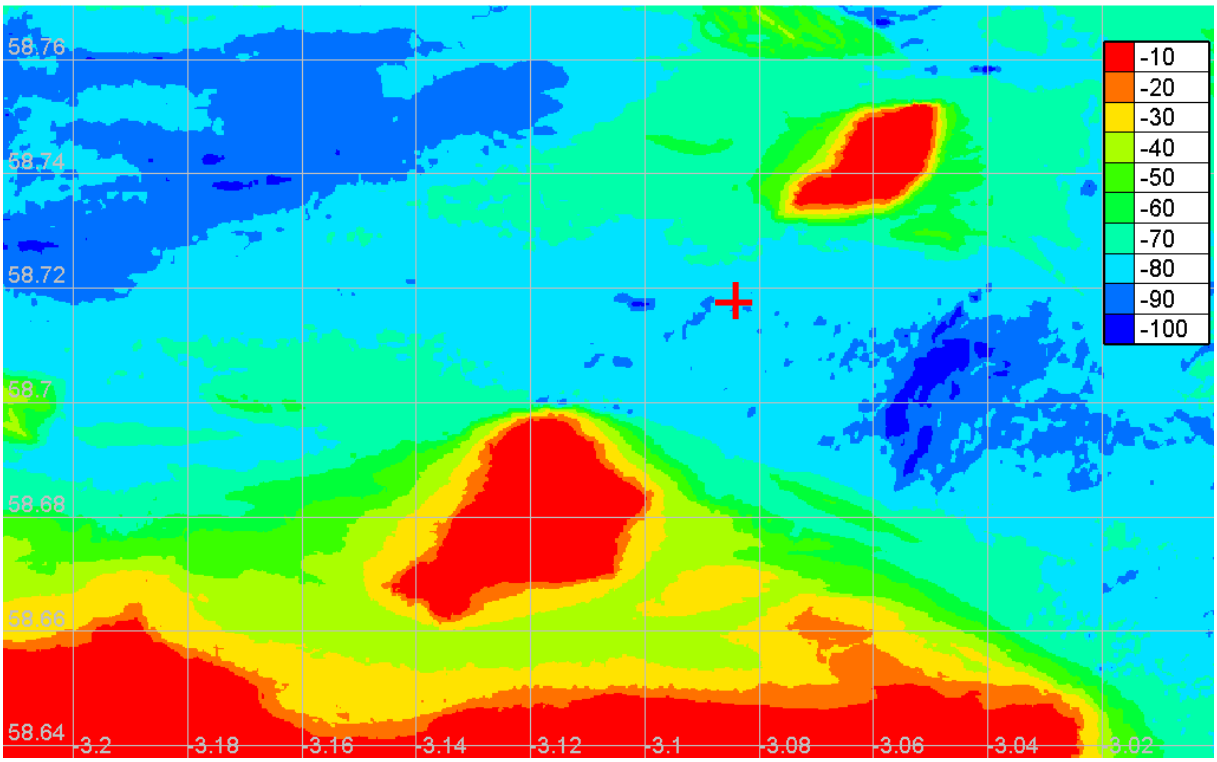

Figure B38 – Zoom on the C2 location (red cross) with bathymetry data in metres.

Given the complexity of the channel, and the model resolution which was chosen (a refined resolution would have been more expensive in terms of CPU time), the conclusion is that the comparison between tidal diamonds is acceptable, and enables further studies with tidal farms.

The mean spring tide simulation is in better agreement with the measurements than the mean neap tide. This is acceptable since the priority is to reproduce high velocities.

Because the only measurement data available correspond to six hours before high water in Aberdeen to six hours after high water in Aberdeen, there is very little information on phase in the measurements. Figure B39, Figure B40 and Figure B41 show that the simulated velocities match the experiments for C2, as expected since this is the calibration point, and are in less good agreement with C1 and C3. Apart from C1, for which there are significant differences between simulations and measurements, the numerical model captures the velocity trends.

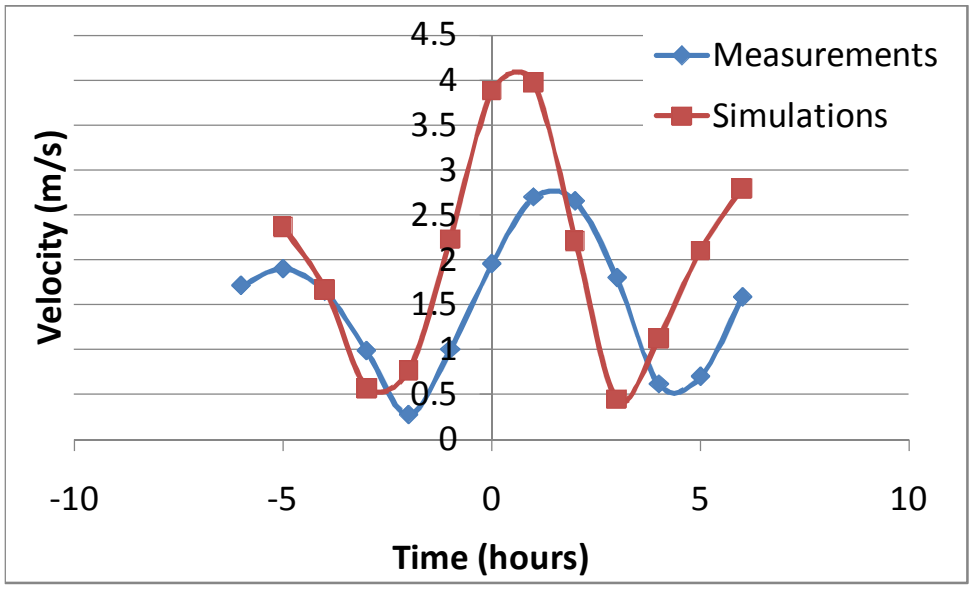

Figure B39 – Velocity time series at C1.

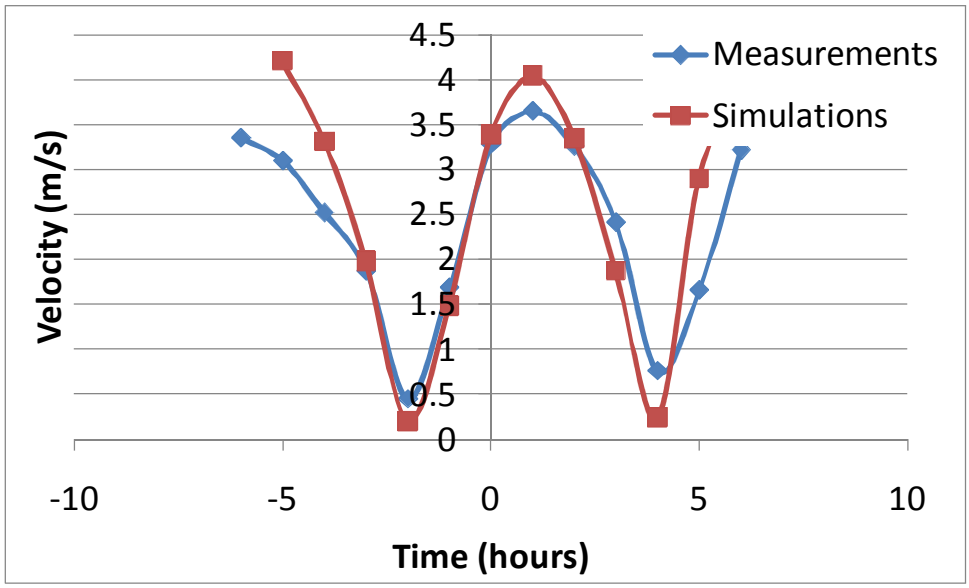

Figure B40 – Velocity time series at C2.

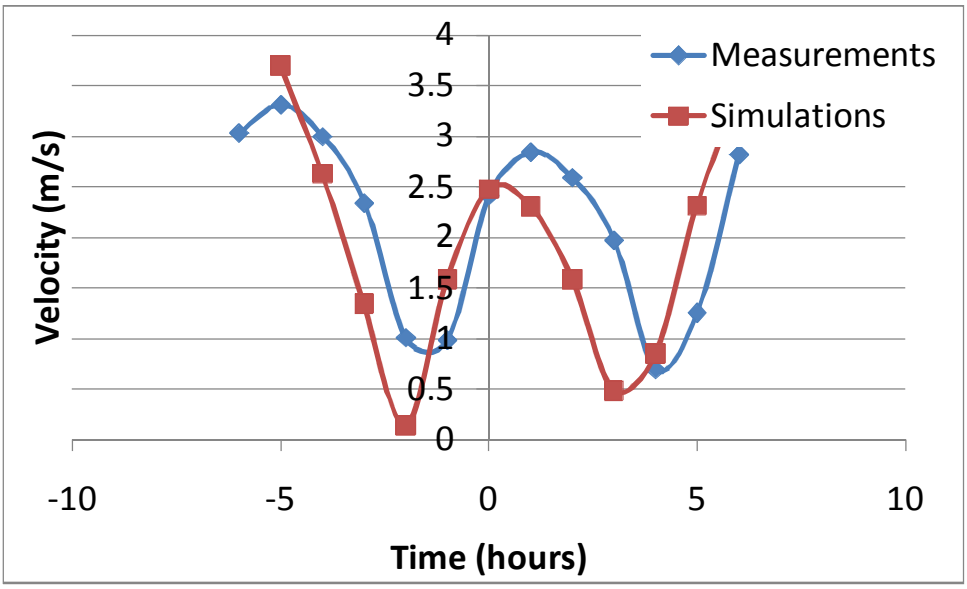

Figure B41 – Velocity time series at C3.

The modelled velocity time-series were then shifted in order to be in phase with the measurements. That operation enables the estimation of quality indices which reflect the ability of the model to reproduce the velocity amplitudes (please see Appendix G1 for more information about quality indices). Results can be observed in Table B11 below. The non-dimensional error in C2 confirms that the calibration operation enables simulations and measurements to match at this location. The other errors (at C1 and C3) are 12% and 25%, and these values illustrate how complex the site is, and how difficult obtaining agreement simultaneously at different locations can be.

Quality indice	C1	C2	C3
Mean error or bias	0,36 m/s	0,04 m/s	0,24 m/s
Root mean square error	0,57 m/s	0,94 m/s	0,4 m/s
Non dimensional bias	25 %	2%	12%
Non dimensional RMS error or scatter index	39%	41%	20%
Pearson linear correlation coefficient	0,92	0,94	0,95

Table B11 - Quality indices of computed tidal velocity intensities compared to ADCP raw measurements at C1, C2 and C3 on 19Th September 2001 (spring tide).

4.2.8 Analysis

The tidal flow conditions during the mean spring tide of 19th September 2001 are detailed below. The figures show the hourly evolution of the tidal currents in the Pentland Firth.

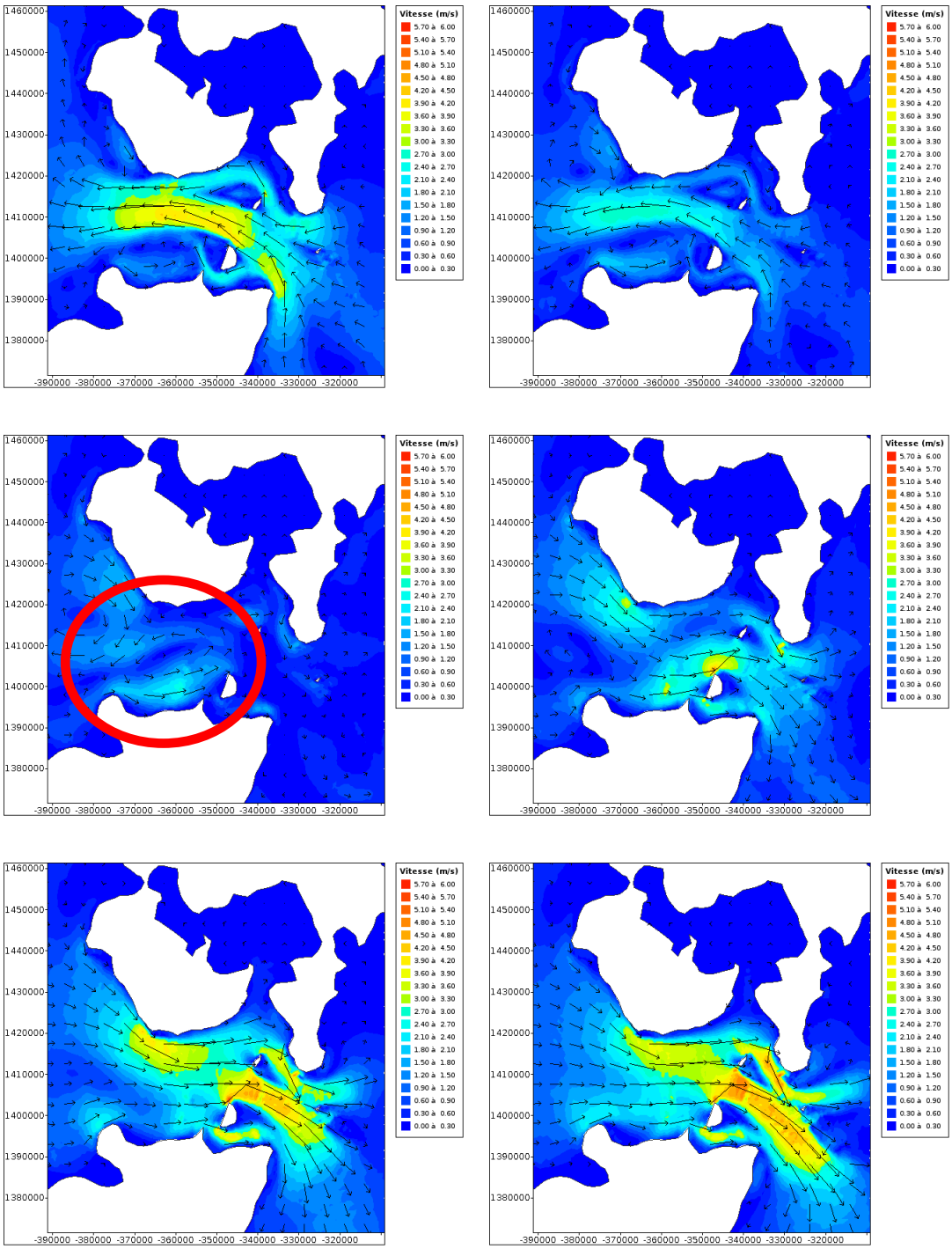
Vitesse (m/s)
5.70 à 6.00
5.40 à 5.70
5.10 à 5.40
4.80 à 5.10
4.50 à 4.80
4.20 à 4.50
3.90 à 4.20
3.60 à 3.90
3.30 à 3.60
3.00 à 3.30
2.70 à 3.00
2.40 à 2.70
2.10 à 2.40
1.80 à 2.10
1.50 à 1.80
1.20 à 1.50
0.90 à 1.20
0.60 à 0.90
0.30 à 0.60
0.00 à 0.30
1460000
1450000
1440000
1430000
1420000
1410000
1400000
1390000
1380000
-390000 -380000 -370000 -360000 -350000 -340000 -330000 -320000

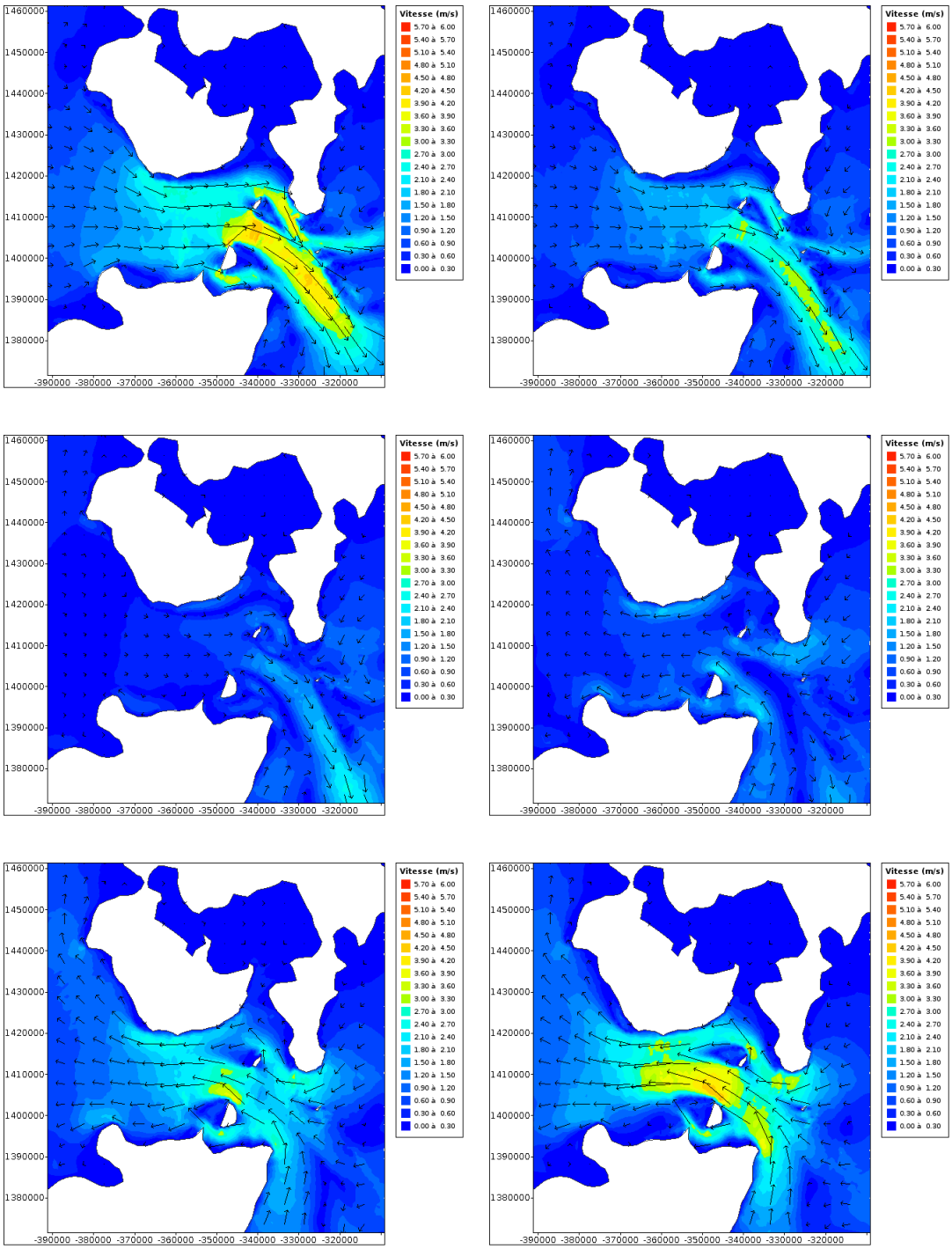
Vitesse (m/s)
5.70 à 6.00
5.40 à 5.70
5.10 à 5.40
4.80 à 5.10
4.50 à 4.80
4.20 à 4.50
3.90 à 4.20
3.60 à 3.90
3.30 à 3.60
3.00 à 3.30
2.70 à 3.00
2.40 à 2.70
2.10 à 2.40
1.80 à 2.10
1.50 à 1.80
1.20 à 1.50
0.90 à 1.20
0.60 à 0.90
0.30 à 0.60
0.00 à 0.30
1460000
1450000
1440000
1430000
1420000
1410000
1400000
1390000
1380000
-390000 -380000 -370000 -360000 -350000 -340000 -330000 -320000

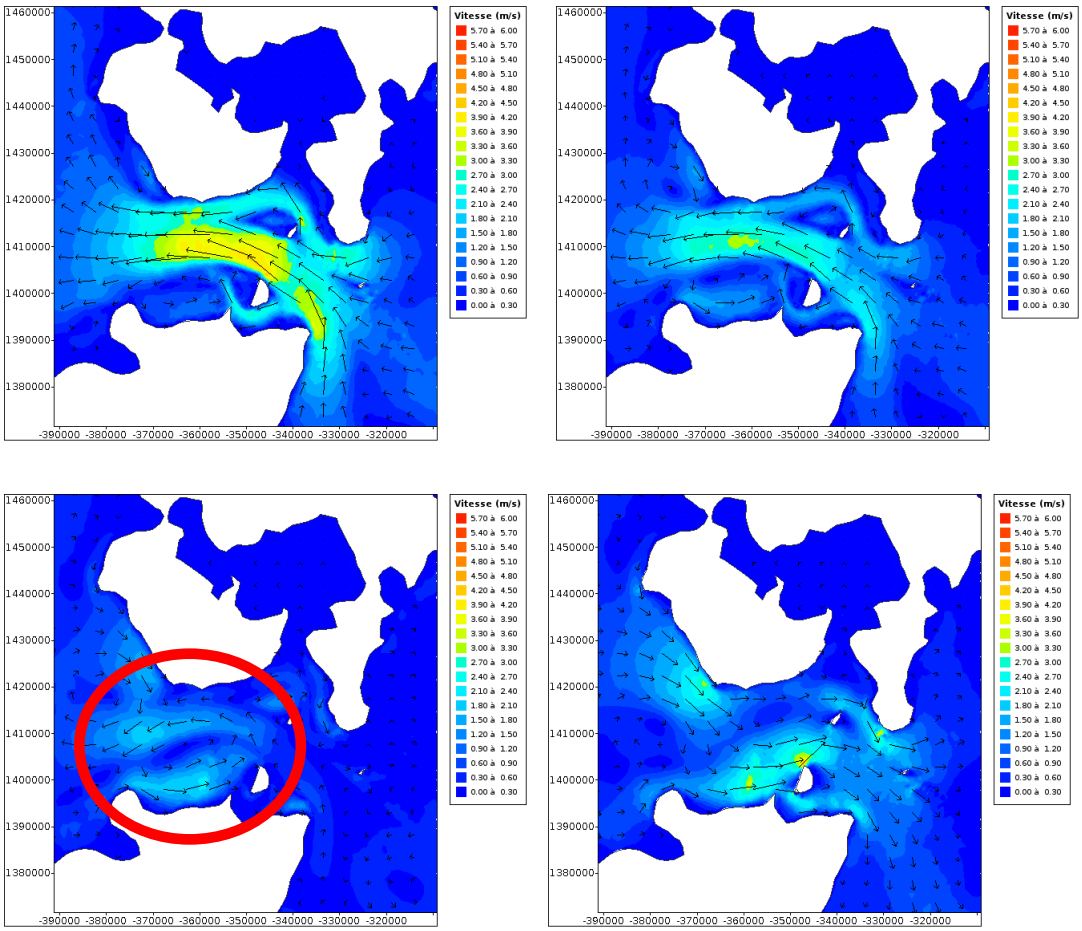

Figure B42 – Current speed evolution between 4h29 and 19h29, on 19th September 2001.

The figures above show all the complexity of the tidal flow in the Pentland Firth area. For example, very important recirculations are observed on the third and on the fifteenth graphs (in the red circles). These rotating flows are not local phenomena, but take place over the entire Firth. They occur at the change between the East to West flow and the West to East flow.

The velocity, which is obtained with this numerical model, goes up to 5 meters/second, when the water flows from West to East. This value is extremely high and, even if it may overestimate the real velocity values, as seen in the previous paragraph, it reveals that the currents in this region can be really important, and it therefore confirrms the potential of the site for the installation of a tidal farm.

4.3 Uncertainties

Uncertainties have been discussed and quantified in the calibration paragraph. As explained in that paragraph, it is believed that there are two major aspects which can explain why the comparison between measured and simulated velocities is not as good as expected. These are the resolution of the model and the site hydrodynamic complexity.

It is also important to underline the fact that Seazone charts data are mainly for navigation safety and can hence display conservative soundings (*i.e.* the sea bed can be over-estimated). Therefore the data may not accurately represent the local features of the seabed morphology which strongly influences the tidal current patterns. This means that the comparison between single point location ADCP measurements and simulation results which come from such an extensive model with bathymetry uncertainties has its limitations.

The numerical errors which are propagated within the TELEMAC-2D model are not quantified at this stage. This extremely complex topic is currently under investigation outside of the PerAWaT project, and may not be available before the end of 2013.

The uncertainties associated to the current measurements are not provided in the available measurement report. However, the data come from moored ADCPs, which are much more reliable than data obtained with transect profiling operations. Therefore, it is believed that these measurement uncertainties must not be significant.

4.4 Computation time

The TELEMAC-2D computations were carried out on 8 processors running at 2.40 GHz. The CPU time required for a simulation of 28 days is approximately five and a half hours.

4.5 Conclusion

The present study enabled the characterisation of tidal flow conditions on the Pentland Firth area. The numerical model was built with the TELEMAC-2D hydro-informatics software developed at EDF R&D.

Calibration results were given in terms of tidal diamonds for the current speed for two different periods (a mean spring tide and a mean neap tide), at three different locations in the Pentland Firth. These simulations were compared to measurements and an analysis of these comparisons was performed.

4.6 References

[B1] Tidal Modelling – D06 Functional summary and Testing Report, version 1.0, May 2012, HR Wallingford, Black & Veatch, the University of Edinburgh. Confidential document.

[B2] The GEBCO_08 Grid, released in Sept 2010; http://www.gebco.net

The GEBCO_08 Grid, Report, 2011.

[B3] Seazone charted grids: NW25600020, NW25600040, NW25600060, NW25600080, NW25600100, NW25800020, NW25800040, NW25800060, NW25800080, NW25800100, NW26000020, NW26000040, NW26000060, NW26000080.

Seazone survey grids: NW55850030, NW55850035, NW55850040, NW56050030, NW56050035, NW56050040

[B4] G. D. Egbert, A. F. Bennett, M. G. G. Foreman, TOPEX/POSEIDON tides estimated using a global inverse model, Journal of geophysical research, VOL. 99, NO. C12, PP. 24,821-24,852, 1994

G. D. Egbert, S. Y. Erofeeva, Efficient Inverse Modeling of Barotropic Ocean Tides, Journal of atmospherical and oceanic Technology, vol.19 – pp.183 – 204, 2002.

[B5] http://volkov.oce.orst.edu/tides/otis.html, May 2012

[B6] Gardline Surveys (2001) 'Pentland Firth – Tidal Stream Observations' Produced for the Navigation Safety Branch of the Maritime and Coastguard Agency, Contract NBSA5B/2959

5 PAIMPOL-BRÉHAT

5.1 Introduction

The aim of this study is to provide a precise characterisation of the tidal conditions, *i. e.* the sea levels and tidal currents, in the Paimpol-Bréhat zone (French department of Côtes-d'Armor in Brittany) using numerical modelling at local scale.

Various measurement campaigns were carried out in the Bréhat zone between 2005 and 2008:

- a marine current measurement campaign, carried out by IXSURVEY, over a period of 17 days from the 5th to the 21st of April 2005 [C1],
- a three-month campaign of marine current and wave measurements performed by IXSURVEY over the period from March 25th to June 25th 2008 [C2],
- a bathymetric measurement campaign conducted by CREOCEAN in April 2008 [C3].

5.2 Geographical location of the site

The Bréhat zone, also known as Paimpol region, is located in the Normandy-Brittany Gulf to the north-west of the Saint-Brieuc Gulf, in the French department of Côtes-d'Armor (22) in Brittany. The major port in the zone is Paimpol. Also located in the sector are Port Clos and Men Joliguet ports on the Isle of Bréhat and the ports of Loguivy, Les Héaux-de-Bréhat and Roches Douvres. In the Bréhat zone, there is a crustacean reserve, in which any type of fishing other than line fishing is forbidden.

5.3 Tidal sea levels

The sea level data, which are characteristic of astronomical tides, are provided by the French Marine Hydrographic and Oceanographic Service (SHOM) and referenced with respect to Chart Datum for the two ports: Paimpol, the major port near the Isle of Bréhat and Men Joliguet, the reference port that is closest to the site and located on the Isle of Bréhat (©SHOM-2010).

Table C1 gives sea level data for the following tides:

- Highest Astronomical Tide (HAT),
- Mean High Water Springs (MHWS),
- Mean High Water Neaps (MHWN),
- Mean Sea Level (MSL),
- Mean Low Water Neaps (MLWN),
- Mean Low Water Springs (MLWS),
- Lowest Astronomical Tide (LAT).

Port	(m CD)						
	HAT	MHWS	MHWN	MSL	MLWN	MLWS	LAT
Paimpol	11,92	10,80	8,35	6,09	3,85	1,35	0,11
Men Joliguet (Isle of Bréhat)	11,68	10,55	8,15	5,95	3,75	1,30	0,10

Table C1: Sea levels characteristic of astronomical tides at Paimpol and Men Joliguet (Isle of Bréhat), (source [C4], ©SHOM-2010).

The following tidal ranges are thus obtained:

Port	(m)		
	Exceptional Spring Tide (ES)	Mean Spring Tide (MS)	Mean Neap Tide (MN)
Paimpol	11,81	9,45	4,50
Men Joliguet (Isle of Bréhat)	11,58	9,25	4,40

Table C2: Tidal ranges at Paimpol and Men Joliguet (Isle of Bréhat).

Certain meteorological conditions can lead to differences between the predicted tide and the actual tide, in particular a combination of a High Astronomical Tide and a surge (extreme high water level), or conversely, a conjunction of a Low Astronomical Tide and a receding surge (extreme low water level).

5.4 Measurement campaigns

Over the course of the IXSURVEY measurement campaign, carried out on the Les Héaux-de-Bréhat zone from the 5th to the 21st April 2005 [C1], two measurement sampling points were studied (points 1 2005 and 2 2005, illustrated on Figure C1). Point 1 2005 is located in the crustacean reserve to the north of La Horaine plateau, while point 2 2005 is situated to the North of Les Héaux-de-Bréhat. The coordinates of these two points (geographic reference coordinate systems WGS84 and NTF Lambert 1 North), as well as the bottom depth, are given in Table C3.

Measurements of flow velocity (magnitude + direction of the velocity) were taken over the full water column at each of the sampling points by two ADCP.

During this first measurement campaign, a fairly large range of French tidal coefficients [C5] were recorded (coefficients 24 to 104, from neap tides to spring tides). During this period in 2005, the ADCP at the point inside the reserve recorded maximum surface velocities in the order of 2.6 m/s at flood tide and 2 m/s at ebb tide, whereas to the north of Les Héaux-de-Bréhat, maximum flows of 2.4 m/s at flood tide and 1.8 m/s at ebb were reached.

Points	WGS84		NTF Lambert 1 North		Depth
	degrees and decimal minutes		metres		(m CD)
	Longitude West	Latitude North	East	North	
1	2°54,6'	48°55,4'	215851	149264	-46
2	3°5'	48°57'	203394	153120	-58

Table C3: Coordinates of the two measurement sample points of the April 2005 campaign [C1].

A second measurement campaign was carried out by IXSURVEY from March 25th to June 25th 2008 [C2]. Two measurement points were instrumented (points 1 2008 and 2 2008 as illustrated on Figure C1, within the vicinity of point 1 2005 of the April 2005 current measurement campaign, to the south-east). These two points are located in the crustacean reserve. Their coordinates (geographic systems WGS84, and NTF Lambert 1 North), as well as the bottom depth, are listed in Table C4.

Measurements recorded at the first point included both tidal flows (by two ADCP) and waves (a wave monitoring buoy and an ADCP of the AWAC type), whereas only tidal flow measurements were recorded at the second point, with the aid of an ADCP.

The chosen sampling period enabled coverage of a large range of French tidal coefficients (from 25 to 109, from neap tides to spring tides) including, in particular, the April 2008 equinox tide and a variety of sea states (calm to stormy).

In comparison to the 2005 measurement campaign, the measurement sampling period was greatly extended, which enabled the characterisation of the site under diverse marine conditions (four spring

tides and six neap tides over the three months) with equally varied sea states (end of winter storms and calm periods in the spring).

In general, maximum velocities are greater at flood tide than at ebb tide, and this is especially so in the case of a spring tide. The maximum surface velocity measured during this campaign was 3.05 m/s, at flood tide (compared to about 2.3 m/s at ebb tide). However, 75% of the velocities measured over the course of the measurement campaign fell within the range of 0.2 to 1.8 m/s, whichever the sector of the water column being considered. Velocities were homogenous over the vertical, although with a slight increase near the surface (a classic profile, due to bed friction and to wind effects at the surface).

The flow is bidirectional with two orientations being clearly predominant (towards 120° and 320° clockwise relative to North). The current has a course towards 120° at flood tide and towards 320° at ebb tide. There is very little directional shear of the current over the vertical. The flow velocity ceases and the flow direction changes after the slack waters of high and low water (around 30 minutes to 2 hours thereafter). This change takes place earlier for spring tides than for neap tides. The tidal current turns through North in general.

Tidal durations are reasonably stable: between 6 h and 6 h 30 min. They are a little longer in the case of neap tides.

Significant wave heights fall within the range of 0.2 to 3.5 m, but are generally below 2 m. Waves arrive from two principal directions: the North-West sector (about 75% of the time) and the East (at about 15% of the time). Waves coming from the North-West sector have higher associated peak periods and significant wave heights than those arriving from the East sector. All episodes of waves above 2 m occurred in the north-west propagation direction, except for one wave event. The wave periods ranged between 1.5 and 18.2 s.

Points	WGS84		NTF Lambert 1 North		Depth
	degrees and decimal minutes		metres		(m CD)
	Longitude West	Latitude North	East	North	
1	2°53,169'	48°54,746'	217510	147934	-44,1
2	2°51,988'	48°54,496'	218918	147372	-43,7

Table C4: Coordinates of the two measurement points for the Spring 2008 campaign [C2].

These two measurement campaigns permitted the calibration of the TELEMAC-2D and TELEMAC-3D numerical models.

5.5 2D numerical model

All flow velocities shown hereafter only take into account the astronomic tide. In particular, no meteorological effects (atmospheric pressure, wind, surge/wane) or wave effects have been considered in the numerical model.

Moreover, in this section, any reference made to the current velocity resulting from the TELEMAC-2D numerical model refers to the vertically averaged velocity. The results given are averages in the Reynolds sense, *i. e.* after smoothing out of the turbulence effects.

The sea levels are referenced with respect to Chart Datum.

5.5.1 Code version

The TELEMAC-2D edition used in this study is version 6.0.

5.5.2 Definition of the domain area / justification

The domain covers an area that is almost square, extending approximately 60 km from North to South and from West to East. Its extent can be seen in Figure C1. The domain extent of the numerical study is, in the WGS84 coordinate system, contained between the coast and 49° 20' N in latitude and, in longitude, between longitudes 2° 30' and 3° 20' W. In addition, the South-East boundary of the domain (segment [E1, E2]) is oblique (with regards to the North-South and East-West directional axes), as can be seen from Figure C1. The orientation of this boundary is thus roughly perpendicular to the flow direction of the marine currents (at the level of La Mauve). The boundary coordinates of the domain covered by the study are given in Table C5.

Outer boundary points of the numerical domain	WGS84 degrees and decimal minutes		NTF Lambert 1 North metres	
	Longitude West	Latitude North	East	North
E1	2°53,4'	48°42'	215591	124387
E2	2°30'	48°48,6'	245020	134678
E3	2°30'	49°20'	248753	192754
E4	3°20'	49°20'	188339	196973
E5	3°20'	48°49,75'	184123	141068

Table C5: Boundary coordinates of the numerical domain extent (Figure C1).

All hydrodynamic numerical models were built with their horizontal geographic coordinates expressed in the Lambert 1 North projection coordinate system (in metres, with the point of origin at the Lambert 1 North projection origin).

5.5.3 Bathymetry

The bathymetry data used in the numerical model is derived from, amongst other sources:

- bathymetric grids # 14582 and 14583 – geographic coverage provided in one degree square blocks without overlap (metropolitan coastal area bathymetry composed of a selection of soundings with a minimum sampling interval of 25 metres, created in February 2006) – provided commercially by the SHOM, covering the zone contained between 2° and 4° W and between 48° and 49° N (WGS84 system),
- a 500 metre grid Digital Terrain Model (DTM) covering the English Channel and Atlantic Ocean metropolitan coasts (October 2006), also commercially available from the SHOM,
- a digitalisation, with the aid of the SINUSX data input tool, of the 0 m CD isobaths of the coastline of charts # 7152 L and # 6966 L,
- a bathymetry measurement campaign (single and multi-beam) carried out in April 2008 [C3]. Grid resolution for the bathymetric soundings on a potential site for installing tidal turbines reaches 10 m.

Figure C1 represents the numerical model bathymetry over the entire study domain.

5.5.4 Mesh

The mesh (see Figure C2) used for this numerical model is a finite element mesh generated with the aid of the MATISSE v1.0 grid-generation software. It consists of 14,129 nodes and 27,425 triangular elements. The mesh size varies from 300 m at the coast to approximately 1.6 km in the zones of the greatest depths (to the West and North of the model). The mesh was progressively refined to 50 m, specifically at potential installation sites for tidal turbines.

5.5.5 Boundary conditions

The boundary conditions are derived from an extended LNHE model covering the near Atlantic, the English Channel and the southern part of the North Sea, from which the following harmonic constituents [G6] were extracted:

- M2, principal lunar semidiurnal constituent, with a period of 44,714 s (12 h 25 min 14 s),
- S2, principal solar semidiurnal constituent, with a period of 43,200 s (12 h),
- N2, larger elliptical lunar semidiurnal constituent, with a period of 45,570 s (12 h 39 min 30 s),
- M4, first harmonic of M2, quarter-diurnal constituent with a period of 22,357 s (6 h 12 min 37 s).

In this study, schematic tides including the mean neap tides, mean spring tides and exceptional spring tides were simulated, as well as real tide cases, reconstructed from the four harmonic constituents cited above.

Water depths and velocities at the boundary are imposed using Thompson-type boundary conditions [G7].

5.5.6 Modifications of standard sources

The bottom elevation of the numerical model is referenced to Chart Datum whereas tide elevation is referenced to the Mean Sea Level (MSL) on open boundaries. Moreover, if no modifications are done, the sea levels for different ports over the area are not well reproduced simultaneously. For the sea level calibration, it was then found to be necessary to introduce a non-constant mean sea level over the extent of the domain, in order to correctly calibrate the sea levels at the ports on the zone. This mean sea level is subtracted from the bottom elevation referenced to Chart Datum so that the bottom elevation is finally referenced to Mean Sea Level. Thus, a “pseudo” mean level was generated based on the LNHE 4-constituent numerical model that covers the near Atlantic Ocean, the English Channel and the southern part of the North Sea. This data is read from a binary data file in Serafin format.

In practice, at the beginning of the computations, the frame of reference of the bottom elevation and free surface elevation is changed (passing from the frame of reference linked to Chart Datum to that linked to the mean sea level in the CORFON subroutine) and all elevations are expressed relative to the Mean Sea Level (MSL). In order to post-treat the results correctly with reference to Chart Datum (the original frame of reference), new post-treatment variables were created (including the original bathymetry of the model and the free surface elevation relative to Chart Datum) in the sub-routines preres_telemac2d and nomvar_telemac2d.

In addition, where the seabed elevation of the nodes at the open liquid boundary – on which tidal conditions are imposed – is liable to be above LAT, it is modified so that these nodes will always be wet (these modifications are again made in the CORFON subroutine. In practice, the nodal bathymetry is clipped to the elevation corresponding to Chart Datum).

Finally, in order to take into account the modification of some of the subroutine arguments, the telemac2d routine was consequently modified.

As discussed in § 5.5.5, tidal signals for the boundary conditions at the liquid border are reconstituted from the extended LNHE model [G6] comprising four harmonic constituents (M2, S2, N2 and M4). The water depths and velocities are reconstituted according to the methodology described in [G6]. In the case of the numerical simulation of schematic tides, a phase shift is applied in relation to a point on the liquid boundary on which the tidal conditions are imposed (in this case, the 22nd node) such that the simulation starts at a time of high water in the zone. A velocity ramp (*i. e.* an increase of the velocity in time over the 30 min of the simulation) is imposed at the beginning of the simulation,

during the first half hour of physical simulation, so that the simulation does not freeze or crash during this period. These modifications are found in the new subroutines BORDTIDE and TIDAL_MODEL_T2D, which isolate the treatment of the tide at the liquid boundaries and have been integrated into version 6.1 of the TELEMAC-2D software.

A calibration parameter was used in order to correctly reproduce the tidal range at the different ports on the zone. It is called CTIDE (for versions 6.1 and above) based on the end users. This parameter is a multiplier coefficient that acts on the amplitude of the tidal signal (sum of the sinusoids of four harmonic constituents for the water depth and the two horizontal velocity components). It varies according to the type of schematic tide being modelled. However, this calibration parameter is not used here for simulations of real tides.

5.5.7 Parameters

An example of the parameter files (those of a mean spring tide) is reproduced in Appendix C1.

Two tidal cycles (as a minimum) are modelled, with a duration for the physical computation (keyword NUMBER OF TIME STEPS associated with the keyword TIME STEP) of 90,000 s = 25 h (93,000 s in the case of a mean neap tide).

The initial condition chosen is a free-surface elevation that is constant over the entire domain extent (keyword INITIAL CONDITIONS assigned to the value CONSTANT ELEVATION), taken as equal to the high water at the port of Men Joliguet (value of the keyword INITIAL ELEVATION) in the chosen frame of reference (in this case relative to the mean sea level). As boundary conditions are treated for open liquid boundaries, in particular they are non reflecting conditions (see subsubsections 5.5.5 and 5.5.7.2), the water can come in or come out freely. The influence of the choice for the initial conditions disappears after around one tidal cycle. There is only a transient period of time when the modelling of tides is not well reproduced, in particular water balances are not good inside the extent of the domain, but after one tidal cycle, it is OK.

The graphic outputs (variable and variable name in the parameter file) routinely viewed for this type of hydrodynamic study are: the water depth H; the horizontal velocity components U and V (averaged over the vertical); scalar velocity (magnitude of the vertically-averaged velocity vector) M; elevation of the seabed, B in general, O in this case (cf. sub-section 5.5.6); free-surface elevation, S in general, but N here (cf. sub-section 5.5.6) and the Courant number L.

For this numerical model and for a mean spring tide or a mean neap tide, the chosen time step (keyword TIME STEP) was 20 s, whereas for an exceptional spring tide it was 6 s.

In order to determine the maximum velocities, the computational results are written to the output file every 5 minutes (real time) = 15 × 20 s = 50 × 6 s (keyword GRAPHIC PRINTOUT PERIOD = 15 or 50 according to the chosen time step).

5.5.7.1 Physical parameters

Dissipation through bed friction was modelled using a uniform Strickler coefficient K over the entire study domain (LAW OF BOTTOM FRICTION = 3 and FRICTION COEFFICIENT VARIABLE IN SPACE = NO, default value).

The Coriolis effect was taken into account (keyword CORIOLIS = YES) with the value of the Coriolis coefficient equal to 1.10×10^{-4}. (= $2\omega\sin(l)$ value obtained for a latitude l equal to 49°N, with $\omega = 2\pi/T$, T = 86,164 s, the duration of a sidereal day. This value is thus assigned to the keyword CORIOLIS COEFFICIENT).

Meteorological effects (wind or atmospheric pressure) were not taken into account in the numerical simulations (keywords WIND and AIR PRESSURE = NO, default values).

No specific turbulence model was employed (value left at 1 by default for keyword TURBULENCE MODEL). Therefore, a constant coefficient of viscosity equal to the default value of 10^{-4} is applied over the whole domain (keyword VELOCITY DIFFUSIVITY).

5.5.7.2 Numerical parameters

The boundary conditions for the open liquid boundaries at which the tidal conditions (depth and/or velocity) were imposed, were treated using the Thompson method [G7] with calculation of characteristics (keyword OPTION FOR LIQUID BOUNDARIES = 2).

The discretisation uses linear triangular elements (DISCRETIZATION IN SPACE = 11; 11 default values) with matrix storage by segments to optimise calculation times (keyword MATRIX STORAGE = 3, default value). For the suppression of free-surface parasite oscillations, the keyword FREE SURFACE GRADIENT COMPATIBILITY was taken to equal 0.9 (recommended value).

Equations were solved in the wave equation form (keyword TREATMENT OF THE LINEAR SYSTEM = 2).

The numerical schemes used were: the method of characteristics for the advection of velocities and, for the water depth, a conservative scheme (keyword TYPE OF ADVECTION = 1; 5 default values).

For solving the propagation step, the conjugate gradient method was the chosen solver (keyword SOLVER = 1), with an accuracy of 10^{-4} which is the default value (keyword SOLVER ACCURACY), a maximum number of 500 iterations (keyword MAXIMUM NUMBER OF ITERATIONS FOR SOLVER) and a diagonal preconditioning (keyword PRECONDITIONING = 2, default value).

5.5.8 Treatment of tidal flats

The tidal flats (keyword TIDAL FLATS = YES, default value) were treated using the first treatment option, which consists of the correction of the free surface computations by elements, to take account of the tidal flats (keyword OPTION FOR THE TREATMENT OF TIDAL FLATS = 1, default value).

In order to ensure that water depths remain positive over the entire study domain (particularly given the presence of tidal flats), an innovation, introduced from TELEMAC version 6.0 onward, was used. This consists of taking the combination of the following four keywords: no upwind for SUPG (SUPG OPTION = 0; 0), total mass-lumping for depth (keyword MASS-LUMPING ON H = 1.), correction of velocities at the points with imposed depth where the continuity equation has not been solved (keyword CONTINUITY CORRECTION = YES) and a treatment to suppress negative depths by a limitation of fluxes (keyword TREATMENT OF NEGATIVE DEPTHS = 2).

5.5.9 Calibration

To test the validity of the model, various comparisons were made between the model results and the sea level data or velocity measurements.

5.5.9.1 Sea levels

The levels calculated with TELEMAC-2D were compared to the sea levels characteristic of astronomical tides for Paimpol, the Isle of Bréhat (Men Joliguet), Roches Douvres and Les Héaux-de-Bréhat, as indicated by the SHOM data (source [C4] « ©SHOM-2010 » for the three first ports). In particular, the TELEMAC-2D model has been calibrated with the data of the Isle of Bréhat for sea levels. The other ports are used to validate the model.

Table C6 gives a quantification of the variance between the TELEMAC-2D numerical model results and the SHOM data.

The following abbreviations are used in Table C6:
- HW: high water (in m CD),
- LW: low water (in m CD),
- ES: exceptional spring tide,
- MS: mean spring tide,
- MN: mean neap tide.

ES	HW (m CD)			LW (m CD)			Tidal range (m)		
	SHOM	TEL2D	Var.	SHOM	TEL2D	Var.	SHOM	TEL2D	Var.
Paimpol	11,92	11,79	0,13	0,11	0,13	-0,02	11,81	11,66	0,15
Isle of Bréhat	11,68	11,66	0,02	0,10	0,08	0,02	11,58	11,58	0,00
Les Héaux-de-Bréhat	10,95	10,84	0,11	0,10	0,08	0,02	10,85	10,76	0,09
Roches Douvres	10,80	10,71	0,09	0,03	0,14	-0,11	10,77	10,57	0,20

MS	HW (m CD)			LW (m CD)			Tidal range (m)		
	SHOM	TEL2D	Var.	SHOM	TEL2D	Var.	SHOM	TEL2D	Var.
Paimpol	10,80	10,65	0,15	1,35	1,33	0,02	9,45	9,32	0,13
Isle of Bréhat	10,55	10,52	0,03	1,30	1,27	0,03	9,25	9,25	0,00
Les Héaux-de-Bréhat	9,80	9,78	0,02	1,20	1,22	-0,02	8,60	8,56	0,04
Roches Douvres	9,80	9,65	0,15	1,30	1,25	0,05	8,50	8,40	0,10

MN	HW (m CD)			LW (m CD)			Tidal range (m)		
	SHOM	TEL2D	Var.	SHOM	TEL2D	Var.	SHOM	TEL2D	Var.
Paimpol	8,35	8,25	0,10	3,85	3,81	0,04	4,50	4,44	0,06
Isle of Bréhat	8,15	8,14	0,01	3,75	3,74	0,01	4,40	4,40	0,00
Les Héaux-de-Bréhat	7,60	7,60	0,00	3,55	3,55	0,00	4,05	4,05	0,00
Roches Douvres	7,60	7,51	0,09	3,55	3,54	0,01	4,05	3,97	0,08

Table C6: Comparison of tide levels provided by SHOM (source [C4] « ©SHOM-2010 ») with levels simulated in TELEMAC-2D, for various tide conditions and ports within the study zone.

To adapt the tidal range, the coefficient CTIDE (cf. §5.5.6) is modified (to the values 1.164, 1.046 and 1.022 respectively for an exceptional spring tide, mean spring tide and mean neap tide).

The tidal ranges, as well as the High Water (HW) and Low Water (LW) levels were very well replicated by the model for an exceptional spring tide (ES), a mean spring tide (MS) and mean neap tide (MN). In general, the variance is less than 10 cm at Les Héaux-de-Bréhat and at Men Joliguet, the closest port to the potential installation site on the Isle of Bréhat. For the port of Paimpol and the same three types of tides, the variances are slightly greater (generally less than 15 cm), whereas for Roches Douvres the tidal ranges are worse replicated.

5.5.9.2 Current velocities

The current measurements resulting from the two campaigns carried out in April 2005 [C1] and in the spring of 2008 [C2] were used in this study to calibrate and validate the model to the best level possible. The locations of the measurement sampling points are indicated on Figure C1. The model has been visually calibrated with ADCP measurements at two locations during a four-day period from June 3rd to 6th 2008 that corresponds to spring tides.

Dissipation by bed friction is modelled by a Strickler coefficient *K* that is uniform over the whole study domain and set at 27 $m^{1/3}/s$. The choice of a Strickler coefficient value of 27 (rather than 25 or 30) was validated by the comparison of the numerical simulations of current velocities performed in TELEMAC-2D with the ADCP measurements of current velocities during periods of spring tides and neap tides. Several exact tide dates were isolated, corresponding to periods of spring tides (7th to 11th

April 2005, 5th to 9th April 2008, 4th to 8th May 2008 and 3rd to 6th June 2008). For each of the above periods, a comparison was then made of the evolution over time of the magnitude of the vertically-averaged velocity vector of the ADCP measurements (red crosses) with the simulations obtained by the TELEMAC-2D numerical model (blue, sky blue or black lines) in Figures C3 to C10. Moreover, Figures C11 to C18 show same comparisons during one tidal cycle – flood/ebb – with a zoom on 8th April 2005, 6th April 2008, 5th May 2008 and 4th June 2008 afternoons. Further comparison was made of the point cloud of ADCP-provided measurements of the vertically averaged velocity with the current roses obtained in the TELEMAC-2D numerical model (Figures C19 to C26).

The qualitative agreement between velocities simulated by the model and the measurements is quite satisfactory with regard to measurement points 1 and 2 of the April 2005 and spring 2008 campaigns (in particular for direction). Nevertheless, when replicating maximum velocity during flood tide, the maximum velocity is not well replicated during ebb (and *vice versa*).

Tables C 7 to C 9 show quality indices (see Appendix G1 for more information about calculated quality indices) at ADCP location 2 for ADCP during the single tidal cycle shown on Figures C11 to C16 in 2008. Only this location has been chosen because ADCP 1 missed one velocity measurement every hour (while measuring wave parameters). Sometimes, one phase shift may appear (10 or 20 min), but no correction has been done to improve the calculated quality indices. The comparison shows medium agreement between model outputs and measurements. The RMS error of current speeds remains relatively high (from 0.2 to 0.3 m/s generally), but this can be partly explained by the nature of the measured tidal speeds. The signal is rather noisy due to the turbulent nature of the flow. Besides, the model only accounts open boundary conditions to force tide, whereas on-site measurements capture wind, wave and atmospheric pressure effects on currents. As it is difficult to replicate maximum velocity during flood and ebb with the same friction coefficient, it is then difficult to conclude correctly when considering bias.

Quality indice	Strickler = 25 $m^{1/3}/s$	Strickler = 27 $m^{1/3}/s$	Strickler = 30 $m^{1/3}/s$
Bias or mean error	-0.03	0.02	0.08
Non dimensional bias	-0.02	0.01	0.06
RMS error	0.20	0.21	0.23
Non dimensional RMS error	0.15	0.15	0.17
Pearson correlation coefficient	0.95	0.94	0.94

Table C7: Quality indices of computed tidal velocity intensities compared to ADCP location 2 raw measurements during one tidal cycle (April 6th 2008) for Strickler coefficient = 25, 27 and 30 $m^{1/3}/s$.

Quality indice	Strickler = 25 $m^{1/3}/s$	Strickler = 27 $m^{1/3}/s$	Strickler = 30 $m^{1/3}/s$
Bias or mean error	0.03	0.07	0.14
Non dimensional bias	0.02	0.05	0.10
RMS error	0.18	0.20	0.24
Non dimensional RMS error	0.14	0.15	0.18
Pearson correlation coefficient	0.95	0.95	0.95

Table C8: Quality indices of computed tidal velocity intensities compared to ADCP location 2 raw measurements during one tidal cycle (May 5th 2008) for Strickler coefficient = 25, 27 and 30 $m^{1/3}/s$.

Quality indice	Strickler = 25 $m^{1/3}/s$	Strickler = 27 $m^{1/3}/s$	Strickler = 30 $m^{1/3}/s$
Bias or mean error	0.18	0.23	0.30
Non dimensional bias	0.15	0.19	0.25
RMS error	0.27	0.31	0.38
Non dimensional RMS error	0.23	0.26	0.32
Pearson correlation coefficient	0.95	0.95	0.95

Table C9: Quality indices of computed tidal velocity intensities compared to ADCP location 2 raw measurements during one tidal cycle (June 4th 2008) for Strickler coefficient = 25, 27 and 30 $m^{1/3}/s$.

5.5.10 Analysis

Various characteristic tidal conditions were simulated:

- an exceptional spring tide,
- a mean spring tide,
- a mean neap tide.

Two locations (A and B, see Figure C1) are introduced to give results for some locations other than the four ADCP locations.

Points	WGS84		NTF Lambert 1 North		Depth
	degrees and decimal minutes		metres		(m CD)
	Longitude West	Latitude North	East	North	
A	2°53.411'	48°54.532'	217188	147558	-35
B	2°53.376'	48°54.547'	217232	147584	-37,5

Table C10: Coordinates of the two locations A and B.

Current fields for the study zone are presented hour-by-hour in Figures C27 to C32: for an exceptional spring tide (Figures C27 and C28); a mean spring tide (Figures C29 and C30) and a mean neap tide (Figures C31 and C32). High water at Paimpol was considered as the reference.

For three ADCP locations and locations A and B, the mean direction of the current flows along the NW-SE axis; the ebb current flows towards the North-West and the flood current to the South-East, with the passage from South-East to North-West occurring through the North.

Maximum current fields, during the flood and ebb tides (defined with reference to the instants of occurrence of high and low waters on the zone), are represented in Figures C33 to C35 for the three schematic tide conditions (an exceptional spring tide, a mean spring tide and a mean neap tide). These fields do not correspond to an instantaneous flow situation; they are constituted from the maximum velocities. Velocities are generally higher during the flood than during the ebb.

Figures C36 to C38 illustrate the time series of the magnitude of velocity, at six locations in the study zone (the four ADCP locations and two locations close to a potential site of installation in the south-west quarter of the crustacean reserve), for three types of tides (an exceptional spring tide, a mean spring tide and a mean neap tide).

Figures C39 to C41 illustrate current roses, at six locations in the study zone (the four ADCP locations and two locations in the south-west quarter of the crustacean reserve), for three types of tides (an exceptional spring tide, a mean spring tide and a mean neap tide).

Table C11 gives the maximum velocities (averaged over the vertical), during a tide cycle at the six locations, for the three types of schematic tide conditions – exceptional spring tide, mean spring tide and mean neap tide.

Location	Exceptional Spring (ES)		Mean Spring (MS)		Mean Neap (MN)	
	(m/s)					
	Flood	Ebb	Flood	Ebb	Flood	Ebb
1 in 2008	2,7	2,5	2,3	2,1	1,2	1,1
2 in 2008	2,5	2,2	2,2	1,9	1,1	0,9
1 in 2005	2,3	2,3	2,0	2,0	1,0	1,0
2 in 2005	2,0	1,8	1,7	1,5	0,8	0,7
A	3,0	2,5	2,6	2,2	1,3	1,1
B	2,9	2,4	2,5	2,1	1,3	1,1

Table C11: Magnitude of maximum flow velocities (averaged over the vertical), during flood and ebb, at six locations in the study zone tested for three tidal conditions.

5.5.11 Uncertainties

In this section, account is given of the main sources of uncertainties concerning the results presented.

Bathymetric data for the study zone was obtained from two principal sources: commercially available SHOM data (digital bathymetric grids, DTMs, charts), with regard to Chart Datum, and measurements carried out by CREOCEAN for EDF that were first expressed relative to NGF-IGN69 zero, then reduced to Chart Datum taking Paimpol as the reference port (translation of +6.65 m). The coherence or continuity (in position and level) of the data is not always perfectly correct. Moreover, there are no SHOM probes in some relatively large areas of the Bréhat zone (areas that can reach a few km^2).

A second limitation is that the model takes into account only four harmonic constituents (M2, S2, N2 and M4) to represent the tide: this representation could be enhanced by taking account of other components of the tidal signal.

In addition, this study used the TELEMAC-2D modelling software, which solves the Saint-Venant two-dimensional equations based on the shallow-water assumption (shallow waters being, in principle, satisfactory for tide representation) [C9]. In order to more closely represent flow velocities in the zone, three-dimensional modelling is performed with the TELEMAC-3D software (see subsection 5.6), which solves the Navier-Stokes equations.

5.5.12 Computation time

The TELEMAC-2D computations were carried out on the EDF R&D IBM Debian “Ivanoé” cluster (200 TFlops). The processor specifications are as follows: 24 GB RAM per node (1 node = 2 hexa-core processors, running at 2.93 GHz). The CPU time required for a 4 or 5 day simulation was approximately 2 hours for a 1-processor run.

5.5.13 Conclusion

The present study enabled the characterisation of tidal flow conditions in the Paimpol-Bréhat zone. It was based on numerical modelling at local scale. The numerical models were built with the TELEMAC-2D hydro-informatics software developed at the LNHE.

Calibration results were given in terms of tidal range, sea level and current velocities. For different types of schematic tide (an exceptional spring tide, a mean spring tide and a mean neap tide), various results were also given: current fields hour-by-hour; maximum current fields during flood and ebb across the area; time series of magnitude of velocity; current roses and maximum velocities during flood and ebb for specific locations in the area.

5.5.14 Figures

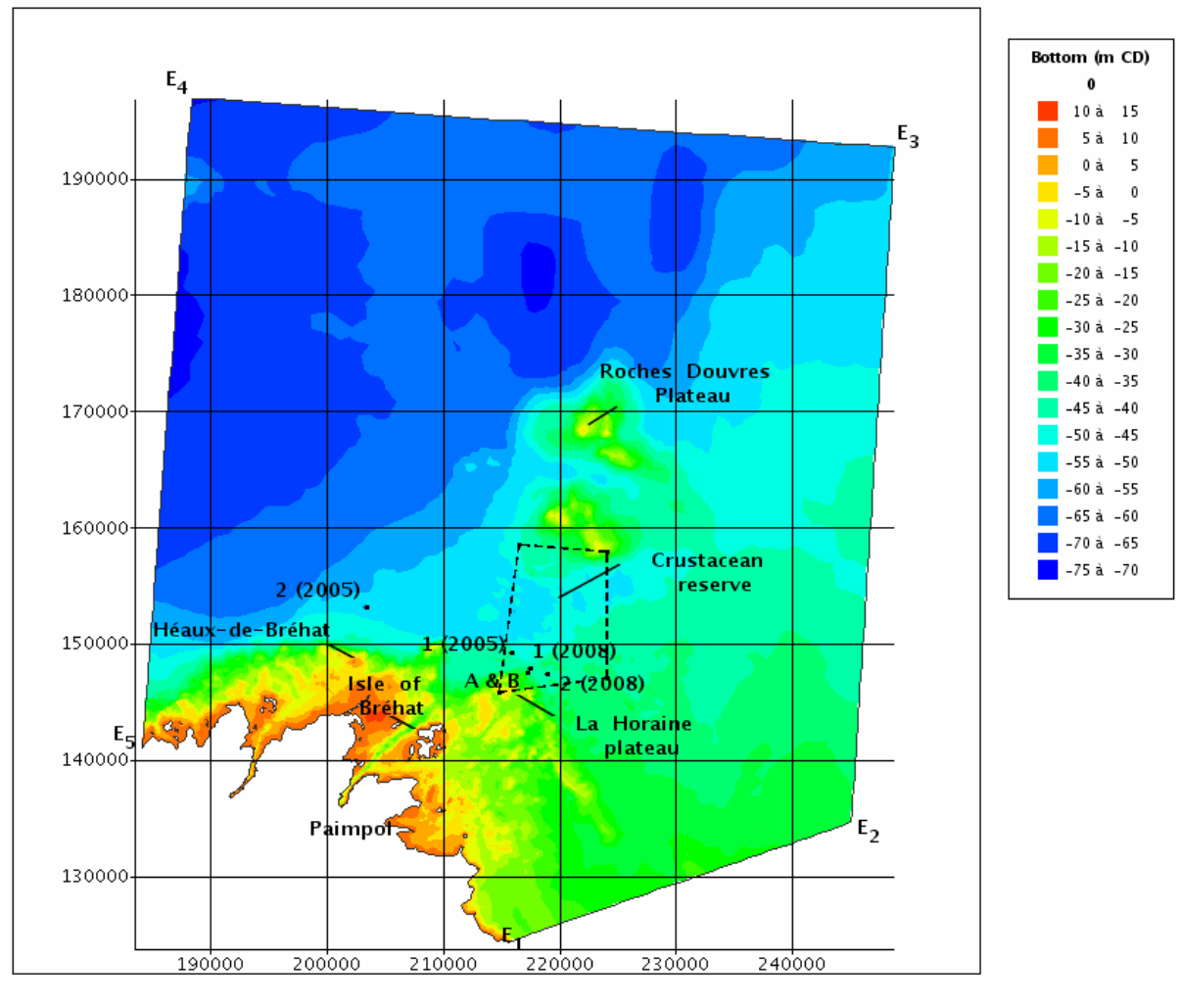

Figure C1: Bathymetry of Paimpol-Bréhat model and location of ADCP deployment.

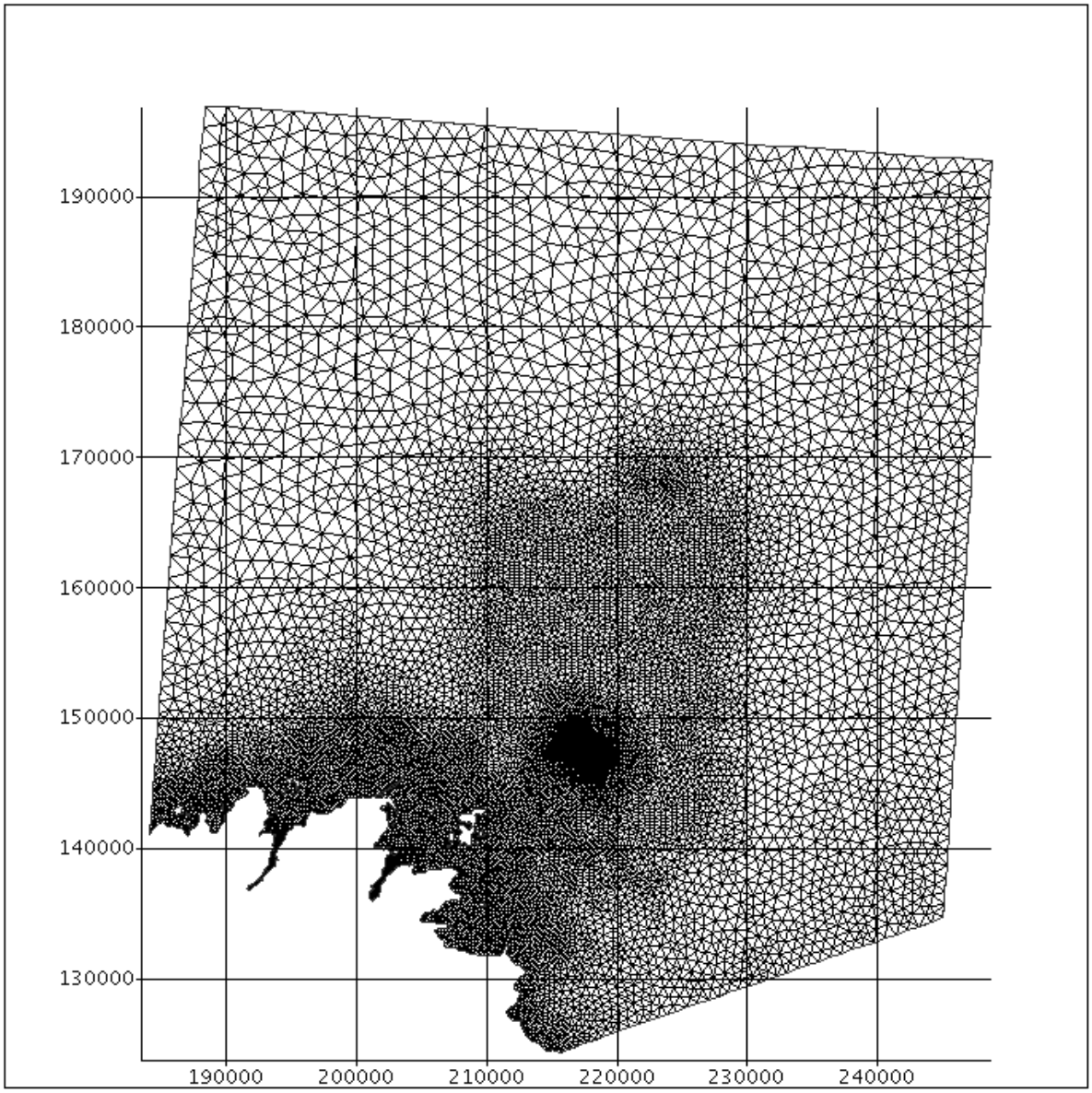

Figure C2: Mesh of Paimpol-Bréhat model.

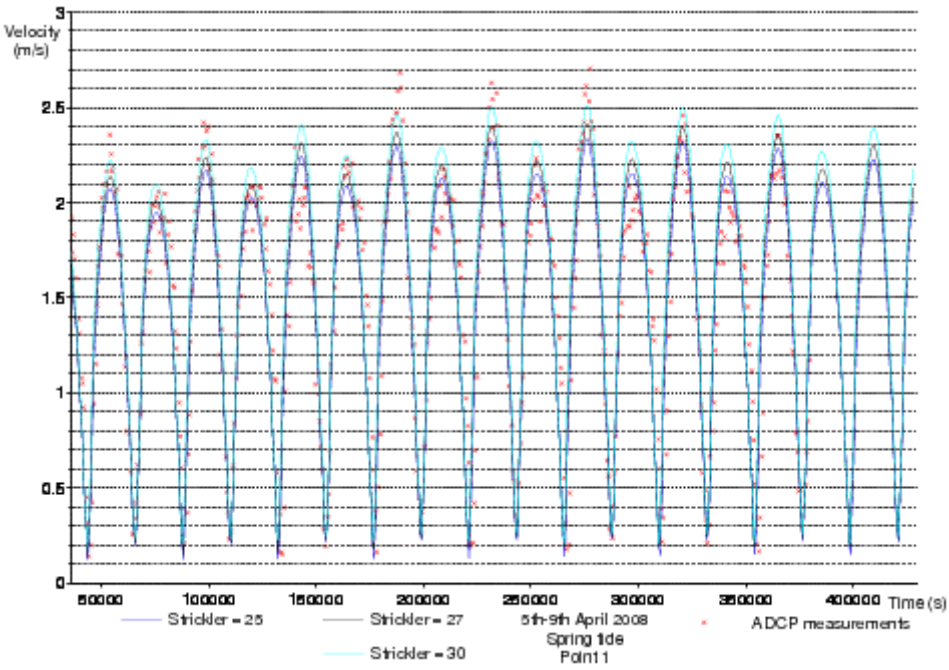

Figure C3: Magnitude of (vertically averaged) current velocity time series. Comparison between ADCP measurements (in red) and Telemac-2D results from April 5th to 9th 2008 at location 1.

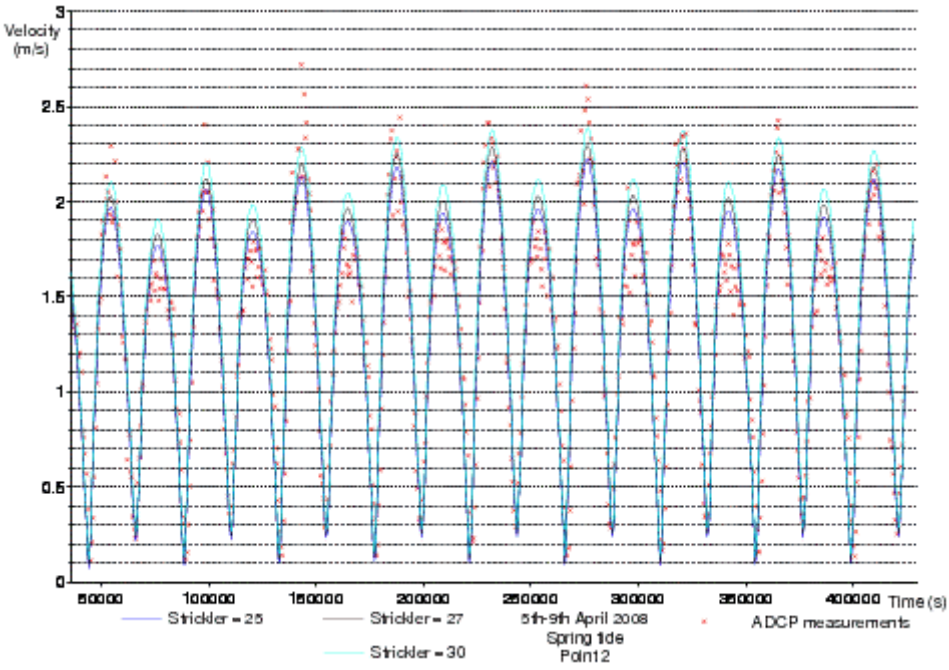

Figure C4: Magnitude of (vertically averaged) current velocity time series. Comparison between ADCP measurements (in red) and Telemac-2D results from April 5th to 9th 2008 at location 2.

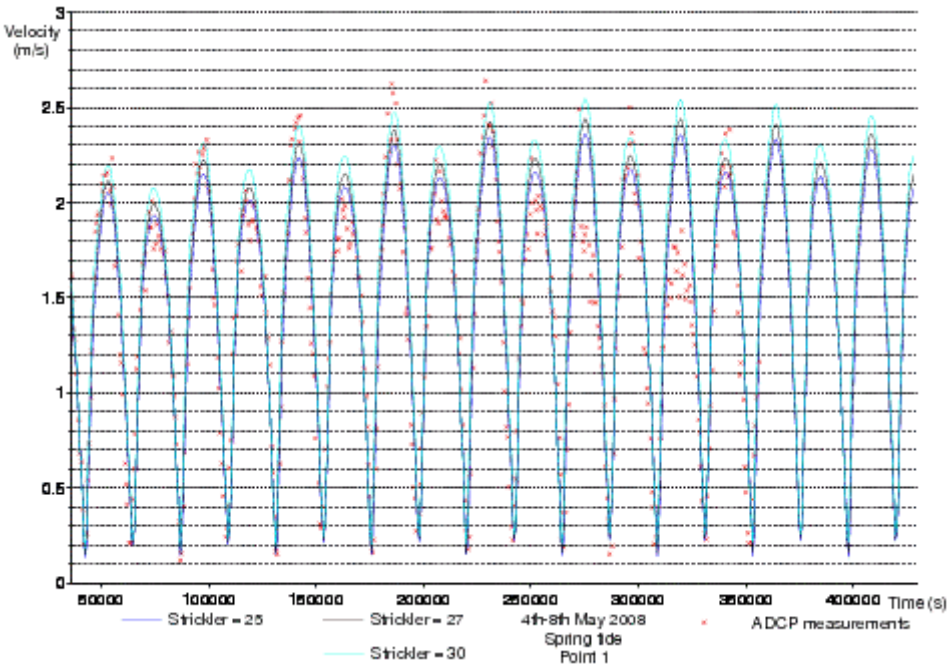

Figure C5: Magnitude of (vertically averaged) current velocity time series. Comparison between ADCP measurements (in red) and Telemac-2D results from May 4th to 8th 2008 at location 1.

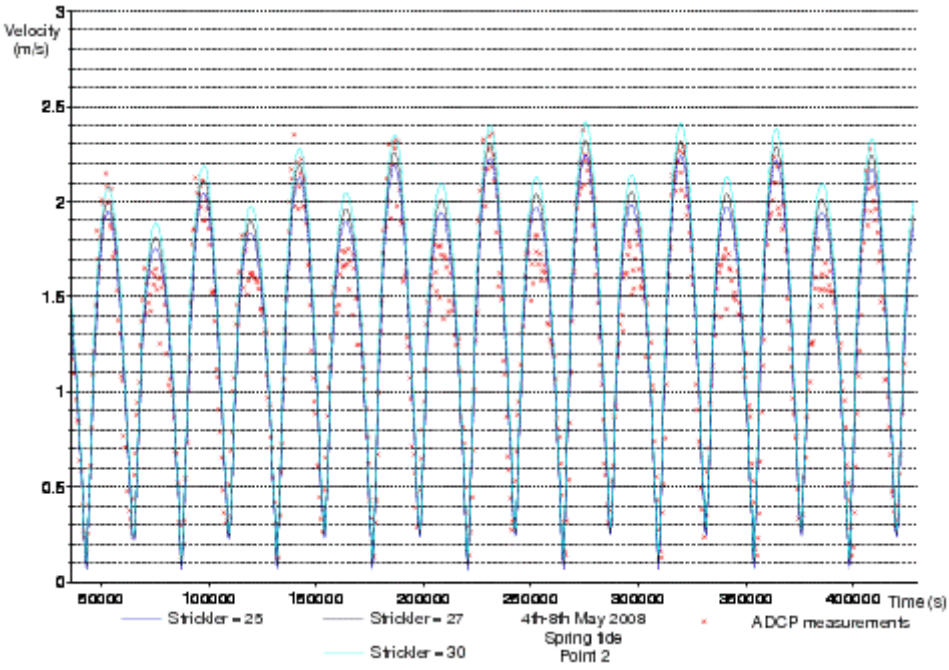

Figure C6: Magnitude of (vertically averaged) current velocity time series. Comparison between ADCP measurements (in red) and Telemac-2D results from May 4th to 8th 2008 at location 2.

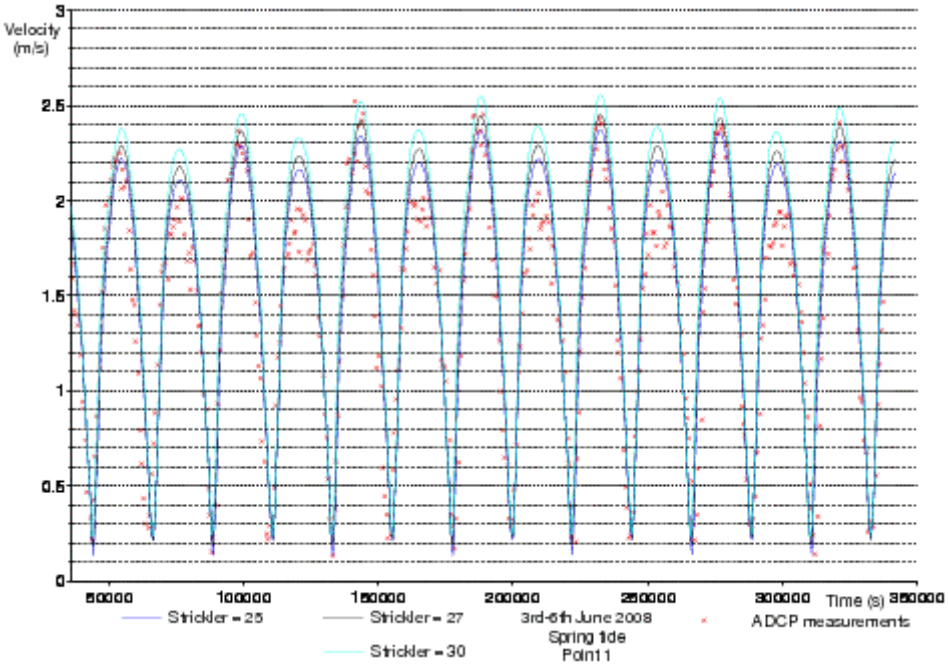

Figure C7: Magnitude of (vertically averaged) current velocity time series. Comparison between ADCP measurements (in red) and Telemac-2D results from June 3rd to 6th 2008 at location 1.

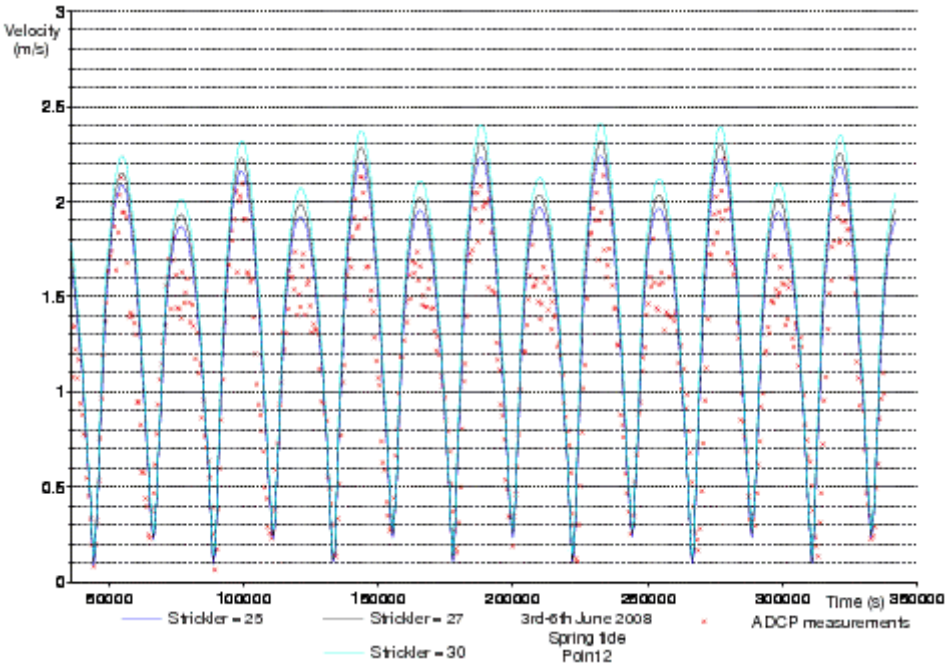

Figure C8: Magnitude of (vertically averaged) current velocity time series. Comparison between ADCP measurements (in red) and Telemac-2D results from June 3rd to 6th 2008 at location 2.

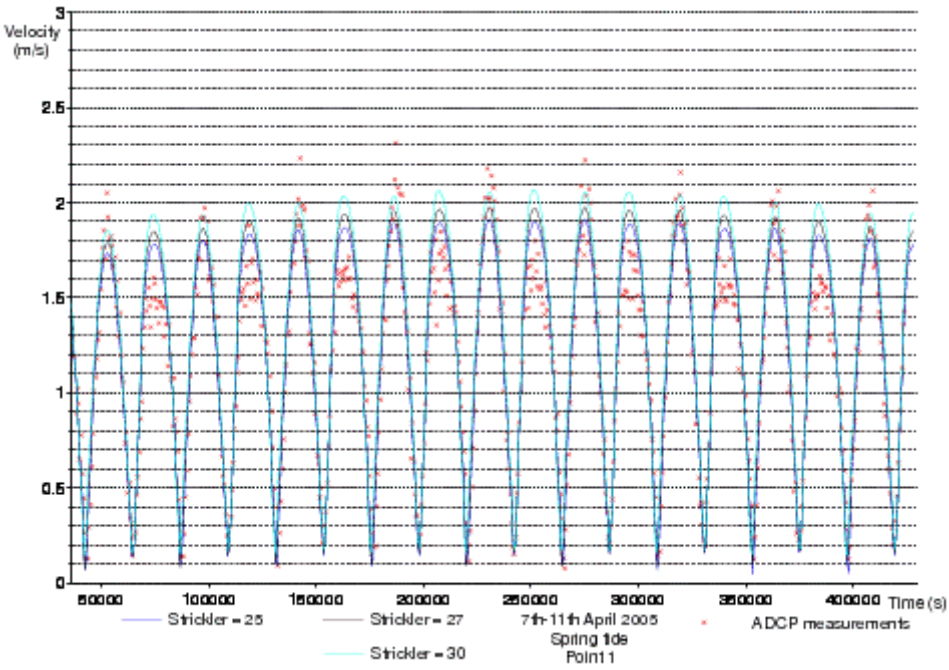

Figure C9: Magnitude of (vertically averaged) current velocity time series. Comparison between ADCP measurements (in red) and Telemac-2D results from April 7th to 11th 2005 at location 1.

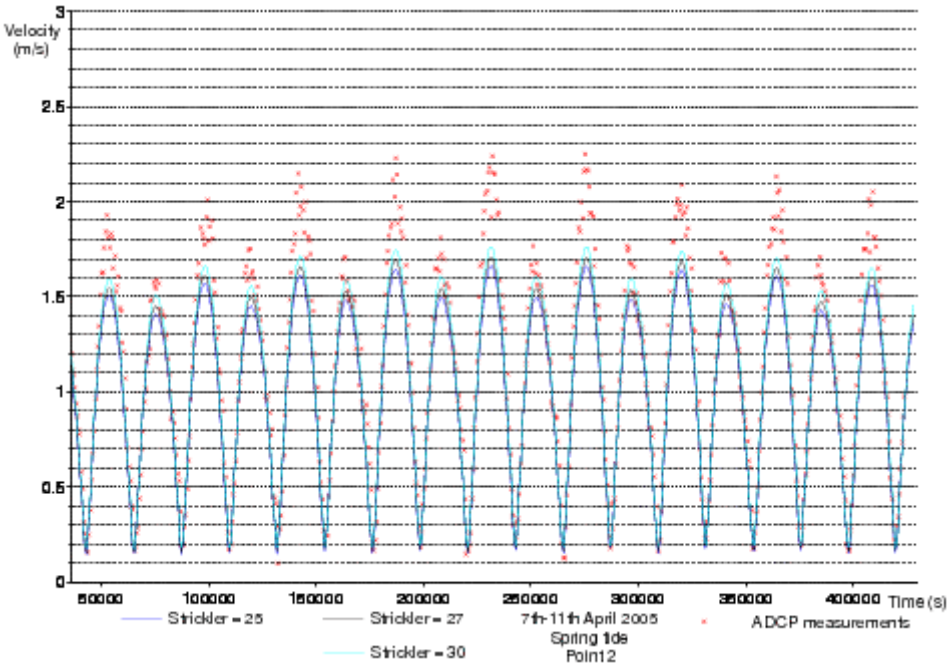

Figure C10: Magnitude of (vertically averaged) current velocity time series. Comparison between ADCP measurements (in red) and Telemac-2D results from April 7th to 11th 2005 at location 2.

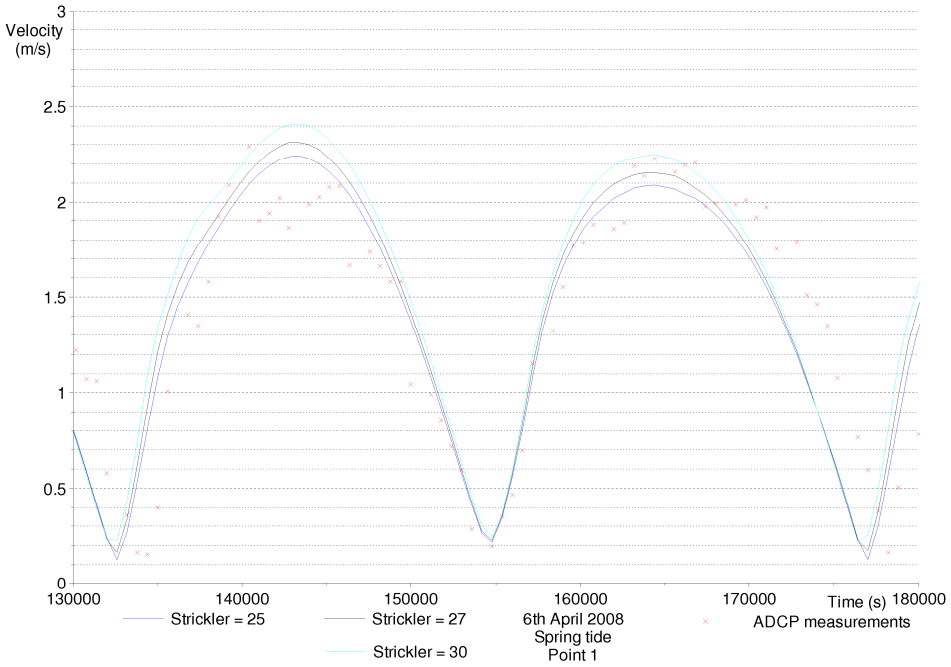

Figure C11: Magnitude of (vertically averaged) current velocity time series. Comparison between ADCP measurements (in red) and Telemac-2D results on April 6th 2008 afternoon at location 1.

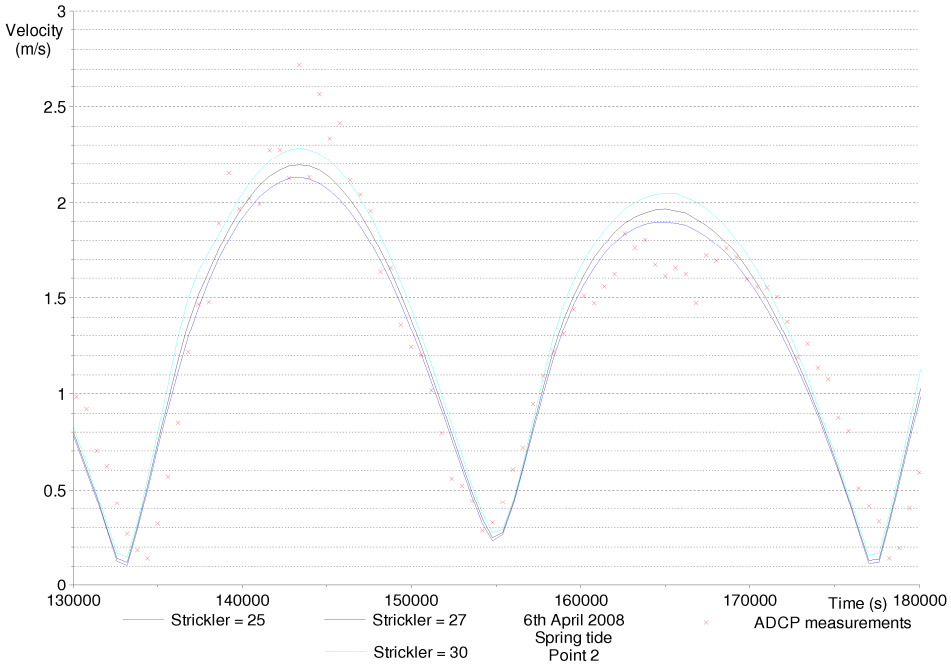

Figure C12: Magnitude of (vertically averaged) current velocity time series. Comparison between ADCP measurements (in red) and Telemac-2D results on April 6th 2008 afternoon at location 2.

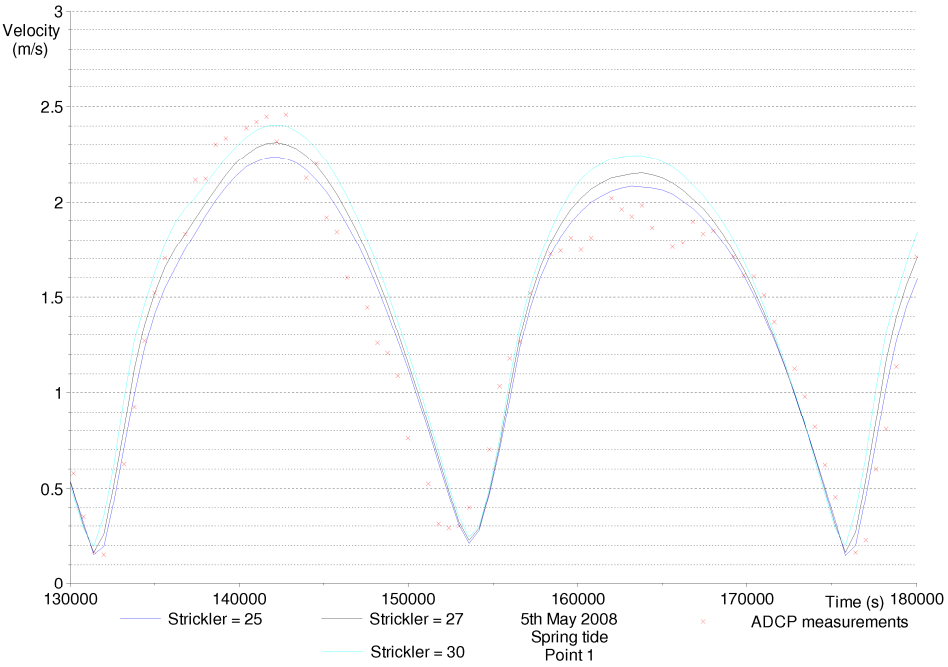

Figure C13: Magnitude of (vertically averaged) current velocity time series. Comparison between ADCP measurements (in red) and Telemac-2D results on May 5th 2008 afternoon at location 1.

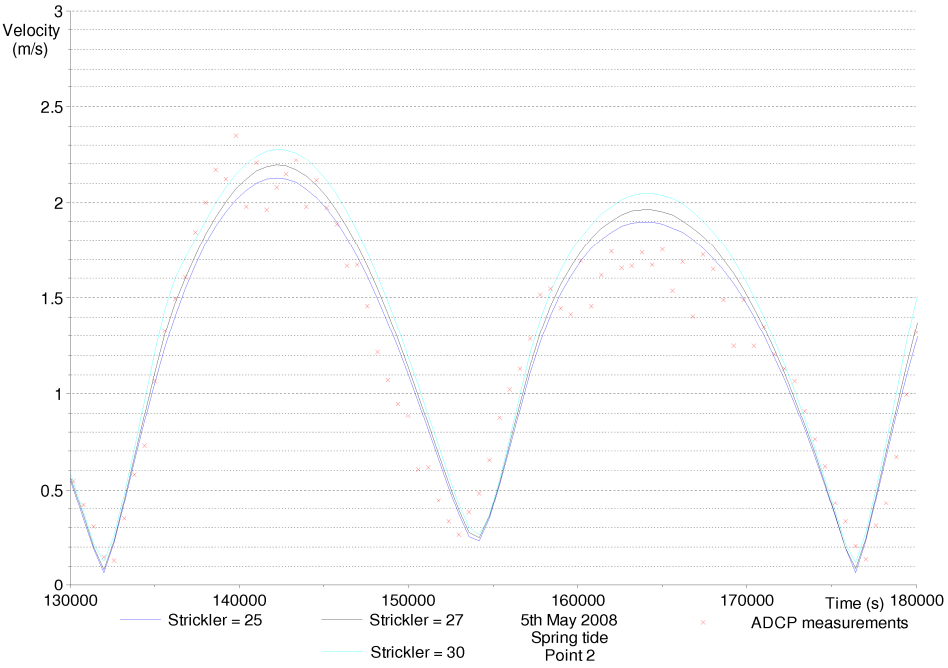

Figure C14: Magnitude of (vertically averaged) current velocity time series. Comparison between ADCP measurements (in red) and Telemac-2D results on May 5th 2008 afternoon at location 2.

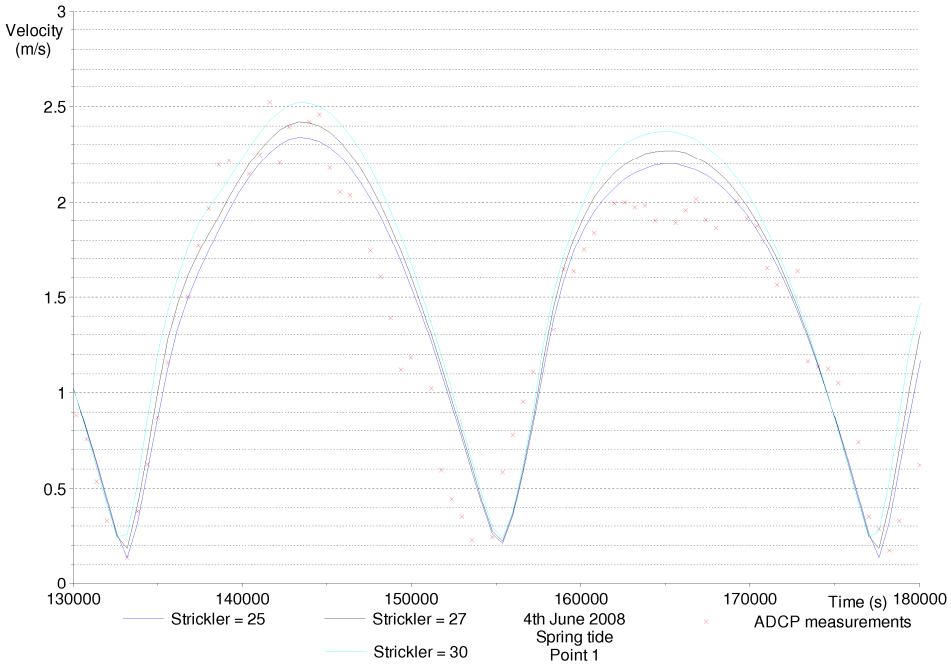

Figure C15: Magnitude of (vertically averaged) current velocity time series. Comparison between ADCP measurements (in red) and Telemac-2D results on June 4th 2008 afternoon at location 1.

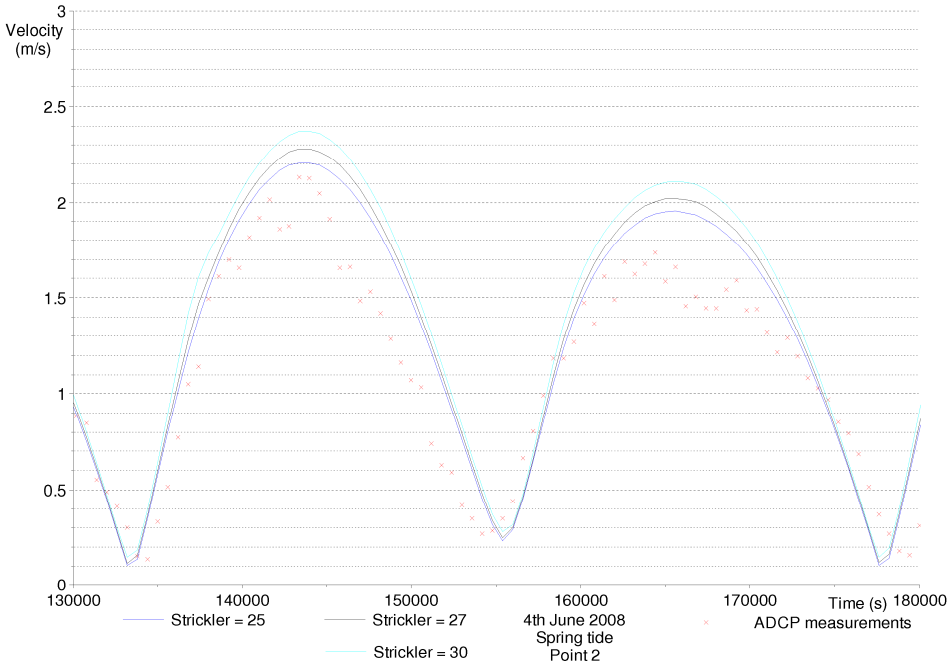

Figure C16: Magnitude of (vertically averaged) current velocity time series. Comparison between ADCP measurements (in red) and Telemac-2D results on June 4th 2008 afternoon at location 2.

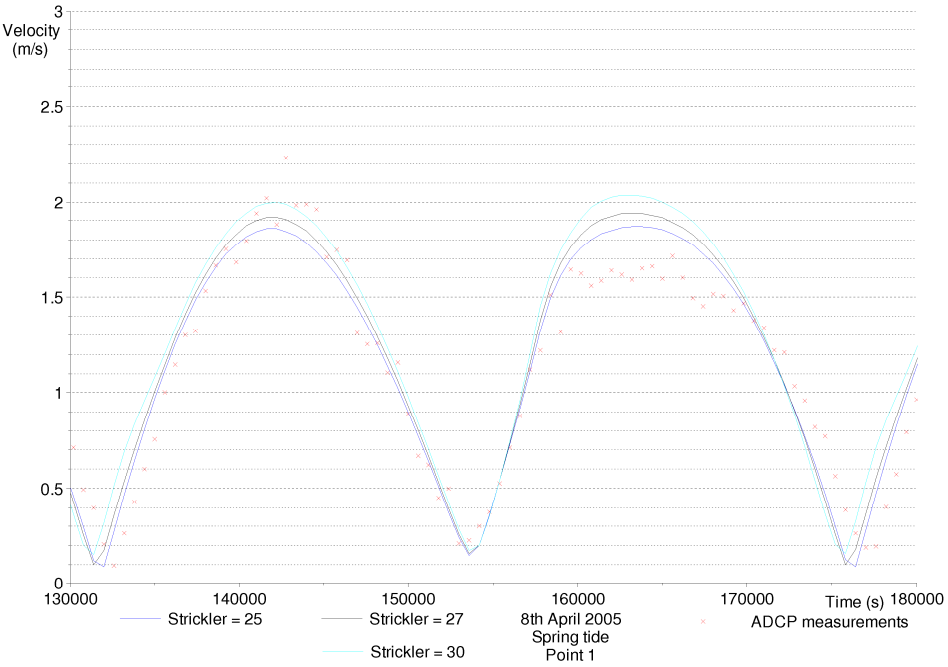

Figure C17: Magnitude of (vertically averaged) current velocity time series. Comparison between ADCP measurements (in red) and Telemac-2D results on April 8th 2005 afternoon at location 1.

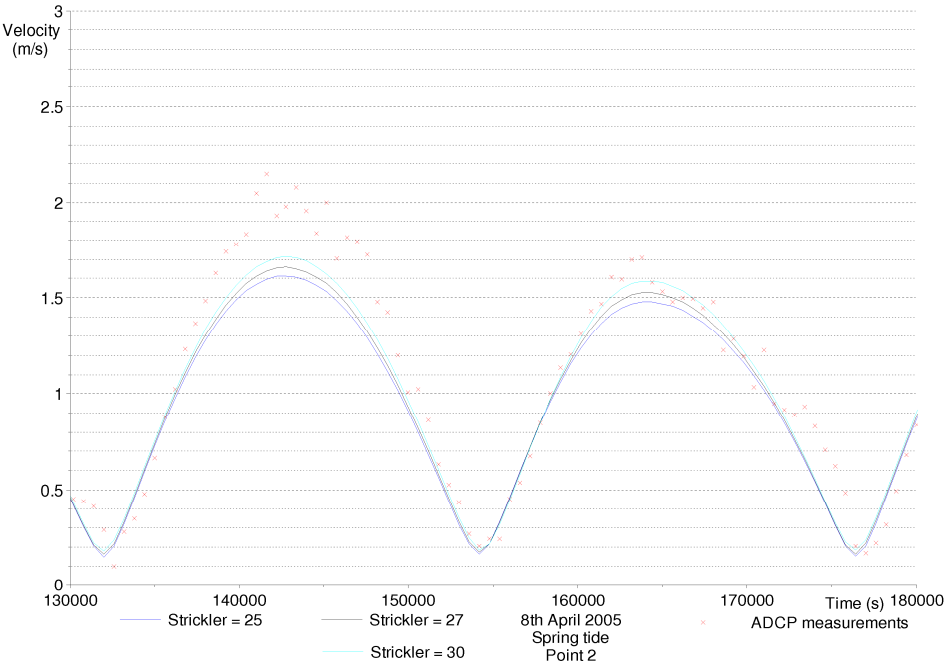

Figure C18: Magnitude of (vertically averaged) current velocity time series. Comparison between ADCP measurements (in red) and Telemac-2D results on April 8th 2005 afternoon at location 2.

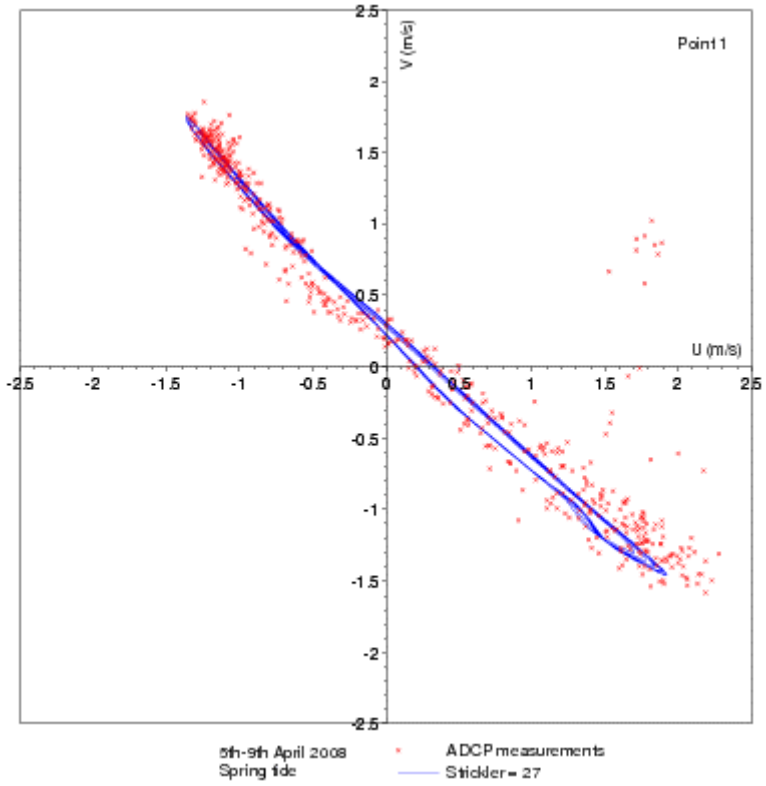

Figure C19: Tidal roses. Comparison between ADCP measurements (in red) and Telemac-2D results from April 5th to 9th 2008 at location 1.

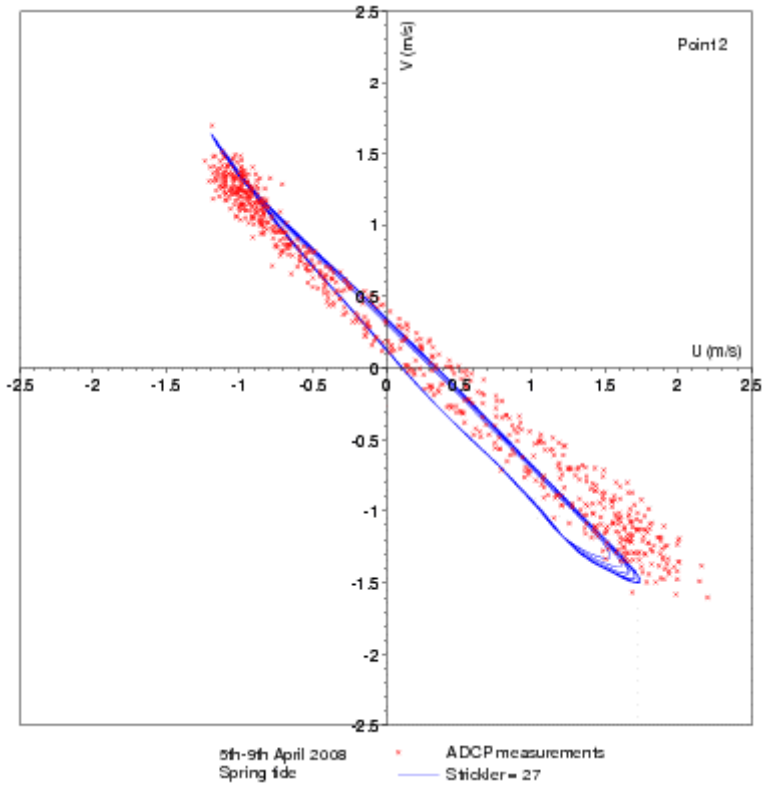

Figure C20: Tidal roses. Comparison between ADCP measurements (in red) and Telemac-2D results from April 5th to 9th 2008 at location 2.

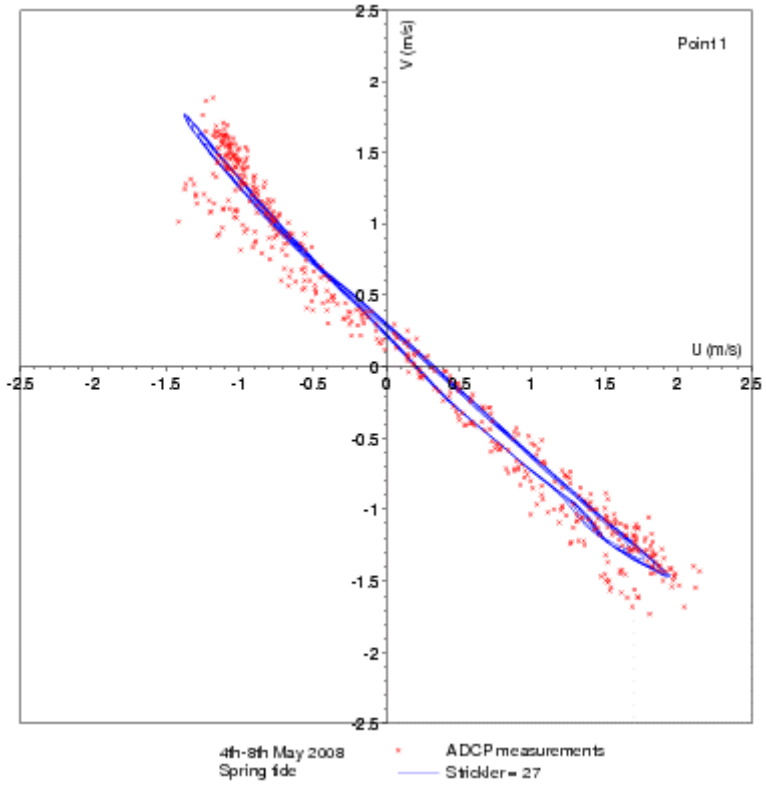

Figure C21: Tidal roses. Comparison between ADCP measurements (in red) and Telemac-2D results from May 4th to 8th 2008 at location 1.

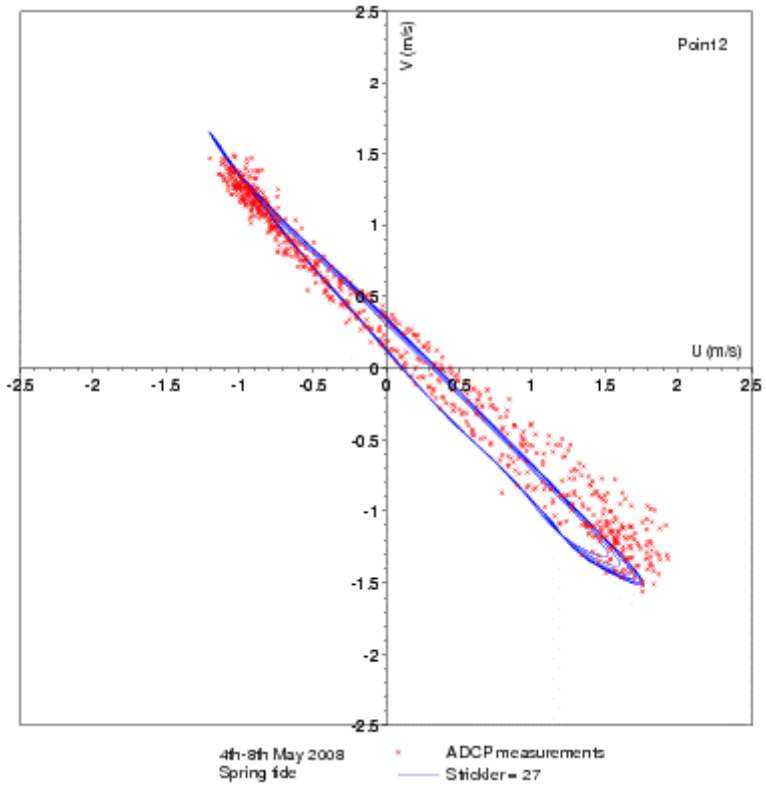

Figure C22: Tidal roses. Comparison between ADCP measurements (in red) and Telemac-2D results from May 4th to 8th 2008 at location 2.

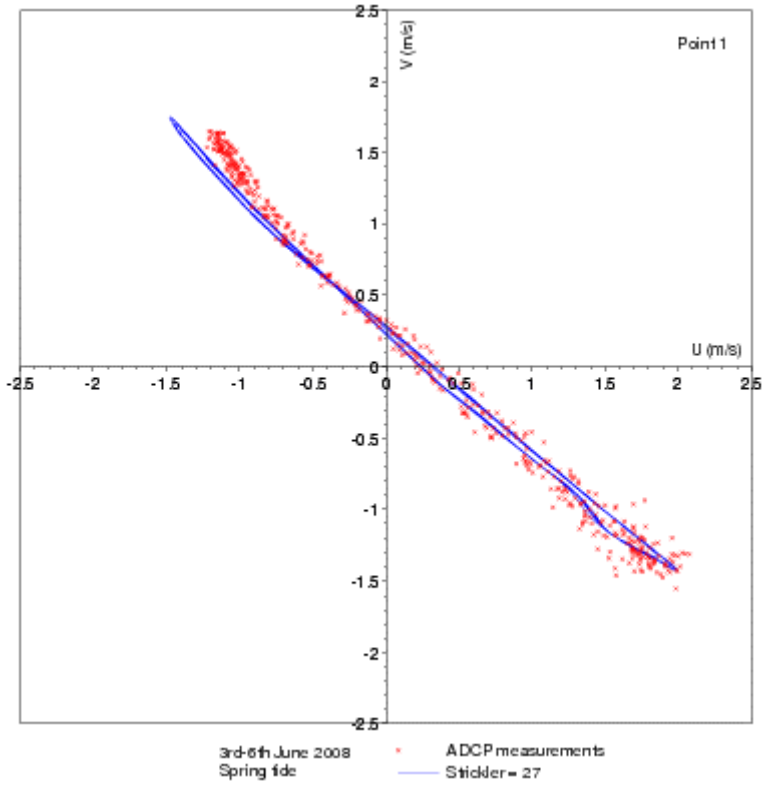

Figure C23: Tidal roses. Comparison between ADCP measurements (in red) and Telemac-2D results from June 3rd to 6th 2008 at location 1.

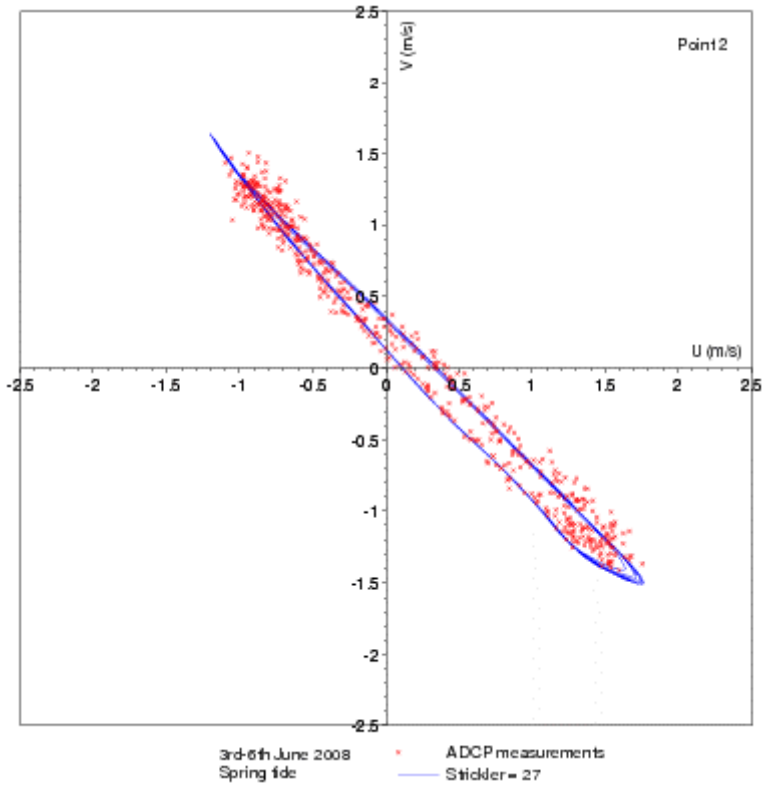

Figure C24: Tidal roses. Comparison between ADCP measurements (in red) and Telemac-2D results from June 3rd to 6th 2008 at location 2.

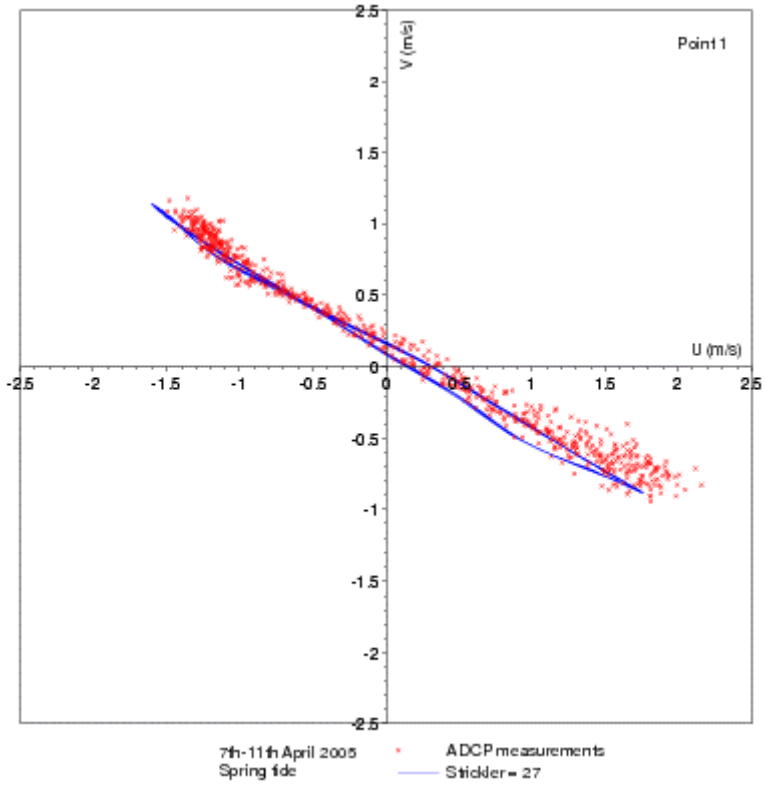

Figure C25: Tidal roses. Comparison between ADCP measurements (in red) and Telemac-2D results from April 7th to 11th 2005 at location 1.

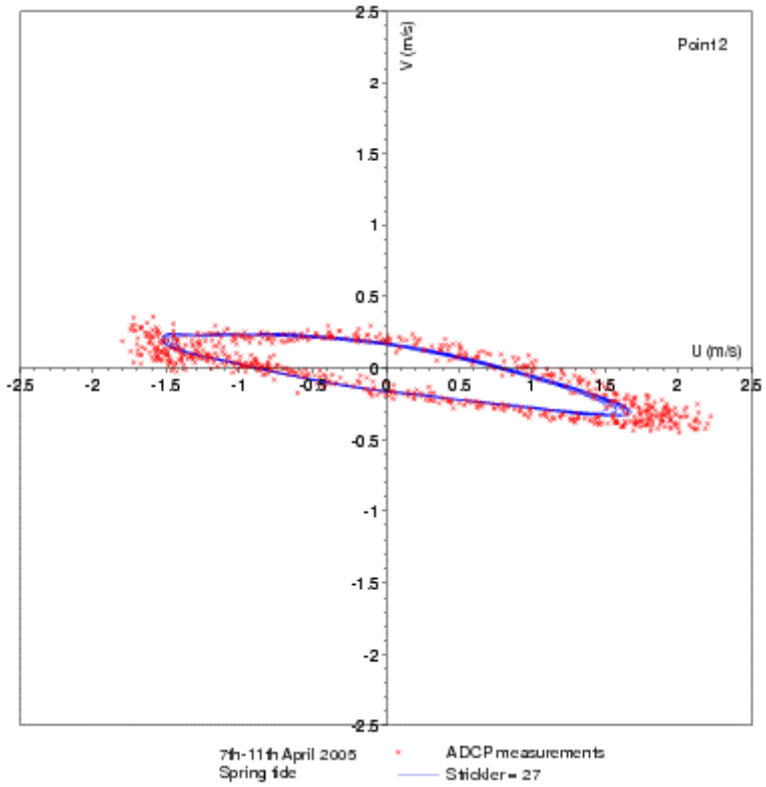

Figure C26: Tidal roses. Comparison between ADCP measurements (in red) and Telemac-2D results from April 7th to 11th 2005 at location 2.

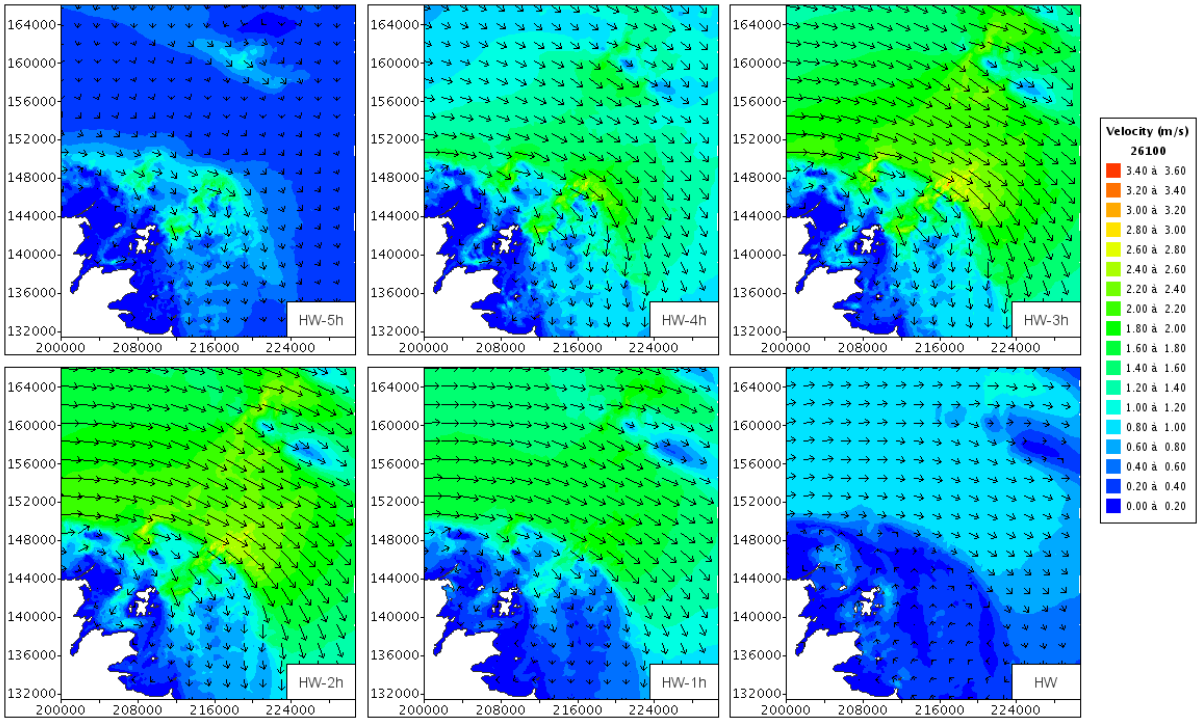

Figure C27: Current fields during an exceptional spring tide.

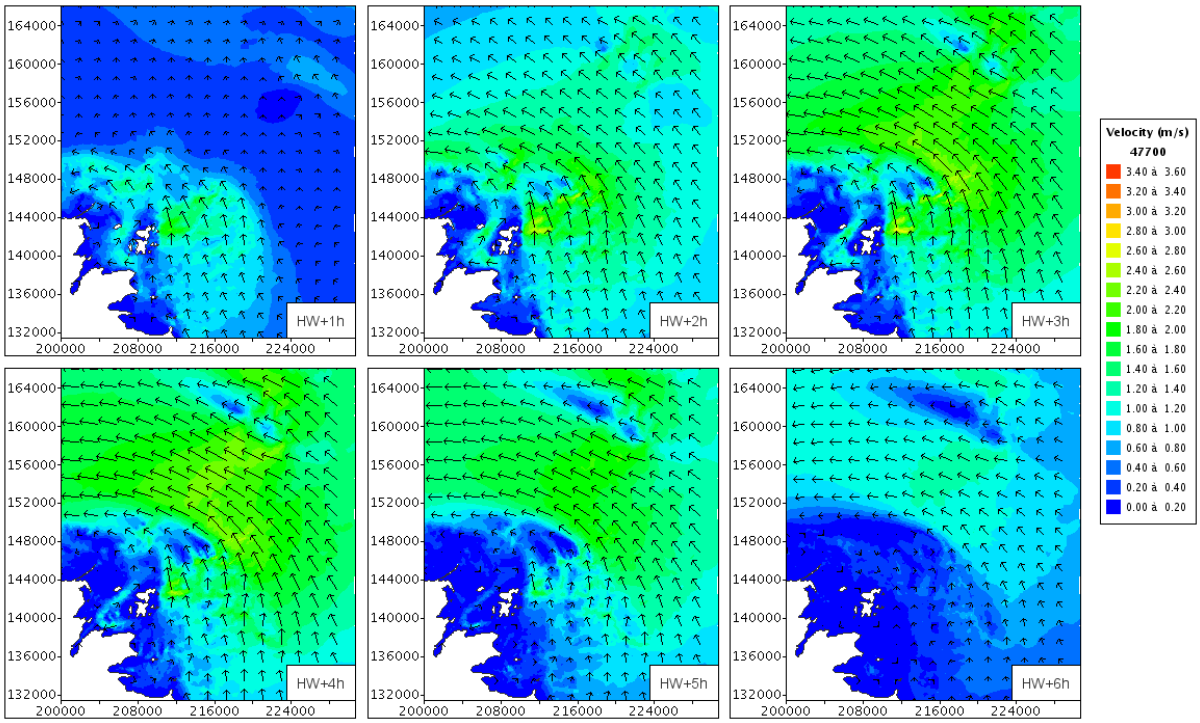

Figure C28: Current fields during an exceptional spring tide.

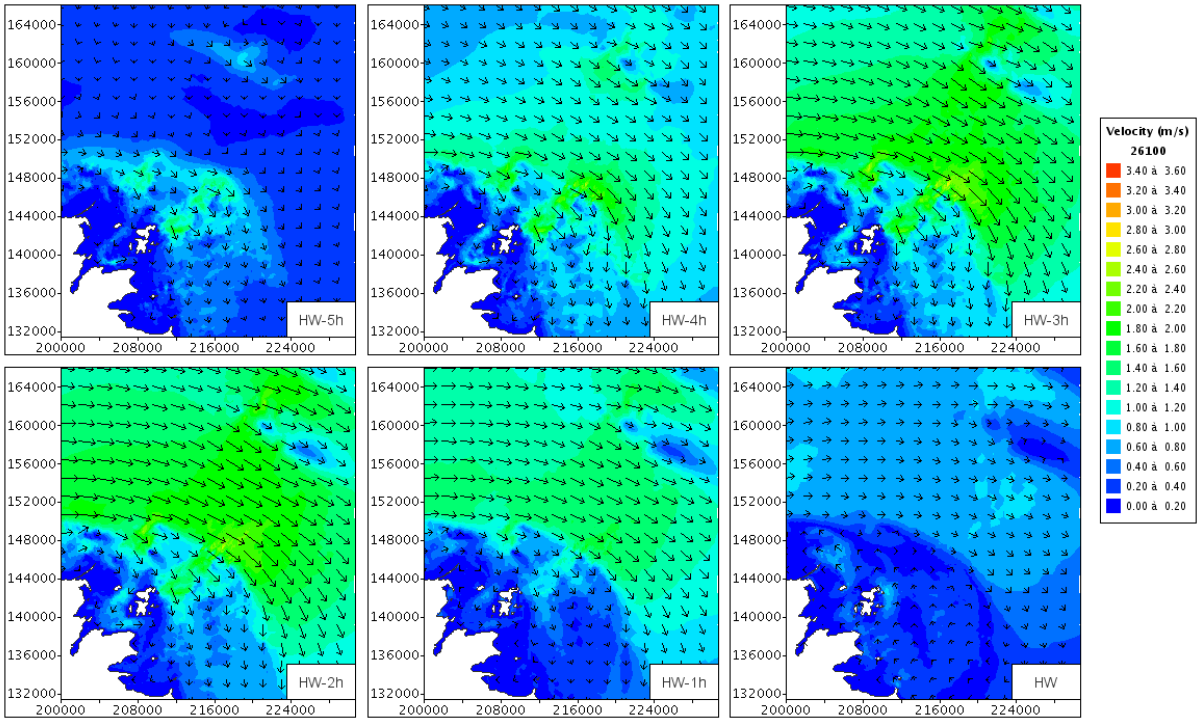

Figure C29: Current fields during a mean spring tide.

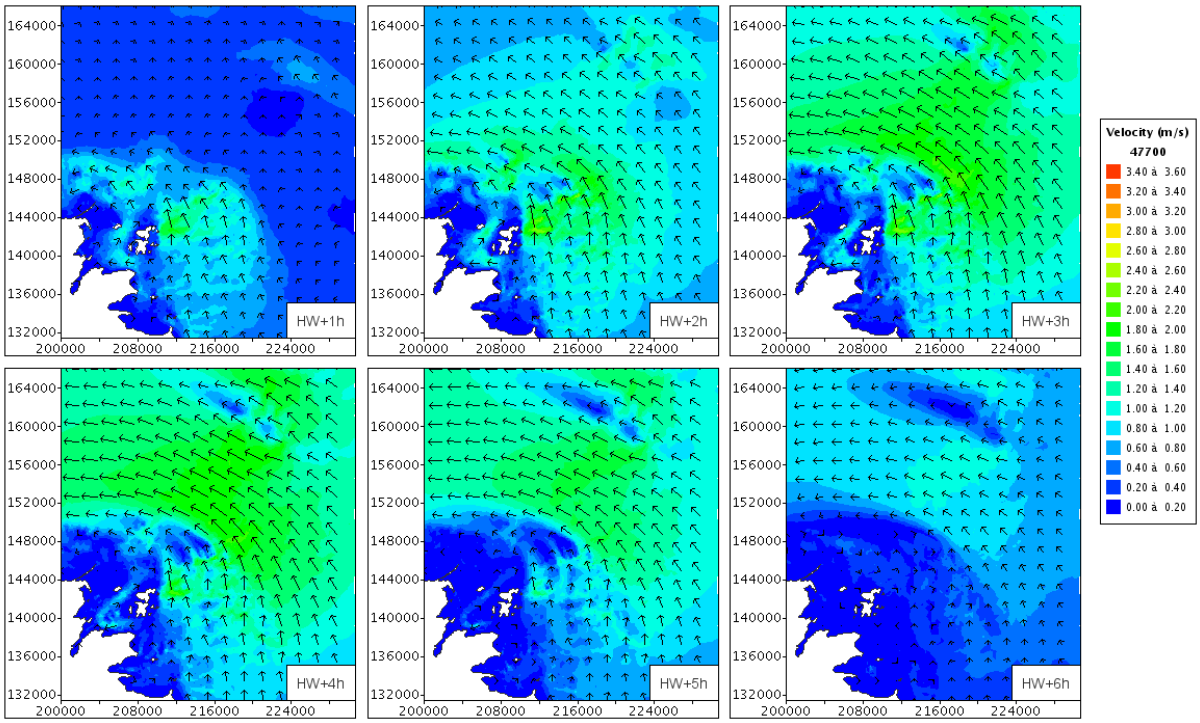

Figure C30: Current fields during a mean spring tide.

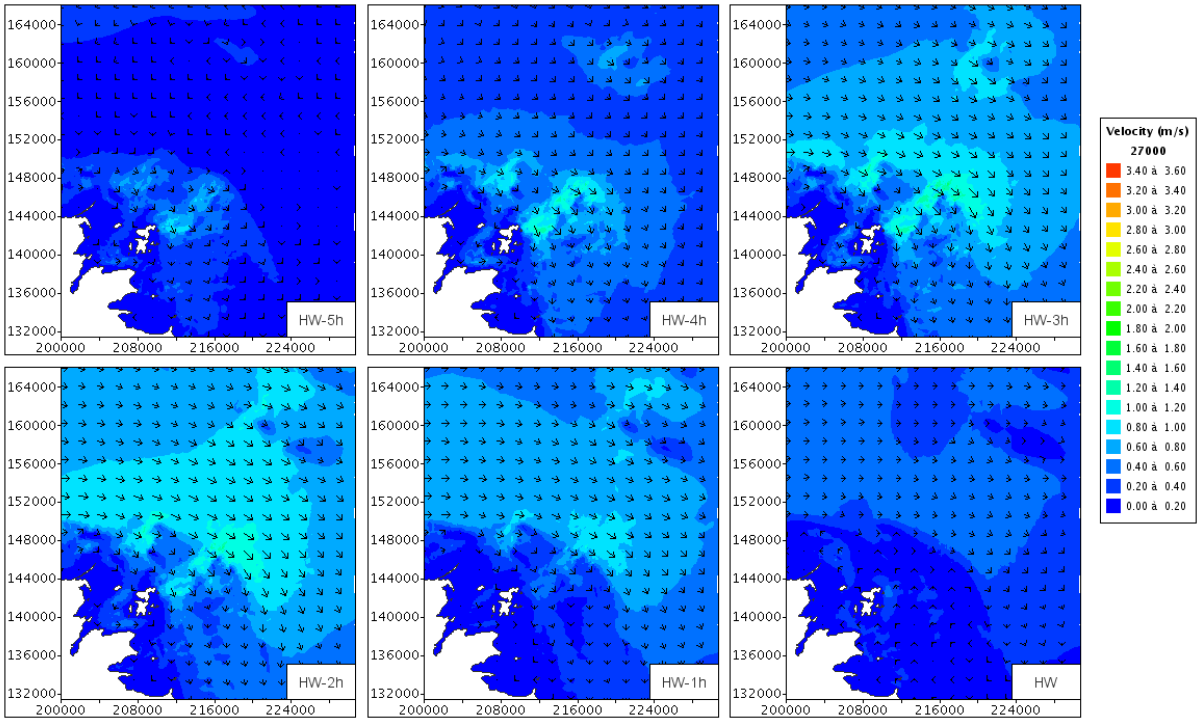

Figure C31: Current fields during a mean neap tide.

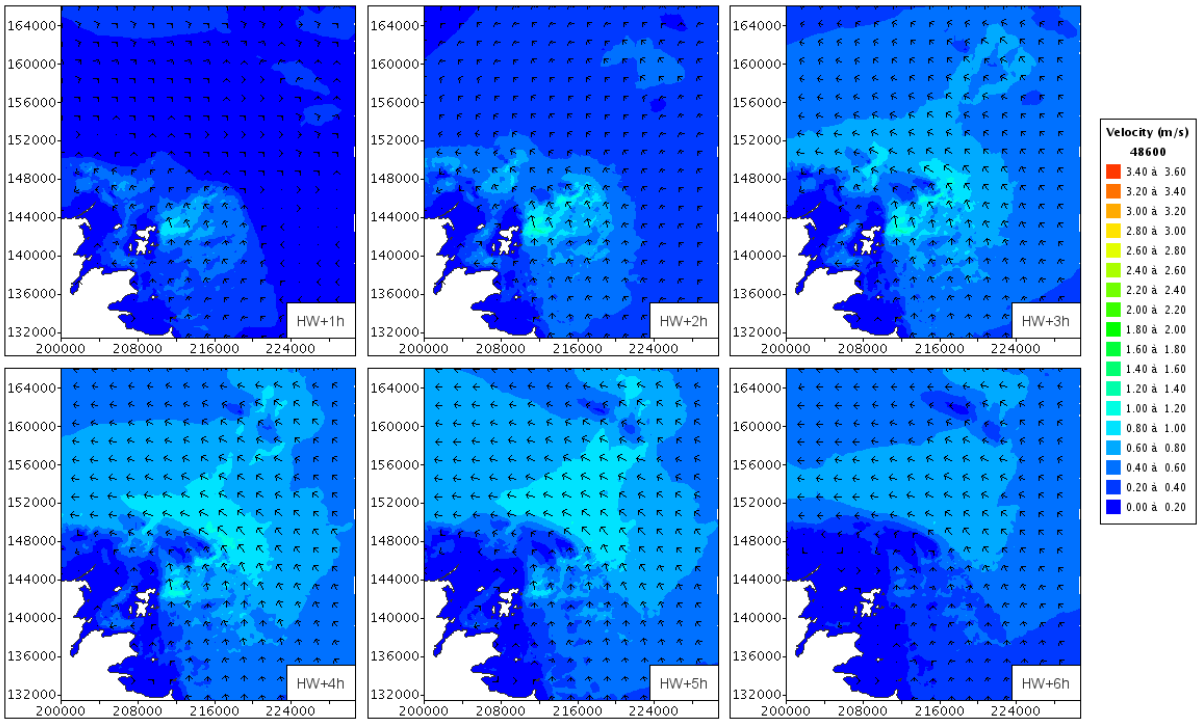

Figure C32: Current fields during a mean neap tide.

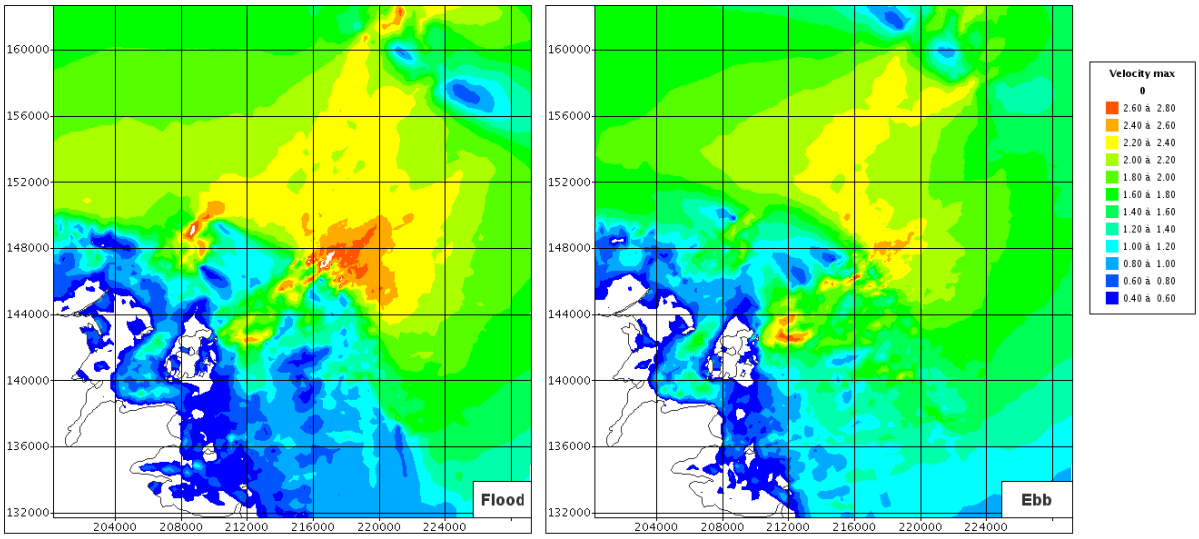

Figure C33: Maximum current fields during flood (left) and ebb (right) of an exceptional spring tide.

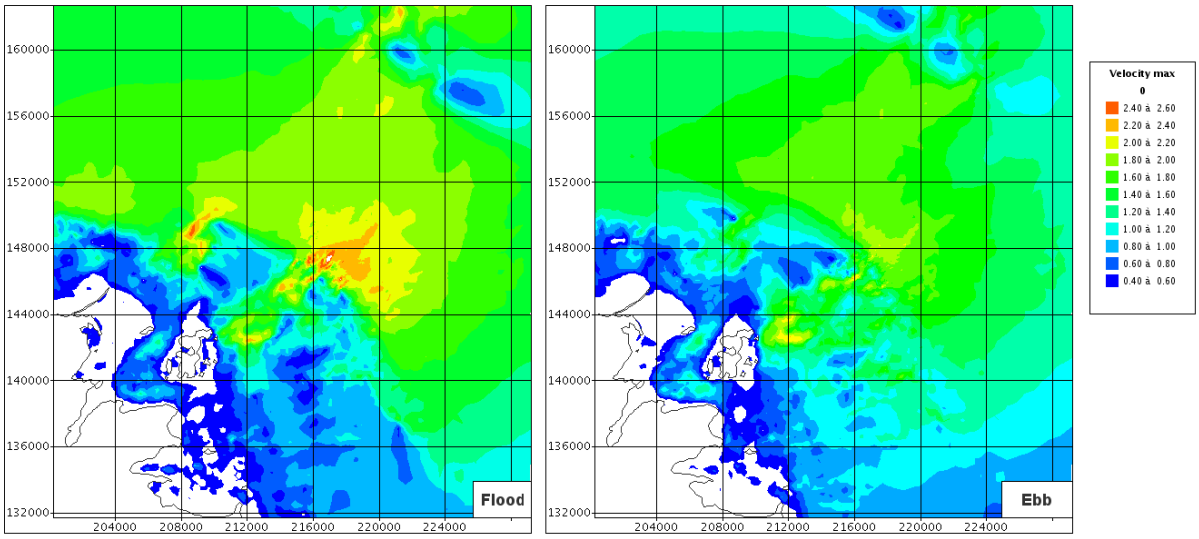

Figure C34: Maximum current fields during flood (left) and ebb (right) of a mean spring tide.

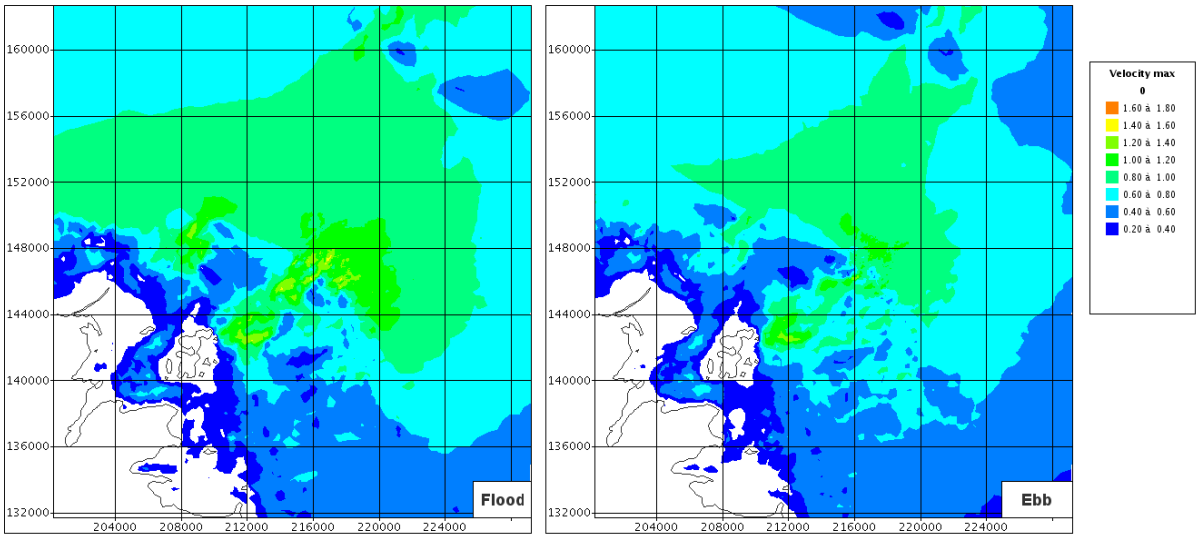

Figure C35: Maximum current fields during flood (left) and ebb (right) of a mean neap tide.

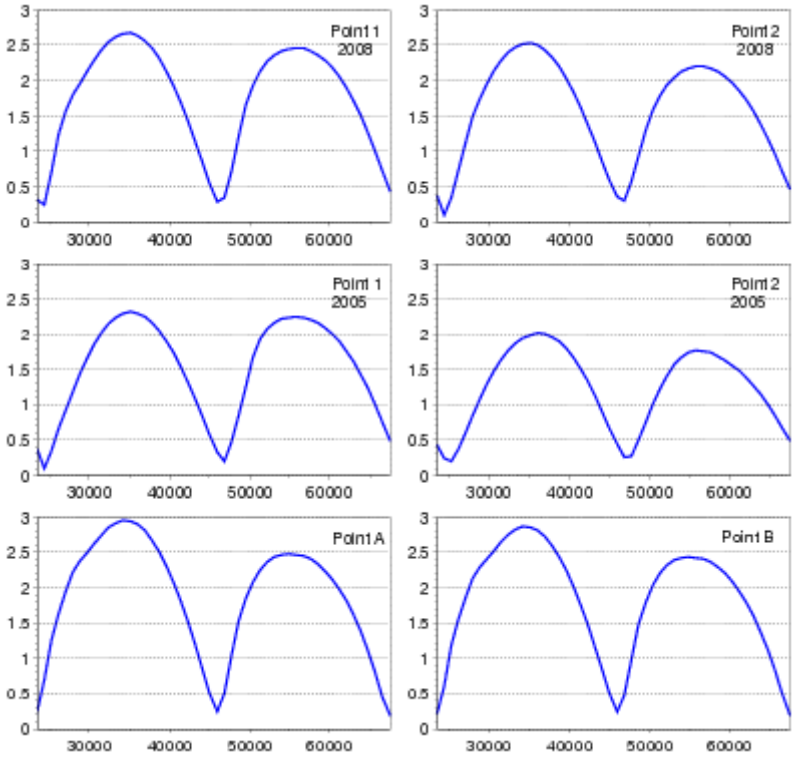

Figure C36: Magnitude of (vertically averaged) current velocity time series during an exceptional spring tide, for six locations.

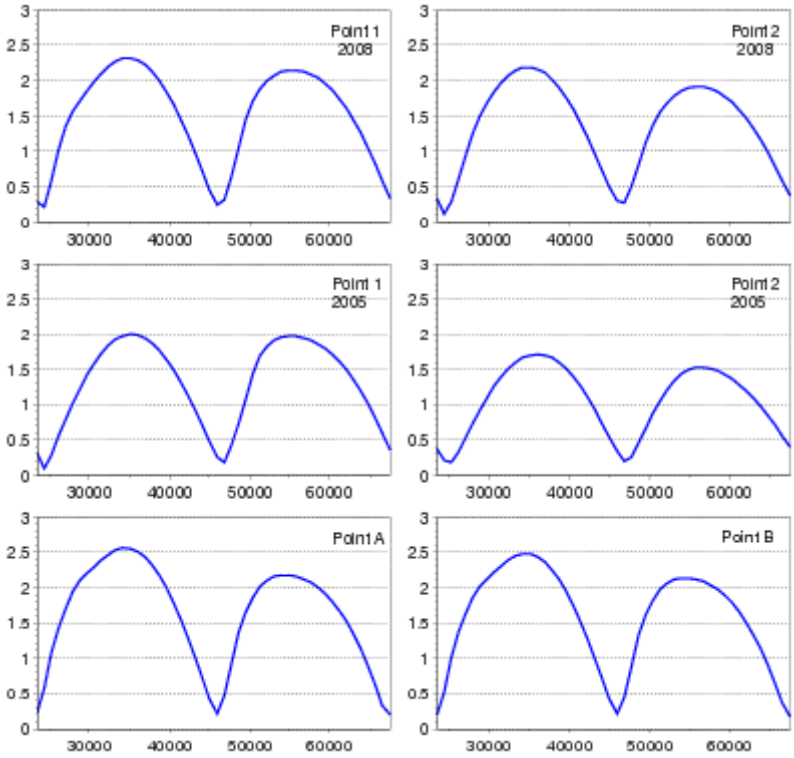

Figure C37: Magnitude of (vertically averaged) current velocity time series during a mean spring tide, for six locations.

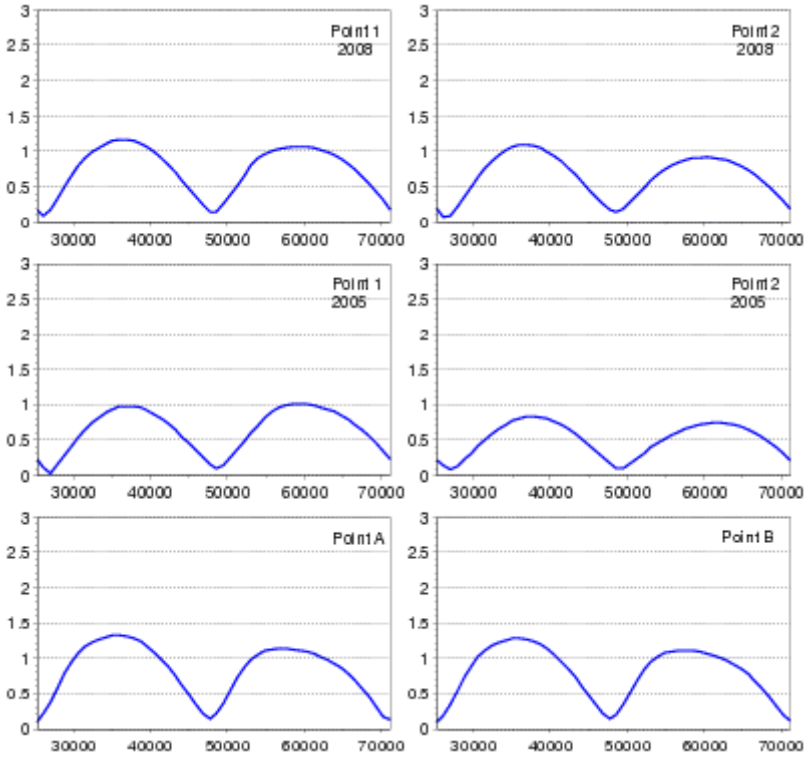

Figure C38: Magnitude of (vertically averaged) current velocity time series during a mean neap tide, for six locations.

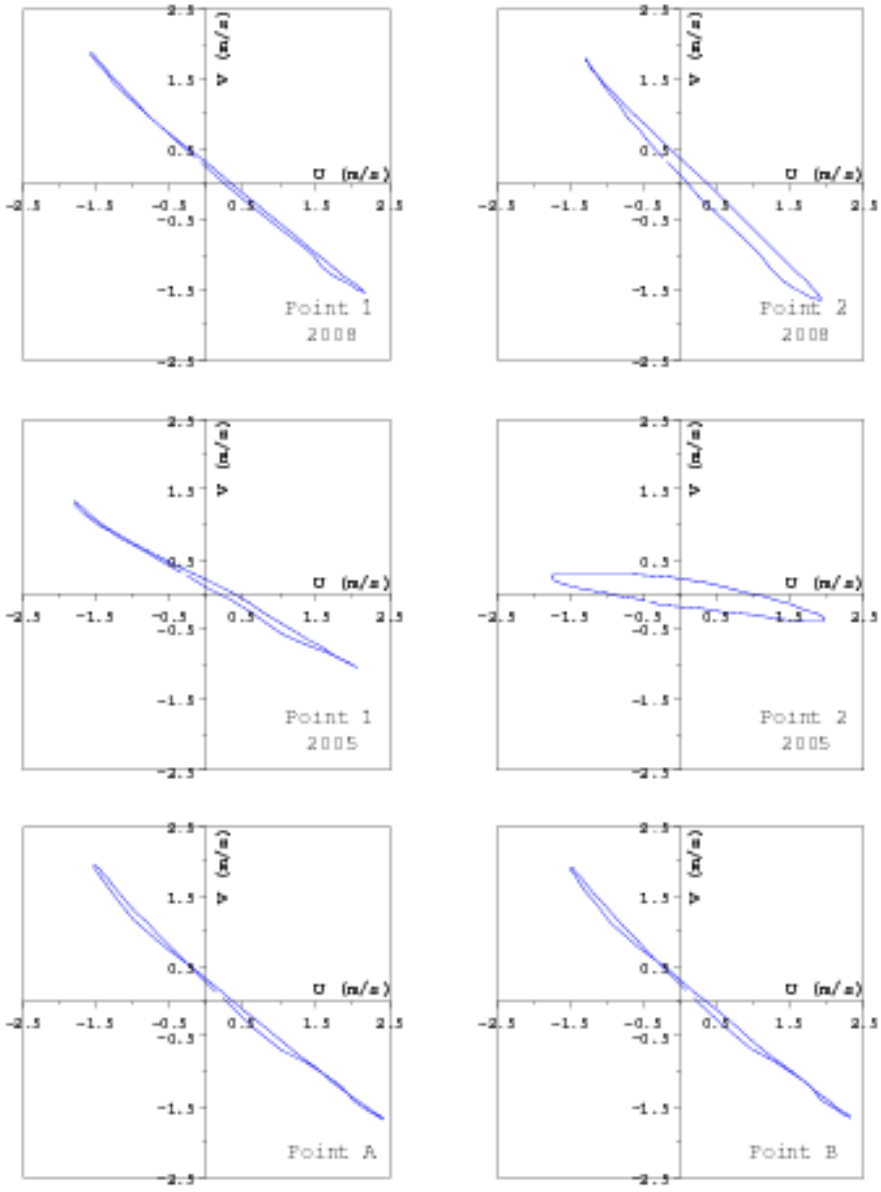

Figure C39: Tidal rose during an exceptional spring tide, for six locations.

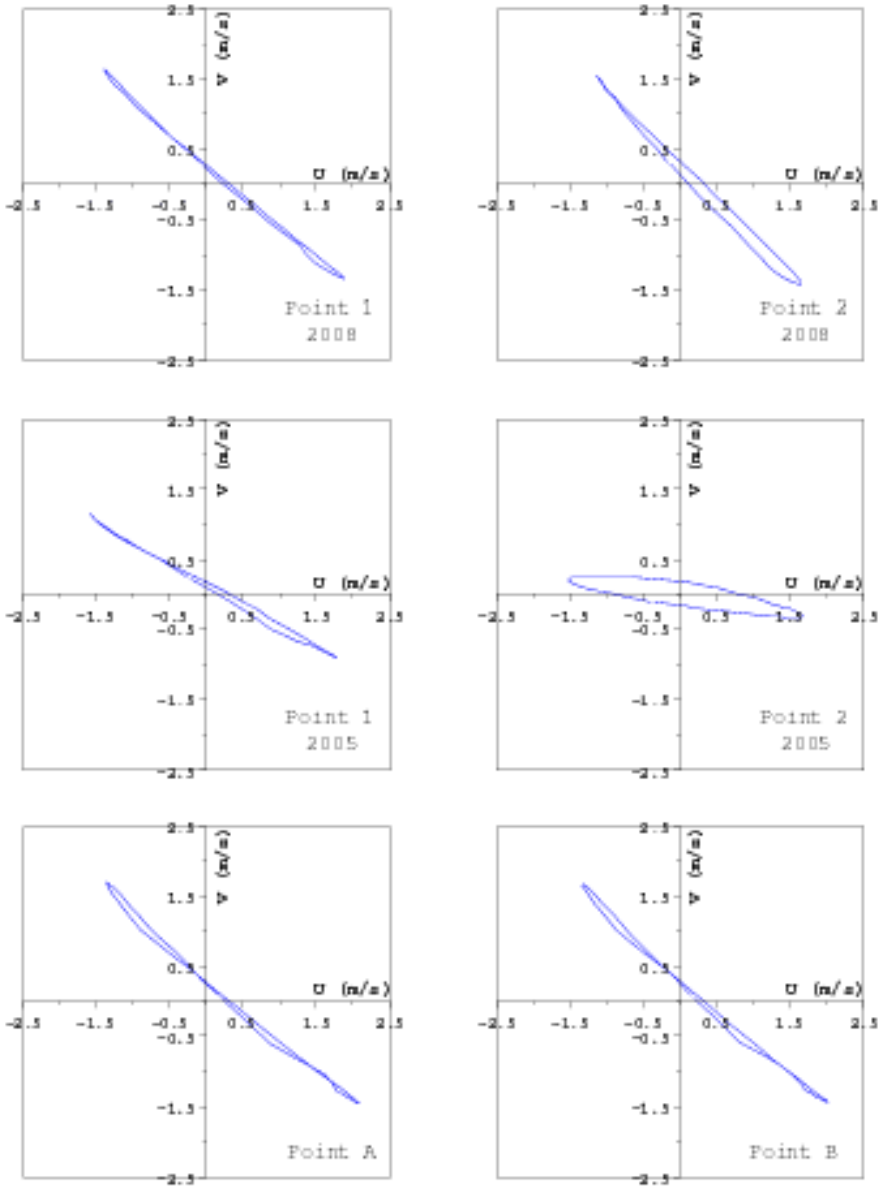

Figure C40: Tidal rose during a mean spring tide, for six locations.

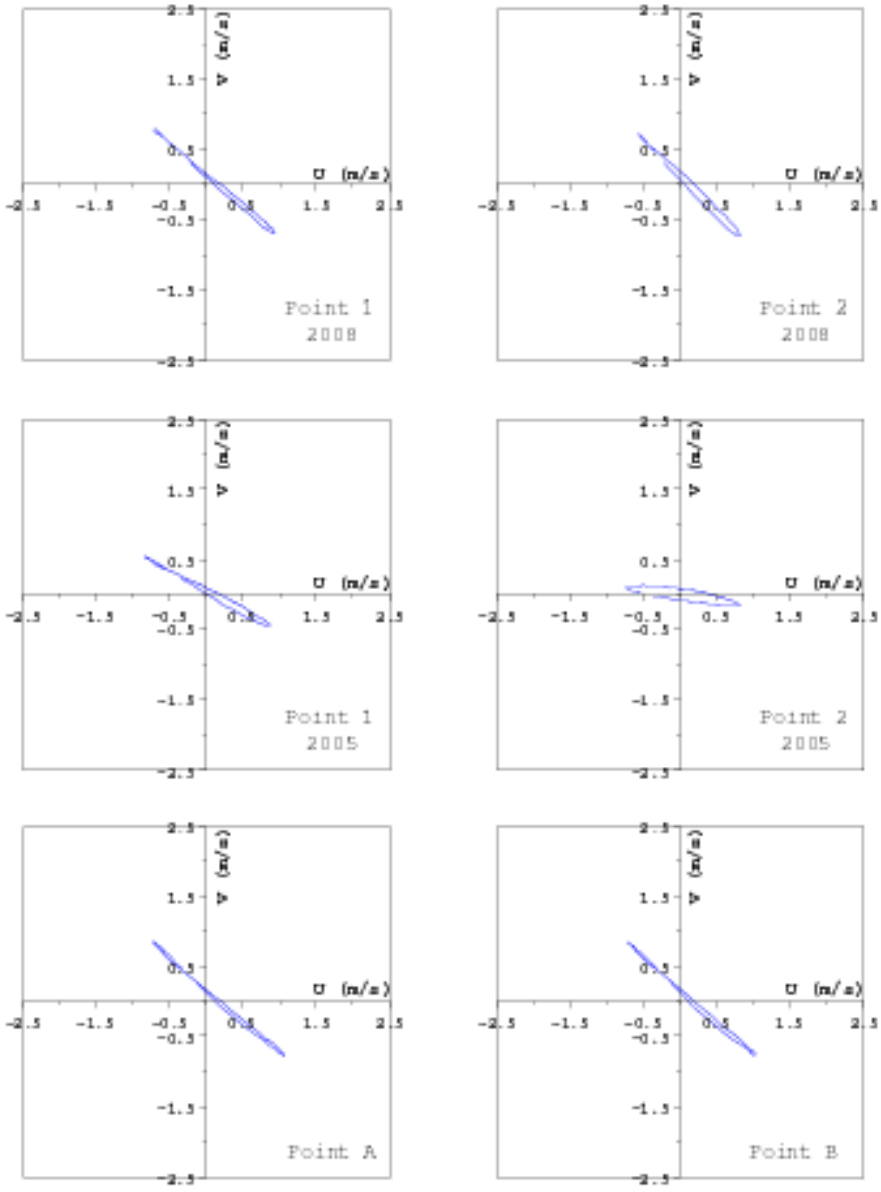

Figure C41: Tidal rose during a mean neap tide, for six locations.

5.6 3D numerical model

All flow velocities shown hereafter only take into account the astronomic tide. In particular, no meteorological effects (atmospheric pressure, wind and surge/wane) or wave effects have been considered in the numerical model.

Moreover, in this section, any reference made to the current velocity resulting from the TELEMAC-3D numerical model does not always refer to the vertically averaged velocity. In particular, the 3D velocity component can be expressed (e.g.: *W*). The results given are averages in the Reynolds sense, *i. e.* after smoothing out of the turbulence effects.

The sea levels are referenced with respect to Chart Datum.

5.6.1 Code version

The TELEMAC-3D edition used in this study is version 6.1.

5.6.2 Definition of the domain area / justification

The domain area of the 3D model is the same as detailed in the 2D (see 5.5.2).

5.6.3 Bathymetry

The bathymetry used for the 3D model is the same as detailed in the 2D (see 5.5.3).

5.6.4 Mesh

The 3D mesh is made of a stack of the same 2D meshes used for Telemac-2D (see 5.5.4). Elements are thus prisms with triangular elements for bases. The 2D mesh (see Figure C2) used for this 3D numerical model is the same as for TELEMAC-2D: it is a finite element mesh generated with the aid of the MATISSE v1.0 grid-generation software. It consists of 14,129 nodes and 27,425 triangular elements. The mesh size varies from 300 m at the coast to approximately 1.6 km at the greatest depths (to the West and North of the model). The mesh was progressively refined to 50 m, specifically at potential installation sites for tidal turbines. Eleven σ-layers are used in this model [G1].

5.6.5 Boundary conditions

The boundary conditions are still derived from an extended LNHE model covering the near Atlantic, the English Channel and the southern part of the North Sea, from which the harmonic constituents of four harmonic constituents [G6] – M2, S2, N2 and M4 – (see 5.5.5) were extracted.

In this study, schematic tides including the mean neap tides, mean spring tides and exceptional spring tides were simulated, as well as real-case tides, reconstructed from the four harmonic constituents cited above.

Contrary to the 2D model, Thompson-type boundary conditions [G7] are not used here because they had not yet been implemented in Telemac-3D v6.1. Velocities are imposed on the two edges parallel to the North-South direction (longitude 2° 30’ W and 3° 20’ W), whereas water depths are imposed on the edge parallel to the West-East direction (latitude 49° 30’ N). Thus, the boundary condition file is slightly different (codes 4 6 6 or 5 4 4, rather than 5 6 6 for each liquid node, *i. e.* velocity exclusive or water depth is imposed on the boundary, rather than both velocity and water depth are imposed on the boundary [G3] or [G5]).

5.6.6 Modifications of standard sources

As was the case in the 2D model, the bottom elevation of the numerical model is referenced to Chart Datum whereas tide elevation is referenced to the Mean Sea Level (MSL) on open boundaries. Moreover, if no modifications are done, the sea levels for different ports over the area are not well reproduced simultaneously. For the sea level calibration, it was then found to be necessary to introduce a non-constant mean sea level over the extent of the domain, in order to correctly calibrate the sea levels at the ports on the zone. This mean sea level is subtracted from the bottom elevation referenced to Chart Datum so that the bottom elevation is finally referenced to Mean Sea Level. Thus, a "pseudo" mean level was generated based on the LNHE 4-constituent numerical model that covers the near Atlantic Ocean, the English Channel and the southern part of the North Sea. This data is read from a binary data file in Serafin format. The same file as for 2D is used.

In practice, at the beginning of the computations, the frames of reference of the bottom elevation and free surface elevation are changed (passing from the frame of reference linked to Chart Datum to that linked to the mean sea level in the CORFON subroutine) and all elevations are expressed relative to the Mean Sea Level (MSL). No special post-treatment is done to convert the results back to correspond with Chart Datum (the original frame of reference), *i. e.* no new post-treatment variables were created as they were in the 2D case.

In addition, where the seabed elevation of the nodes at the open liquid boundary – on which tidal conditions are imposed – is susceptible to be above the LAT, it is modified so that these nodes will always be wet (these modifications are again made in the CORFON subroutine. In practice, the nodal bathymetry is clipped to the elevation corresponding to Chart Datum).

As discussed in § 5.5.5 and § 5.6.5, tidal signals for the boundary conditions at the liquid border are reconstituted from the extended LNHE model [G6] comprising four harmonic constituents (M2, S2, N2 and M4). The water depths and velocities are reconstituted according to the methodology described in [G6]. In the case of the numerical simulation of schematic tides, a phase shift is applied in relation to a point on the liquid boundary on which the tidal conditions are imposed (in this case, the 22nd node), such that the simulation starts at a time of high water on the zone. A velocity ramp (*i. e.* an increase of the velocity in time over the 30 min of the simulation) is imposed at the beginning of the simulation, during the first half hour of physical simulation, so that the simulation does not freeze or crash during this period. These modifications are found in the new subroutines BORDTIDE and TIDAL_MODEL_T3D, which isolate the treatment of the tide on the liquid boundaries and will be integrated into version 6.2 of the TELEMAC-3D software.

A calibration parameter was used in order to correctly reproduce the tidal range at the different ports in the zone. It is called CTIDE (for versions 6.1 and above), based on the end users. This parameter is a multiplier coefficient that acts on the amplitude of the tidal signal (sum of the sinusoids of four harmonic constituents for the water depth and the two horizontal velocity components). It varies according to the type of schematic tide being modelled. However, this calibration parameter is not used here for simulations of real tides.

5.6.7 Parameters

An example of the parameter files (those of a mean spring tide) is reproduced in Appendix C2.

Two tidal cycles (as a minimum) are modelled, with a duration for the physical computation (keyword NUMBER OF TIME STEPS associated with the keyword TIME STEP) of 90,000 s = 25 h (93,000 s in the case of a mean neap tide).

The initial condition chosen is a free-surface elevation that is constant over the entire domain extent (keyword INITIAL CONDITIONS assigned to the value 'CONSTANT ELEVATION'), taken as equal to the high water at the port of Men Joliguet (value of the keyword INITIAL ELEVATION') in

the chosen frame of reference (in this case relative to the mean sea level). As boundary conditions are treated for open liquid boundaries, in particular they are non reflecting conditions (see subsubsection 5.6.5), the water can come in or come out freely. The influence of the choice for the initial conditions disappears after around one tidal cycle. There is only a transient period of time when the modelling of tides is not well reproduced, in particular water balances are not good inside the extent of the domain, but after one tidal cycle, it is OK.

The graphic outputs (variable and variable name in the parameter file) routinely viewed in 2D for this type of hydrodynamic study are: the water depth H; the horizontal velocity components U and V (averaged over the vertical); scalar velocity (magnitude of the vertically-averaged velocity vector) M; elevation of the seabed B (with respect to mean sea level); free-surface elevation S (with respect to mean sea level) and the Courant number L.

The graphic outputs (variable and variable name in the parameter file) routinely viewed in 3D for this type of hydrodynamic study are: the 3D velocity components U, V and W and the elevation of each node, Z.

For this numerical model and for all types of tides, the chosen time step (keyword TIME STEP) was 20 s.

In order to determine the maximum velocities, the computational results are written to the output file every 5 minutes (real time) = 15 × 20 s (keyword GRAPHIC PRINTOUT PERIOD = 15).

5.6.7.1 Physical parameters

Dissipation through bed friction was modelled using a uniform Strickler coefficient *K* over the entire study domain (LAW OF BOTTOM FRICTION = 3).

The Coriolis effect was taken into account (keyword CORIOLIS = YES) with the value of the Coriolis coefficient equal to 1.10×10^{-4}. (= $2\omega\sin(l)$ value obtained for a latitude l equal to 49°N, with $\omega = 2\pi/T$, T = 86,164 s, the duration of a sidereal day. This value is thus assigned to the keyword CORIOLIS COEFFICIENT).

Meteorological effects (wind or atmospheric pressure) were not taken into account in the numerical simulations (keywords WIND and AIR PRESSURE = NO, default values).

No specific turbulence model was employed on the horizontal (value left at 1 by default for keyword HORIZONTAL TURBULENCE MODEL). Therefore, a constant coefficient of viscosity, equal to the default value of 10^{-4}, is applied over the whole domain (keyword COEFFICIENT FOR HORIZONTAL DIFFUSION OF VELOCITIES). A mixing length model (keyword VERTICAL TURBULENCE MODEL = 2) using Nezu Nakagawa's model [C10] (keyword MIXING LENGTH MODEL = 3) is used on the vertical.

5.6.7.2 Numerical parameters

A σ transformation of the mesh is used (keyword MESH TRANSFORMATION = 1, default value) with the number of horizontal levels equal to 11 (keyword NUMBER OF HORIZONTAL LEVELS).

Matrix storage by segments is used to optimise calculation times (keyword MATRIX STORAGE = 3). For the suppression of free-surface parasite oscillations, the keyword FREE SURFACE GRADIENT COMPATIBILITY was taken to equal 0.9 (recommended value).

The non-hydrostatic version of TELEMAC-3D is recommended to better model the vertical velocity *w* (keyword NON-HYDROSTATIC VERSION = YES). Hydrostatic step is solved using in the wave equation option (keyword OPTION FOR THE HYDROSTATIC STEP = 2, which is the only option presently available).

The numerical schemes used were: the method of characteristics for the advection of velocities and, for the water depth, a conservative scheme (keywords SCHEME FOR ADVECTION OF VELOCITIES = 1 and SCHEME FOR ADVECTION OF DEPTH = 5, default values).

For solving the propagation step, the conjugate residual method was the chosen solver (keyword SOLVER FOR PROPAGATION = 2), whereas the conjugate gradient method was chosen for the other steps, each with an accuracy of 10^{-6} (keywords ACCURACY FOR DIFFUSION OF VELOCITIES, ACCURACY FOR PROPAGATION and ACCURACY FOR PPE), a maximum number of 500 iterations (keywords MAXIMUM NUMBER OF ITERATIONS FOR DIFFUSION OF VELOCITIES, MAXIMUM NUMBER OF ITERATIONS FOR PROPAGATION and MAXIMUM NUMBER OF ITERATIONS FOR PPE) and various preconditionings: (keywords PRECONDITIONING FOR DIFFUSION OF VELOCITIES = 34, *i. e.* diagonal and direct solver on the vertical, PRECONDITIONING FOR PROPAGATION = 2, *i. e.* diagonal, PRECONDITIONING FOR PPE = 17, *i. e.* direct solver on the vertical).

Full implicitations are used for the different equations (keywords IMPLICITATION FOR DEPTH, IMPLICITATION FOR VELOCITIES and IMPLICITATION FOR DIFFUSION equal to 1.) and total mass-lumping for depth, velocities and diffusion are used (keywords MASS-LUMPING FOR DEPTH, MASS-LUMPING FOR VELOCITIES and MASS-LUMPING FOR DIFFUSION equal to 1.).

5.6.8 Treatment of tidal flats

The tidal flats (keyword TIDAL FLATS = YES, default value) were treated using the first treatment option, which consists of the correction of the free surface computations by elements, to take account of the tidal flats (keyword OPTION FOR THE TREATMENT OF TIDAL FLATS = 1, default value).

In order to ensure that water depths remain positive over the entire study domain (particularly given the presence of tidal flats), an innovation, introduced from TELEMAC version 6.0 onward, was used. This consists of taking the combination of the following four keywords: no upwind for SUPG (SUPG OPTION = 0; 0), total mass-lumping for depth (keyword MASS-LUMPING FOR DEPTH = 1.), and a treatment to suppress negative depths by a limitation of fluxes (keyword TREATMENT OF NEGATIVE DEPTHS = 2).

5.6.9 Calibration

To test the validity of the model, various comparisons were made between the model results and the sea level data or velocity measurements.

5.6.9.1 Sea levels

The levels calculated with TELEMAC-3D were compared to the sea levels characteristic of astronomical tides for Paimpol, the Isle of Bréhat (Men Joliguet), Roches Douvres and Les Héaux-de-Bréhat, as indicated by the SHOM data (source [C4] « ©SHOM-2010 » for the three first ports). In particular, the TELEMAC-3D model has been calibrated with the data of the Isle of Bréhat for sea levels. The other ports are used to validate the model.

Table C12 gives a quantification of the variance between the TELEMAC-3D numerical model results and the SHOM data.

The following abbreviations are used in Table C12:
- HW: high water (in m CD),
- LW: low water (in m CD),
- ES: exceptional spring tide,
- MS: mean spring tide,
- MN: mean neap tide.

ES	HW (m CD)			LW (m CD)			Tidal range (m)		
	SHOM	TEL3D	Var.	SHOM	TEL3D	Var.	SHOM	TEL3D	Var.
Paimpol	11,92	11,79	0,13	0,11	0,13	-0,02	11,81	11,66	0,15
Isle of Bréhat	11,68	11,65	0,03	0,10	0,07	0,03	11,58	11,58	0,00
Les Héaux-de-Bréhat	10,95	10,80	0,15	0,10	0,11	-0,01	10,85	10,69	0,16
Roches Douvres	10,80	10,66	0,14	0,03	0,21	-0,18	10,77	10,45	0,32

MS	HW (m CD)			LW (m CD)			Tidal range (m)		
	SHOM	TEL3D	Var.	SHOM	TEL3D	Var.	SHOM	TEL3D	Var.
Paimpol	10,80	10,65	0,15	1,35	1,32	0,03	9,45	9,33	0,12
Isle of Bréhat	10,55	10,52	0,03	1,30	1,27	0,03	9,25	9,25	0,00
Les Héaux-de-Bréhat	9,80	9,76	0,04	1,20	1,26	-0,06	8,60	8,50	0,10
Roches Douvres	9,80	9,62	0,18	1,30	1,31	-0,01	8,50	8,31	0,19

MN	HW (m CD)			LW (m CD)			Tidal range (m)		
	SHOM	TEL3D	Var.	SHOM	TEL3D	Var.	SHOM	TEL3D	Var.
Paimpol	8,35	8,23	0,12	3,85	3,79	0,06	4,50	4,44	0,06
Isle of Bréhat	8,15	8,12	0,03	3,75	3,72	0,03	4,40	4,40	0,00
Les Héaux-de-Bréhat	7,60	7,57	0,03	3,55	3,54	0,01	4,05	4,03	0,02
Roches Douvres	7,60	7,47	0,13	3,55	3,56	-0,01	4,05	3,91	0,14

Table C12: Comparison of tide levels provided by SHOM (source [C4] « ©SHOM-2010 ») with levels simulated with TELEMAC-3D, for various tide conditions and ports within the study zone.

To adapt the tidal range, the coefficient CTIDE (cf. §5.5.6 or §5.6.6) is modified (to the values 1.120, 1.005 and 0.971 respectively for an exceptional spring tide, mean spring tide and mean neap tide).

The tidal ranges, as well as the High Water (HW) and Low Water (LW) levels were very well replicated by the model for an exceptional spring tide (ES), a mean spring tide (MS) and mean neap tide (MN). In general, the variance is less than 10 cm at Les Héaux-de-Bréhat and at Men Joliguet, which is on the Isle of Bréhat, the closest port to the potential installation site. For the port of Paimpol and the same three types of tides, the variances are slightly greater (generally less than 15 cm), whereas for Roches Douvres the tidal ranges are worse replicated.

5.6.9.2 Current velocities

The current measurements resulting from the two campaigns carried out in April 2005 [C1] and in the spring of 2008 [C2] were used in this study to calibrate and validate the model to the best level possible. The locations of the measurement sampling points are indicated on Figure C1. The model has been visually calibrated with ADCP measurements at two locations during a four-day period from June 3rd to 6th 2008 that corresponds to spring tides.

Dissipation by bed friction is modelled by a Strickler coefficient *K* that is uniform over the whole study domain and set at 27 m$^{1/3}$/s, as it was for the 2D numerical model. The choice of a Strickler coefficient value of 27 (rather than 25 or 30) was validated by the comparison of the numerical simulations of current velocities performed in TELEMAC-3D with the ADCP measurements of current velocities during periods of spring tides and neap tides. This choice was also made to compare the 2D and the 3D numerical model with the same calibration coefficient. Several exact tide dates were isolated, corresponding to periods of spring tides (from 7th to 11th April 2005, 5th to 9th April 2008, 4th to 8th May 2008 and 3rd to 6th June 2008). For each of the above periods, a comparison was

then made of the evolution over time of the magnitude of the vertically-averaged velocity vector of the ADCP measurements (red crosses) with the simulations obtained by the TELEMAC-3D numerical model (blue, sky blue or black lines) in Figures C42 to C49. Moreover, Figures C50 to C57 show same comparisons during one tidal cycle – flood/ebb – with a zoom on 8th April 2005, 6th April 2008, 5th May 2008 and 4th June 2008 afternoons. Further comparison was made of the point cloud of ADCP-provided measurements of the vertically averaged velocity with the current roses obtained with the TELEMAC-3D numerical model (Figures C58 to C65).

The qualitative agreement between velocities simulated by the model and the measurements is quite correct with regard to measurement points 1 and 2 of the April 2005 and spring 2008 campaigns. Nevertheless, when predicting maximum velocity during flood tide, the maximum velocity during ebb can be underestimated or overestimated by 20% (and *vice versa*).

Tables C 13 to C 15 show quality indices (see Appendix A2 for more information about calculated quality indices) at ADCP location 2 for ADCP during the single tidal cycle shown on Figures C50 to C57 in 2008. Only this location has been chosen because ADCP 1 missed one velocity measurement every hour (while measuring wave parameters). Sometimes, one phase shift may appear (10 or 20 min), but no correction has been done to improve the calculated quality indices. The comparison shows medium agreement between model outputs and measurements. The RMS error of current speeds remains relatively high (from 0.2 to 0.4 m/s), but this can be partly explained by the nature of the measured tidal speeds. The signal is rather noisy due to the turbulent nature of the flow. Besides, the model only accounts open boundary conditions to force tide, whereas on-site measurements capture wind, wave and atmospheric pressure effects on currents. As it is difficult to replicate maximum velocity during flood and ebb with the same friction coefficient, it is then difficult to conclude correctly when considering bias.

Quality indice	Strickler = 25 $m^{1/3}/s$	Strickler = 27 $m^{1/3}/s$	Strickler = 30 $m^{1/3}/s$
Bias or mean error	0.04	0.07	0.09
Non dimensional bias	0.03	0.05	0.07
RMS error	0.23	0.24	0.25
Non dimensional RMS error	0.17	0.17	0.18
Pearson correlation coefficient	0.94	0.93	0.93

Table C13: Quality indices of computed tidal velocity intensities compared to ADCP location 2 raw measurements during one tidal cycle (April 6th 2008) for Strickler coefficient = 25, 27 and 30 $m^{1/3}/s$.

Quality indice	Strickler = 25 $m^{1/3}/s$	Strickler = 27 $m^{1/3}/s$	Strickler = 30 $m^{1/3}/s$
Bias or mean error	0.10	0.12	0.15
Non dimensional bias	0.08	0.09	0.11
RMS error	0.23	0.24	0.26
Non dimensional RMS error	0.18	0.18	0.20
Pearson correlation coefficient	0.95	0.95	0.95

Table C14: Quality indices of computed tidal velocity intensities compared to ADCP location 2 raw measurements during one tidal cycle (May 5th 2008) for Strickler coefficient = 25, 27 and 30 $m^{1/3}/s$.

Quality indice	Strickler = 25 $m^{1/3}/s$	Strickler = 27 $m^{1/3}/s$	Strickler = 30 $m^{1/3}/s$
Bias or mean error	0.27	0.29	0.32
Non dimensional bias	0.22	0.24	0.27
RMS error	0.36	0.38	0.41
Non dimensional RMS error	0.30	0.32	0.34
Pearson correlation coefficient	0.94	0.94	0.94

Table C15: Quality indices of computed tidal velocity intensities compared to ADCP location 2 raw measurements during one tidal cycle (June 4th 2008) for Strickler coefficient = 25, 27 and 30 $m^{1/3}/s$.

5.6.10 Analysis

Various characteristic tidal conditions were simulated:

- an exceptional spring tide,
- a mean spring tide,
- a mean neap tide.

Current fields for the study zone are presented hour-by-hour in Figures C66 to C71: for an exceptional spring tide (Figures C66 and C67); a mean spring tide (Figures C68 and C69) and a mean neap tide (Figures C70 and C71). High water at Paimpol was considered as the reference.

For three ADCP locations and locations A and B, the mean direction of the current flows along the NW-SE axis; the ebb current flows towards the North-West and the flood current to the South-East, with the passage from South-East to North-West occurring through the North.

Maximum current fields, during the flood and ebb tides (defined with reference to the instants of occurrence of high and low waters on the zone), are represented in Figures C72 to C74 for the three schematic tide conditions (an exceptional spring tide, a mean spring tide and a mean neap tide). These fields do not correspond to an instantaneous flow situation; they are constituted from the maximum velocities. Velocities are generally higher during the flood than during the ebb.

Figures C75 to C77 illustrate the time series of the magnitude of velocity at six locations in the study zone (the four ADCP locations and two locations close to a potential site of installation in the south-west quarter of the crustacean reserve), for three types of tides (an exceptional spring tide, a mean spring tide and a mean neap tide).

Figures C78 to C80 illustrate current roses at six locations in the study zone (the four ADCP locations and two locations in the south-west quarter of the crustacean reserve), for three types of tides (an exceptional spring tide, a mean spring tide and a mean neap tide).

Table C16 gives the maximum velocities (averaged over the vertical), during a tide cycle at the six locations, for the three types of schematic tide conditions – exceptional spring tide, mean spring tide and mean neap tide.

Location	Exceptional Spring (ES)		Mean Spring (MS)		Mean Neap (MN)	
	(m/s)					
	Flood	Ebb	Flood	Ebb	Flood	Ebb
1 in 2008	2,8	2,6	2,3	2,2	1,1	1,0
2 in 2008	2,6	2,4	2,2	2,0	1,0	0,9
1 in 2005	2,4	2,3	2,0	2,0	1,0	1,0
2 in 2005	2,1	1,8	1,8	1,6	0,8	0,7
A	3,0	2,6	2,6	2,2	1,2	1,1
B	2,9	2,6	2,5	2,2	1,2	1,1

Table C16: Magnitude of maximum flow velocities (averaged over the vertical), during flood and ebb, at six locations in the study zone tested for three tidal conditions.

Figures C81 to C92 illustrate velocity profiles along the vertical direction at six different instants (flood and ebb during April, May and June 2008) at the two ADCP locations of the 2008 measurement campaign. In addition to perform a detailed sensitivity analysis of the Strickler coefficient, three simulations were performed with TELEMAC-3D using different values of Strickler coefficients (25, 27 and 30 $m^{1/3}/s$). As for calibration subsection 5.6.9.2, when replicating maximum velocity during flood, the maximum velocity is not well replicated during ebb (and *vice versa*), whatever friction

coefficient is used. New developments to enable the use of two other sets of harmonic constants to calculate boundary conditions for tides in TELEMAC-(2D or 3D) have been integrated in version 6.2 during Summer 2012. On the Paimpol-Bréhat zone, it is shown that the modelling of tides is better replicated when using these two other sets of harmonic constants [C11]. Thus, the results of the present studies must be improved by using such new harmonic constants databases.

5.6.11 Comparison of the 2D and 3D studies

As discussed in subsection 5.6.9.2, the final results for 3D studies use the same friction coefficient as for 2D studies to compare 2D and 3D results. Yet, when modelling schematic tides the parameter CTIDE, which enables adaptation of tidal range, may differ. Besides, the pseudo mean sea level file used for the 3D study is the same as for 2D, especially calibrated for 2D.

Sea levels are generally better replicated in 2D than in 3D for schematic tides (see subsections 5.5.9.1 and 5.6.9.1). Absolute differences can reach 12 cm, but compared to relative differences, they are only a few percents. Nevertheless, one main reason to explain why the 2D models better replicate SHOM data may be that these data are generated from a Telemac-2D model that solves the shallow water equations, along the French coasts [C12]. Moreover, the accuracy of the data for sea levels (for mean spring or mean neap tides) is between 5 and 10 cm. Figures for the hour-by-hour velocity fields, the maximum current fields during flood or ebb tide, the times series of magnitude of current velocity and tidal roses during a tide at specific locations are approximately the same for 2D and 3D studies. Differences in magnitudes of maximum flow velocities, during flood and ebb at various locations, are mostly less than 0.1 m/s between the 2D and 3D studies.

5.6.12 Uncertainties

In this section account is given of the main sources of uncertainties concerning the results presented.

Bathymetric data for the study zone was obtained from two principal sources: commercially available SHOM data (digital bathymetric grids, DTMs, charts), with regard to Chart Datum, and measurements carried out by CREOCEAN for EDF that were first expressed relative to NGF-IGN69 zero, then reduced to Chart Datum taking Paimpol as the reference port (translation of +6.65 m). The coherence or continuity (in position and level) of the data is not always perfectly correct. Moreover, there are no SHOM probes in some relatively large areas of the Bréhat zone (area that can reach a few km^2).

A second limitation is that the model takes into account only four harmonic constituents (M2, S2, N2 and M4) to represent the tide: this representation could be enhanced by taking account of other components of the tidal signal.

5.6.13 Computation time

The TELEMAC-3D computations were carried out on the EDF R&D IBM Debian “Ivanoé” cluster (200 TFlops). The processor specifications are as follows: 24 GB RAM per node (1 node = 2 hexa-core processors, running at 2.93 GHz). The CPU time required for a 4 or 5 day simulation was approximately 7 min for a 96-processor run (optimal speed-up of the 3D model with 11 planes was found for this number of processors).

5.6.14 Conclusion

The present study enabled the characterisation of tidal flow conditions in the Paimpol-Bréhat zone. It was based on numerical modelling at local scale. The numerical models were built with the TELEMAC-3D hydro-informatics software developed at the LNHE.

Calibration results were given in terms of tidal range, sea level and current velocities. For different types of schematic tide (an exceptional spring tide, a mean spring tide and a mean neap tide), various

results were also given: current fields hour-by-hour; maximum current fields during flood and ebb across the area; time series of magnitude of velocity; current roses and maximum velocities during flood and ebb for specific locations in the area. Moreover, for velocity profiles along the vertical direction comparisons are given between ADCP measurements and the TELEMAC-3D model.

5.6.15 Figures

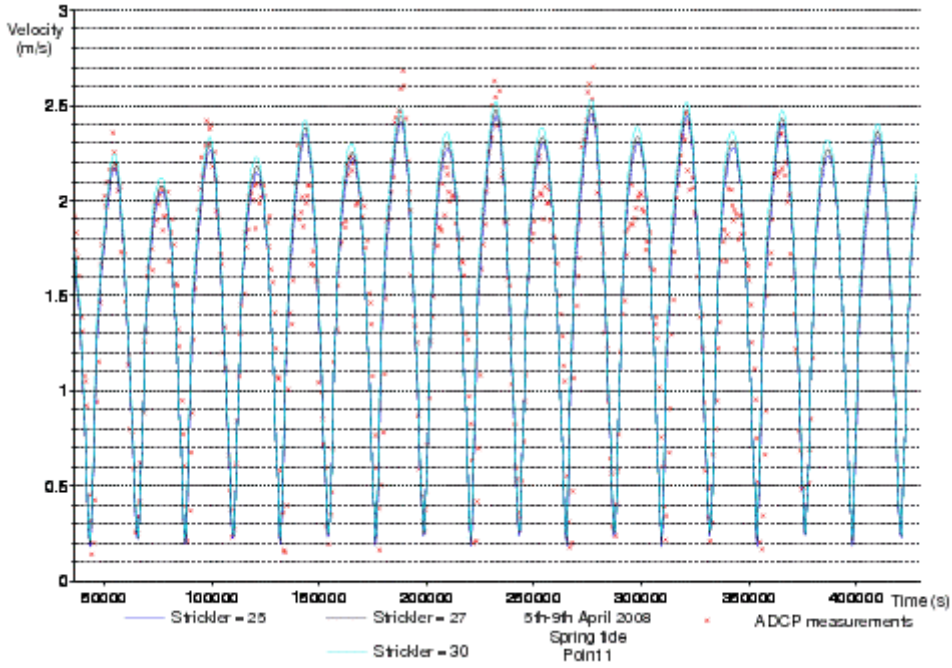

Figure C42: Magnitude of (vertically averaged) current velocity time series. Comparison between ADCP measurements (in red) and Telemac-3D results from April 5th to 9th 2008 at location 1.

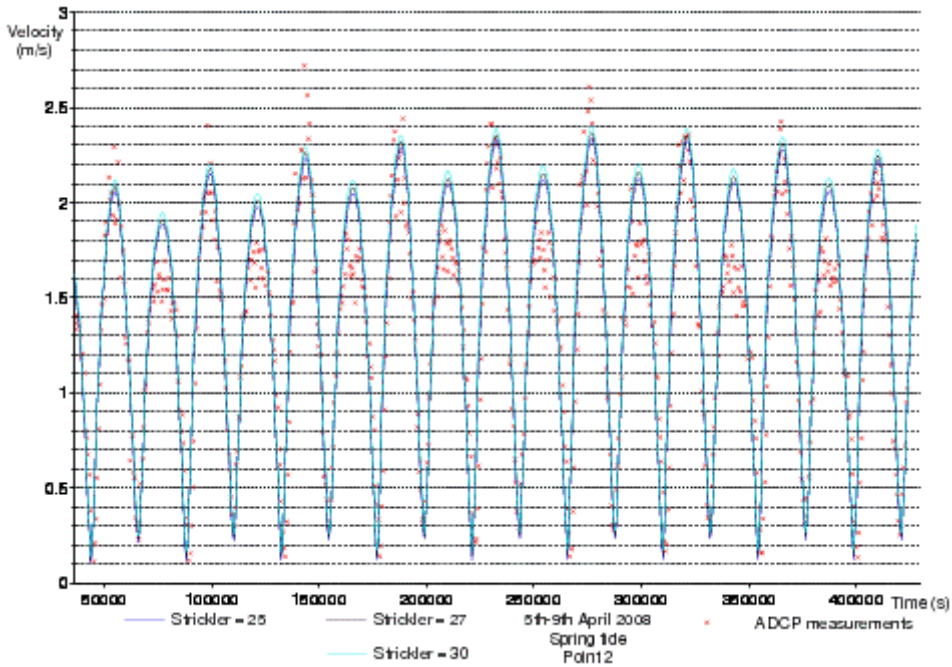

Figure C43: Magnitude of (vertically averaged) current velocity time series. Comparison between ADCP measurements (in red) and Telemac-3D results from April 5th to 9th 2008 at location 2.

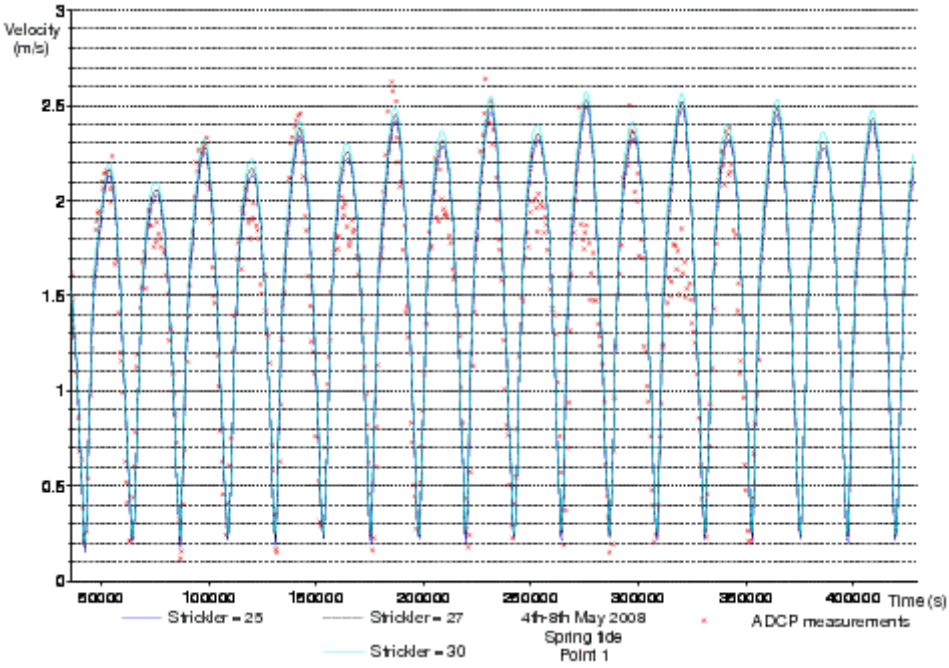

Figure C44: Magnitude of (vertically averaged) current velocity time series. Comparison between ADCP measurements (in red) and Telemac-3D results from May 4th to 8th 2008 at location 1.

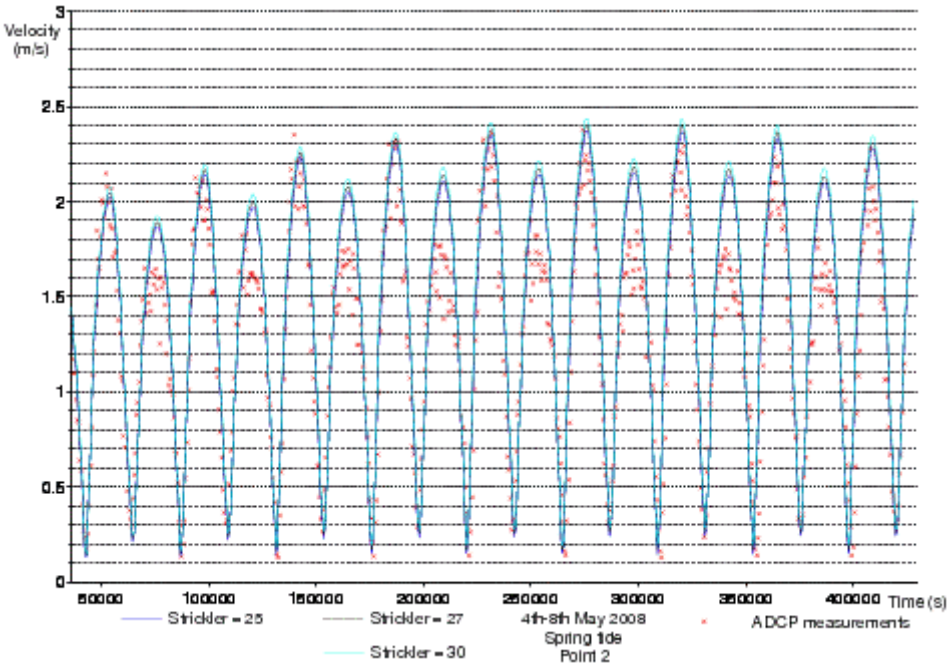

Figure C45: Magnitude of (vertically averaged) current velocity time series. Comparison between ADCP measurements (in red) and Telemac-3D results from May 4th to 8th 2008 at location 2.

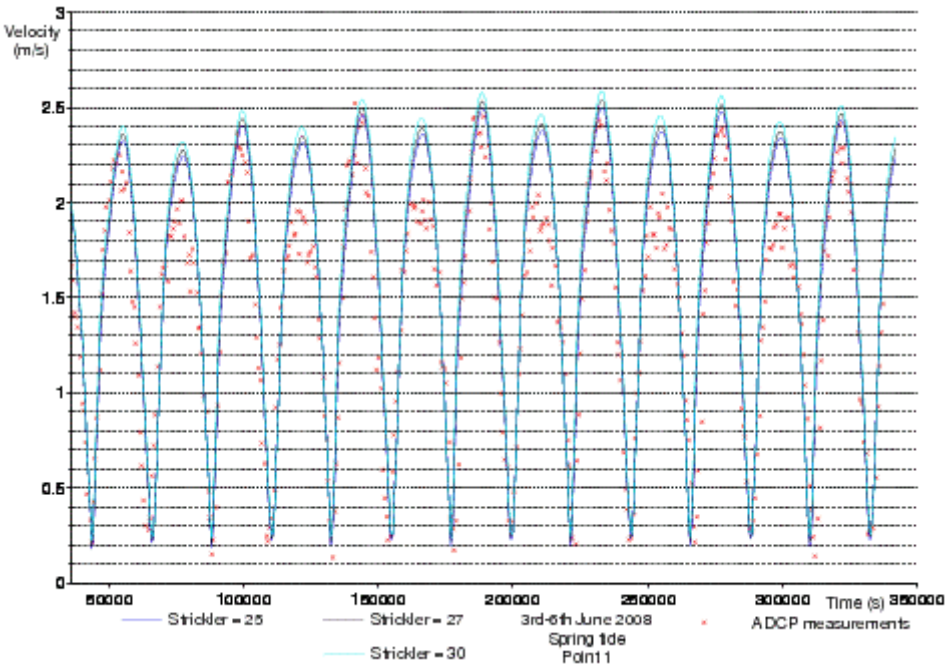

Figure C46: Magnitude of (vertically averaged) current velocity time series. Comparison between ADCP measurements (in red) and Telemac-3D results from June 3rd to 6th 2008 at location 1.

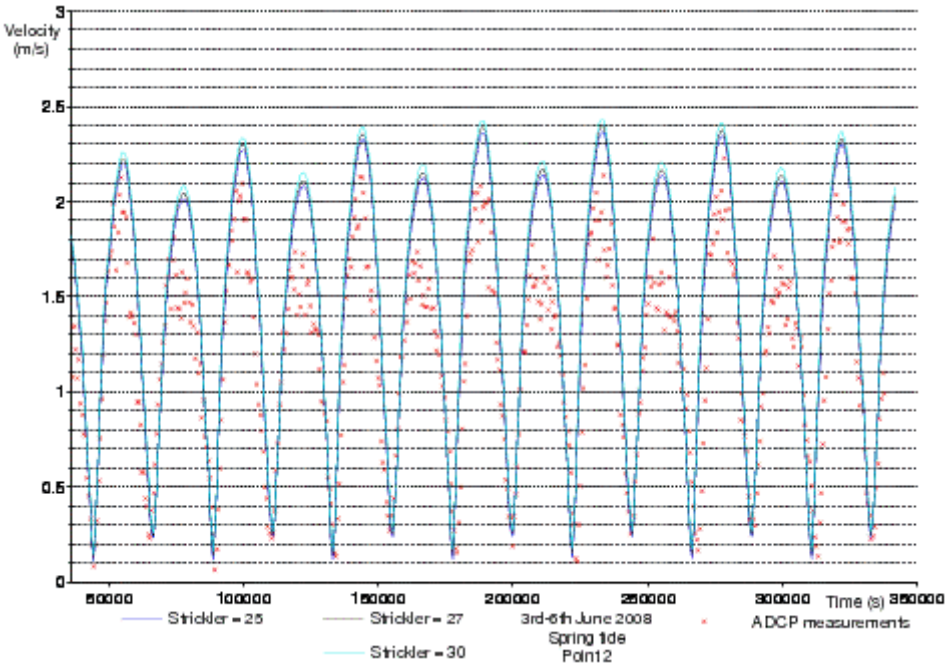

Figure C47: Magnitude of (vertically averaged) current velocity time series. Comparison between ADCP measurements (in red) and Telemac-3D results from June 3rd to 6th 2008 at location 2.

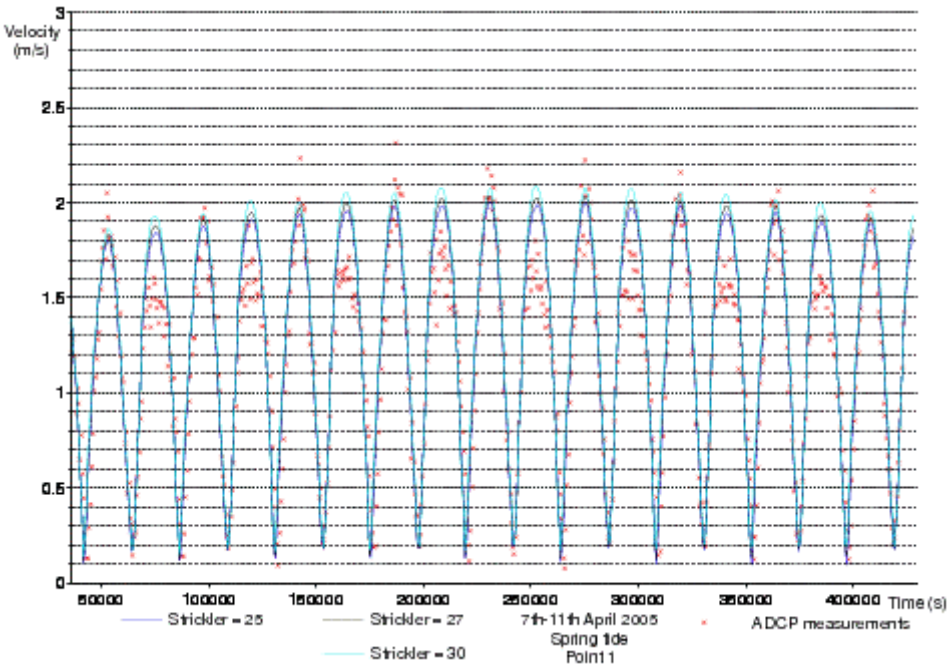

Figure C48: Magnitude of (vertically averaged) current velocity time series. Comparison between ADCP measurements (in red) and Telemac-3D results from April 7th to 11th 2005 at location 1.

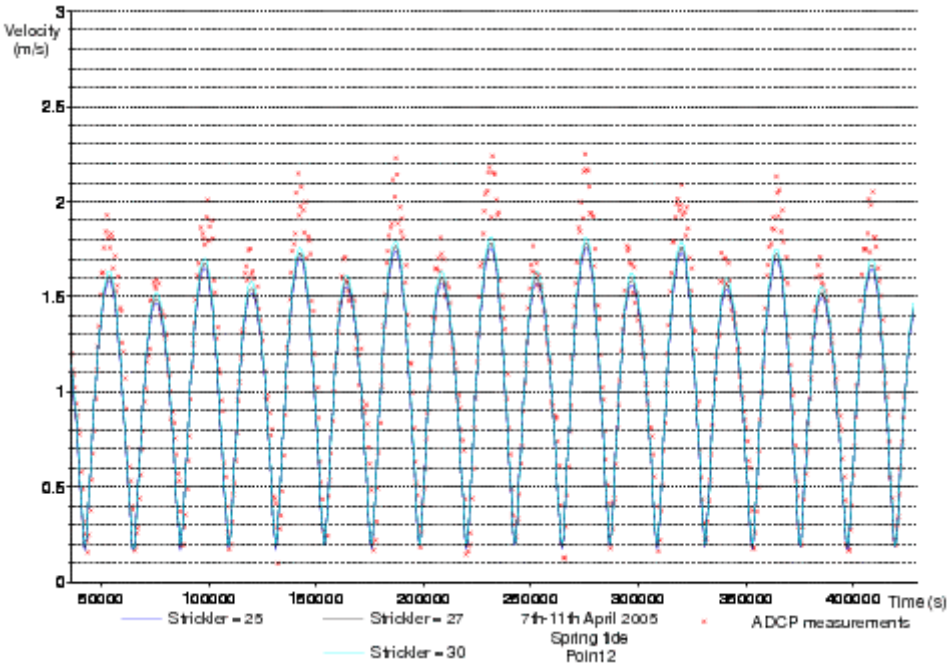

Figure C49: Magnitude of (vertically averaged) current velocity time series. Comparison between ADCP measurements (in red) and Telemac-3D results from April 7th to 11th 2005 at location 2.

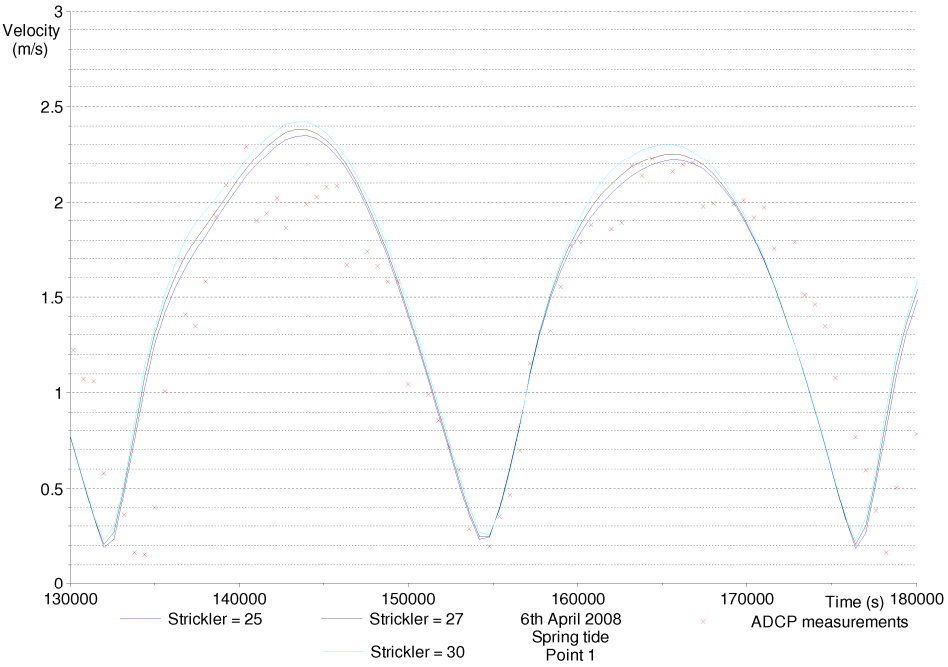

Figure C50: Magnitude of (vertically averaged) current velocity time series. Comparison between ADCP measurements (in red) and Telemac-2D results on April 6th 2008 afternoon at location 1.

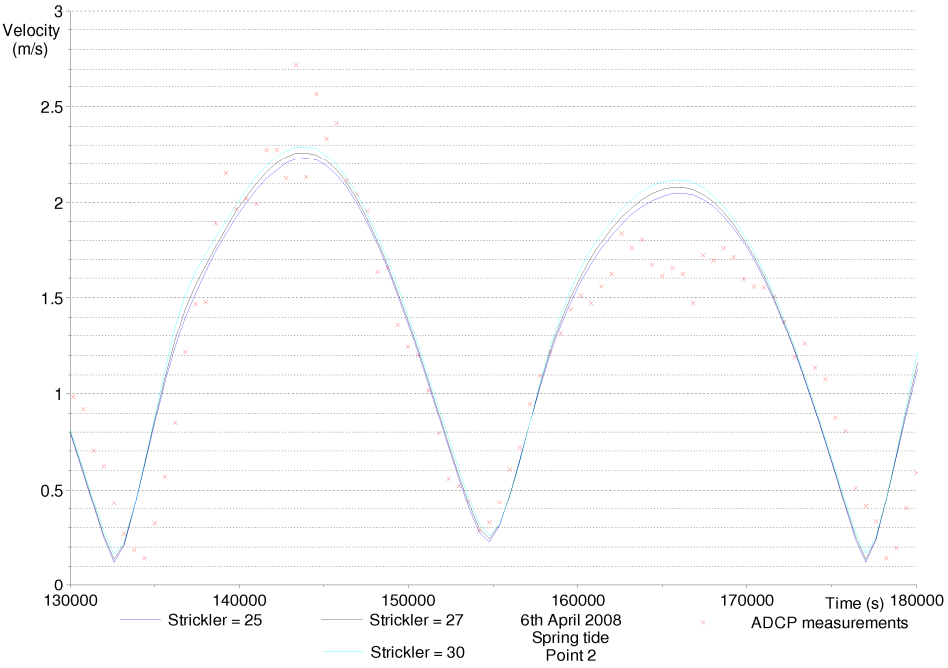

Figure C51: Magnitude of (vertically averaged) current velocity time series. Comparison between ADCP measurements (in red) and Telemac-2D results on April 6th 2008 afternoon at location 2.

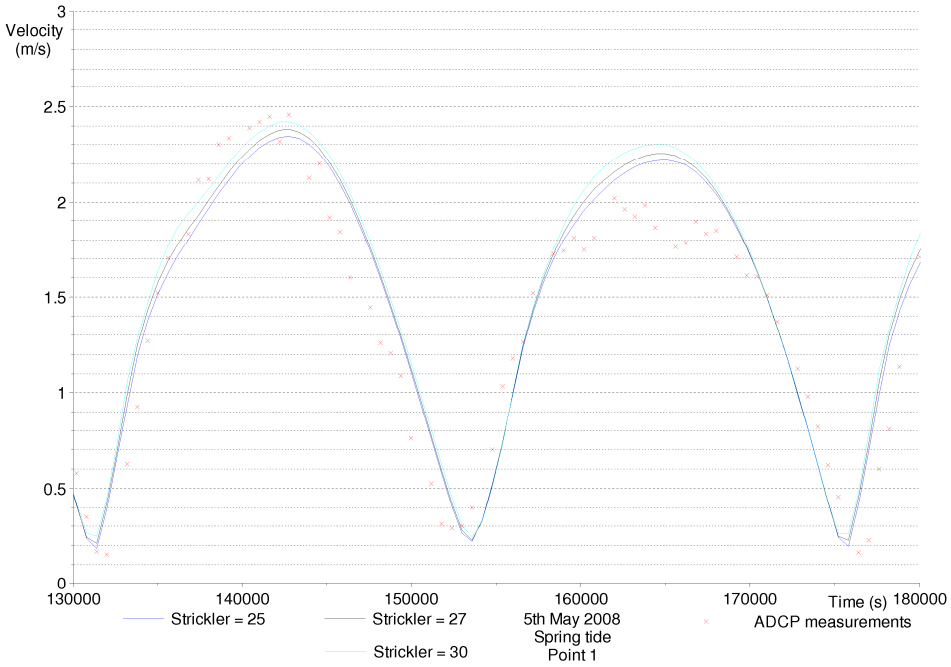

Figure C52: Magnitude of (vertically averaged) current velocity time series. Comparison between ADCP measurements (in red) and Telemac-2D results on May 5th 2008 afternoon at location 1.

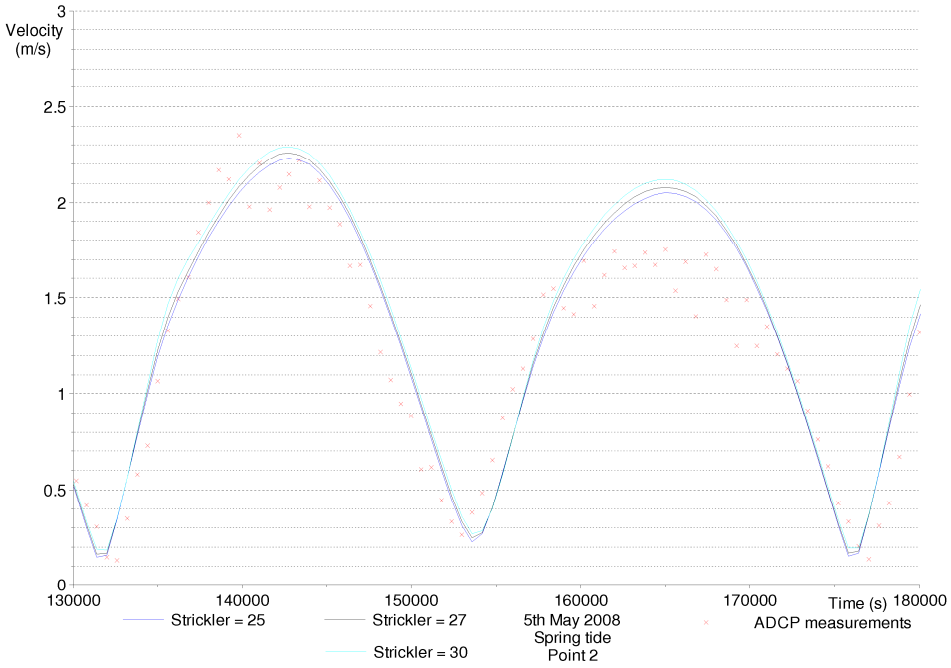

Figure C53: Magnitude of (vertically averaged) current velocity time series. Comparison between ADCP measurements (in red) and Telemac-2D results on May 5th 2008 afternoon at location 2.

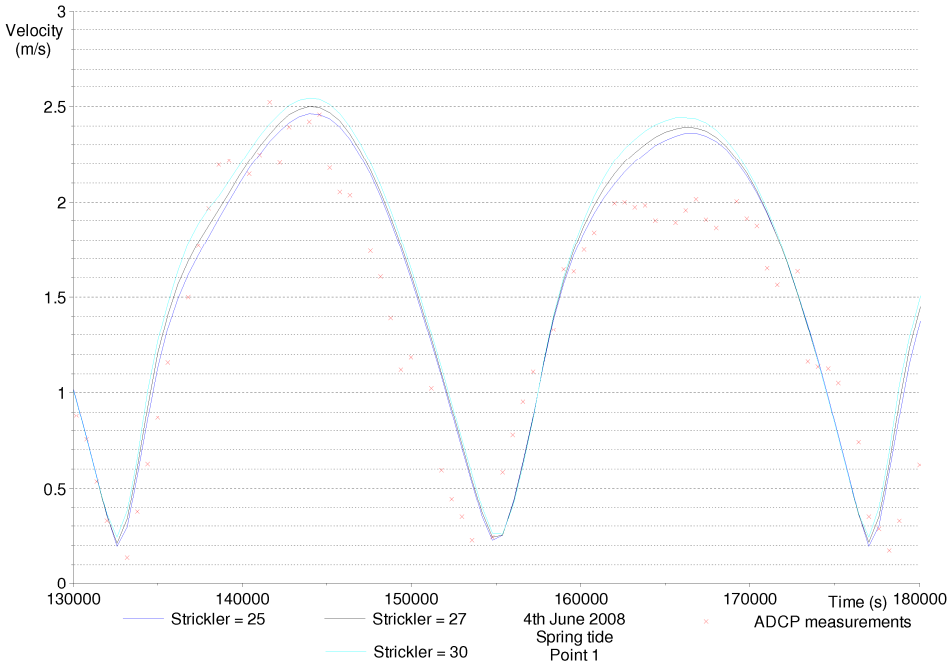

Figure C54: Magnitude of (vertically averaged) current velocity time series. Comparison between ADCP measurements (in red) and Telemac-2D results on June 4th 2008 afternoon at location 1.

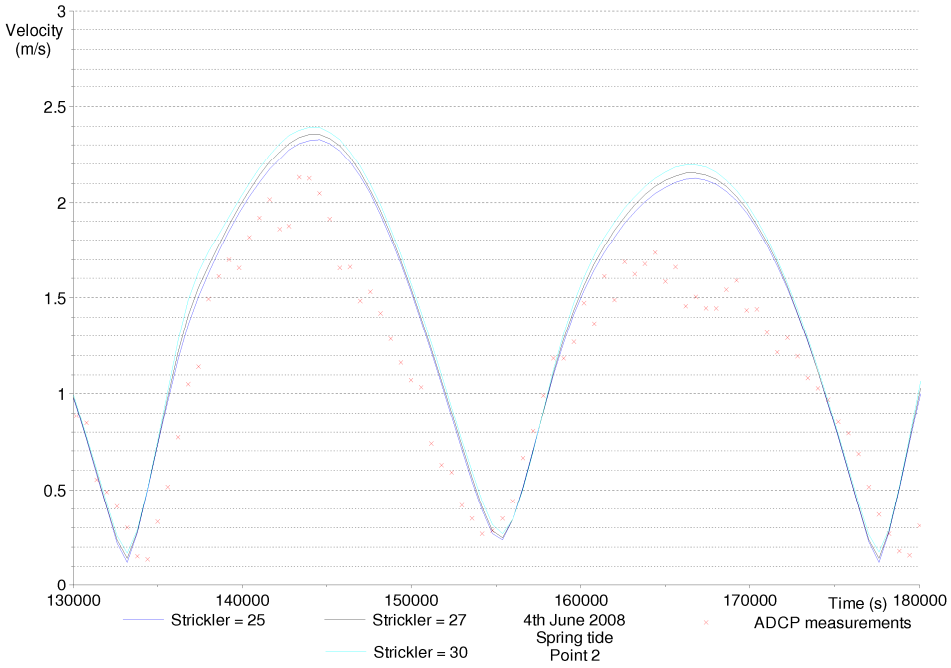

Figure C55: Magnitude of (vertically averaged) current velocity time series. Comparison between ADCP measurements (in red) and Telemac-2D results on June 4th 2008 afternoon at location 2.

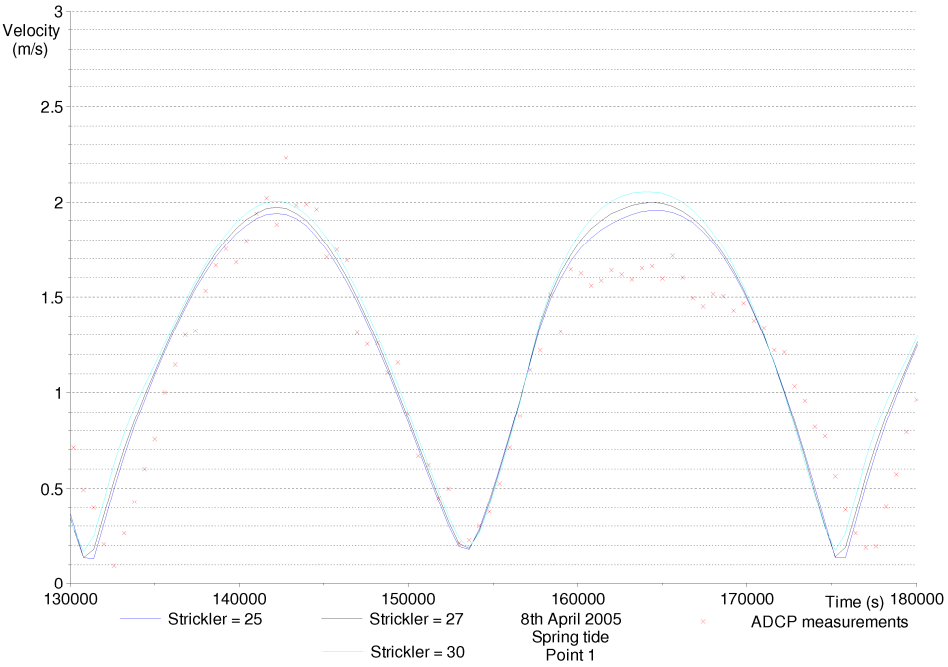

Figure C56: Magnitude of (vertically averaged) current velocity time series. Comparison between ADCP measurements (in red) and Telemac-2D results on April 8th 2005 afternoon at location 1.

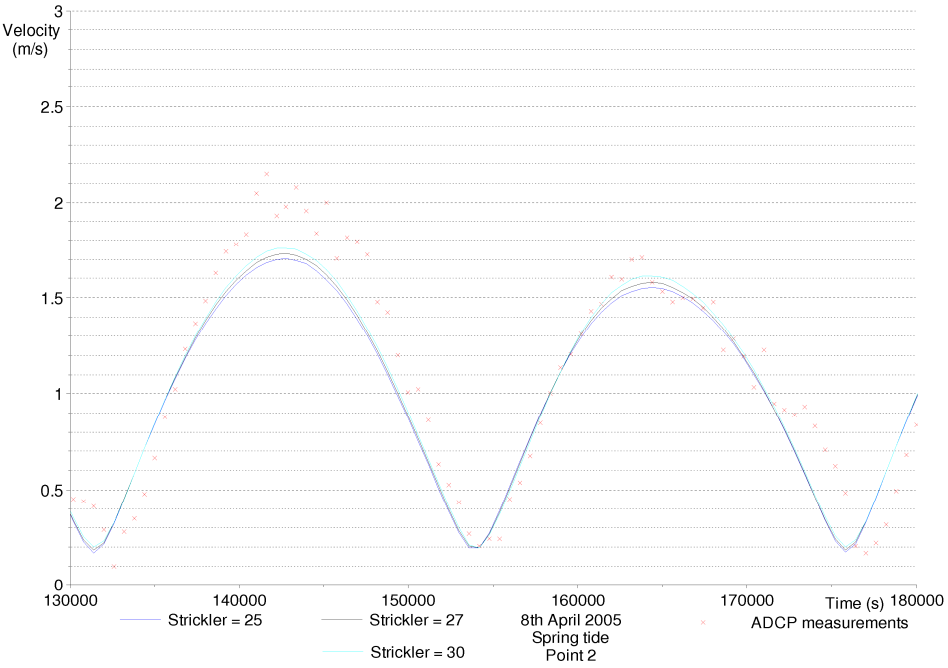

Figure C57: Magnitude of (vertically averaged) current velocity time series. Comparison between ADCP measurements (in red) and Telemac-2D results on April 8th 2005 afternoon at location 2.

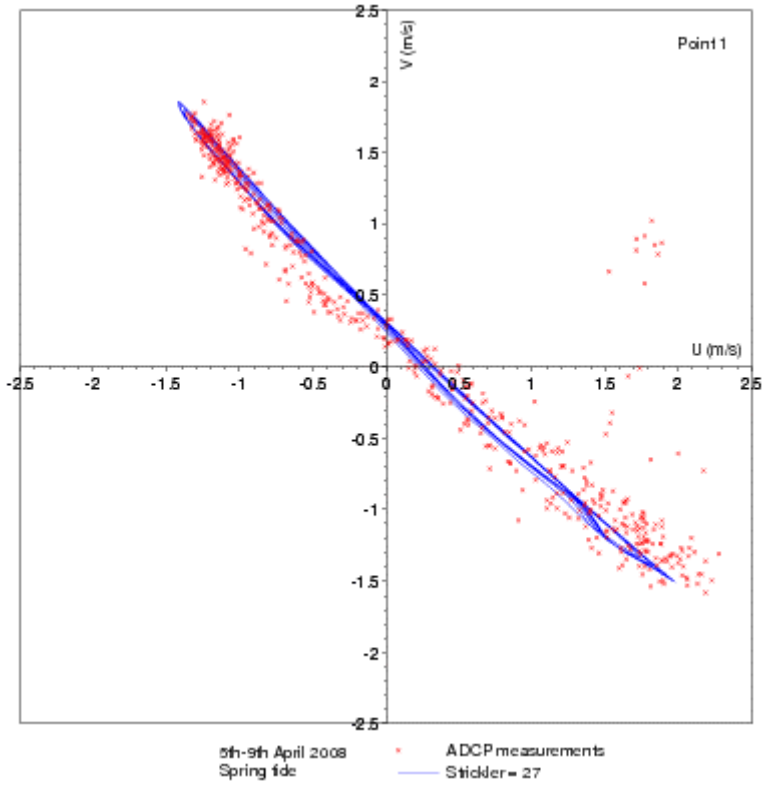

Figure C58: Tidal roses. Comparison between ADCP measurements (in red) and Telemac-3D results from April 5th to 9th 2008 at location 1.

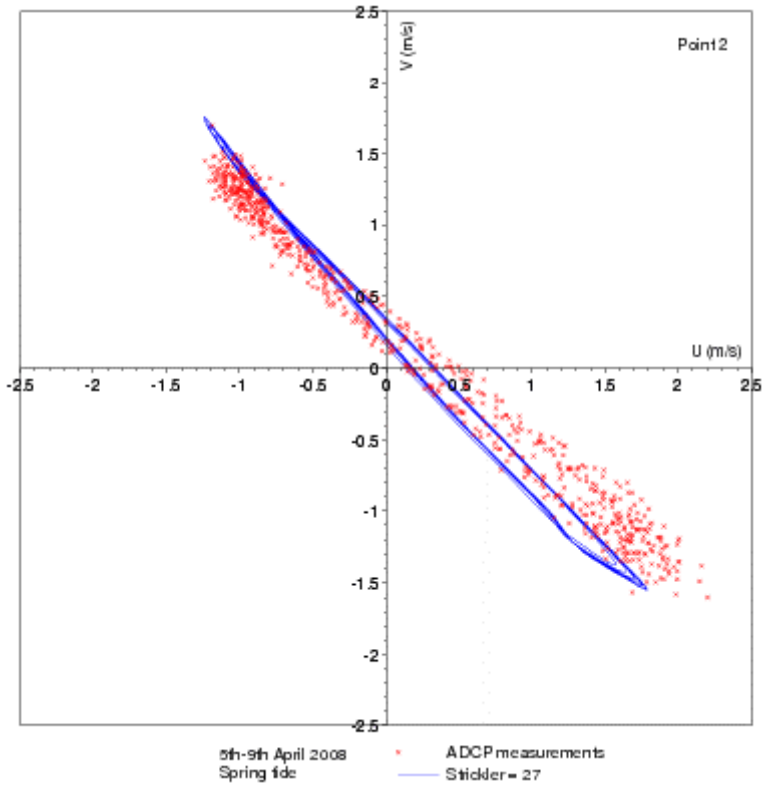

Figure C59: Tidal roses. Comparison between ADCP measurements (in red) and Telemac-3D results from April 5th to 9th 2008 at location 2.

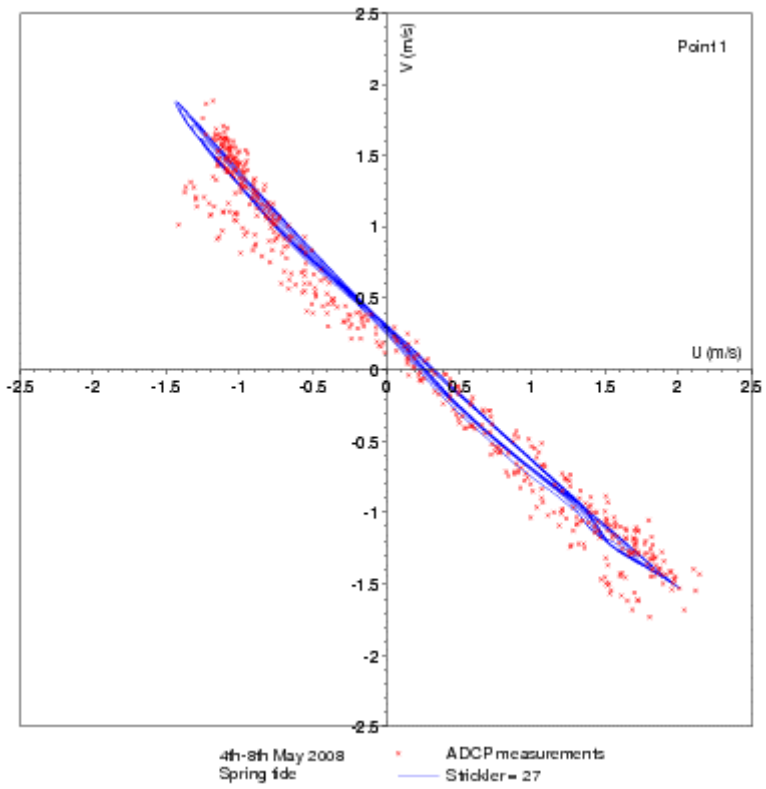

Figure C60: Tidal roses. Comparison between ADCP measurements (in red) and Telemac-3D results from May 4th to 8th 2008 at location 1.

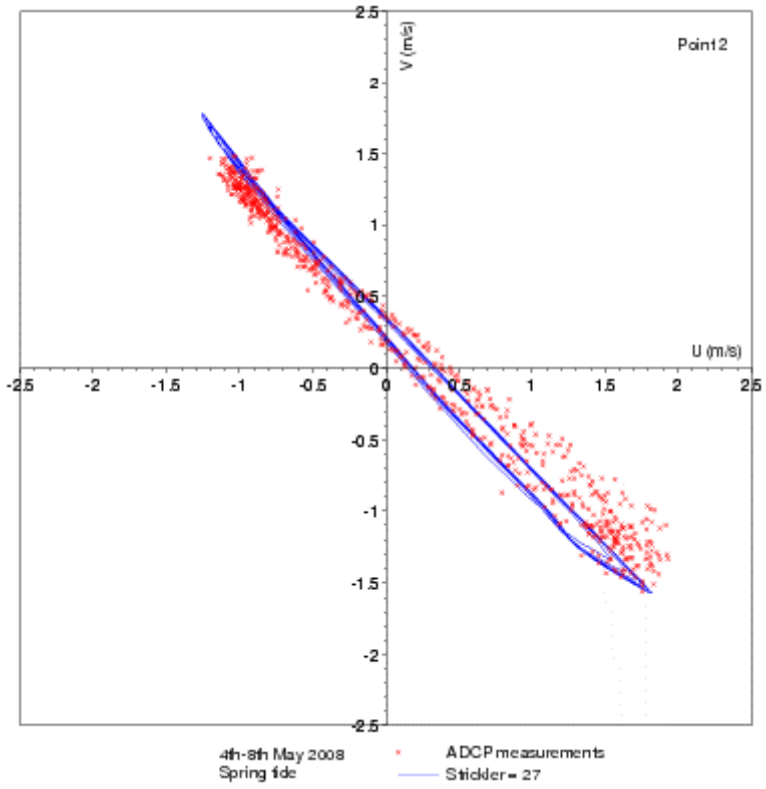

Figure C61: Tidal roses. Comparison between ADCP measurements (in red) and Telemac-3D results from May 4th to 8th 2008 at location 2.

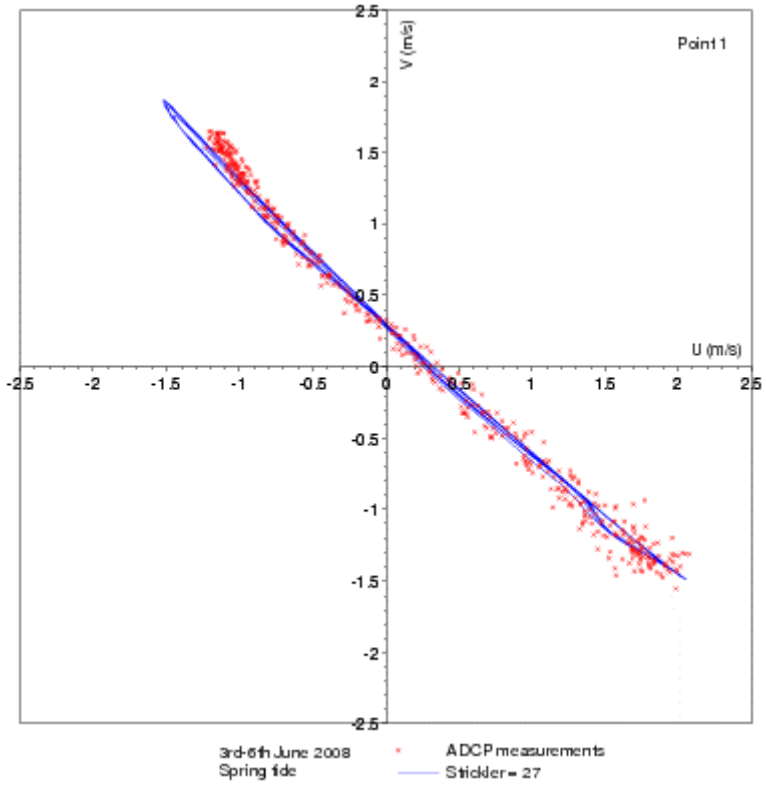

Figure C62: Tidal roses. Comparison between ADCP measurements (in red) and Telemac-3D results from June 3rd to 6th 2008 at location 1.

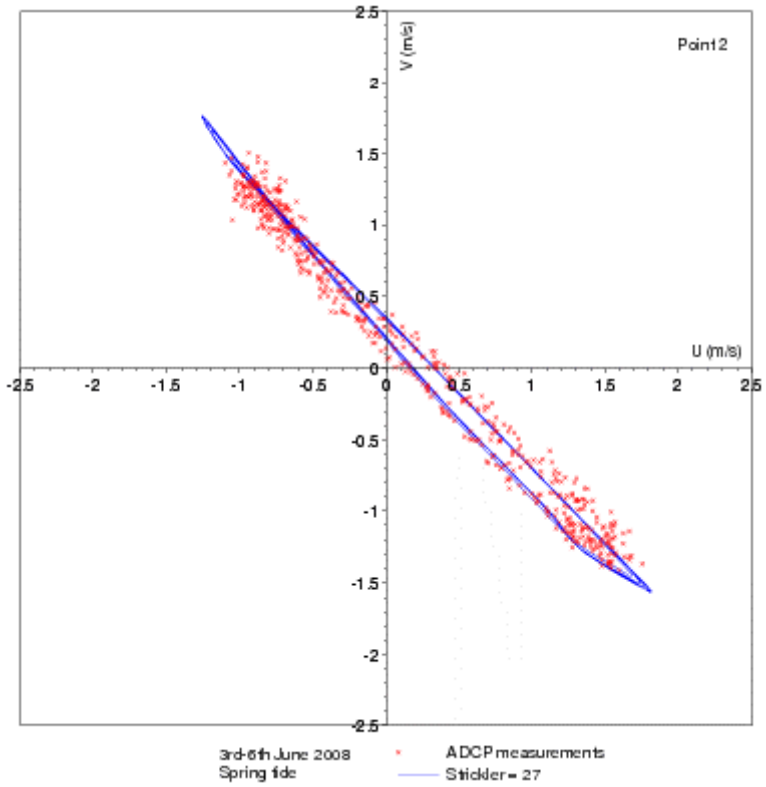

Figure C63: Tidal roses. Comparison between ADCP measurements (in red) and Telemac-3D results from June 3rd to 6th 2008 at location 2.

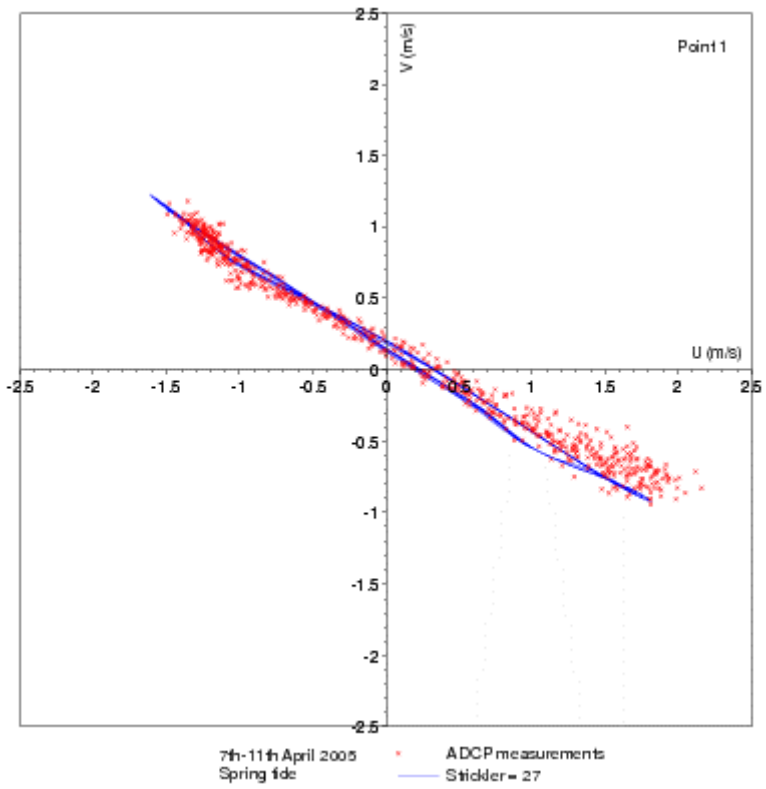

Figure C64: Tidal roses. Comparison between ADCP measurements (in red) and Telemac-3D results from April 7th to 11th 2005 at location 1.

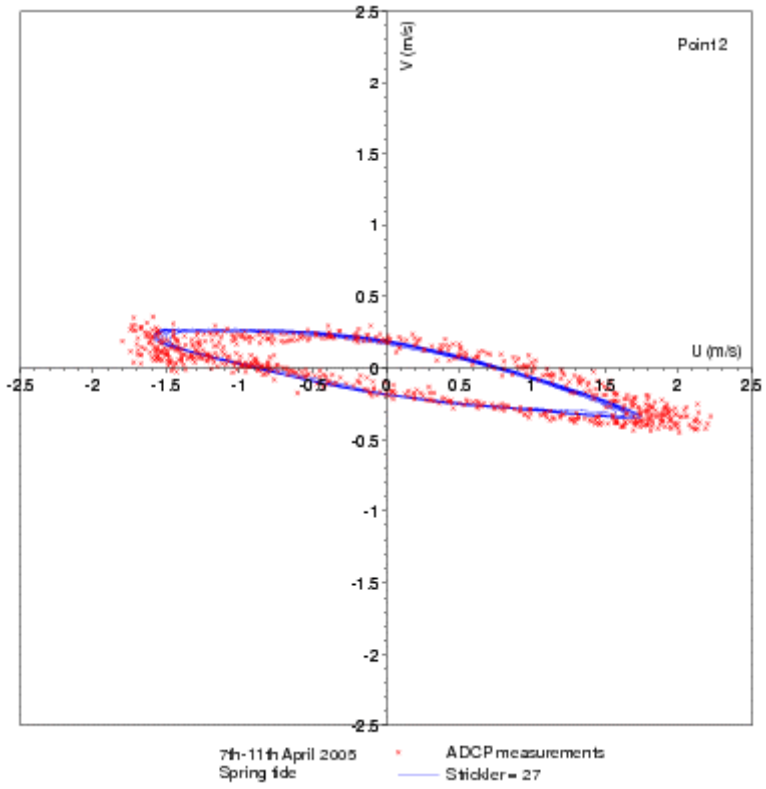

Figure C65: Tidal roses. Comparison between ADCP measurements (in red) and Telemac-3D results from April 7th to 11th 2005 at location 2.

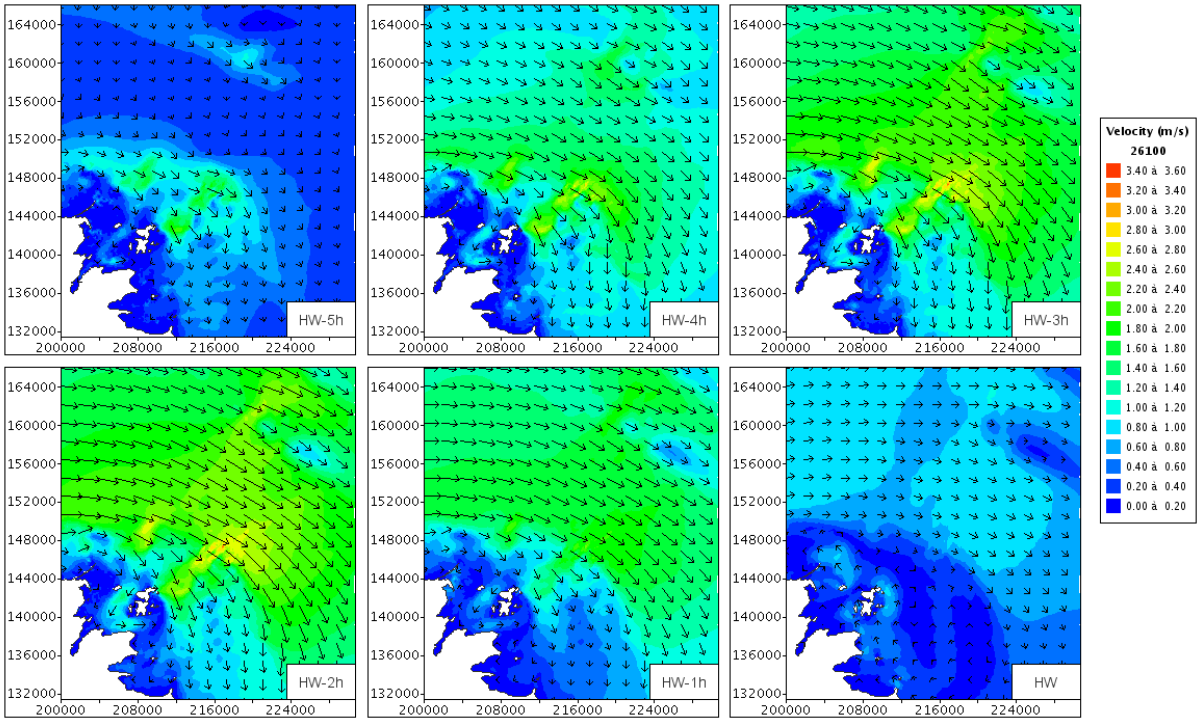

Figure C66: Current fields during an exceptional spring tide.

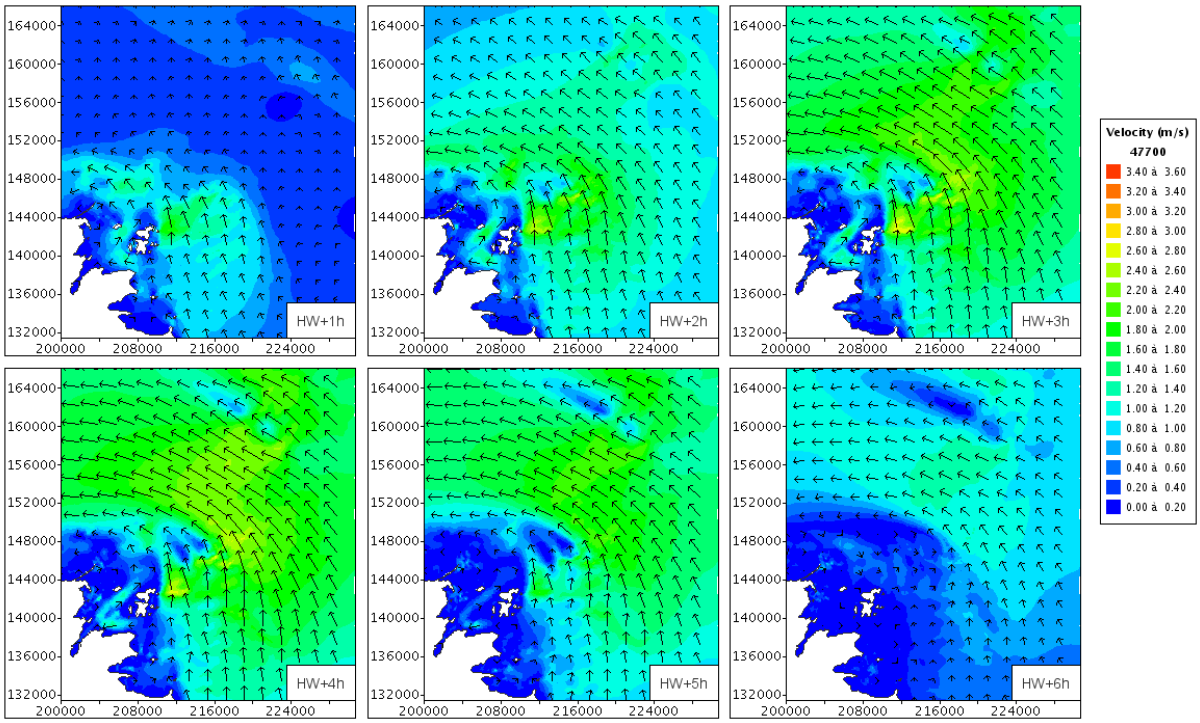

Figure C67: Current fields during an exceptional spring tide.

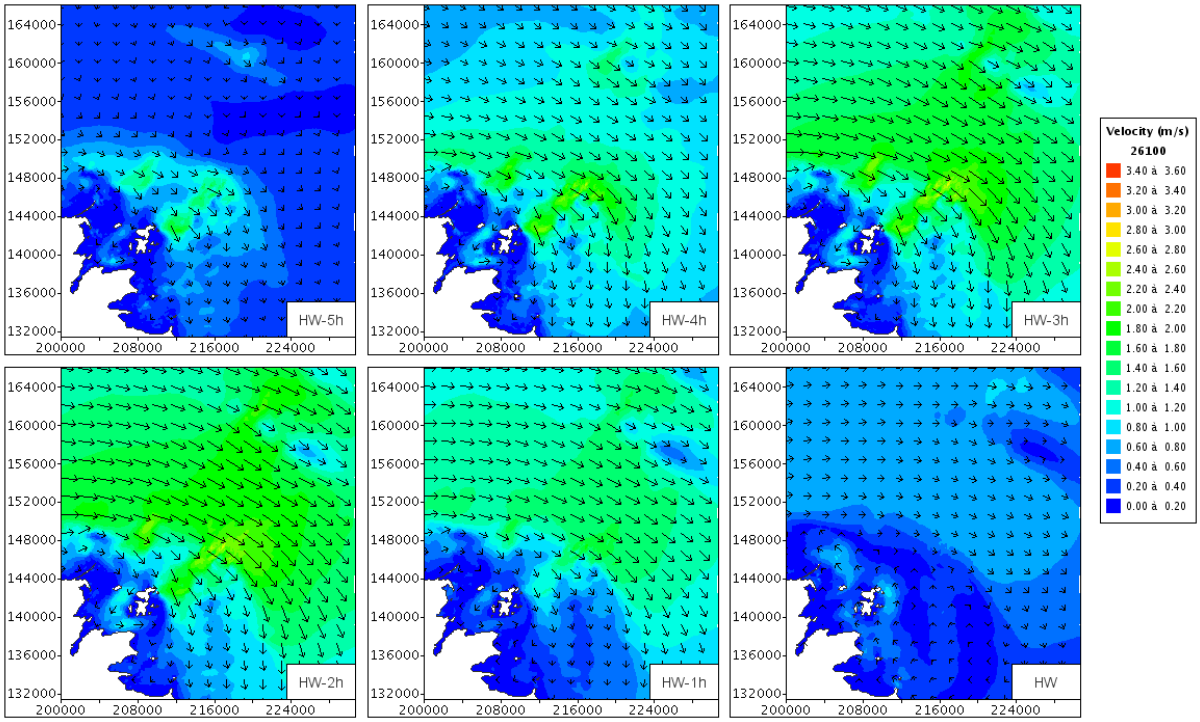

Figure C68: Current fields during a mean spring tide.

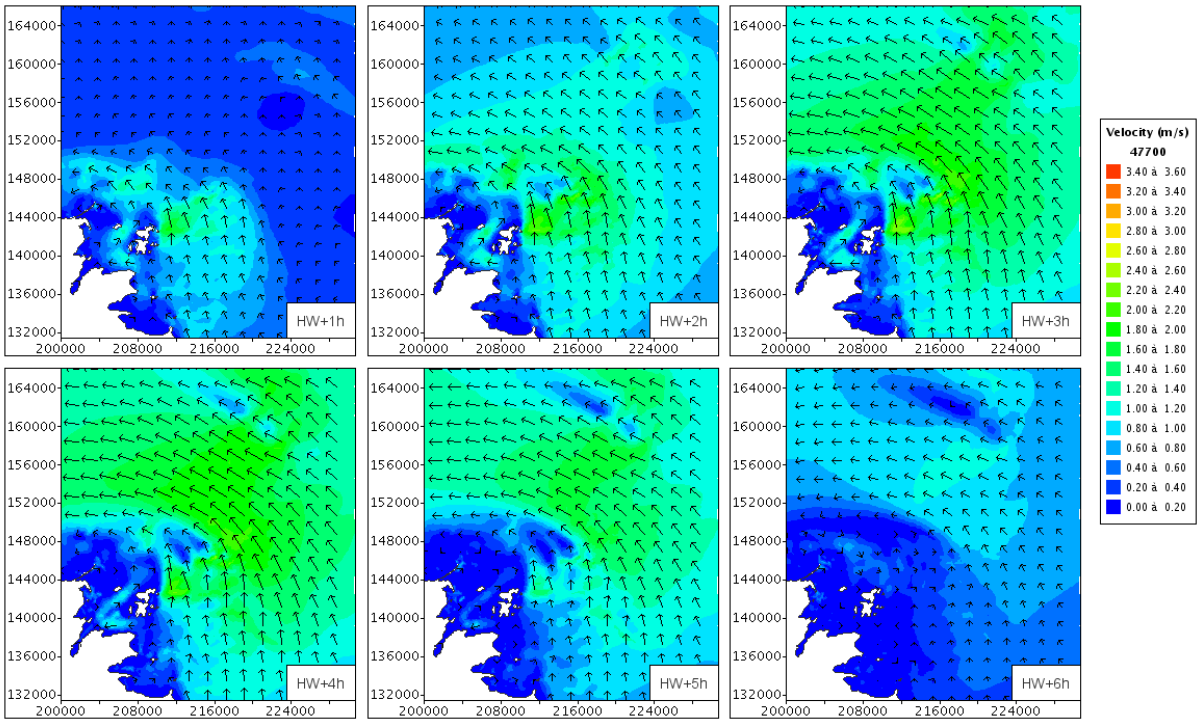

Figure C69: Current fields during a mean spring tide.

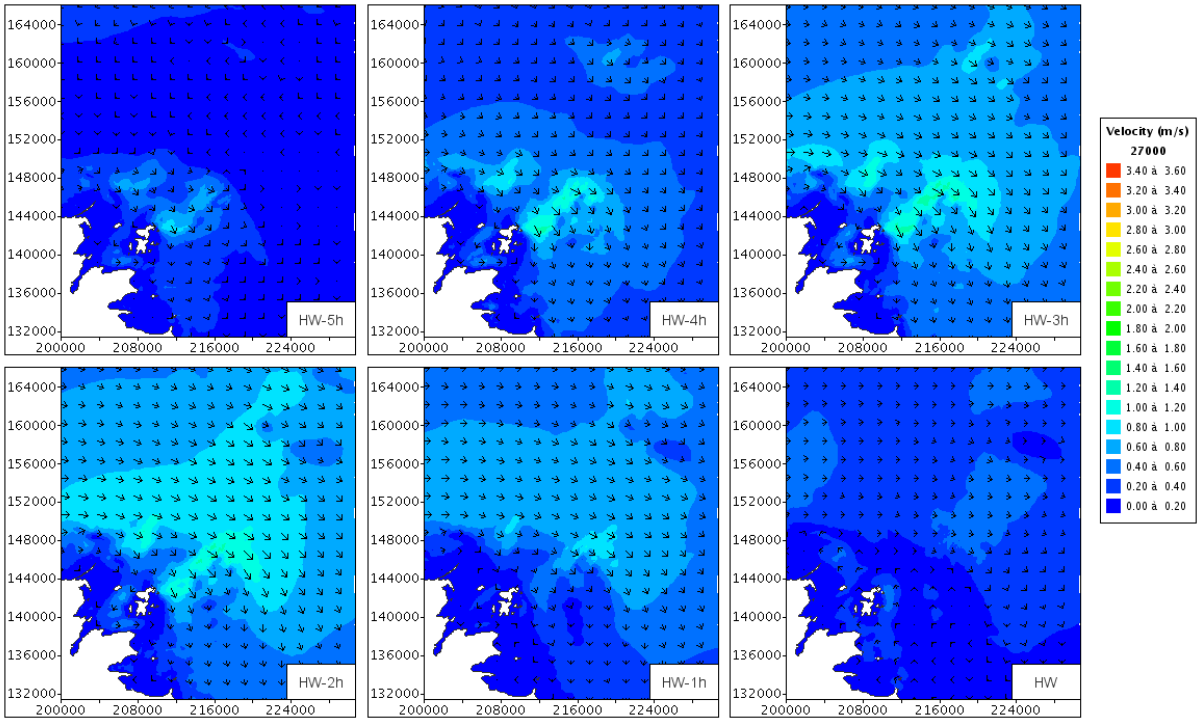

Figure C70: Current fields during a mean neap tide.

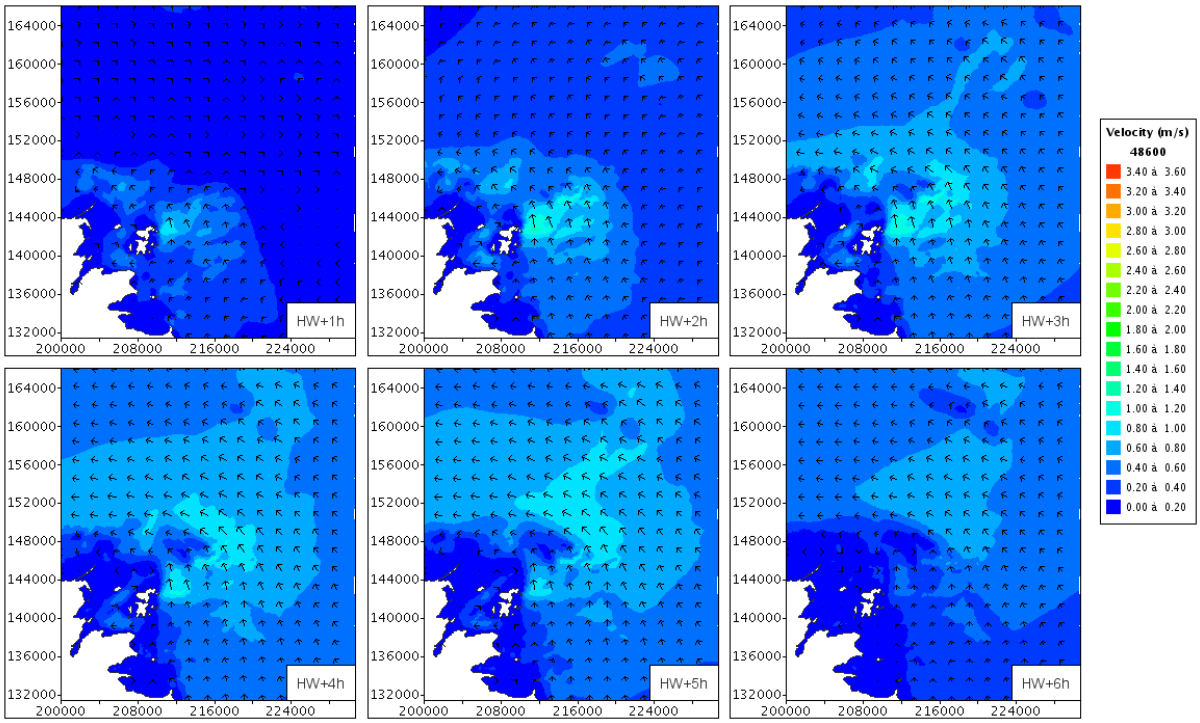

Figure C71: Current fields during a mean neap tide.

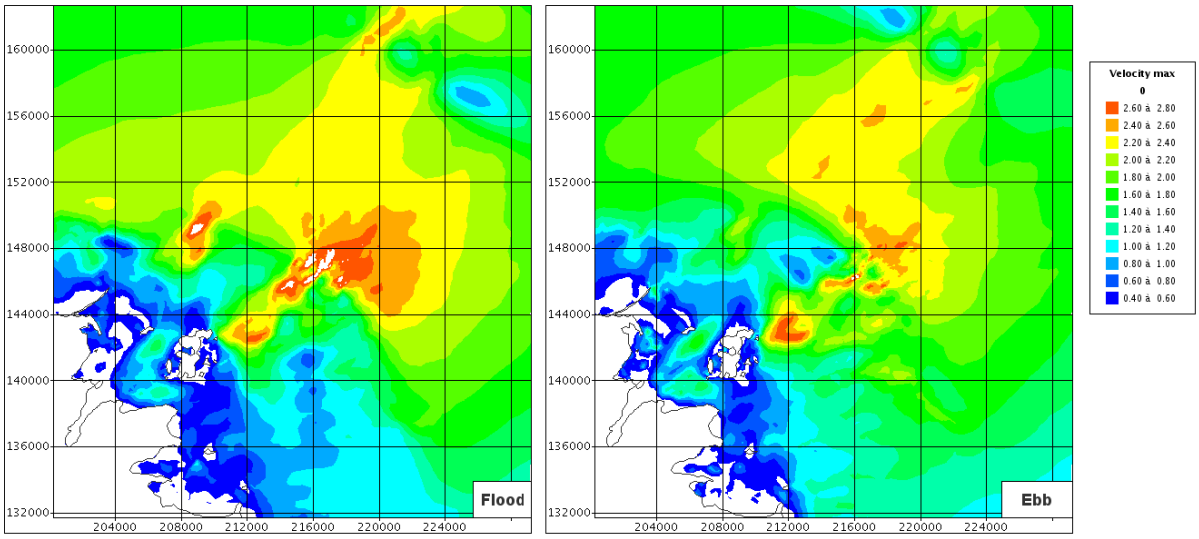

Figure C72: Maximum current fields during flood (left) and ebb (right) of an exceptional spring tide.

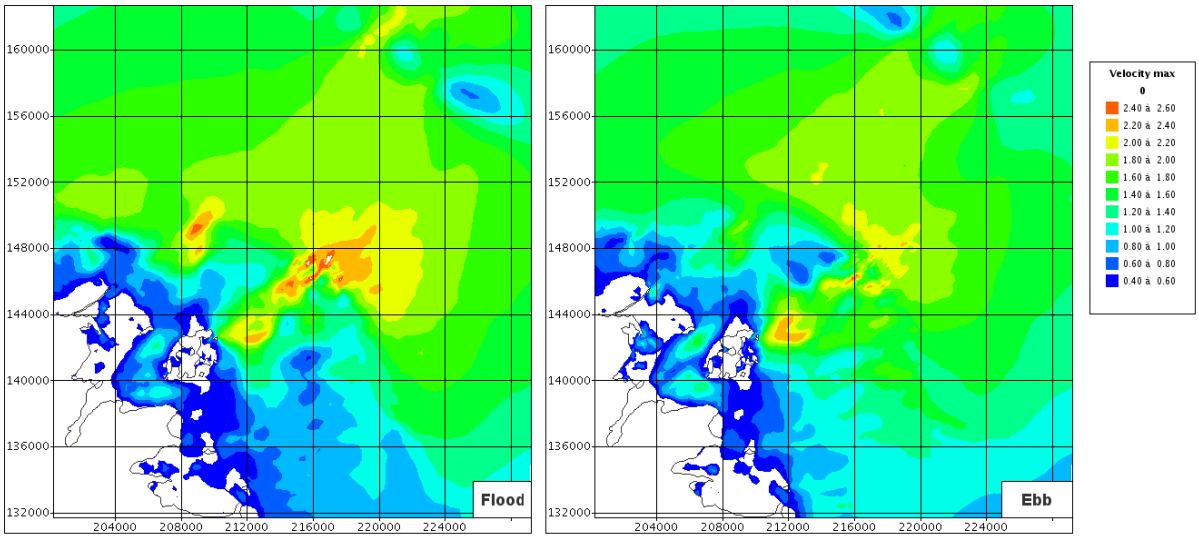

Figure C73: Maximum current fields during flood (left) and ebb (right) of a mean spring tide.

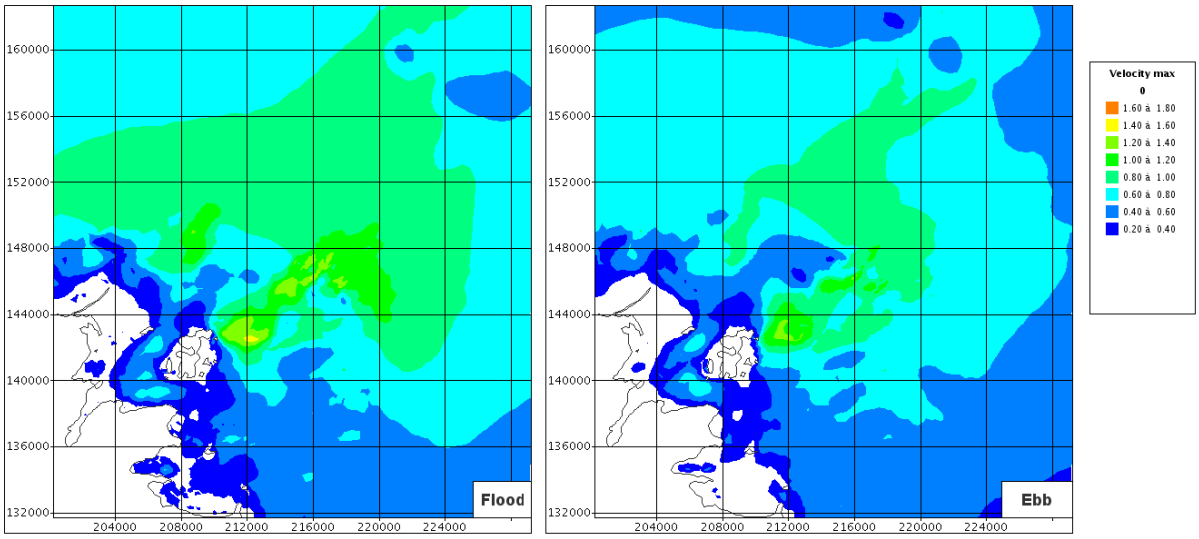

Figure C74: Maximum current fields during flood (left) and ebb (right) of a mean neap tide.

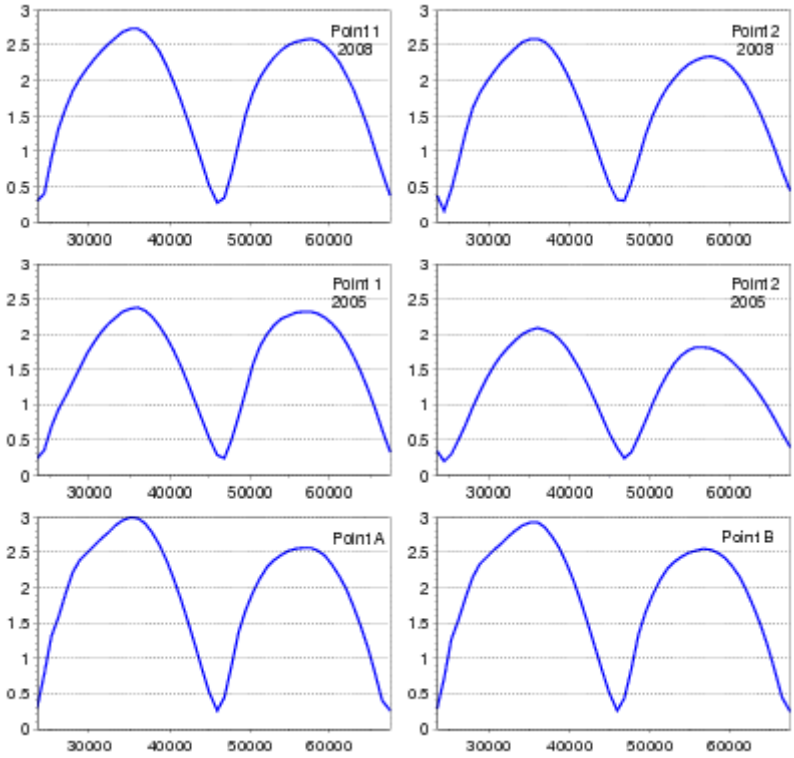

Figure C75: Magnitude of (vertically averaged) current velocity time series during an exceptional spring tide, for six locations.

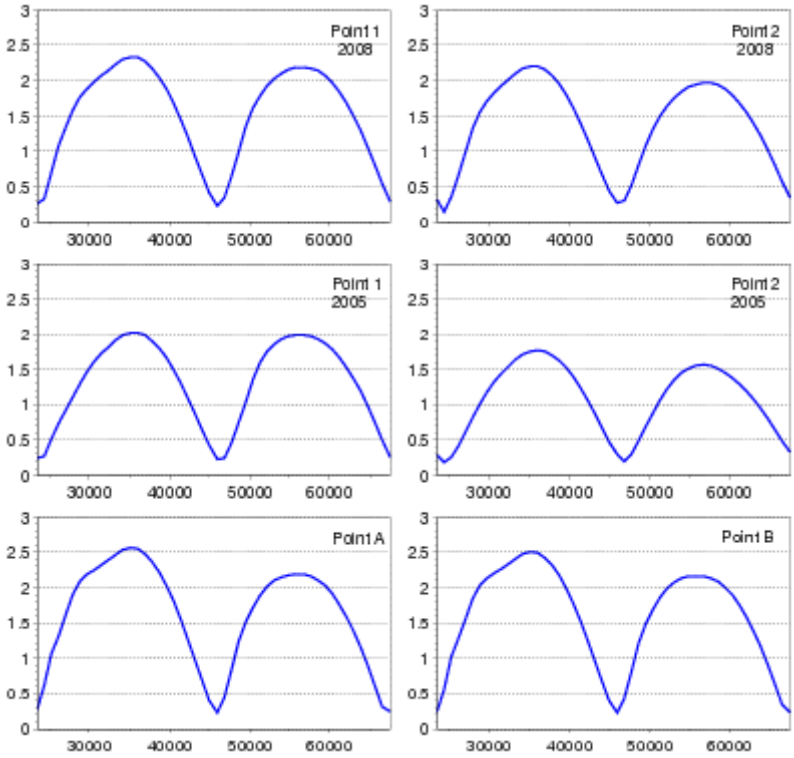

Figure C76: Magnitude of (vertically averaged) current velocity time series during a mean spring tide, for six locations.

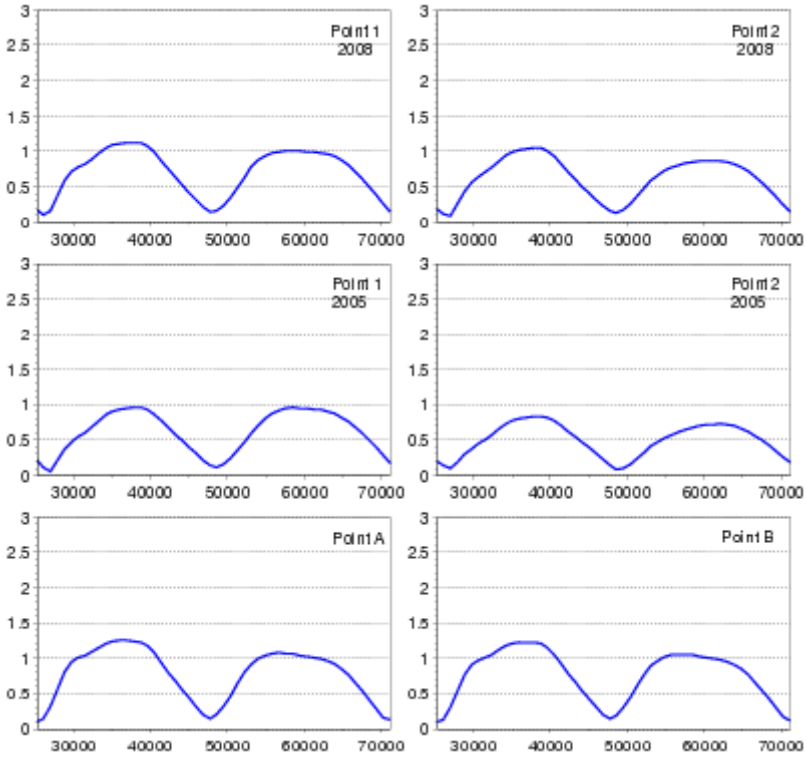

Figure C77: Magnitude of (vertically averaged) current velocity time series during a mean neap tide, for six locations.

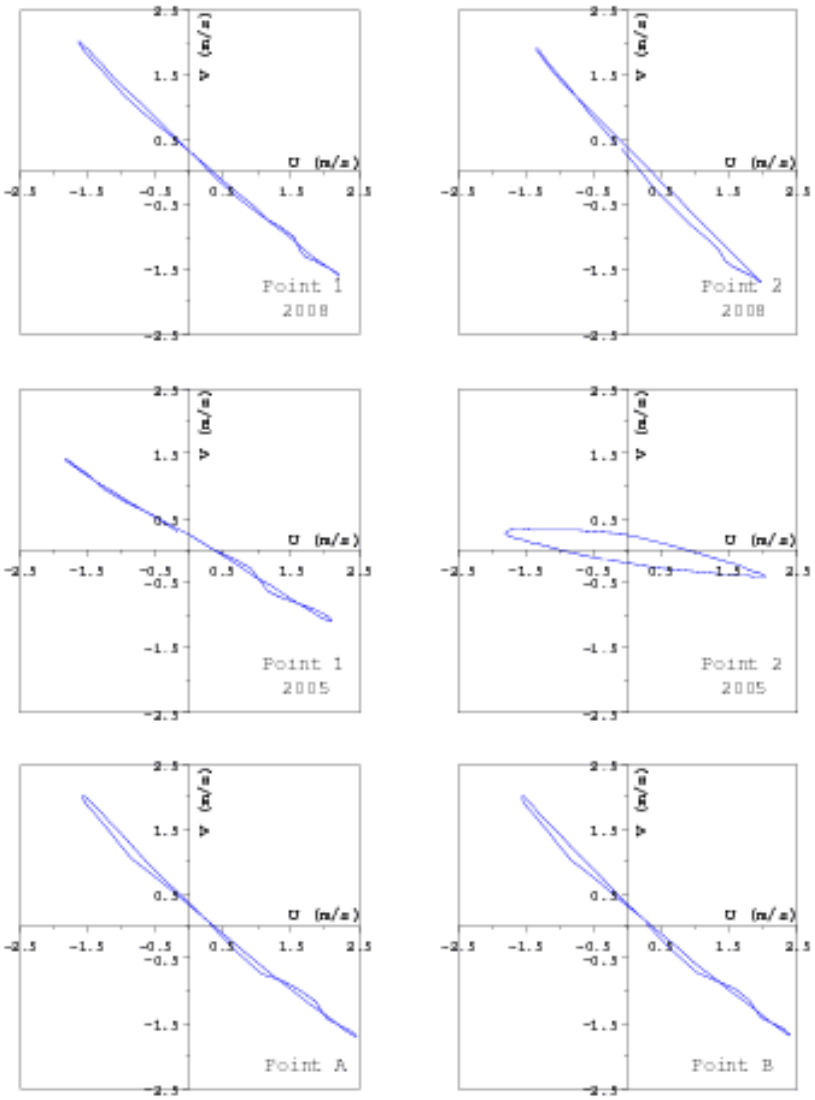

Figure C78: Tidal rose during an exceptional spring tide, for six locations.

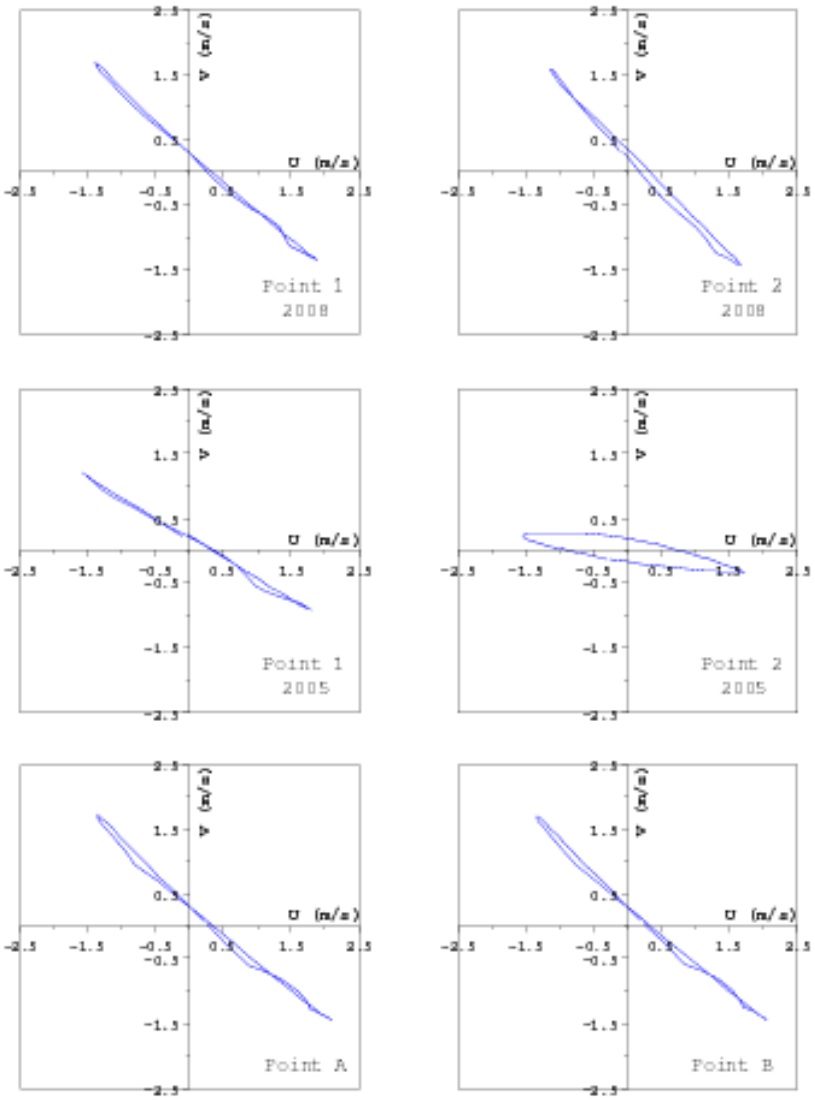

Figure C79: Tidal rose during a mean spring tide, for six locations.

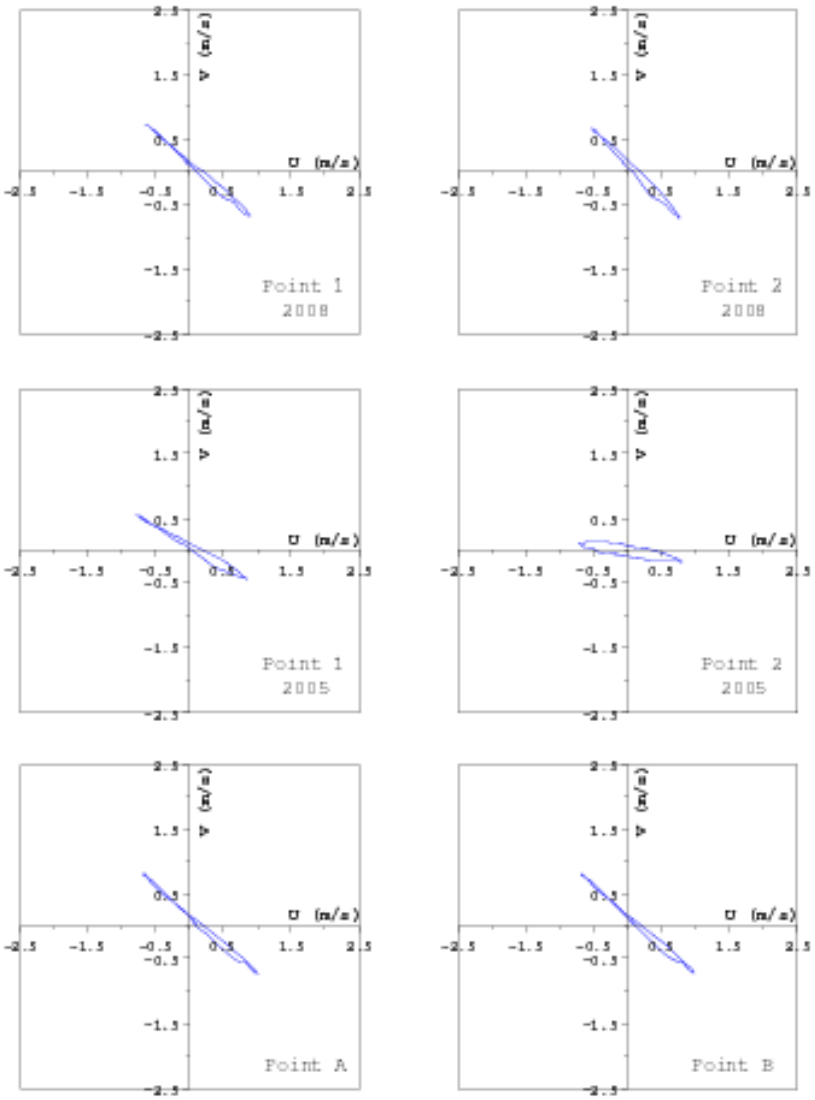

Figure C80: Tidal rose during a mean neap tide, for six locations.

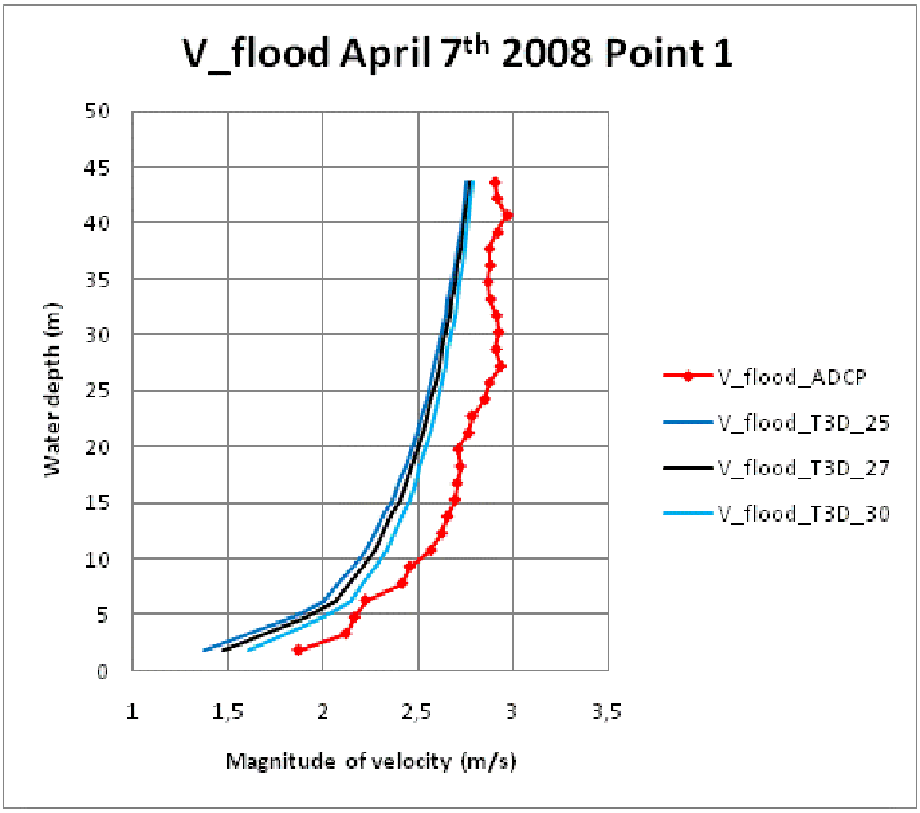

Figure C81: Velocity profile along the vertical during flood (April 7th 2008) at location 1. Comparison between ADCP measurements (in red) and Telemac-3D results.

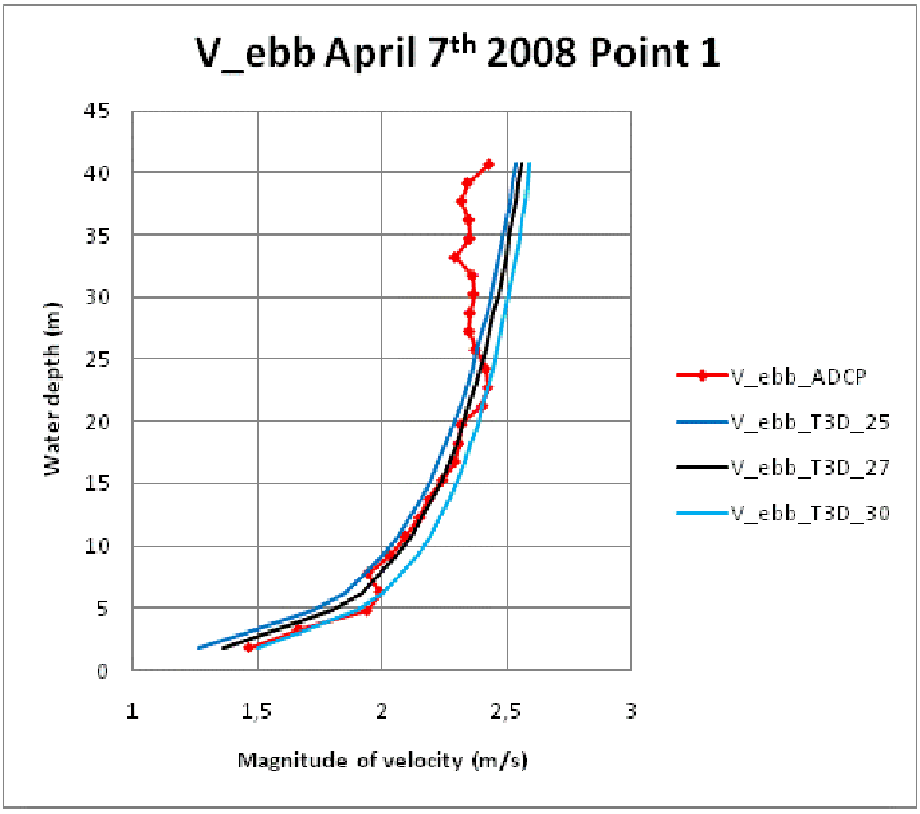

Figure C82: Velocity profile along the vertical during ebb (April 7th 2008) at location 1. Comparison between ADCP measurements (in red) and Telemac-3D results.

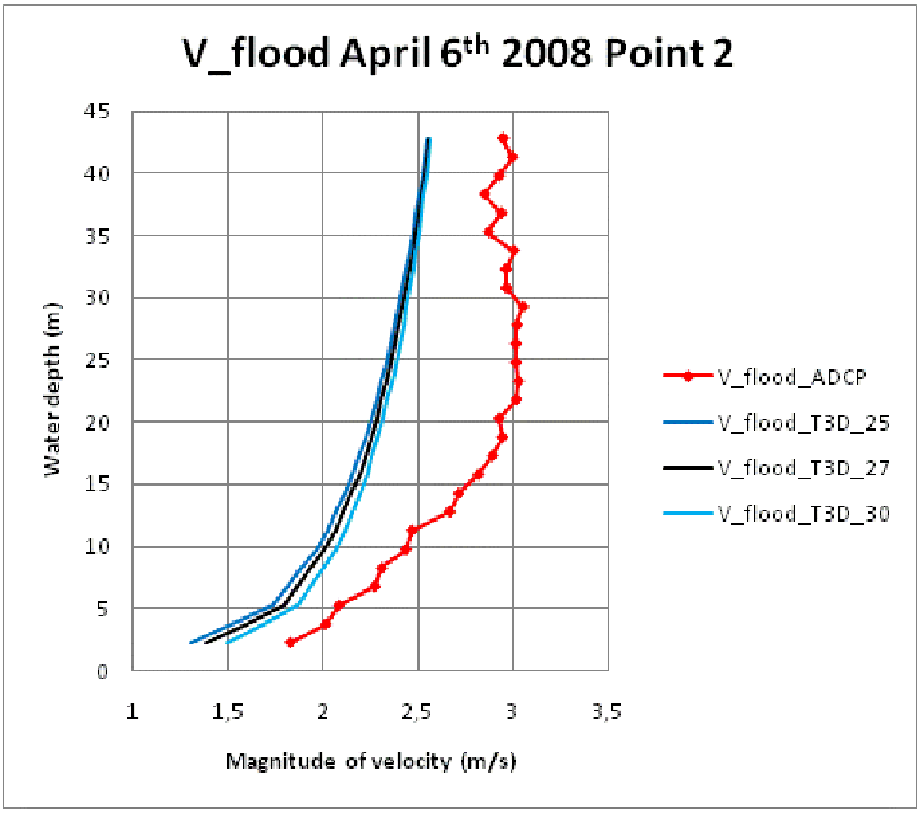

Figure C83: Velocity profile along the vertical during flood (April 6th 2008) at location 2. Comparison between ADCP measurements (in red) and Telemac-3D results.

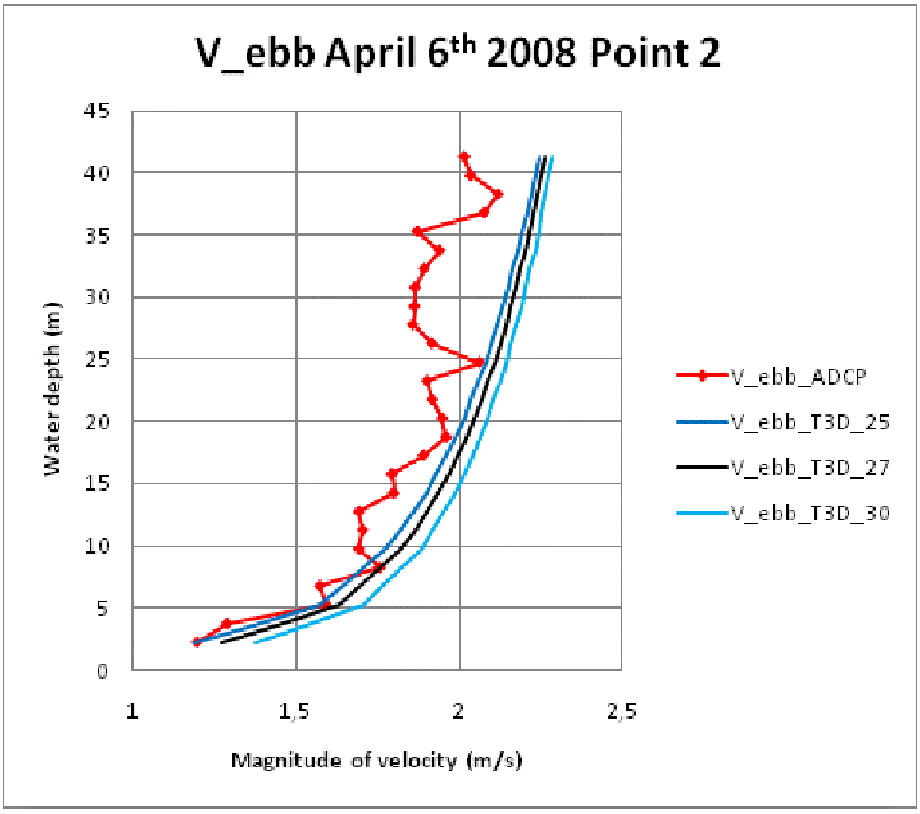

Figure C84: Velocity profile along the vertical during ebb (April 6th 2008) at location 2. Comparison between ADCP measurements (in red) and Telemac-3D results.

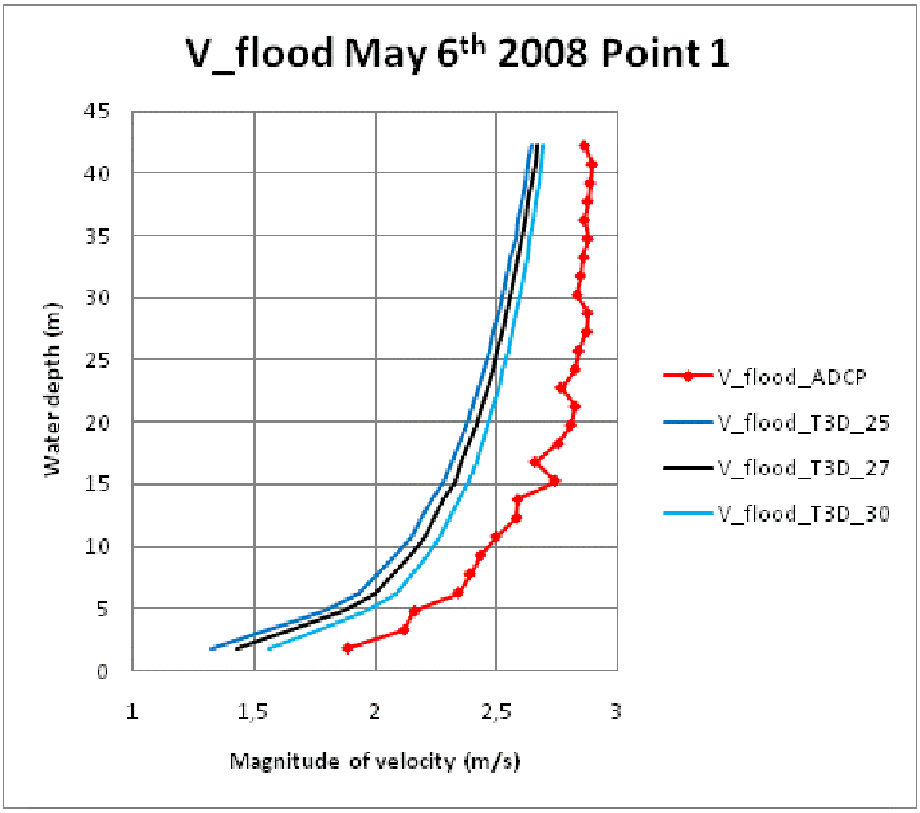

Figure C85: Velocity profile along the vertical during flood (May 6th 2008) at location 1. Comparison between ADCP measurements (in red) and Telemac-3D results.

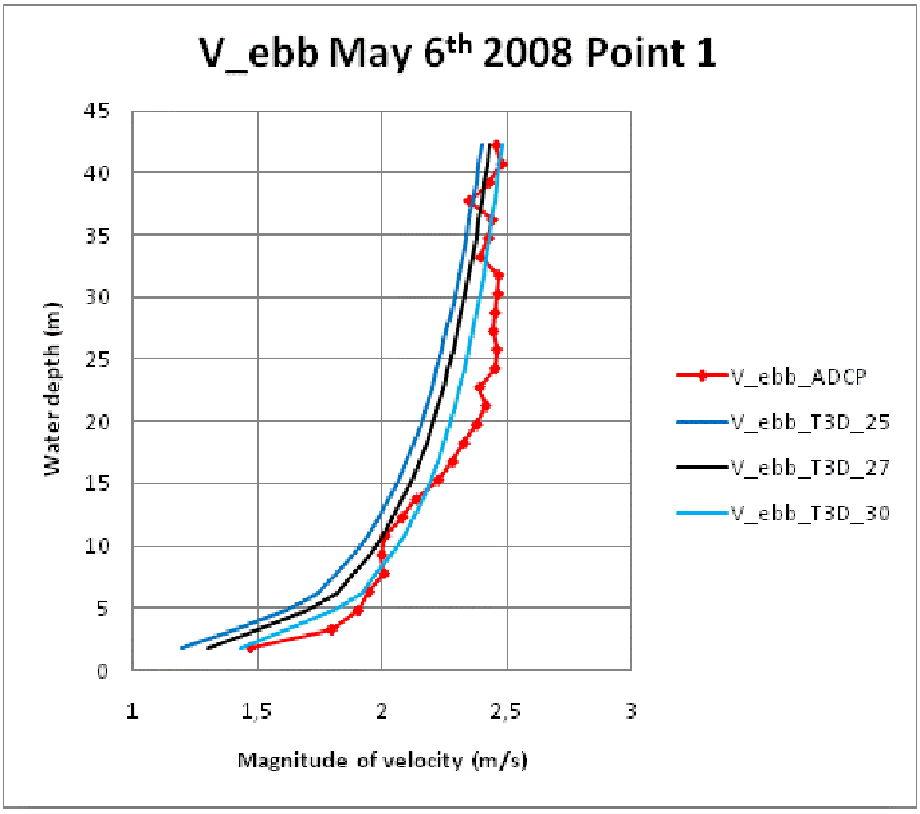

Figure C86: Velocity profile along the vertical during ebb (May 6th 2008) at location 1. Comparison between ADCP measurements (in red) and Telemac-3D results.

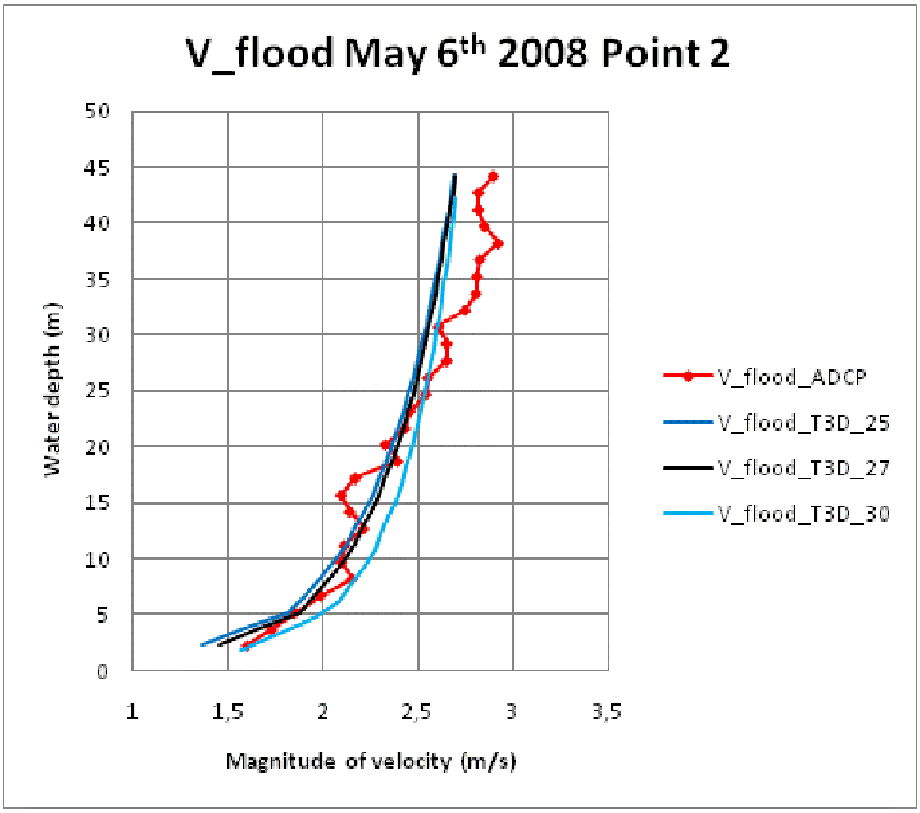

Figure C87: Velocity profile along the vertical during flood (May 6th 2008) at location 2. Comparison between ADCP measurements (in red) and Telemac-3D results.

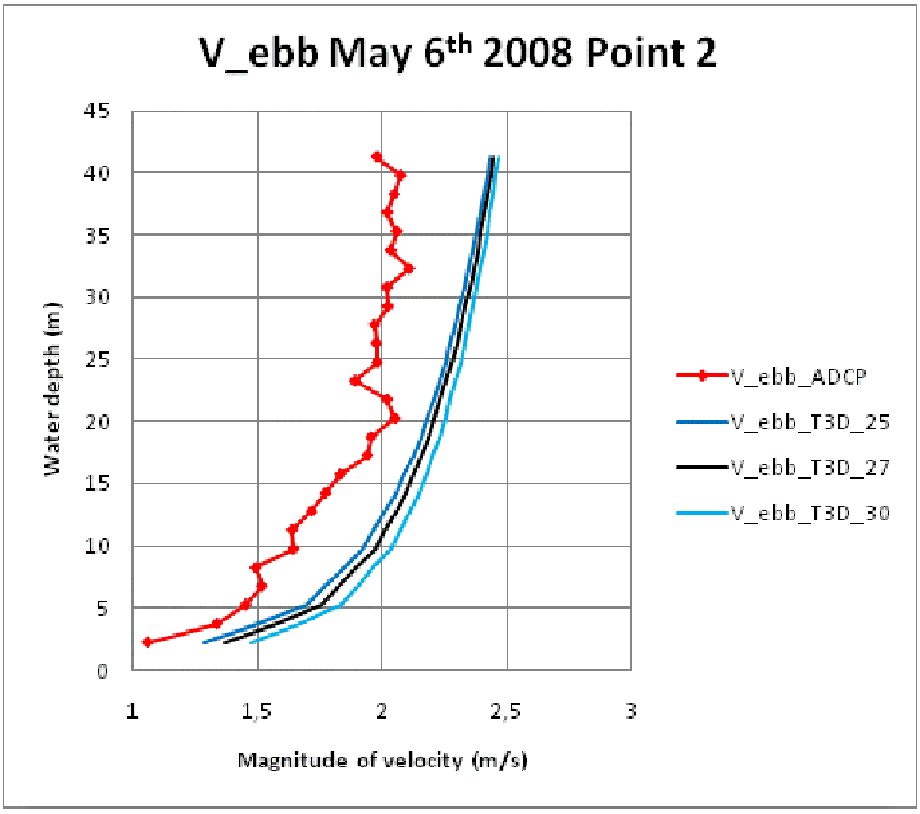

Figure C88: Velocity profile along the vertical during ebb (May 6th 2008) at location 2. Comparison between ADCP measurements (in red) and Telemac-3D results.

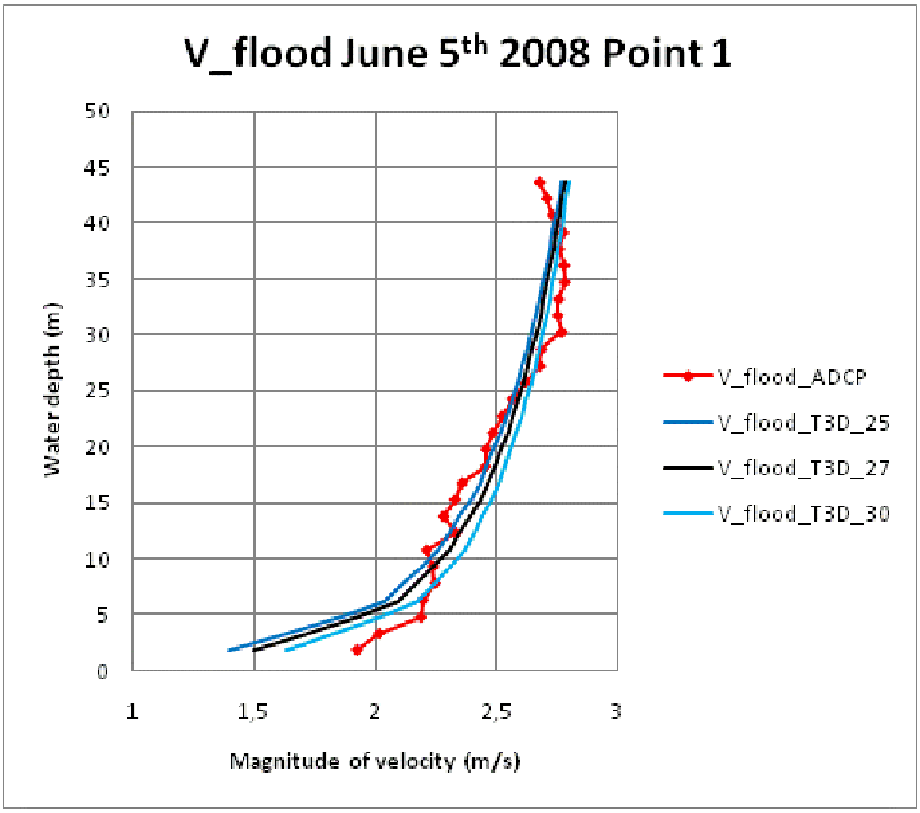

Figure C89: Velocity profile along the vertical during flood (June 5th 2008) at location 1. Comparison between ADCP measurements (in red) and Telemac-3D results.

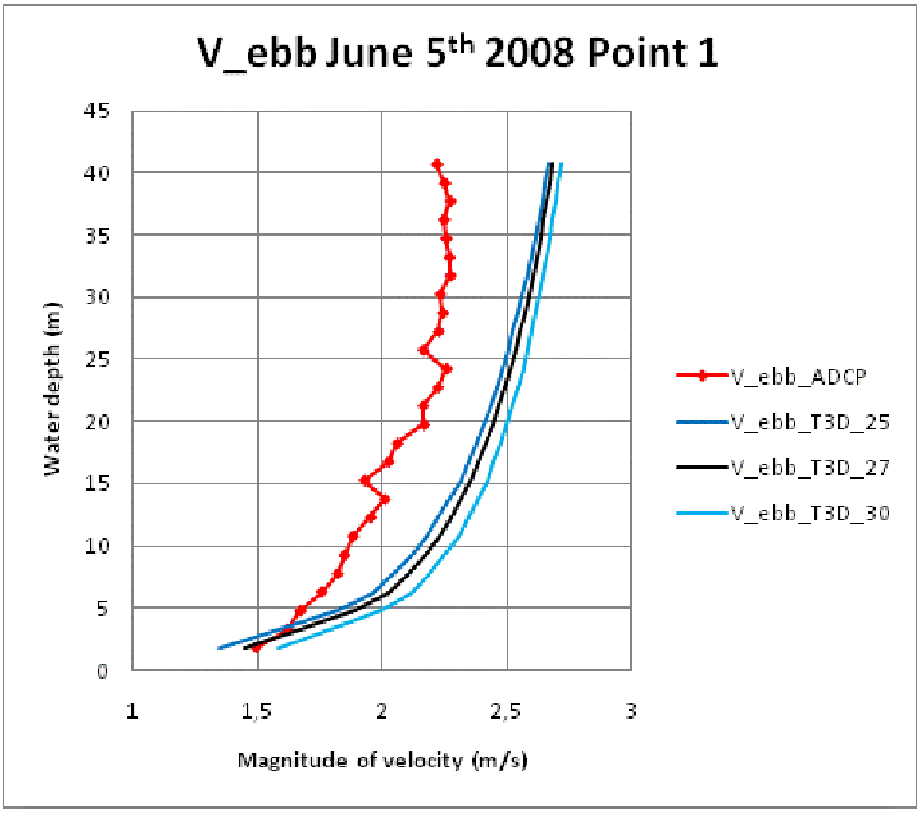

Figure C90: Velocity profile along the vertical during ebb (June 5th 2008) at location 1. Comparison between ADCP measurements (in red) and Telemac-3D results.

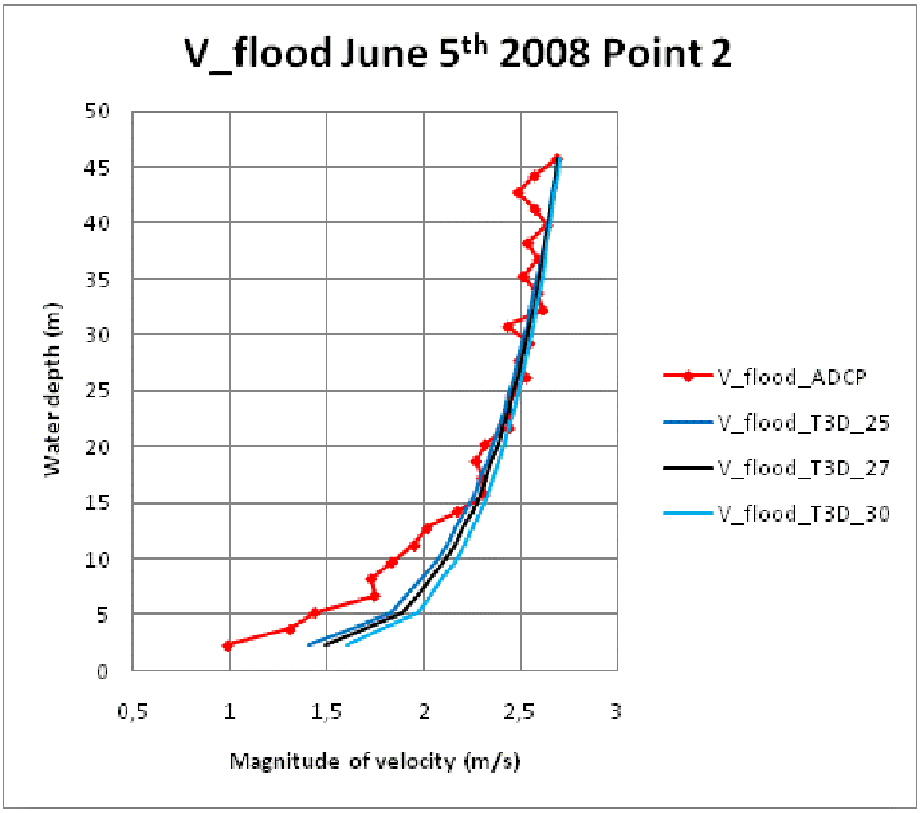

Figure C91: Velocity profile along the vertical during flood (June 5th 2008) at location 2. Comparison between ADCP measurements (in red) and Telemac-3D results.

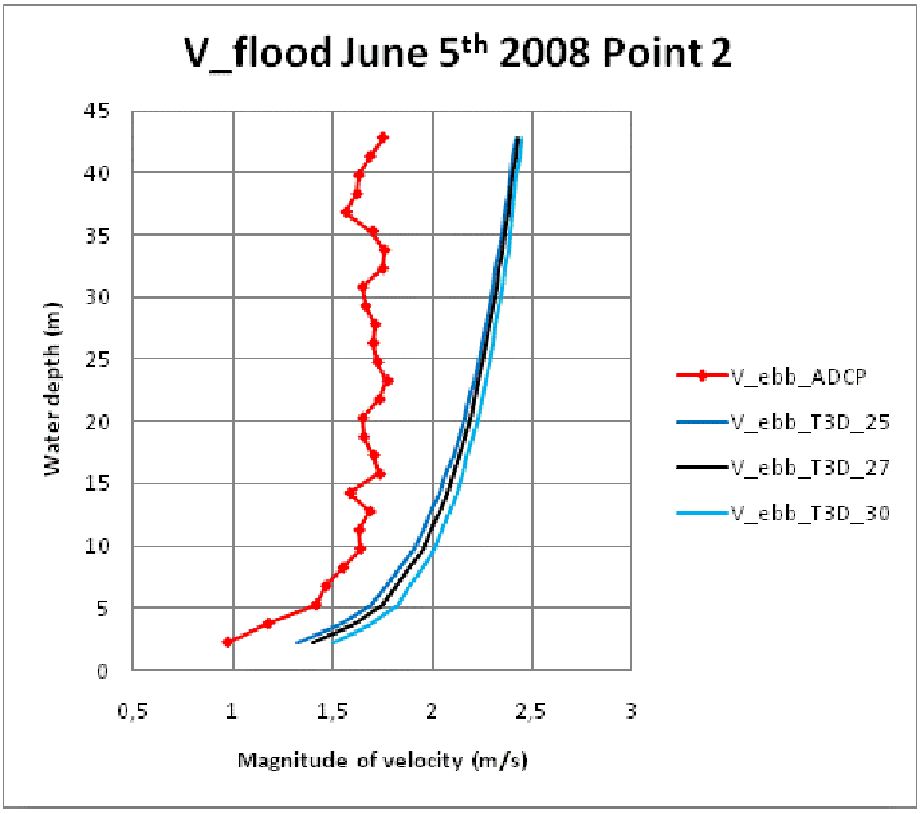

Figure C92: Velocity profile along the vertical during ebb (June 5th 2008) at location 2. Comparison between ADCP measurements (in red) and Telemac-3D results.

5.7 Site references

[C1] IXSURVEY (2005). « Analyse des mesures de courant dans les Héaux de Bréhat ». Document T1441. [Analysis of flow measurements in Les Héaux-de-Bréhat].

[C2] IXSURVEY (2008). Projet « Énergies marines ». Mesures de courants marins et de houle dans la zone de Bréhat. Mars-juin 2008. Document T1706. ["Marine Energies" Project: "Marine current and wave measurements in the Bréhat zone. March-June 2008"].

[C3] CREOCEAN (2008). Projet d'hydroliennes au Nord de Bréhat. Campagne de reconnaissance en mer : bathymétrie, sonar à balayage latéral, sismique réflexion, magnétisme. Rapport intermédiaire. Dossier 1081017_RA1. [Tidal turbines project to the North of Bréhat. Marine reconnaissance campaign: bathymetry, side scanning sonar, seismic reflection, magnetism. Intermediate Report].

[C4] SHOM (2010). Références altimétriques maritimes (zéros hydrographiques) – SHOM 2010. Zone Manche Centre. Site Internet SHOM : www.shom.fr. [Marine altimetric references (Chart Datums) – SHOM 2010. Central English Channel Zone].

[C5] http://www.shom.fr/les-activites/activites-scientifiques/maree-et-courants/marees/coefficient-de-maree

[C6] SHOM (2004). "De l'île de Bréhat au Plateau des Roches Douvres". Nautical chart # 7153 L.

[C7] SHOM (2004). "Des Héaux-de-Bréhat au Cap Lévi". Nautical chart # 6966 L, 3rd edition.

[C8] SHOM (2004). "De l'île Grande à l'île de Bréhat". Nautical chart # 7152 L.

[C9] Salmon R. (1998). Lectures on Geophysical Fluid Dynamics.

[C10] Nezu I., Nakagawa H. (1993). Turbulence in Open-Channel Flows. IAHR monograph series. Balkema.

[C11] Pham C.-T., Lyard F. (2012). Use of tidal harmonic constants databases to force open boundary conditions in TELEMAC. 19th TELEMAC-MASCARET User Conference, Oxford, UK.

[C12] Desmare S., Nicolle A. (2011). Hydrodynamique côtière : les applications du système de modélisation TELEMAC au SHOM. JIST 2011.

6 GENERAL REFERENCES

[G1] Hervouet J.-M. (2007). Hydrodynamics of Free Surface Flows. Modelling with the finite element method. Wiley.

[G2] Telemac modelling system (2010). 2D Hydrodynamics. TELEMAC-2D Software. Version 6.0. Reference manual.

[G3] Telemac modelling system (2010). 2D Hydrodynamics. TELEMAC-2D Software. Version 6.0. User manual.

[G4] Telemac modelling system (2010). 2D Hydrodynamics. TELEMAC-2D Software. Version 6.0. Validation document.

[G5] Telemac modelling system (2008). 3D Hydrodynamics. TELEMAC-3D Code. Release 5.8. Operating manual.

[G6] Janin J.-M., Blanchard X. (1992). Simulations des courants de marée en Manche et Proche Atlantique. Rapport EDF DER – LNH n° HE-42/92.58. [Simulations of tidal flows in the English Channel and Near Atlantic Ocean].

[G7] Thompson K. W. (1987). Time dependent boundary conditions for hyperbolic systems. Journal of Computational Physics, vol. 68, pp. 1-24.

7 CONCLUSIONS / NEXT STEPS

7.1 Conclusions

The selected sites have been modelled, and the models have been calibrated against available data. A considerable amount of work has been produced in order to build the different models, find the suitable boundary conditions, and find the appropriate calibration data.

The Alderney Race and the Pentland Firth have been modelled in 2D, while the Paimpol-Brehat area has been modelled in both 2D and 3D. The comparison between 2D and 3D will be detailed in another deliverable of the present work package.

7.2 Next deliverables

- D2 - Code development for 2D shallow water model in Telemac 2D of the Telemac software suite, in order to allow for the implementation of parametric characterization of arrays.

- D3 – Incorporation of parametric characterization of an axial flow turbine array (obtained in WG3 WP2) into the 2D basin scale numerical models.

- D4 - Assessment of the effects of energy extraction at various UK sites with the 2D model: Macroscopic, but still reliable, study of the large scale impact of a tidal farm on the hydrodynamics of the area, and accurate assessment of the site tidal resource.

- D5 - Cross-comparison of 2D and 3D results, in terms of energy extraction, for the selected site.

8 APPENDIX A1

Only available to PerAWaT participants.

9 APPENDIX B1

Only available to PerAWaT participants.

10 APPENDIX C1

Only available to PerAWaT participants.

11 APPENDIX C2

Only available to PerAWaT participants.

12 APPENDIX G1

Be x_i the measured values and y_i the modelled values, the quality indices used in this study are calculated as follows:

Standard quality indice	Expression
Mean error or bias	$\frac{1}{n}\sum_i (y_i - x_i)$
Root Mean Square error	$\sqrt{\frac{1}{n}\sum_i (y_i - x_i)^2}$
Non dimensional bias	$\frac{\sum_i (y_i - x_i)}{\sum_i (x_i)}$
Non dimensional RMS error or scatter index	$\frac{\sqrt{\frac{1}{n}\sum_i (y_i - x_i)^2}}{\frac{1}{n}\sum_i (x_i)}$
Pearson linear correlation coefficient	$\frac{\sum_i \left(x_i - \frac{1}{n}\sum_j (x_j)\right)\left(y_i - \frac{1}{n}\sum_j (y_j)\right)}{\sqrt{\sum_i \left(x_i - \frac{1}{n}\sum_j (x_j)\right)^2 \sum_i \left(y_i - \frac{1}{n}\sum_j (y_j)\right)^2}}$